2018-03-02

Molecular Mechanisms Underlying Synaptic Connectivity in C. elegans

Alison M. Philbrook
University of Massachusetts Medical School

MOLECULAR MECHANISMS UNDERLYING SYNAPTIC CONNECTIVITY IN *C. ELEGANS*

A Dissertation Presented

By

Alison Philbrook

Submitted to the Faculty of the
University of Massachusetts Graduate School of Biomedical Sciences, Worcester
in partial fulfillment of the requirements for the degree of

DOCTOR OF PHILOSOPHY

MARCH 2nd, 2018

NEUROBIOLOGY

MOLECULAR MECHANISMS UNDERLYING SYNAPTIC CONNECTIVITY IN *C. ELEGANS*

A Dissertation Presented
By
Alison Philbrook

This work was undertaken in the Graduate School of Biomedical Sciences
Program in Neuroscience

Michael Francis, Ph.D., Thesis Advisor

Vivian Budnik, Ph.D., Member of the Committee

Kensuke Futai, Ph.D., Member of the Committee

Andrew Tapper, Ph.D., Member of the Committee

Kenneth Norman, Ph.D., External Member of the Committee

Claire Bénard, Ph.D., Chair of Committee

Mary Ellen Lane, Ph.D.,
Dean of the Graduate School of Biomedical Sciences

March 2nd, 2018

ACKNOWLEDGEMENTS

First, I would like to thank my mentor, Mike, for his endless support during my graduate studies. His constant encouragement and enthusiasm has been a driving force for me. I am truly appreciative of all the time he spent sitting through practice talks, editing my writing, or meeting with me to discuss my work. He has provided me with so many opportunities, and I feel fortunate to have had such an exceptional mentor.

Next, I want to thank all members, past and present, of the Francis lab. It is inspiring to work in an environment where everyone is passionate about their research, and even more inspiring to work with such an amazingly supportive group of people. I am grateful for all of the pow-wows and coffee breaks, and our festive celebrations of birthdays and holidays. You all make it exciting to come into lab each day.

I would also like to thank my committee members past and present for all of their advice and helpful feedback about my project. I am extremely grateful to have had Claire Bénard as my Chair over the years, who has gone out of her way to provide me with guidance and advice. Claire has helped me to become more confident as a scientist and I can't thank her enough for her continued support. I would also like to thank my committee members Vivian Budnik, Kenny Futai, and Andrew Tapper for encouraging me to pursue my goals and to not be afraid of presenting my science.

Thank you to the wonderful FABB group for creating an environment of scientific discussion that is lively and supportive, and to the entire Neurobiology department, for creating a fantastic place to work.

Last but certainty not least, thank you especially to my family and friends, who have always provided unconditional support. To my mom: thank you for your endless patience with me. You were always willing to listen to all of the ups and downs of grad school. To my dad, who possesses a tireless work ethic, and has inspired me to work hard and stay focused. To Jason, who has been by my side every step of the way and is always supportive of my goals, lifting my spirits whenever I have doubts or need an extra boost. And finally to my sister Lauren, who is my role model in all aspects of life. I am lucky to be surrounded by a loving group of people and I thank you all.

ABSTRACT

Proper synaptic connectivity is critical for communication between cells and information processing in the brain. Neurons are highly interconnected, forming synapses with multiple partners, and these connections are often refined during the course of development. While decades of research have elucidated many molecular players that regulate these processes, understanding their specific roles can be difficult due to the large number of synapses and complex circuitry in the brain. In this thesis, I investigate mechanisms that establish neural circuits in the simple organism *C. elegans*, allowing us to address this important problem with single cell resolution *in vivo*.

First, I investigate remodeling of excitatory synapses during development. I show that the immunoglobulin domain protein OIG-1 alters the timing of remodeling, demonstrating that OIG-1 stabilizes synapses in early development but is less critical for the formation of mature synapses. Second, I explore how presynaptic excitatory neurons instruct inhibitory synaptic connectivity. My work shows that disruption of cholinergic neurons alters the pattern of connectivity in partnering GABAergic neurons, and defines a time window during development in which cholinergic signaling appears critical. Lastly, I define novel postsynaptic specializations in GABAergic neurons that bear striking similarity to dendritic spines, and show that presynaptic *nrx-1*/neurexin is required for the development of spiny synapses. In contrast, cholinergic connectivity with their other postsynaptic partners, muscle cells, does not require *nrx-1*/neurexin. Thus, distinct molecular signals govern connectivity with these two cell types. Altogether, my

findings identify fundamental principles governing synapse development in both the developing and mature nervous system.

TABLE OF CONTENTS

List of tables

List of figures

Figures in Chapter I

Figures in Chapter II

Figures in Chapter III

Figures in Chapter IV

Figures in Chapter V

List of copyrighted materials produced by the author

A figure in **Chapter I** (General Introduction) has been previously published in a book chapter written by the author and is presented in accordance with copyright law.

Philbrook, A. & Francis, M. “Emerging technologies in the analysis of *C. elegans* nicotinic acetylcholine receptors.” *Nicotinic Acetylcholine Receptor Technologies.* Ed. Ming Li. Humana Press, 2016. 77-96. Print. The final publication is available at link.springer.com via http://dx.doi.org/10.1007/978-1-4939-3768-4_5

Chapter II represents work previously published and is presented in accordance with copyright law.

*He, S., *Philbrook, A., McWhirter, R., Gabel, C., Taub, D., Carter, M., Hanna, I., Francis, M., & Miller, D. (2015) Transcriptional control of synaptic remodeling through regulated expression of an immunoglobulin superfamily protein. *Current Biology.* 25(19):2541-8. doi:10.1016/j.cub.2015.08.022

*co-first authors

Chapter III represents work previously published and is presented in accordance with copyright law.

*Barbagallo, B., *Philbrook, A., Touroutine, D., Banerjee, N., Oliver, D., Lambert, C., & Francis, M. (2017) Excitatory neurons sculpt GABAergic neuronal connectivity in the *C. elegans* motor circuit. *Development.* 144(10):1807-1819. doi:10.1242/dev.141911

*co-first authors

List of symbols, abbreviations, or nomenclature

ACh: acetylcholine

AChR: acetylcholine receptor

ADAMTS: disintegrin and metalloprotease with thrombospondin repeats

ATR: all-trans-retinal

AMPA: α-amino-3-hydroxy-5-methyl-4-isoxazolepropionic acid

BDNF: brain-derived neurotrophic factor

CaMKII: Ca^{2+}/calmodulin-dependent protein kinase II

CASK: calcium/calmodulin-dependent serine protein kinase

ChAT: choline acetyltransferase

CNS: central nervous system

COE: Collifer/Olf/EBF

COUP-TF: chicken ovalbumin upstream promoter transcription factor

DEG/ENaC: degenerin/epithelial sodium channel

EBF: early B cell factor

EGF: epidermal growth factor

E/I balance: excitation/inhibition balance

EM: electron microscopy

FRAP: fluorescence recovery after photobleaching

GABA: γ-aminobutyric acid

GFP: green fluorescent protein

iAChR: ionotropic acetylcholine receptor

Ig: immunoglobulin

IgSF: immunoglobulin superfamily

L1-L4: first, second, third, and fourth larval stages

L-AChR: levamisole-sensitive acetylcholine receptor

LNS: laminin/neurexin/sex hormone-binding globulin

Lrp4: low-density lipoprotein receptor-related protein 4

LRRTM: leucine-rich repeat transmembrane

MB: mushroom body

mEPSC/IPSC: miniature excitatory/inhibitory postsynaptic current

Mint: Munc18 interacting protein

MuSK: muscle-specific kinase

nAChR: nicotinic acetylcholine receptor

NGM: nematode growth media

NMDA: N-methyl-D-aspartate

NMJ: neuromuscular junction

Npas4: Neuronal Per Arnt Sim domain protein 4

PDZ: postsynaptic density protein (PSD95), *Drosophila* disc large tumor suppressor (Dlg1), and zonula occludens-1 protein (zo-1)

PSD: postsynaptic density

smFISH: single molecule fluorescent *in situ* hybridization

TetTx: tetanus toxin light chain

TGFβ: transforming growth factor beta

TM: transmembrane

TrkB: tropomyosin receptor kinase B

vAChT: vesicular acetylcholine transporter

Veli: vertebrate LIN-7 homolog

Preface

The work presented in **Chapter II** is previously published.

*He, S., ***Philbrook, A.,*** McWhirter, R., Gabel, C., Taub, D., Carter, M., Hanna, I., Francis, M., & Miller, D. (2015) Transcriptional control of synaptic remodeling through regulated expression of an immunoglobulin superfamily protein. *Current Biology.* 25(19):2541-8.

*co-first authors

The work presented in **Chapter III** is previously published.

*Barbagallo, B., ***Philbrook, A.,*** Touroutine, D., Banerjee, N., Oliver, D., Lambert, C., & Francis, M. (2017) Excitatory neurons sculpt GABAergic neuronal connectivity in the *C. elegans* motor circuit. *Development.* 144(10):1807-1819.

*co-first authors

The work presented in **Chapter IV** represents unpublished work that is under review at *eLIFE*.

Philbrook, A., Ramachandran, S., Lambert, C., Oliver, D., Florman, J., Alkema, M., Lemons, M., & Francis, M. Neurexin directs partner-specific synaptic connectivity in *C. elegans.*

Contributions of the authors are addressed at the beginning of each chapter.

CHAPTER I

General Introduction

Establishing synaptic connectivity: a multistep process

Synapses are specialized junctions that serve as communication nodes between neurons in the brain. Information is transferred between connected neurons, ultimately forming neural circuits that are thought to underlie behavior. The correct wiring of appropriate synaptic partners is essential for nervous system function, and understanding the mechanisms that drive this process remains an important question in neurobiology.

The formation of synaptic connections requires a series of steps including neurogenesis, the guidance of axons to their target cells, and the assembly and organization of synaptic machinery. Following initial synapse establishment, connections can be further remodeled or refined. In this thesis, I examine how genetically encoded and activity-dependent processes shape the construction and refinement of neural circuits. Through the investigation of synaptic connectivity in *C. elegans*, this work advances our understanding of the processes governing neural circuit wiring in the brain.

Synapse assembly and circuit formation

Circuit formation involves a series of developmental events. My thesis work specifically examines the molecular mechanisms driving synaptic connectivity following neurogenesis and axon pathfinding, two processes that are critical for early nervous system development (Reviewed in (Chilton, 2006; Dickson, 2002; Gotz and Huttner, 2005; Martynoga et al., 2012; Raper and Mason, 2010; Robichaux and Cowan, 2014)). After spatiotemporal cues guide axons to their target areas, many molecular components

act to coordinate the formation of a synapse. Regulatory signals orchestrate the precise wiring of synaptic connections, enabling synapse specificity. Neuronal activity and transmitter release can also help shape the process of synapse formation. While studies of the vertebrate neuromuscular junction (NMJ) have identified an agrin/Lrp4/MuSK pathway that guides synapse development, the mechanisms governing central synapse formation are less well understood. In this thesis, I investigate how excitatory synapses onto neurons and muscle are differentially established in the model organism *C. elegans*. Additionally, I examine how neuronal activity shapes the formation of inhibitory synapses, a process that helps maintain excitatory/inhibitory balance in the brain. Together, this work aims to identify conserved mechanisms that shape the development of neural circuits.

Synapse formation at the neuromuscular junction

Studies at the vertebrate neuromuscular junction, a large chemical synapse that is experimentally easily accessible, have helped elucidate general principles of synaptogenesis. The NMJ is a synapse between motor neurons and skeletal muscle fibers, and uses the neurotransmitter acetylcholine (ACh) to mediate muscle contraction. During development, acetylcholine receptors (AChRs) initially prepattern in the muscle (Lin et al., 2001; Yang et al., 2001), and the arrival of the motor neurons induces the differentiation of the postsynaptic specialization (McMahan, 1990; Sanes and Lichtman, 2001). Specifically, motor neuron derived agrin acts to stabilize AChRs in muscle through the agrin/Lrp4/MuSK pathway. Agrin binds to Lrp4 (low-density lipoprotein

receptor-related protein 4), which forms a complex with the receptor tyrosine kinase MuSK (muscle-specific kinase) to stimulate neuromuscular synapse formation through the effector protein rapsyn (Apel et al., 1997; DeChiara et al., 1996; Gautam et al., 1995; Gillespie et al., 1996; Kim et al., 2008b). These events in turn trigger the assembly of the presynaptic terminal, including its alignment with the postsynaptic domain (DeChiara et al., 1996; Gautam et al., 1996). Glia-derived signals, such as transforming growth factor β (TGFβ) (Feng and Ko, 2008), and Wnt signaling (Kim et al., 2003; Messeant et al., 2017) also play critical roles in NMJ development.

Excitatory synapse development at the *C. elegans* NMJ similarly involves a well-characterized scaffold. *C. elegans* NMJs form *en passant*, where muscles send projections called muscle arms to form synapses with motor neuron axons (Sulston and Horvitz, 1977; White et al., 1986). Two types of AChRs, levamisole-sensitive acetylcholine receptors (L-AChRs) and homomeric ACR-16 receptors, mediate excitatory signaling onto muscle (Boulin et al., 2008; Francis et al., 2005; Richmond and Jorgensen, 1999; Touroutine et al., 2005).

The clustering of L-AChRs requires postsynaptic scaffolding proteins expressed in muscle and presynaptic secretion of a critical signaling component, similar to the expression of postsynaptic Lrp4/MuSK and motor neuron secretion of agrin in vertebrates. Specifically, the transmembrane protein LEV-10 localizes postsynaptically in *C. elegans* muscle (Gally et al., 2004), and this protein physically interacts with the muscle-secreted extracellular protein LEV-9 to regulate L-AChR clustering (Gendrel et al., 2009). The single immunoglobulin (Ig) domain protein OIG-4 is also secreted from

muscle cells and acts to stabilize the L-AChR/LEV-9/LEV-10 complex (Rapti et al., 2011). Interestingly, LEV-10 contains an LDLa (low-density lipoprotein receptor domain class A) domain, similar to LDLa domain repeats in the vertebrate agrin receptor Lrp4 (Gally et al., 2004; Zong et al., 2012). Following this work, a screen for abnormal L-AChR distribution identified the ADAMTS-like protein MADD-4, the *C. elegans* ortholog of Punctin-1 and Punctin-2 (Pinan-Lucarre et al., 2014). MADD-4 is secreted presynaptically from cholinergic motor neurons to localize AChRs at excitatory NMJs, and in the absence of *madd-4,* L-AChRs are localized in extrasynaptic regions of the muscle cells (Pinan-Lucarre et al., 2014). While agrin directly binds to postsynaptic Lrp4 in vertebrates (Kim et al., 2008b), the relationship between MADD-4 and the LEV-9/LEV-10 complex is unclear. The extrasynaptic and remaining synaptic L-AChR clusters in *madd-4* mutants still contain LEV-9 and LEV-10, arguing against a direct interaction (Pinan-Lucarre et al., 2014). Disruption of L-AChR clustering does not alter the distribution of presynaptic boutons, suggesting that pre- and post-synaptic development can be genetically uncoupled (Gally et al., 2004; Gendrel et al., 2009; Pinan-Lucarre et al., 2014; Rapti et al., 2011).

The clustering of ACR-16 homomeric receptors requires the Ror receptor tyrosine kinase CAM-1 (Francis et al., 2005). *C. elegans* CAM-1 shares homology with MuSK (Forrester et al., 1999; Francis et al., 2005), a critical organizer at the vertebrate NMJ, suggesting that this protein may act to regulate synapse formation across systems. Cholinergic synaptic vesicle clustering is also disrupted in *cam-1* mutants; however, it is unclear whether these alterations are secondary to disruptions in ACR-16 receptor

clustering or whether they result from CAM-1 requirements in pre- and post-synaptic development independently (Francis et al., 2005). Similar to the case in vertebrates, Wnt signaling plays critical roles at the *Drosophila* (Mathew et al., 2005; Packard et al., 2002) and *C. elegans* (Babu et al., 2011; Jensen et al., 2012; Klassen and Shen, 2007) NMJs. In *C. elegans*, photoconversion experiments demonstrated that Wnt signaling, mediated by CAM-1 (in a heteromeric complex with LIN-17/Frizzled), regulates the translocation of ACR-16 receptors to synapses (Jensen et al., 2012).

In the central nervous system (CNS), similar principles guide excitatory synapse formation, such as diffusible presynaptic signaling molecules and Wnt signaling. Additionally, cell-adhesion molecules play a predominant role in directing synapses, coordinating pre- and post-synaptic assembly. However, the mechanisms of central synapse formation are less well understood due to the complexity of synaptic connections and heterogeneity of cell types.

Developing excitatory synapses in the central nervous system

Most excitatory synapses in the brain are glutamatergic and they occur on the surface of membranous protrusions called dendritic spines. The first description of these structures emerged in 1888, when Santiago Ramón y Cajal examined the cerebellum of birds using Golgi staining and observed that the surfaces of Purkinje cells were covered with “espinas” (i.e. “thorns” or “spines”) (Cajal, 1888). Since then, an explosion of literature has supported the idea that spines are present on many neurons, including pyramidal neurons of the neocortex and hippocampus (Cajal, 1891; Harris and Stevens,

1989), granule cells in the olfactory cortex (Woolf et al., 1991), and GABAergic neurons in the striatum (Smith and Bolam, 1990; Wilson et al., 1983).

Dendritic spines can be generally characterized as actin-filled structures (Matus et al., 1982) that anchor the postsynaptic density (PSD) opposite presynaptic inputs, allowing for rapid transmission from cell to cell (Gray, 1959). Both AMPA (α-amino-3-hydroxy-5-methyl-4-isoxazolepropionic acid) and NMDA (N-methyl-D-aspartate) type glutamate receptors are present in the PSD (Aoki et al., 1994; Martin et al., 1993). Spines are categorized based on their morphology, including mushroom-shaped, branched, thin, and stubby spines (Harris et al., 1992; Peters and Kaiserman-Abramof, 1970). Many, but not all, dendritic spines are formed after thin, transient structures called filopodia evolve into spines containing functional synapses (Ziv and Smith, 1996). In early development, dendritic spine density increases, followed by a period of pruning of inappropriate connections (Markus and Petit, 1987; Rakic et al., 1986; Zuo et al., 2005). A host of factors have been identified as regulators of spine development and stabilization, including proteins that bind to or modify the actin cytoskeleton such as spinophilin and small GTPases (Feng et al., 2000; Luo et al., 1996).

To form glutamatergic synapses on dendritic spines, extracellular molecules and their receptors help guide the navigation of axons to appropriate target regions. Many of these guidance-related cues also appear to play a secondary role in synapse formation, such as BDNF/TrkB signaling, which acts to increase synapse number in the hippocampus by increasing the probability of cell-cell interactions (Luikart et al., 2008). Developing glutamatergic synapses contain a large number of diverse proteins, and many

of these molecules must work in concert to build a synapse. Secreted proteins such as Wnts (Davis et al., 2008; Hall et al., 2000; Sahores et al., 2010) and glia-derived signals such as thrombospondins (Christopherson et al., 2005) help regulate synapse formation in multiple regions of the CNS. At the postsynapse, the widely-expressed proteins Homer and Shank act as scaffolding proteins for the PSD and play critical roles in spine morphogenesis (Hayashi et al., 2009; Sala et al., 2001). Additionally, several cell adhesion molecules have been implicated in synapse assembly and the coordinated development of both pre- and post-synaptic terminals. Examples include Ig superfamily members, cadherins, neurexin-neuroligin complexes, and proteoglycans. Many of these cell adhesion molecules also contribute to spine formation (Chih et al., 2005; Liu et al., 2016; Togashi et al., 2002), but defining their specific roles *in vivo* has remained difficult. The molecular diversity of these trans-synaptic complexes helps establish the specificity of synaptic connections in the nervous system.

One of the most well-characterized examples of trans-synaptic signaling in the CNS is the neurexin-neuroligin adhesion complex, which has been implicated in both excitatory and inhibitory synapse development (Chih et al., 2005; Graf et al., 2004; Ichtchenko et al., 1995). Neurexins and neuroligins are single pass transmembrane domain proteins and are thought to be primarily expressed pre- and post-synaptically, respectively (Hata et al., 1993; Song et al., 1999; Ushkaryov et al., 1992). Through PDZ binding domains, neurexins and neuroligins are also coupled to intracellular partners. At the postsynapse, neuroligin binds to PSD-95, a major component of the glutamatergic postsynaptic scaffold, and the coordinated actions of neuroligin and PSD-95 regulate

synapse development (Irie et al., 1997; Prange et al., 2004). Neurexins have been shown to interact with a complex of PDZ domain containing proteins including CASK (calcium/calmodulin-dependent serine protein kinase), Velis (vertebrate LIN-7 homolog), and Mint (Munc18 interacting protein) (Biederer and Sudhof, 2000; Butz et al., 1998; Hata et al., 1996). Previous studies in vertebrates have largely implicated a requirement for neurexin in Ca^{+2}-induced synaptic release, primarily through coupling Ca^{+2} channels to the presynaptic machinery (Dean et al., 2003; Missler et al., 2003), and have suggested that neurexin is not essential for synapse formation (Dudanova et al., 2007). However, more recent work has demonstrated that neurexins serve as context-dependent synaptic organizers, implicating a role for neurexin in both synapse formation and function depending on synapse type (Chen et al., 2017).

There are three neurexin genes in mammals and they are subject to extensive alternative splicing, resulting in thousands of isoforms (Ullrich et al., 1995). The two major neurexin isoforms (α and β) are broadly expressed throughout the brain (Ullrich et al., 1995), while a short γ isoform originating from the Nrxn1 gene has recently been shown to be highly expressed in the cerebellum (Sterky et al., 2017). Notably, in *C. elegans* there is one neurexin gene (*nrx-1*) that encodes both long and short isoforms, but loss of either isoform has not yet been associated with disrupted synapses in worms. *C. elegans* NRX-1/neurexin function has been characterized almost exclusively in the context of its partnership with NLG-1/neuroligin (Hart and Hobert, 2018; Hu et al., 2012; Maro et al., 2015; Tong et al., 2015; Tong et al., 2017), and NRX-1 can directly bind NLG-1 (Hu et al., 2012).

Recent work has demonstrated that neurexins are also capable of binding many other extracellular ligands, including calsyntenins (Lu et al., 2014; Pettem et al., 2013; Um et al., 2014), neurexophilins (Beglopoulos et al., 2005; Missler et al., 1998; Missler and Sudhof, 1998; Petrenko et al., 1996), cerebellins (Joo et al., 2011; Matsuda and Yuzaki, 2011; Uemura et al., 2010), dystroglycans (Reissner et al., 2014; Sugita et al., 2001), latrophilins (Boucard et al., 2012), hevins (Singh et al., 2016), leucine-rich repeat transmembrane proteins (LRRTMs) (de Wit et al., 2009; Ko et al., 2009; Siddiqui et al., 2010; Um et al., 2016), and, in *C. elegans*, the synapse-organizing molecule MADD-4 (Maro et al., 2015). Many of these proteins have been shown to be important for promoting synapse formation, such as LRRTMs and calsyntenins (de Wit et al., 2009; Ko et al., 2009; Pettem et al., 2013; Um et al., 2014). Given the large number of ligands that can bind neurexins, an interesting possibility is that the organization of synapses can be specified by the interactions of neurexins with different partners.

In the central nervous system, ionotropic acetylcholine receptors (iAChRs) are primarily expressed presynaptically or extrasynaptically, and they perform mostly modulatory roles (Dani and Bertrand, 2007). However, like glutamate receptors, some cholinergic receptor subtypes can also localize to dendritic spines (Shoop et al., 1999; Yang et al., 2013). While protein complexes likely mediate the clustering of neuronal iAChRs, these synapses appear to require a distinct molecular scaffold from that at the NMJ (Feng et al., 1998). Recent work has provided evidence that PDZ domain-containing scaffolding proteins, which play a critical role in the clustering of brain glutamatergic receptors, may also cluster neuronal iAChRs, including PICK1 and PSD-

95 (Baer et al., 2007; Conroy et al., 2003; Neff et al., 2009). However, the mechanisms regulating iAChR localization in the brain have not been fully elucidated.

Notably, the major excitatory neurotransmitter in *C. elegans* is acetylcholine, and more than a third of all neurons release ACh (Rand, 2007). In Chapter IV, I present evidence demonstrating that cholinergic receptors are clustered at the tips of spine-like protrusions in *C. elegans* inhibitory neurons. Early electron microscopy studies reported the presence of spine-like processes on inhibitory neurons (White et al., 1976, 1986), but these features have remained uncharacterized. Spiny processes have also been observed in other invertebrates, such as *Drosophila* (Leiss et al., 2009), crickets (Frambach et al., 2004), and bees (Farris et al., 2001). This discovery in *C. elegans* allows us to investigate how spiny synapses are formed *in vivo* using the advantages of a genetic model organism. I demonstrate that the presynaptic organizer neurexin directs cholinergic receptor localization and spine outgrowth, acting independently of its typical binding partner neuroligin. This work addresses a critical need to understand neurexin's multifaceted roles at synapses, as disruption of neurexin in the brain is associated with several neuropsychiatric and neurodevelopmental disorders (Kim et al., 2008a; Martinez-Mir et al., 2013; Reichelt et al., 2012; Rujescu et al., 2009).

The role of neuronal activity on inhibitory synapse formation

Inhibitory interneurons make up approximately 15-25% of cortical neurons in the brain (Hendry et al., 1987; Meinecke and Peters, 1987), and release of the principal inhibitory neurotransmitter γ-aminobutyric acid (GABA) is critical for nervous system

function, including the regulation of neuronal excitability (Lee and Maguire, 2013, 2014). Studies in mammals have demonstrated that inhibitory network development is regulated by sensory experience through activity-dependent pathways. In the visual cortex, for example, light deprivation disrupts the maturation of GABAergic circuits (Morales et al., 2002). In the developing hippocampus, neuronal activity regulates inhibitory synapse density through the expression of brain-derived neurotrophic factor (BDNF) (Marty et al., 2000). Further, activity-dependent transcriptional pathways play an important role in inhibitory network development. The expression of the transcription factor Npas4 is rapidly activated by excitatory activity, regulating the expression of target genes such as BDNF to control inhibitory synapse development (Bloodgood et al., 2013; Lin et al., 2008). 270 unique genes are differentially regulated by knockdown of Npas4 (Bloodgood et al., 2013), suggesting that a wide variety of genes may affect inhibitory synapses. Thus, the precise mechanisms underlying activity-dependent changes in inhibitory network development still remain inadequately understood.

In *C. elegans*, muscle fibers receive both excitatory and inhibitory inputs. Two classes of iAChRs (discussed above) mediate cholinergic signaling, while GABAergic receptors mediate inhibitory neurotransmission onto muscle (Richmond and Jorgensen, 1999). As in mammals, inhibitory signaling is critical for neural circuit activity and behavior. Release of acetylcholine onto body wall muscles results in muscle contraction, while GABA release causes relaxation of the muscle. To generate the sinusoidal movement characteristic of *C. elegans*, the contraction and relaxation of body wall muscle must be out of phase. Using the genetic advantages afforded in the model

organism *C. elegans*, I investigate the role of neuronal activity on GABAergic synapse formation. This work suggests that similar processes may be important for establishing GABAergic connectivity across systems, and identifies a model to examine the mechanisms driving activity-dependent changes in connectivity.

Synaptic refinement

After initial synaptic connections are established, circuits can further refine or rewire their connectivity. For example, the pruning of synaptic connections is required for the maturation of the vertebrate neuromuscular junction and rearrangement of retinogeniculate synapses. Similarly, developmental remodeling shapes neural circuitry in *C. elegans* GABAergic DD motor neurons and mushroom body neurons in *Drosophila.* Further, activity-dependent reorganization of pre-existing structures is thought to enable both learning and memory and the stability of the adult brain. These processes of refinement reflect an ongoing need to maintain appropriate synaptic connections in the nervous system.

Developmental synaptic remodeling

In vertebrates, development of both the neuromuscular junction (Brown et al., 1976; Sanes and Lichtman, 1999; Walsh and Lichtman, 2003) and visual cortex (Campbell and Shatz, 1992; Shatz and Kirkwood, 1984) have been extensively studied as examples of activity-dependent synapse elimination. Early in postnatal development at the vertebrate NMJ, multiple motor neurons send axons to the same muscle cell.

However, within a few weeks, all but one of the axonal inputs are eliminated. This establishes a one-to-one connection between the motor neuron and muscle cell in adulthood (Brown et al., 1976). Removal of excess connections is a competitive process, where the remaining axon takes over the space formerly occupied by its neighbor, and stronger inputs are favored (Buffelli et al., 2003; Walsh and Lichtman, 2003). Similarly, remodeling in the visual system involves the elimination of excess inputs onto geniculate neurons of the visual thalamus. Prior to eye opening, each geniculate neuron receives inputs from twenty or more retinal ganglion cells. Within about two weeks, approximately 1-3 inputs remain, and these connections are now significantly strengthened (Chen and Regehr, 2000). Refinement is dependent on neuronal activity, as microglia can engulf weaker presynaptic inputs (Schafer et al., 2012; Schafer and Stevens, 2015). These retinogeniculate rearrangements are thought to help with the fine tuning of cortical receptive fields (Tavazoie and Reid, 2000), illustrating the importance of eliminating excess connections during development.

In *Drosophila,* a clear example of neuronal rewiring during development is the remodeling of mushroom body (MB) neurons. MB neurons fall into 3 major classes, including α'β', αβ and γ neurons (Lee et al., 1999), and they are essential for olfactory learning and memory in the fly (Heisenberg et al., 1985; McGuire et al., 2001). The γ neurons are born during embryonic and larval development, extending bifurcated axons. However, the lifestyle of the fly dramatically changes as the fly advances to the pupa and adult stages. To accommodate this, axons and dendrites in the γ neurons are pruned during the early stages of pupation and replaced by adult-specific processes (Lee et al.,

1999). Studies investigating the molecular mechanisms underlying pruning in MB γ neurons have since implicated a heterodimer consisting of ultraspiracle and the ecdysone receptor as a cell-autonomous regulator of this pruning process (Lee et al., 2000).

Similar to the rewiring of synaptic connections in vertebrates and *Drosophila,* remodeling also occurs within DD GABAergic neurons in the model organism *C. elegans,* suggesting that synaptic refinement is a conserved feature across organisms. Early electron microscopy studies indicated that the DD neurons reverse polarity during larval development in the late first larval (L1) stage, beginning approximately 12 hours after hatch at 22°C (White et al., 1978). In newly born larvae, DD motor neurons innervate ventral muscles and receive cholinergic input (DA/DB) on the dorsal side. At the end of the first larval stage, DD neurons reverse polarity to relocate output to dorsal muscles and receive ventral input from newly born cholinergic motor neurons (VA/VB) (White et al., 1978). However, DD remodeling in *C. elegans* does not require changes in neuronal morphology. Instead, DD neurons reverse their polarity by exchanging the locations of signaling components (**Figure 1.1**).

To monitor DD remodeling, prior studies have examined the relocation of pre-synaptic components. This work has demonstrated that the timing of DD remodeling during development is subject to transcriptional control. The heterochronic gene *lin-14* was the first factor identified that regulates the timing of this reorganization, and loss-of-function mutants show precocious DD remodeling (Hallam and Jin, 1998). In contrast, the Iroquois homeodomain protein IRX-1 promotes remodeling, and *irx-1* knockdown results in delayed remodeling (Petersen et al., 2011). This work demonstrated that the

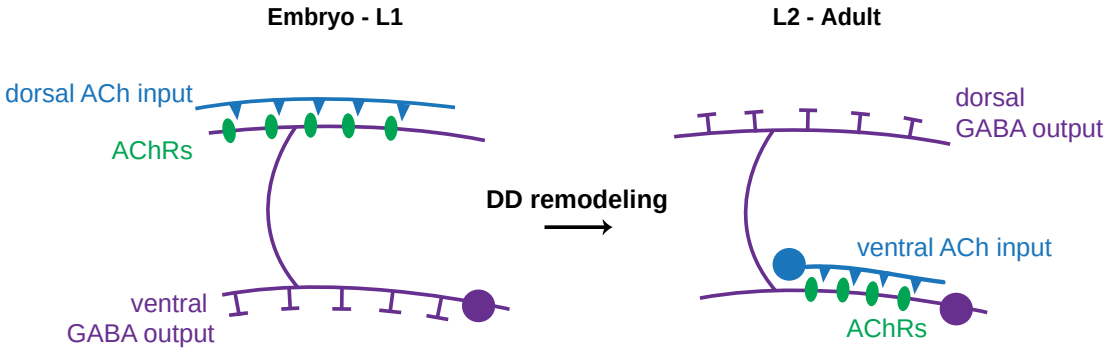

Figure 1.1 Schematic of DD remodeling in *C. elegans*
In the embryo and L1 larval stage, DD motor neurons (purple) innervate ventral muscles and extend commissures to the dorsal side for cholinergic input (blue) from DA/DB motor neurons. After remodeling at the end of the L1 larval stage, postsynaptic receptors (green) switch locations to receive input ventrally from newly born VA/VB cholinergic motor neurons, while GABA outputs are relocated to innervate muscles dorsally.

PITX transcription factor UNC-30 promotes IRX-1 expression, facilitating the remodeling process (Petersen et al., 2011). The transcription factor *hbl-1* also acts to promote DD remodeling, and expression of this heterochronic gene is activity-dependent (Thompson-Peer et al., 2012). Specifically, mutations that decrease circuit activity through defects in synaptic vesicle priming or docking (i.e. *unc-13*/Munc13 or *unc-18*/Munc18) decrease *hbl-1* expression and consequently delay DD remodeling (Thompson-Peer et al., 2012), suggesting that the timing of DD plasticity is activity-dependent. Further, two ER-bound transcription factors, MYRF-1 and MYRF-2 (myelin-regulatory factor), were recently shown to be indispensable for synaptic rewiring; loss of *myrf-1* and *myrf-2* causes a complete failure in the relocation of presynaptic components (Meng et al., 2017). Thus, transcription factors act as key regulators of the remodeling program.

DD remodeling of presynaptic components appears to require the disassembly of synapses ventrally and trafficking of these components to the dorsal nerve cord (Park et al., 2011). This process is mediated by the actions of CYY-1, a cyclin box-containing protein that drives synapse removal, and CDK-5, a cyclin-dependent kinase that regulates the transport of synaptic vesicles to dorsal synapses (Park et al., 2011). Interestingly, *Cdk5* also regulates synapse removal in *Drosophila* mushroom body remodeling, suggesting that conserved mechanisms may regulate developmental remodeling across systems (Smith-Trunova et al., 2015). Further, the Degenerin/Epithelial Sodium Channel (DEG/ENaC) protein UNC-8 has also been shown to promote DD synapse disassembly in an activity-dependent pathway (Miller-Fleming et al., 2016).

Monitoring of postsynaptic remodeling, however, was previously unapproachable due to the lack of available markers labeling the postsynapse. Thus, it was unknown whether genes required for setting the timing of presynaptic remodeling (e.g. *lin-14, irx-1, hbl-1*) are also required for postsynaptic remodeling, or if the relocation of postsynaptic structures similarly requires the removal and trafficking of signaling components. Recent work from the Francis lab identified a postsynaptic receptor complex that regulates the activity of inhibitory motor neurons and localizes opposite cholinergic presynaptic inputs (Petrash et al., 2013). Expression of this tagged cholinergic receptor in DD neurons enabled the investigation of mechanisms that differentially drive pre- and post-synaptic remodeling, discussed in Chapter II and in other recent work (Howell et al., 2015) (**Figure 1.1**).

The GABAergic VD motor neurons, which are born post-embryonically, do not normally undergo remodeling due to expression of the COUP-TF nuclear hormone receptor UNC-55 (Walthall and Plunkett, 1995; White et al., 1986; Zhou and Walthall, 1998). In *unc-55* mutants, the VD neurons ectopically remodel and synaptic outputs relocate to the dorsal side (Petersen et al., 2011; Shan et al., 2005). Cell-specific expression profiling has demonstrated that both *irx-1* and *hbl-1*, two factors discussed above that promote DD remodeling, are transcriptional targets of *unc-55* (Petersen et al., 2011; Thompson-Peer et al., 2012). UNC-55 blocks expression of HBL-1 and IRX-1 to inhibit VD remodeling (Petersen et al., 2011; Thompson-Peer et al., 2012). My work and others (Howell et al., 2015) have characterized a role for the single immunoglobulin

domain protein OIG-1 in the regulation of both wild type DD remodeling and ectopic VD remodeling, discussed further in Chapter II.

Initially, DD motor neurons innervate ventral muscle and GABAergic receptors are expressed exclusively on the ventral side (Gally and Bessereau, 2003). Following the birth of the VD motor neurons, GABAergic receptors in muscle appear both ventrally (to receive input from VD motor neurons) and dorsally (to receive input from remodeled DD motor neurons) (Gally and Bessereau, 2003). In Chapter III, I demonstrate that reduced presynaptic activity during the process of rewiring GABAergic outputs results in altered synapse patterning in the adult. This work illustrates how activity-dependent processes are critical for the wiring of mature synaptic connections.

Plasticity of mature synapses

Structural changes in the brain can occur throughout life, modifying pre-existing connections. In particular, the plasticity of dendritic spines has been extensively studied, as the shape, size, and/or number of spines can be modified by activity and experience. Enhanced glutamate release, for example, induces an enlargement of spines on the dendrites of hippocampal neurons in rat slice preparations (Matsuzaki et al., 2004). Additionally, inducing long-term depression in cultured rat neurons results in spine shrinkage (Henson et al., 2017; Zhou et al., 2004).

In vivo work has elucidated a connection between learning and memory and spine formation. Learning and novel sensory experiences, for example, lead to newly formed spines in the mouse cortex which persist for months after training (Yang et al., 2009a).

These stabilized connections are thought to represent long-term encoding of memory (Yang et al., 2009a). Further, disruption of newly formed spines after a learning task using an optical probe can “erase” the acquired skill (Hayashi-Takagi et al., 2015). Many neurological diseases are associated with the loss or disruption of spiny synapses, including autism spectrum disorders, schizophrenia, and Alzheimer’s disease (Glantz and Lewis, 2000; Hutsler and Zhang, 2010; Probst et al., 1983), emphasizing the importance of elucidating mechanisms involved in spine formation and stabilization. My work in Chapter IV establishes a dendritic spine model in *C. elegans*, enabling future investigation of plasticity in the nervous system.

Alterations in neuronal activity can also result in the up/down regulation of receptors at synapses. With tetanic stimulation of hippocampal slice neurons, GFP-tagged AMPARs are rapidly recruited to synaptic sites (Shi et al., 1999). This example illustrates the strengthening of synaptic connections in response to coincident pre- and post-synaptic activity, a principle first described by Donald Hebb in the 1940s (termed Hebbian plasticity) that is thought to provide the basis for learning and memory (Hebb, 1949). To keep nervous system function within a normal range, homeostatic mechanisms can compensate for alterations in circuit activity, a process first described in cultured cortical neurons (Turrigiano et al., 1998). Compensatory mechanisms are particularly important for establishing excitatory/inhibitory (*E/I*) balance in the brain. Following activity deprivation, GABA receptor redistribution may help regulate *E/I* imbalances. Activity blockade in cell culture scales up the strength of mEPSCs (O'Brien et al., 1998), while mIPSC amplitudes and the number of GABA receptors clustered at postsynaptic sites

decrease (Kilman et al., 2002). Homeostatic regulation of inhibitory synapse number may involve the expression of CaMKII (Flores et al., 2015), which has also been implicated in excitatory synapse plasticity (Lisman et al., 2012). Importantly, *E/I* imbalance is associated with a number of neurological diseases, including schizophrenia and epilepsy (Fritschy, 2008; Wassef et al., 2003). Although the literature on homeostatic inhibitory plasticity has expanded in recent years, the molecular mechanisms underlying this negative feedback response are not well understood. In Chapter III, I describe a homeostatic process that may shape inhibitory synapses at the mature *C. elegans* NMJ, providing a potential model to explore compensatory mechanisms that shape synapses.

Synapse formation and refinement drive synaptic specificity

Neural circuits in the brain rely on the specificity of synaptic connections, and the precise wiring of synapses and further refinement of existing connections is central to this process. In Chapter II, I investigate the mechanisms underlying synaptic remodeling in *C. elegans* DD neurons, a process of refinement that is critical for the formation of mature connections in the nervous system. My work in Chapter III demonstrates that excitatory cholinergic neurons sculpt GABAergic connectivity, highlighting key roles for neuronal activity in circuit formation and maintenance. This work also suggests that a transcriptional target of the COE-type transcription factor *unc-3* is required to establish synapses onto GABAergic neurons. Prior studies have shown that transcriptional regulation of signals involved in cell-cell interactions help shape synaptic connectivity. In mice, for example, loss of the transcription factor Pea3 deregulates motor neuron

expression of cadherins, which results in the mispositioning of neurons within the spinal cord (Livet et al., 2002). Additionally, the transcription factor *senseless* regulates expression of the cell adhesion molecule *capricious* in the *Drosophila* visual system, which acts to distinguish synaptic layers (Morey et al., 2008; Shinza-Kameda et al., 2006). In Chapter IV, I identify this transcriptional target of *unc-3* as the cell adhesion molecule *nrx-1*/neurexin, and I explore how *nrx-1* directs partner-specific connectivity, enabling precise connections in the *C. elegans* motor circuit.

C. elegans as a model system to study synaptic connectivity

C. elegans offers many advantages for studies of synapse development. First, the basic features of the worm make it an ideal system for genetic analysis. There are two sexes in *C. elegans*, self-fertilizing hermaphrodites which can produce homozygous progeny, and males, which allows for cross-fertilization. The life cycle of *C. elegans* is very short, and a worm will grow from an egg to fertile adult in about three days at 20°C. Between the embryonic stage and adulthood, the worm goes through four larval stages (L1-L4), marking the end of each stage with a molt. Importantly, strains carrying mutations in genes that are essential for viability in mammals are in many cases viable and easily propagated, allowing for studies of conserved gene function that would otherwise be unapproachable. The *C. elegans* genome is small, containing about 20,000 genes, and approximately 40% of the predicted protein products have mammalian homologs (Consortium, 1998).

The transparency of the worm cuticle allows one to easily visualize the subcellular distribution of proteins tagged with fluorescent markers and GCaMP signaling in live, intact animals. Further, a variety of cell-specific promoters are available for precise spatial control of transgene expression using microinjection techniques (Mello et al., 1991). With just 302 neurons, the connectivity of the nervous system has been well defined by serial electron microscopy (EM) (White et al., 1976), and powerful genetic experiments enable *in vivo* investigation of altered connectivity. Forward genetic screens have enabled the discovery of novel genes involved in synapse formation, many of which have been shown to play conserved roles at mammalian synapses (e.g. *ric-3* and the maturation of AChRs (Halevi et al., 2002; Halevi et al., 2003)). Through pharmacological analysis (such as drug assays like aldicarb or levamisole), electrophysiological techniques, and calcium imaging, the functional consequences of altered connectivity can be examined. Additional approaches to study gene function, such as CRISPR knock-outs and RNAi, are also commonly used to address questions of synapse development in the worm.

The C. elegans motor circuit

113 of the 302 neurons in *C. elegans* are motor neurons (White et al., 1986). In the motor circuit, both cholinergic (excitatory) and GABAergic (inhibitory) motor neurons coordinate sinusoidal movement (**Figure 1.2**). Ventral body wall muscles are innervated by motor neurons with cell bodies and axons in the ventral cord (VA, VB, VC, VD). Dorsal muscles are innervated by motor neurons with cell bodies located ventrally

and axons dorsally (DA, DB, DD, AS) (Hall and Altun, 2008). Cholinergic neurons include A- and B- type motor neurons, in addition to AS and VC neurons, while the D-type motor neurons are inhibitory. Command interneurons innervate cholinergic neurons via *en passant* synapses along the length of the ventral nerve cord, while D-type inhibitory motor neurons do not receive input from interneurons. Cholinergic motor neurons form dyadic synapses onto both body wall muscles and GABAergic neurons at process swellings. GABAergic neurons in turn project to opposing body wall muscle, causing relaxation (**Figure 1.2**).

Motor neurons are developed during two distinct developmental periods. At hatch, the DA, DB, and DD motor neurons are present, while the VA, VB, VC, AS, and VD motor neurons are born towards the end of the first larval stage (Sulston, 1976; Sulston and Horvitz, 1977). As mentioned above, the GABAergic DD motor neurons reverse their synaptic polarity at the end of the first larval stage, when the VD motor neurons are born and incorporated into the motor circuit to receive input from DA/DB cholinergic neurons (White et al., 1978) (**Figure 1.2**). My thesis investigates the mechanisms underlying DD remodeling (Chapter II) and the integration of VD motor neurons (Chapter III) into the *C. elegans* motor circuit.

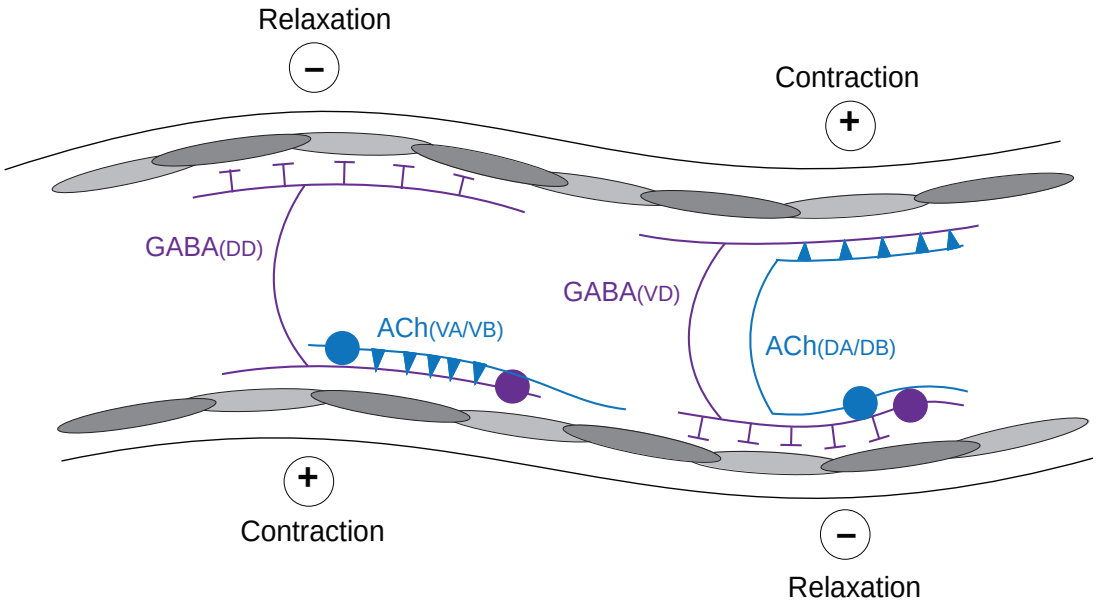

Figure 1.2 The *C. elegans* motor circuit
Schematic of *C. elegans* motor circuit. Purple coloring indicates GABAergic motor neurons (DD/VD), blue coloring indicates cholinergic motor neurons (VA/VB and DA/DB). Gray shading represents body wall muscles.

Motor neurons in *C. elegans* do not fire action potentials and instead produce graded signals, as they do not contain voltage gated sodium channels (Goodman et al., 1998). Body wall muscles, however, do fire action potentials (Gao and Zhen, 2011), and both excitatory cholinergic and inhibitory GABAergic postsynaptic receptors mediate neurotransmission onto muscle. At the *C. elegans* NMJ, muscle cells are arranged into four quadrants, with two dorsal and two ventral rows, and the cells extend projections called muscle arms to the nerve cord to form synapses with motor neuron axons (Sulston and Horvitz, 1977; White et al., 1986). $GABA_A$ receptors that inhibit muscle activity through GABA-gated chloride channels are encoded by the *unc-49* gene that produces three subunits, two of which coassemble to form a heteromeric GABA receptor (UNC-49_B and UNC-49_C form the UNC-49 $GABA_A$ receptor) (Bamber et al., 1999). Two types of cholinergic receptors, levamisole-sensitive L-AChRs and homomeric ACR-16 receptors, mediate excitatory signaling onto muscle (**Figure 1.3**). L-AChRs are composed of five distinct subunits, many of which also show expression in ventral nerve cord neurons (Boulin et al., 2008; Cinar et al., 2005; Culetto et al., 2004; Fleming et al., 1997; Fox et al., 2005; Lewis et al., 1980; Towers et al., 2005).

Neuronal cholinergic receptors

While the postsynaptic apparatus anchoring iAChRs at the *C. elegans* neuromuscular junction has been well characterized, less is known about iAChR clustering in neurons. Early expression profiling studies showed expression of many iAChR subunits in ventral cord motor neurons, highlighting their important roles in

mediating *C. elegans* locomotion (Cinar et al., 2005; Fox et al., 2005). Among these, the iAChR subunit *acr-2* is exclusively expressed in cholinergic motor neurons (Hallam et al., 2000). Four partnering subunits (ACR-3, ACR-12, UNC-63, and UNC-38) coassemble with ACR-2 to form heteromeric receptor complexes (Barbagallo et al., 2010; Jospin et al., 2009), referred to as ACR-2 receptors (**Figure 1.3**). iAChRs containing the ACR-2 subunit are diffusely localized in dendrites, and loss of *acr-2* function impairs neurotransmission from cholinergic motor neurons (Barbagallo et al., 2010; Jospin et al., 2009), suggesting that these complexes modulate cholinergic activity. Additionally, reconstitution of these receptors in *Xenopus* oocytes demonstrated that the ancillary proteins UNC-50, UNC-74, and RIC-3, which are involved in the assembly and trafficking of iAChR subtypes (Boulin et al., 2008; Eimer et al., 2007; Halevi et al., 2002; Haugstetter et al., 2005), are required for functional expression (Jospin et al., 2009).

A second population of ACR-12 containing AChRs is expressed in GABAergic motor neurons, and these complexes regulate inhibitory signaling (Petrash et al., 2013). Genetic ablation of *acr-12* significantly reduces inhibitory postsynaptic currents at the NMJ, and these effects can be rescued with GABA-specific expression of *acr-12* (Petrash et al., 2013). *acr-12* mutants display subtle movement defects, including variability in the sinusoidal movement pattern (Petrash et al., 2013). Unlike ACR-2 receptors, ACR-12 receptor complexes in inhibitory neurons are localized at discrete puncta at synapses, opposite presynaptic inputs (Petrash et al., 2013). In my thesis work, I use this tagged cholinergic receptor (ACR-12::GFP) as a tool to investigate the remodeling of DD

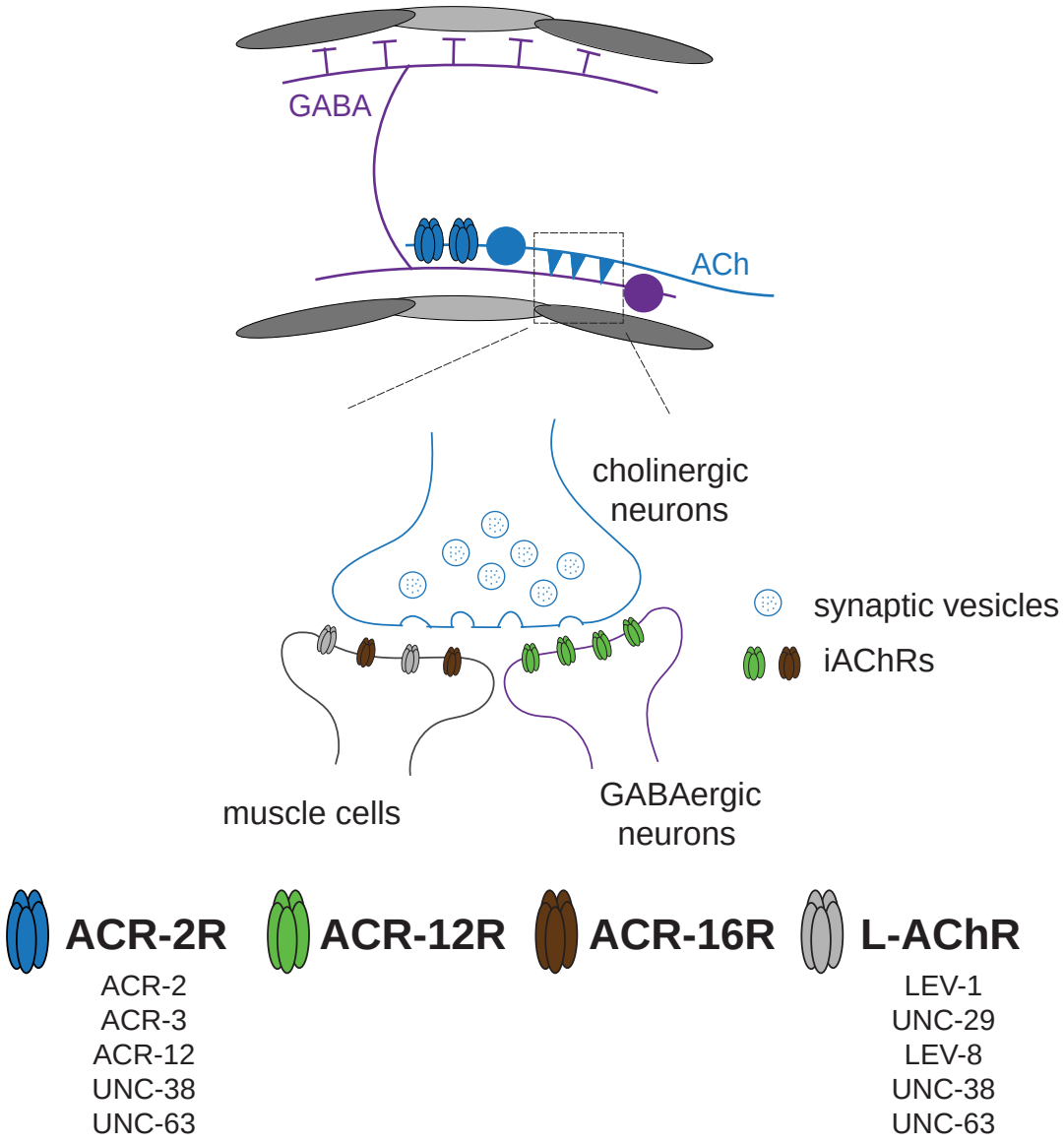

Figure 1.3 Overview of AChRs in the *C. elegans* motor circuit
Top: ACh motor neurons synapse onto both body wall muscle, causing contraction, and onto inhibitory GABA motor neurons. GABA motor neurons in turn project to opposing muscle, causing relaxation. ACR-2 receptors (blue) are localized to the dendritic region of ACh motor neurons.
Bottom: ACR-12 receptors (green) localize postsynaptically at GABA motor neuron dendrites, and ACR-16 and L-AChRs (brown and gray, respectively) tile the NMJ. (Reproduced from (Philbrook and Francis, 2016))

GABAergic neurons (Chapter II) and the molecular mechanisms responsible for the formation of excitatory synapses (Chapters III and IV).

The molecular composition of these ACR-12-containing receptors has not yet been elucidated. Despite considerable progress in assigning functions to brain AChRs carrying specific subunits (Deneris et al., 1991; Gotti et al., 2009; Yang et al., 2009b), many questions remain about the *in vivo* subunit composition and functional significance of AChR subtypes. In Chapter IV, I assess subunit composition of this neuronal AChR using a genetic approach, allowing us to examine how individual subunits may contribute to receptor localization and function. Further, my work demonstrates that these heteromeric receptors are clustered at the tips of spine-like processes in inhibitory neurons, providing an *in vivo* model to study the development of spiny synapses.

Thesis overview

Together, my thesis work aims to address the molecular mechanisms that are used to establish, maintain, or remodel synaptic connectivity during development. Because synapses are so densely packed in the brain, defining the precise processes that drive synapse development and stabilization remains a challenge. The genetically tractable model organism *C. elegans* provides an ideal system to tackle this question.

In Chapter II, I first investigate the regulation of neuronal remodeling during development. Prior work characterizing DD GABAergic remodeling in *C. elegans* has identified genes required for remodeling of axonal components. Does remodeling of the postsynapse occur via a distinct mechanism? In mammals, rewiring of synaptic

connections is critical for mature nervous system function, such as the development of the neuromuscular junction or retinogeniculate synapses. My studies of synaptic remodeling in *C. elegans* aim to advance our understanding of this conserved process.

In Chapter III, I address how excitatory neurons sculpt inhibitory connectivity. Specifically, I investigate how cholinergic signaling shapes GABAergic inputs (synapses onto GABA neurons) and outputs (synapses onto muscle) through studies of fluorescently-tagged synaptic markers. Is neuronal activity required for synapse formation? Surprisingly, work using mammalian model systems suggests that synaptogenesis may still occur in the absence of activity (Varoqueaux et al., 2002; Verhage et al., 2000). My results here indicate that synaptic connections are differentially sensitive to alterations in activity, supporting recent work highlighting cell-type specific effects (Andreae and Burrone, 2014; Morgan et al., 2011). Additionally, my work demonstrates that an identified transcriptional target of the COE-type transcription factor *unc-3* is required for synapses onto GABA neurons. What are the molecular components required for synapses onto this cell type?

Chapter IV targets this important question. A challenge in the studies of cholinergic synapses in the central nervous system is the relatively low expression level of AChRs and the tightly packed organization of neuronal processes. *In vivo* genetic analysis of receptor clustering in *C. elegans* allows for the study of synapse development at the resolution of a single dendritic process, an approach that is unattainable in other systems. Additionally, I find that excitatory receptors are clustered at the tips of spine-like processes, allowing us to examine how spiny synapses may similarly develop in the

brain. Altogether, the studies presented in this dissertation aim to advance our understanding of how synaptic connectivity is established and maintained in the nervous system.

CHAPTER II

Transcriptional control of synaptic remodeling through regulated expression of an immunoglobulin superfamily protein

Siwei He[1,5], Alison Philbrook[3,5], Rebecca McWhirter[2], Christopher V. Gabel[4], Daniel G. Taub[4], Maximilian H. Carter[2], Isabella M. Hanna[2], Michael M. Francis[3], and David M. Miller III[1,2]

[1]Neuroscience Graduate Program, Vanderbilt International Scholar Program

[2]Department of Cell and Developmental Biology

Vanderbilt University, 465 21st Avenue South, Nashville, TN 37240

[3]Department of Neurobiology, University of Massachusetts Medical School,

364 Plantation Street, Worcester MA 01605

[4]Department of Physiology and Biophysics, Boston University Medical Campus,

700 Albany Street, Boston, MA 02118

[5]Co-first authors

Contribution Summary

S.H. generated transgenic lines, collected confocal images, and quantified results for *oig-1*, *irx-1*, and *unc-55* mutant phenotypes. A.P. generated transgenic lines, collected confocal images, and quantified results for *oig-1* mutant effects. R.M. collected and analyzed DD microarray data. A.P., C.V.G., and D.G.T. conducted laser ablation

experiments. M.H.C., I.M.H., and S.H. performed the swimming assays. M.M.F. and D.M.M. wrote the final document.

Abstract

Neural circuits are actively remodeled during brain development, but the molecular mechanisms that trigger circuit refinement are poorly understood. Here, we describe a transcriptional program in *C. elegans* that regulates expression of an Ig domain protein, OIG-1, to control the timing of synaptic remodeling. DD GABAergic neurons reverse polarity during larval development by exchanging the locations of pre- and post-synaptic components. In newly born larvae, DD neurons receive cholinergic inputs in the dorsal nerve cord. These inputs are switched to the ventral side by the end of the first larval (L1) stage. VD class GABAergic neurons are generated in the late L1 and are postsynaptic to cholinergic neurons in the dorsal nerve cord but do not remodel. We investigated remodeling of the postsynaptic apparatus in DD and VD neurons using targeted expression of the acetylcholine receptor (AChR) subunit, ACR-12::GFP. We determined that OIG-1 antagonizes the relocation of ACR-12 from the dorsal side in L1 DD neurons. During the L1/L2 transition, OIG-1 is downregulated in DD neurons by the transcription factor IRX-1/Iroquois, allowing the repositioning of synaptic inputs to the ventral side. In VD class neurons, which normally do not remodel, the transcription factor UNC-55/COUP-TF turns off IRX-1, thus maintaining high levels of OIG-1 to block the removal of dorsally located ACR-12 receptors. OIG-1 is secreted from GABA neurons, but its anti-plasticity function is cell autonomous and may not require secretion. Our study provides a novel mechanism by which synaptic remodeling is set in motion through regulated expression of an Ig domain protein.

Results and Discussion

GABAergic DD motor neurons remodel postsynaptic components during larval development

Motor neurons located in the ventral nerve cord drive locomotion in *C. elegans*. Sinusoidal waves are generated by cholinergic motor neurons that signal at dyadic synapses to excite contraction of ipsilateral body muscles while simultaneously stimulating GABA neurons to induce muscle relaxation on the contralateral side (**Figure 2.1A**) (White et al., 1986; Zhen and Samuel, 2015). We have previously shown that transgenic expression of a functional ionotropic acetylcholine receptor (iAChR) subunit ACR-12::GFP in GABAergic motor neurons marks these connections with punctate clusters that are closely apposed to cholinergic presynaptic regions labeled with mCherry::RAB-3 (**Figure 2.1B and C**) (Petrash et al., 2013). Reconstruction of the DD motor circuit by serial section electron microscopy indicated that cholinergic inputs to DD neurons are switched from dorsal to ventral locations late in the first larval (L1) stage (White et al., 1978). To confirm this observation, we used the *flp-13* promoter to express both ACR-12::GFP and mCherry::RAB-3 in DD neurons. In this case, ACR-12::GFP clusters are confined to the dorsal side, whereas mCherry::RAB-3-labeled synaptic vesicles are limited to the ventral nerve cord in early L1 larvae (**Figure 2.2A-C, top**). By the adult stage, this configuration is reversed with ACR-12::GFP puncta on the ventral side and mCherry::RAB-3 restricted to presynaptic outputs to dorsal muscles (**Figure 2.2A-C, bottom**). The repositioning of ACR-12::GFP from dorsal to ventral locations was mimicked by another iAChR subunit, UNC-29::GFP, which shows robust expression

in GABA neurons (**Figure 2.1D and E**) (Spencer et al., 2011). These results confirm that DD remodeling involves a polarity reversal with presynaptic and postsynaptic components switching places at opposite ends of a morphologically intact GABAergic neuron.

In principle, remodeling of the postsynaptic domain could occur either by translocation of existing receptor complexes from the dorsal to the ventral side or by elimination of dorsal receptors and concomitant synthesis of new receptor subunits that assume a ventral position. To distinguish between these possibilities, we used laser microsurgery to sever the commissural process of the DD1 neuron in the early L1 when ACR-12-containing iAChRs are restricted to the dorsal side (**Figure 2.1F**). We then monitored the appearance of ACR-12::GFP in the ventral DD1 process and found that ventral ACR-12::GFP clusters were indistinguishable from those in mock-axotomized animals, suggesting that an intact commissural connection between the dorsal and ventral DD processes is not required for postsynaptic remodeling (**Figure 2.1G**). These results indicate that ACR-12 receptor translocation from the dorsal to the ventral side is not essential for remodeling and provide evidence that a primary contribution to the ventral receptor pool occurs through de novo ACR-12 synthesis.

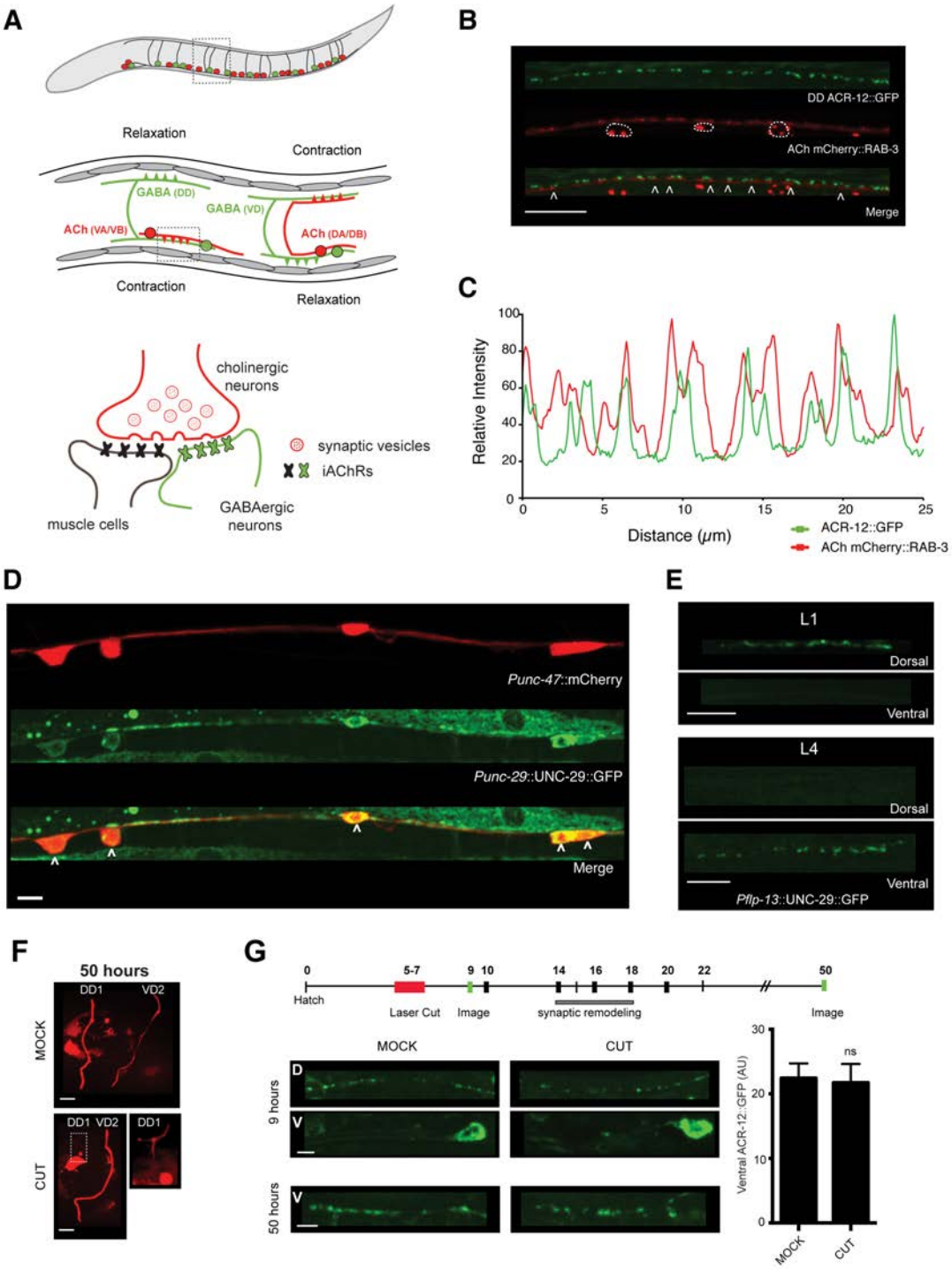
A
Relaxation
Contraction
GABA (DD)
GABA (VD)
ACh (VA/VB)
ACh (DA/DB)
Contraction
Relaxation
cholinergic neurons
synaptic vesicles
iAChRs
muscle cells
GABAergic neurons
B
DD ACR-12::GFP
ACh mCherry::RAB-3
Merge
C
Relative Intensity
Distance (μm)
ACR-12::GFP
ACh mCherry::RAB-3
D
Punc-47::mCherry
Punc-29::UNC-29::GFP
Merge
E
L1
Dorsal
Ventral
L4
Dorsal
Ventral
Pflp-13::UNC-29::GFP
F
50 hours
DD1
VD2
MOCK
CUT
DD1 VD2
DD1
G
Hatch
Laser Cut
Image
synaptic remodeling
Image
MOCK
CUT
9 hours
50 hours
Ventral ACR-12::GFP (AU)
ns
MOCK
CUT

Figure 2.1 Postsynaptic AChRs remodel in DD motor neurons independent of ablating the connecting commissure

(A) For all panels, anterior is to the left and ventral down. Diagram of the adult *C. elegans* motor circuit. Top, the cell bodies of inhibitory GABAergic (green) and excitatory cholinergic (red) motor neurons are located in the ventral nerve cord. GABA motor neurons innervate either dorsal (DD) or ventral (VD) muscles (green triangles). Cholinergic DA and DB motor neurons synapse with dorsal muscles, and VA and VB motor neurons innervate ventral muscles (red triangles) (middle). Cholinergic motor neurons also form synapses with GABA neurons (inset) to effect muscle relaxation on the contralateral side. Specific ionotropic acetylcholine receptors (iAChR) are localized to postsynaptic sites in muscle cells and in GABAergic motor neurons at cholinergic synapses (bottom). (B) Confocal image of the ventral nerve cord showing apposition (arrowheads) of ACR-12::GFP puncta (green) expressed in DD GABAergic motor neurons (*Pflp-13*::ACR-12::GFP, *ufIs126*) and mCherry::RAB-3 (red) expressed in ACh motor neurons (*Pacr-2*::mCherry::RAB-3, *ufIs63*) in a young adult animal. Motor neuron cell bodies are encircled with a dashed white line. Scale bar is 10 µm. (C) Representative line scan depicting co-localization of ACR-12::GFP and mCherry::RAB-3 in a 25 µm region of the ventral nerve cord. Pearson correlation coefficient = 0.93. (D) Confocal image of the ventral nerve cord showing the acetylcholine receptor subunit UNC-29 (*Punc-29*::UNC-29::GFP, green) expressed in GABAergic motor neurons (*Punc-47*::mCherry, red). Arrowheads denote GABA neuron cell bodies. Scale bar is 5 µm. (E) UNC-29::GFP puncta are dorsally localized in early L1 DD motor neurons but are strictly ventral by the L4 larval stage. Scale bars are 5 µm. (F) Laser surgery was performed on young L1 larvae (5-7 hr after hatching) to cut the DD1 commissure or for a mock laser ablation control. Confocal images were obtained at 50 hr post hatch. GABA neurons were marked with *Pflp-13*::ACR-12::GFP; *Punc-47*::mCherry. Inset in cut condition shows fragmented DD1 commissure. Scale bars are 5 µm. (G) Laser ablation of DD1 commissure does not prevent assembly of ventral ACR-12 AChR subunits in remodeling neurons. Top panel shows schematic depicting time line (hours) of DD synaptic remodeling and for laser ablation (red bar) and imaging (green bars). Bottom panel shows ACR-12::GFP (green) in dorsal (D) and ventral (V) nerve cords for mock control and for laser cut DD1 neurons immediately after surgery (9 hr) or in the adult (50 hr). Scale bars are 2 µm. The fluorescence intensity of ACR-12::GFP is not significantly different between mock and cut conditions at 50 hours post hatch (right panel), ($n \geq 6$). Error bars represent SEM.

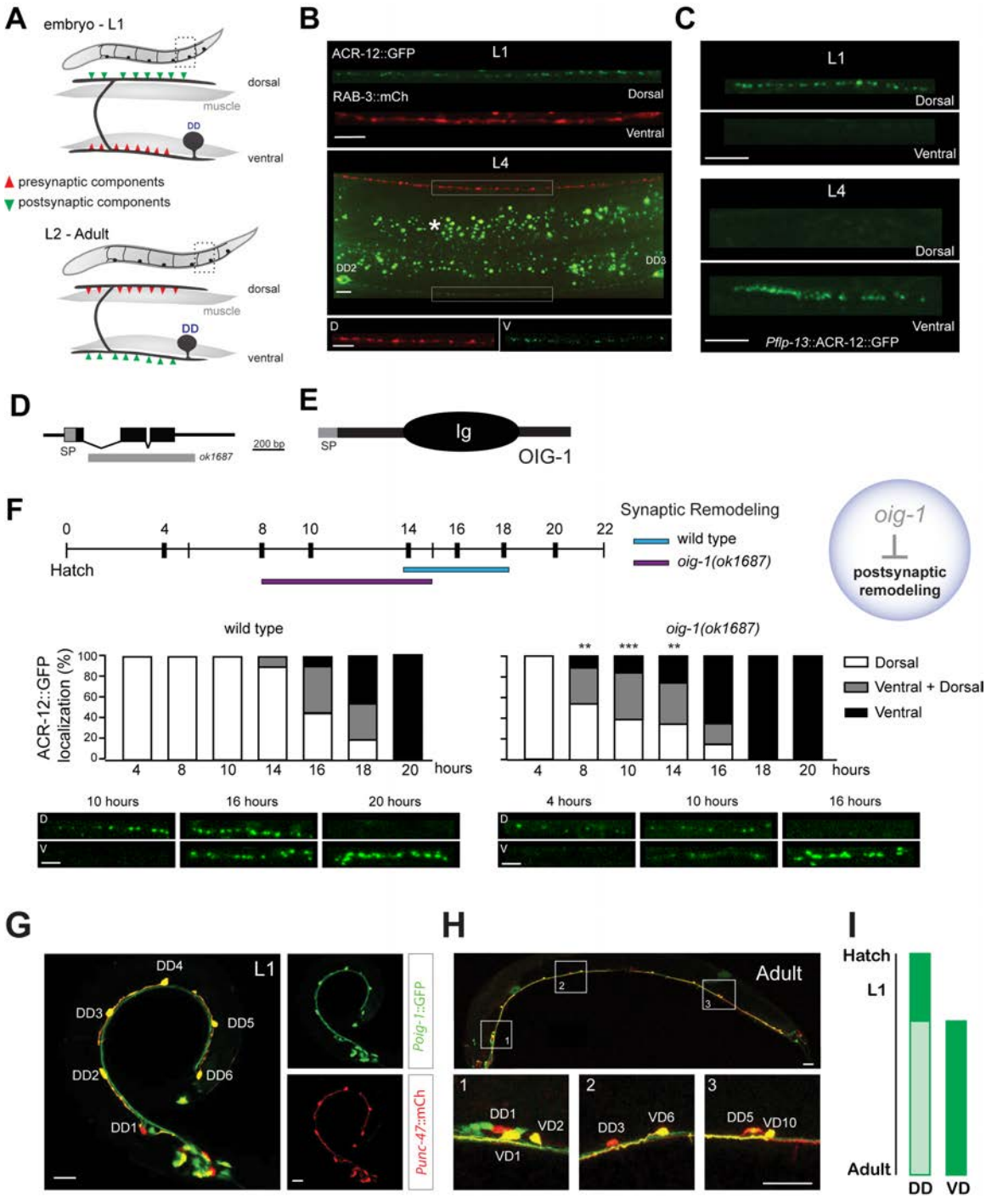
A
embryo - L1
dorsal
muscle
DD
ventral
presynaptic components
postsynaptic components
L2 - Adult
B
ACR-12::GFP
L1
RAB-3::mCh
Dorsal
Ventral
L4
DD2
DD3
D
V
C
L1
Dorsal
Ventral
L4
Pflp-13::ACR-12::GFP
D
SP
ok1687
200 bp
E
SP
Ig
OIG-1
F
Hatch
Synaptic Remodeling
wild type
oig-1(ok1687)
oig-1
postsynaptic remodeling
wild type
oig-1(ok1687)
ACR-12::GFP localization (%)
hours
Dorsal
Ventral + Dorsal
Ventral
10 hours
16 hours
20 hours
4 hours
10 hours
16 hours
G
L1
DD4
DD3
DD5
DD2
DD6
DD1
Poig-1::GFP
Punc-47::mCh
H
Adult
1
2
3
DD1
VD2
VD1
DD3
VD6
DD5
VD10
I
Hatch
L1
Adult
DD
VD

Figure 2.2 OIG-1 inhibits postsynaptic remodeling of DD motor neurons
(A) Embryonic DD motor neurons innervate ventral muscles and extend commissures to the dorsal side for input from cholinergic motor neurons. Toward the end of the L1 larval stage, presynaptic vesicles (red) and postsynaptic acetylcholine receptors (AChRs) (green) switch locations as DD neurons remodel. (B) In a newly hatched L1 larva, RAB-3::mCherry (red) marks DD synapses with ventral muscle, and ACR-12::GFP (green) labels postsynaptic DD regions in the dorsal nerve cord. In an L4 larva, presynaptic RAB-3::mCherry (red) labels DD inputs to dorsal muscles and ACR-12::GFP (green) is restricted to ventral DD postsynaptic locations. Asterisk denotes gut autofluorescence. Scale bars, 5 μm. (C) ACR-12::GFP AChR subunits are dorsally localized in early L1 DD motor neurons but are strictly ventral by the L4 larval stage. Scale bars, 5 μm. (D) The *oig-1* gene includes three exons (black boxes) with a canonical N-terminal signal peptide (SP) sequence. Exons 2 and 3 are deleted in *oig-1(ok1687)*. (E) The OIG-1 protein includes an N-terminal signal peptide (SP) and a single immunoglobulin (Ig) domain. (F) Postsynaptic remodeling is precocious in *oig-1(ok1687)*. Wild-type DD neurons remodel 14–18 hr after hatching, whereas *oig-1* mutant DD neurons remodel 8–16 hr post-hatching. Quantification and representative images of DD remodeling are shown at the bottom. The x axis denotes time since hatching (hr). L1 larvae were binned according to the distribution of *Pflp-13*::ACR-12::GFP puncta as dorsal only (white), ventral only (black), or dorsal and ventral (gray). $**p<0.005$, $***p<0.0005$, versus wild-type (dorsal only versus dorsal + ventral and ventral only) (n = 20 for each time point), Fisher's exact test. Scale bars, 2 μm. (G) In L1 larvae, *Poig-1*::GFP is highly expressed in all six DD neurons as shown by co-localization of *Poig-1*::GFP (green) and *Punc-47*::mCherry (red). Scale bars, 10 μm. (H) By the adult stage, *Poig-1*::GFP is not detected in DD motor neurons but is strongly expressed in VD motor neurons. Insets show representative examples of adjacent DD and VD neurons with differential *Poig-1*::GFP expression. Scale bars, 20 μm. (I) Schematic denoting periods of strong *Poig-1*::GFP expression (dark green) in developing DD and VD neurons.

An immunoglobulin superfamily protein, OIG-1, antagonizes postsynaptic remodeling of GABAergic motor neurons

We used cell-specific microarray analysis to detect strong expression of a transcript encoding a short single-immunoglobulin (Ig) domain protein, OIG-1, in early L1 DD motor neurons (see Materials and Methods; GEO:GSE71618) (**Figure 2.2D and E**). A canonical N-terminal signal peptide predicts that the mature OIG-1 protein (137 amino acids in length) is secreted (Aurelio et al., 2002). Because recent work established that a closely related paralog, OIG-4, stabilizes iAChR complexes in *C. elegans* body muscle cells (Rapti et al., 2011), we wondered whether OIG-1 might exert a similar role and thus potentially retard the dissociation of ACR-12 receptor complexes in remodeling GABA neurons. To address this question, we monitored *Pflp-13*::ACR-12::GFP localization in the null allele, *oig-1(ok1687)* (**Figure 2.2D**) and observed that DD postsynaptic remodeling was initiated significantly earlier than in the wild-type (8–16 hr versus 14–18 hr post-hatching) (**Figure 2.2F, top**) with the precocious removal of dorsal ACR-12::GFP puncta coinciding with their early appearance on the ventral side (**Figure 2.2F, bottom**). This result suggests that OIG-1 normally functions to antagonize the relocation of ACR-12 in L1 stage DD motor neurons (**Figure 2.2F**). This model also predicts, however, that OIG-1 expression should be downregulated by the late L1 stage to allow the normal onset of DD remodeling. To test this hypothesis, we used a GFP reporter gene that includes the *oig-1* upstream region (*Poig-1*::GFP) to confirm expression in DD motor neurons in early L1 larvae (**Figure 2.2G**) (Aurelio et al., 2002; Cinar et al., 2005). As development proceeds, the *Poig-1*::GFP signal declines in DD motor neurons but shows

strong expression in VD motor neurons beginning soon after their birth at the end of the L1 stage (**Figure 2.2H**). This temporal pattern of expression (**Figure 2.2I**) prompted us to ask whether OIG-1 is also necessary to prevent the dorsal to ventral translocation of the ACR-12 receptor in VD neurons, which normally do not remodel. Indeed, *oig-1* mutants showed fewer dorsal ACR-12::GFP puncta than wild-type in both L2 and L4 larval stages (**Figure 2.3A–F**) and a reciprocal relative increase in ventral ACR-12::GFP (**Figure 2.4G**). This result suggests that *oig-1* mutant VD motor neurons undergo ectopic remodeling (e.g., removal of dorsal ACR-12::GFP puncta with reassembly on the ventral side). Notably, *oig-1* mutant animals showed significantly less dorsal ACR-12::GFP than wild-type before remodeling (i.e., 4 hr post hatch), and an overall lower level of ACR-12::GFP in L4 larvae, suggesting that OIG-1 might have an additional role of stabilizing the initial clusters of ACR-12::GFP (**Figure 2.3G and H; Figure 2.4F and G**).

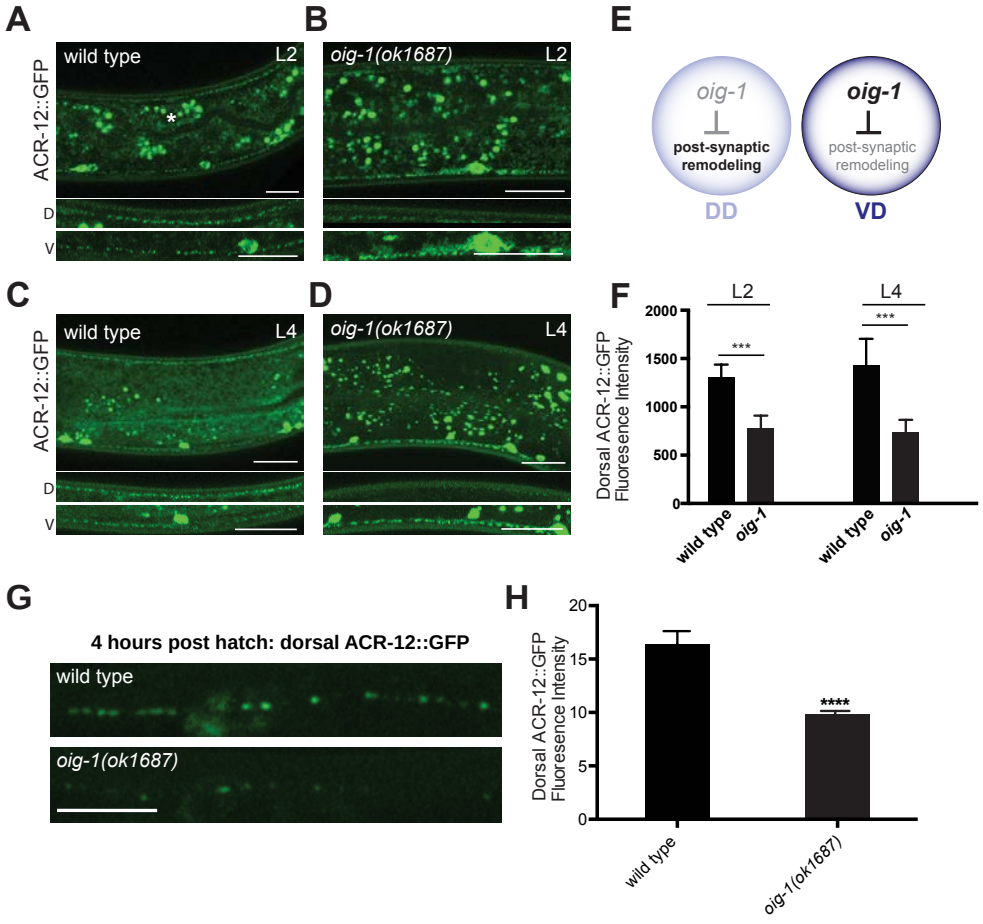

Figure 2.3 OIG-1 inhibits postsynaptic remodeling of VD motor neurons
(A and B) Representative images of *Punc-47*::ACR-12::GFP in L2 wild-type and *oig-1(ok1687)* larvae showing ACR-12::GFP puncta in both dorsal (D) and ventral (V) nerve cords. In *oig-1* mutants, dorsal ACR-12::GFP is significantly reduced compared to wild-type by the L2 stage. Asterisk denotes gut autofluorescence. Scale bars, 20 µm. (C and D) Representative images of *Punc-47*::ACR-12::GFP puncta in L4 wild-type and *oig-1(ok1687)* larvae. Insets (bottom) show ACR-12::GFP puncta in dorsal (D) and ventral (V) nerve cords. Note depletion of dorsal ACR-12::GFP puncta in *oig-1(ok1687)*. Scale bars, 20 µm. (E) Model depicting *oig-1* expression in DD and VD motor neurons (L2 – adult) and negative regulation of postsynaptic remodeling. (F) Quantification of dorsal ACR-12::GFP fluorescence intensity comparing wild-type and *oig-1(ok1687)* L2 and L4 larvae. ***p<0.001, Student's t test, n > 15 for each group. Error bars, SD. (G) Representative images of dorsal ACR-12::GFP puncta in wild-type and *oig-1* mutant L1 animals (4 hr post-hatch). Scale bar, 5 µm. (H) Quantification of ACR-12::GFP localization in the dorsal nerve cord detects a weaker signal in *oig-1* mutants than in wild-type at 4 hr post-hatch. ****p<0.0001 versus wild-type. n = 10 for each group, Student's t test. Error bars, SEM.

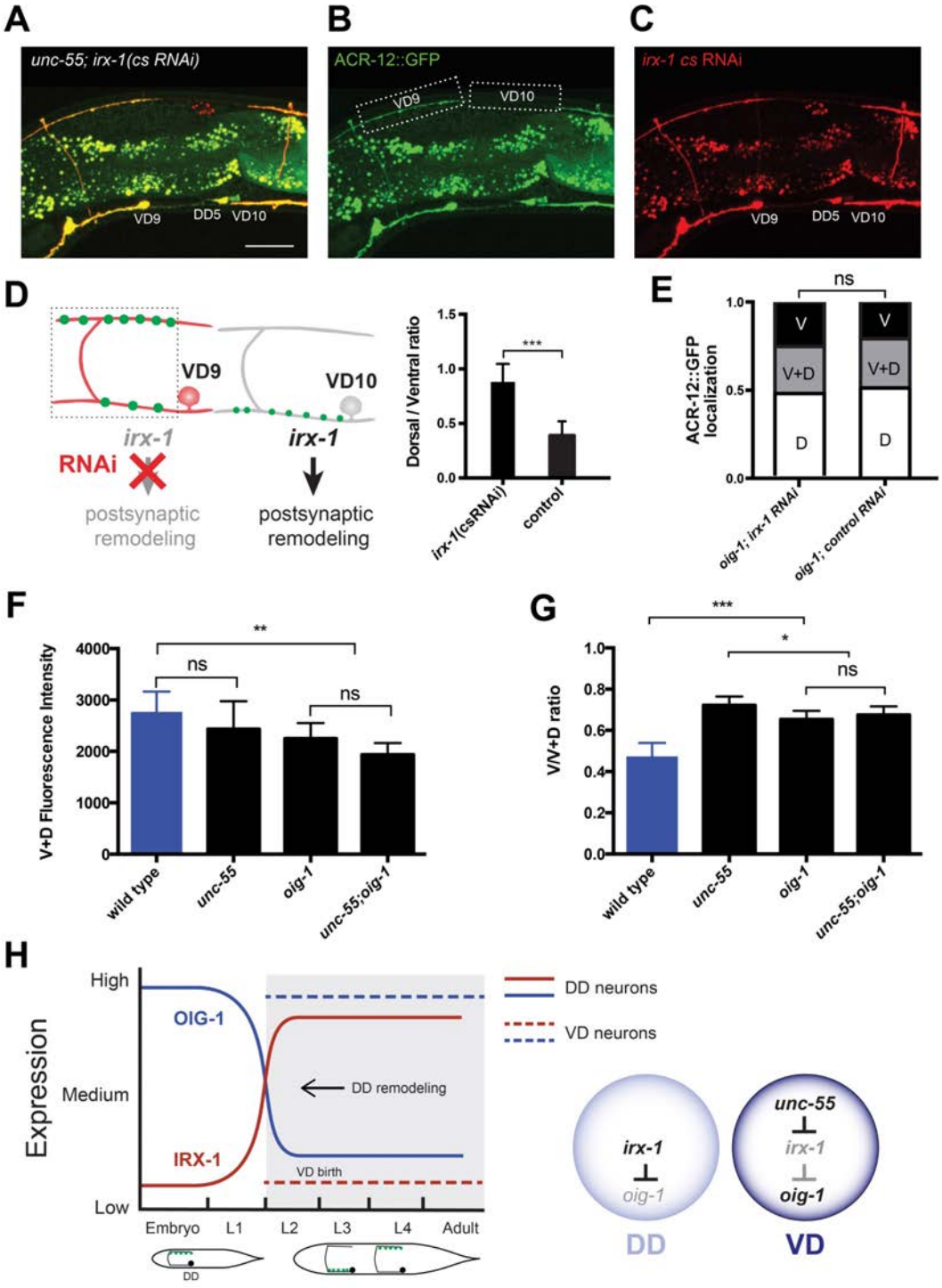
A
unc-55; irx-1(cs RNAi)
VD9
DD5
VD10
B
ACR-12::GFP
VD9
VD10
C
irx-1 cs RNAi
VD9
DD5
VD10
D
VD9
VD10
irx-1
RNAi
irx-1
postsynaptic remodeling
postsynaptic remodeling
Dorsal / Ventral ratio
***
irx-1(csRNAi)
control
E
ns
ACR-12::GFP localization
V
V+D
D
oig-1; irx-1 RNAi
oig-1; control RNAi
F
V+D Fluorescence Intensity
**
ns
ns
wild type
unc-55
oig-1
unc-55;oig-1
G
V/V+D ratio
***
*
ns
wild type
unc-55
oig-1
unc-55;oig-1
H
Expression
High
Medium
Low
OIG-1
IRX-1
DD remodeling
VD birth
Embryo
L1
L2
L3
L4
Adult
DD
DD neurons
VD neurons
irx-1
oig-1
DD
unc-55
irx-1
oig-1
VD

Figure 2.4 *irx-1* functions autonomously in GABAergic motor neurons to promote postsynaptic remodeling

(A, B, C) *irx-1* functions autonomously in GABAergic motor neurons to promote postsynaptic remodeling. Panels depict an *unc-55* mutant adult with mosaic expression of the *irx-1(csRNAi)* transgene and co-selectable mCherry marker. In these experiments, a co-selectable mCherry marker identifies individual GABA neurons that carry the *irx-1(csRNAi)* transgenic array (See Materials and Methods). We exploited this mosaic pattern of transgene expression to distinguish between *irx-1(csRNAi)*- affected neurons and adjacent controls. For example, as shown in a representative image of an *unc-55* mutant carrying the *irx-1(csRNAi)* transgene (**Figure 2.4A-C**), ACR-12::GFP puncta are restored to the dorsal side in mCherry-labeled VD9 but not in the adjacent VD10 motor neuron that does not express mCherry. We attribute the reduced intensity of the ACR-12::GFP signal in VD10 to an overall role of OIG-1 of stabilizing ACR-12::GFP. Dorsal regions of VD9 and VD10 are denoted with dashed boxes. The partial remodeling of DD5 which also expresses *irx-1(csRNAi)* in this animal is consistent with earlier findings that this treatment delays but does not completely block DD presynaptic remodeling (Petersen et al., 2011). Scale bar is 20 μm. (D) Quantification of *irx-1(csRNAi)* results. ACR-12::GFP fluorescence intensity was measured in the dorsal and ventral nerve cords within the anterior regions of each VD neuron that expresses the co-selectable mCherry marker and control VD neurons (See Materials and Methods). VD neurons expressing *irx-1*(*csRNAi*) show a higher ratio of dorsal vs ventral ACR-12::GFP puncta than controls. ***p<0.0001, n = 15, Student's t-test. (E) Quantification of DD postsynaptic remodeling 10 hours post hatch in *oig-1* mutant worms treated with *irx-1* RNAi or control RNAi. n>30 for each group. Fisher's exact test. (F) Quantification of overall fluorescence intensity (ventral and dorsal) of ACR-12::GFP in wild-type, *unc-55*, *oig-1*, and in *unc-55*; *oig-1* mutant worms. Compared with wild type, the overall ACR-12::GFP fluorescence intensity is not decreased in *unc-55* mutants but is reduced in *oig-1* and in *oig-1;unc-55* double mutants likely due to the ACR-12-stabilizing effect of OIG-1. (G) Quantification of ventral *Punc-47::*ACR-12::GFP in *oig-1* and *unc-55*. The fraction of ventral ACR-12::GFP puncta in *unc-55*; *oig-1* double mutants does not differ from that of *oig-1* mutants and is slightly less severe than *unc-55*. These results suggest that *oig-1* is the principal downstream effector in an *unc-55*-regulated pathway that antagonizes postsynaptic remodeling. For E and F, *p<0.05, **p<0.01, ***p<0.001. n>15 for each group, one-way ANOVA test followed by Turkey multiple comparison. Error bars represent SD. (H) A model for *oig-1* temporal regulation and postsynaptic remodeling in GABAergic motor neurons. OIG-1 is highly expressed in early L1 DD motor neurons to prevent precocious remodeling of postsynaptic components. Postsynaptic remodeling ensues in late L1 larval DD neurons as IRX-1 levels rise to block OIG-1 expression. UNC-55 inhibits expression of IRX-1 in VD motor neurons to maintain high levels of OIG-1 which antagonizes the postsynaptic remodeling program.

A transcriptional switch regulates expression of OIG-1 to control postsynaptic remodeling in GABAergic neurons

The strong expression of OIG-1 in VD neurons resembles that of the COUP-TF family transcription factor, UNC-55, which has been previously shown to block presynaptic remodeling in VD neurons (Petersen et al., 2011; Shan et al., 2005; Walthall and Plunkett, 1995; Zhou and Walthall, 1998). We thus asked whether OIG-1 is a downstream target of UNC-55. The *Poig-1*::GFP signal is significantly weaker in *unc-55* mutant VD motor neurons but is unaffected in other *Poig-1*::GFP-positive neurons in the head region (**Figure 2.5A, B, and E**). Because UNC-55 is likely to function as a transcriptional repressor (Petersen et al., 2011; Shan et al., 2005), we reasoned that this effect should depend on an intermediate target in the *unc-55* pathway. An obvious candidate for this role is the Iroquois family homeodomain transcription factor *irx-1*, which is upregulated in *unc-55* mutant VD motor neurons (Petersen et al., 2011). Consistent with this model, treatment of *unc-55* mutant animals with *irx-1* RNAi restores *Poig-1*::GFP expression to VD motor neurons (**Figure 2.5C and E**). *irx-1* RNAi also results in ectopic expression of *Poig-1::*GFP in late larval and adult DD motor neurons (**Figure 2.5D and E**). These data point to related genetic pathways in which *irx-1* antagonizes *oig-1* expression in DD motor neurons, while *unc-55* blocks *irx-1* expression in VD motor neurons to prevent negative regulation of *oig-1*.

We confirmed the roles of these regulatory cascades in postsynaptic remodeling with additional genetic experiments. In wild-type adults, expression of ACR-12::GFP with the *unc-47* GABA neuron promoter results in comparable levels of postsynaptic

ACR-12::GFP clusters on dorsal (VD) and ventral (DD) sides (**Figure 2.5F, J, and M**). At the L2 stage, *unc-55* mutants show a similar distribution of ACR-12::GFP (**Figure 2.5M**). Later, in L4 larvae, however, ACR-12::GFP puncta are largely localized to the ventral side of *unc-55* mutants (**Figure 2.4F and G; Figure 2.5G, K, and M**). This result suggests that *unc-55* mutant VD neurons initially establish postsynaptic ACR-12 receptor domains in the dorsal nerve cord as in the wild-type, but then reposition these ACR-12::GFP puncta to the ventral side as predicted by our model (**Figure 2.5G**). This ectopic postsynaptic remodeling effect in VD neurons can be reversed by global RNAi knockdown of *irx-1* (**Figure 2.5I, L, and M**). Moreover, the ACR-12::GFP remodeling phenotype of *unc-55;oig-1* double mutants is not more severe than that of *oig-1* and shows a slightly weaker phenotype than *unc-55* (**Figure 2.4G**). We interpret these findings to indicate that *oig-1* is the principal downstream effector of *unc-55* in a pathway that blocks postsynaptic remodeling in VD neurons. To ask whether *irx-1* is also required for postsynaptic remodeling in DD motor neurons, we used RNAi to downregulate *irx-1* expression in wild-type animals expressing *Pflp-13*::ACR-12::GFP. More than half (66%) of control L1 larvae showed strictly ventral ACR-12::GFP puncta by 27 hr after egg-laying, whereas significantly fewer (39%) of *irx-1* RNAi- treated animals completed postsynaptic remodeling (**Figure 2.5N**). The partial remodeling of DD neurons could result from either inefficient RNAi knockdown of *irx-1* or the parallel function of another transcriptionally regulated pathway in the DD remodeling program (Thompson-Peer et al., 2012). In any case, the delay in DD remodeling in *irx-1*-RNAi-treated animals requires *oig-1* activity (**Figure 2.4E**). Finally, we confirmed that *irx-1* function is cell

autonomous in DD and VD neurons using cell-specific RNAi (**Figure 2.4A–D**). Taken together, our results demonstrate that postsynaptic remodeling in GABA neurons is modulated by the opposing roles of UNC-55 and IRX-1 in the regulation of OIG-1 expression (**Figures 2.4H and 2.5H**). These findings parallel earlier results showing that UNC-55 and IRX-1 also control presynaptic GABA neuron plasticity (Petersen et al., 2011; Thompson-Peer et al., 2012) and thus suggest that this genetic pathway orchestrates the overall remodeling program (see below).

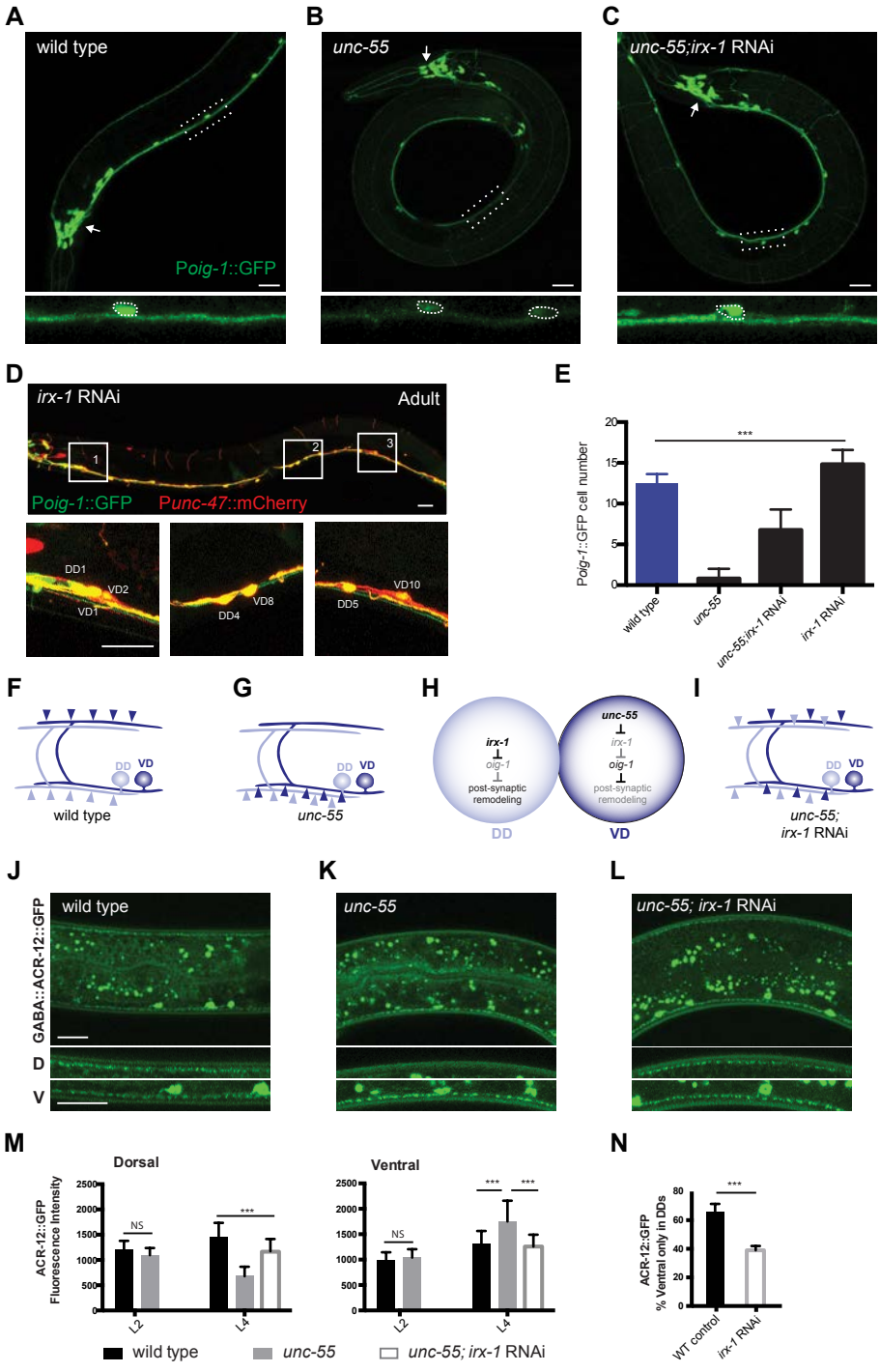
A
wild type
Poig-1::GFP
B
unc-55
C
unc-55;irx-1 RNAi
D
irx-1 RNAi
Adult
1
2
3
Poig-1::GFP
Punc-47::mCherry
DD1
VD2
VD1
VD8
DD4
VD10
DD5
E
Poig-1::GFP cell number
***
wild type
unc-55
unc-55;irx-1 RNAi
irx-1 RNAi
F
DD
VD
wild type
G
unc-55
H
irx-1
oig-1
post-synaptic remodeling
DD
unc-55
irx-1
oig-1
post-synaptic remodeling
VD
I
unc-55;
irx-1 RNAi
J
wild type
GABA::ACR-12::GFP
D
V
K
unc-55
L
unc-55; irx-1 RNAi
M
Dorsal
Ventral
ACR-12::GFP
Fluorescence Intensity
NS
***
L2
L4
wild type
unc-55
unc-55; irx-1 RNAi
N
ACR-12::GFP
% Ventral only in DDs
WT control
irx-1 RNAi

Figure 2.5 A transcriptional cascade involving UNC-55/COUP-TF and IRX-1/Iroquois regulates *oig-1* expression in GABA neurons

All panels depict adults; dorsal is up, and anterior is to left.

(A–C) *Poig-1*::GFP is highly expressed in wild-type VD motor neurons in the ventral nerve cord and in a subset of head neurons (arrow). In *unc-55* mutants, *Poig-1*::GFP is decreased in VD neurons but is maintained in head neurons (arrow). *irx-1* RNAi restores *Poig-1*::GFP expression to ventral cord motor neurons. Insets (bottom) feature enlarged and straightened segments of the ventral nerve cord. Dotted circles denote *Poig-1*::GFP-expressing ventral cord neurons. Scale bars, 20 μm for (A)–(C). (D) RNAi knockdown of *irx-1* restores *Poig-1*::GFP expression to DD neurons in wild-type adults; *Poig-1*::GFP is maintained in the VDs. Inserts (1, 2, 3) show adjacent DD and VD neurons expressing *Poig-1*::GFP. *Punc-47*::mCherry marks GABAergic motor neurons and was merged with *Poig-1*::GFP images to produce yellow overlays. Scale bars, 20 μm. (E) Quantification of *Poig-1*::GFP expression in adult ventral cord GABAergic motor neurons. *Poig-1*::GFP is expressed in all 13 VD motor neurons in the wild-type but is rarely detected in the ventral cord of *unc-55* mutants. *Poig-1*::GFP expression is partially restored in *irx-1* RNAi-treated *unc-55* mutants and is ectopically expressed in adult DD neurons with *irx-1* RNAi of wild-type animals. ***$p<0.001$. One-way ANOVA followed by Tukey multiple comparison test, n > 30 for each group. Error bars, SD. (F and G) In wild-type adults, DD postsynaptic AChRs (light blue) are located on the ventral side, whereas VD postsynaptic receptors (dark blue) are located dorsally. In *unc-55* mutants, postsynaptic ACh receptors are ectopically relocated to the ventral side in VD motor neurons. (H) Model: IRX-1 is expressed in DD motor neurons to promote postsynaptic remodeling by inhibiting OIG-1 expression. IRX-1 is repressed by UNC-55 in VD motor neurons to prevent ectopic remodeling of postsynaptic components to the ventral side. (I) *irx-1* RNAi suppresses postsynaptic remodeling of both DD neurons and ectopically remodeled VD neurons in *unc-55* mutants. (J–L) GABA::ACR-12::GFP (or *Punc-47*::ACR-12::GFP) puncta are detected in both dorsal and ventral nerve cords of wild-type L4 larval animals due to contributions of VD (dorsal) and DD (ventral) neurons (J). In *unc-55* mutants, GABA::ACR-12::GFP puncta are largely ventral (K) but are relocated to the dorsal side in animals treated with *irx-1* RNAi (L). Scale bars, 20 μm for (J)–(L). (M) Quantification of dorsal and ventral GABA::ACR-12::GFP fluorescence intensity for wild-type (black), *unc-55* (gray), and *unc-55;irx-1* RNAi (white) at L2 and L4 stages. In L2 larvae, the distribution of ACR-12::GFP puncta in the dorsal nerve cord does not differ between *unc-55* versus wild-type indicating that the initial assembly of the VD postsynaptic apparatus is not perturbed in *unc-55* animals. In contrast, in L4 larvae, *unc-55* mutant animals show significantly fewer dorsal ACR-12::GFP puncta than wild-type; this ectopic remodeling effect was blocked by *irx-1* RNAi. ***$p<0.001$, one-way ANOVA, n > 15 for each group. Error bars, SD. (N) *irx-1* RNAi knockdown delays DD postsynaptic remodeling. By 27 hr after egg laying (16 hr post-hatch), 66% ± 6% of wild-type (WT) control larvae have completed DD remodeling (i.e., show ventral GABA::ACR-12::GFP only), whereas only 39% ± 3% of *irx-1* knockdown animals have completed DD remodeling, ***$p<0.001$ (n = 113), Fisher's exact test. Error bars, SD.

OIG-1 functions in GABA neurons to block postsynaptic remodeling

Although OIG-1 is strongly expressed in DD and VD neurons, the OIG-1 protein is predicted to be secreted, and thus could potentially function as an extracellular antagonist of postsynaptic remodeling in a non-autonomous fashion. To test for this possibility, we used transgenic reporters in which mCherry was inserted immediately after the signal peptide (SP) to label the OIG-1 protein (**Figure 2.6A**). Expression of the mCherry::OIG-1 construct with the GABA-neuron specific *unc-25* promoter (GABA::OIG-1) resulted in bright punctate mCherry signals along both ventral and dorsal nerve cords (**Figure 2.6B, top**). Similar results were obtained using the native promoter driving OIG-1 fused to superfolder GFP (**Figure 2.7A and B**). A robust mCherry signal in coelomocytes, macrophage- like cells in the body cavity, confirms that mCherry::OIG-1 is secreted (**Figure 2.6B, top**). mCherry::OIG-1 expression in the GABAergic neurons of *oig-1* mutant animals restored dorsal *Punc-47*::ACR-12::GFP to a wild-type level, thus demonstrating that the mCherry::OIG-1 fusion protein is functional and that expression of OIG-1 in GABA neurons is sufficient to rescue the Oig-1 postsynaptic remodeling defect (**Figure 2.6B, top, and 2.6C**). Secretion of mCherry::OIG-1 from neighboring cholinergic neurons (ACh::OIG-1), however, did not rescue the Oig-1 phenotype (**Figure 2.6B, middle, and 2.6C**). This result indicates either that OIG-1 function is cell autonomous and requires expression in GABA neurons or that the secreted form of OIG-1 is not actively involved in postsynaptic remodeling.

To distinguish between these possibilities, we generated a mCherry::OIG-1 protein that excludes the N-terminal signal peptide, thus preventing secretion, and

expressed it in GABA neurons [GABA::OIG-1-SP] (see Materials and Methods). Transgenic *oig-1(ok1687)* animals expressing GABA::OIG-1-SP showed strong mCherry puncta in GABA neuron processes in both the dorsal and ventral nerve cords (**Figure 2.6B, bottom**). As predicted for a non-secreted form of OIG-1, coelomocytes were not labeled with mCherry in this strain; however, ACR-12::GFP was restored to the dorsal nerve cord indicating strong rescue of the Oig-1 postsynaptic remodeling defect (**Figure 2.6B, bottom, and 2.6C**). We note that transgenic expression of OIG-1 and OIG-1-SP appears to elevate ACR-12::GFP levels in comparison to wild-type perhaps due to the overall role of OIG-1 in stabilizing ACR-12::GFP clusters (**Figure 2.6C**). We used a live animal antibody labeling method (Gottschalk and Schafer, 2006) to further investigate OIG-1 secretion in each situation. The external cell membranes of GABA neurons showed strong immunostaining in animals expressing full-length OIG-1, but no extracellular signal was detected in animals expressing OIG-1-SP (**Figure 2.7C**). While we cannot exclude the possibility OIG-1-SP may reach the extracellular environment at low levels that are below the threshold of detection in our experiments, our evidence points to an alternative model in which postsynaptic remodeling does not require the secreted form of OIG-1, but instead involves an intracellular OIG-1 function in GABA neurons. In an additional experiment to define a location for OIG-1 function, we used mosaic expression of a low-copy number GABA::mCherry::OIG-1 transgene to show that localization of mCherry::OIG-1 puncta to the dorsal nerve cord is correlated with the restoration of dorsal ACR-12::GFP puncta in an *oig-1* mutant (**Figure 2.7E and F**). This result points to a local role for OIG-1 in antagonizing the removal of ACR-12 receptors

by the remodeling program. We note, however, that mCherry::OIG-1 and ACR-12::GFP do not overlap in the dorsal nerve cord but instead adopt a striking pattern of alternating mCherry and GFP puncta (**Figure 2.7G**). This finding argues against the idea that OIG-1 stabilizes ACR-12-containing iACh receptors by direct interaction at the synapse and favors an alternative model potentially involving additional components (**Figure 2.8F**). The proposed role for OIG-1 in postsynaptic remodeling is further reinforced by our findings that *oig-1* and *acr-12* mutants display similar locomotory defects that depend on GABA neuron dysfunction (**Figure 2.6D**).

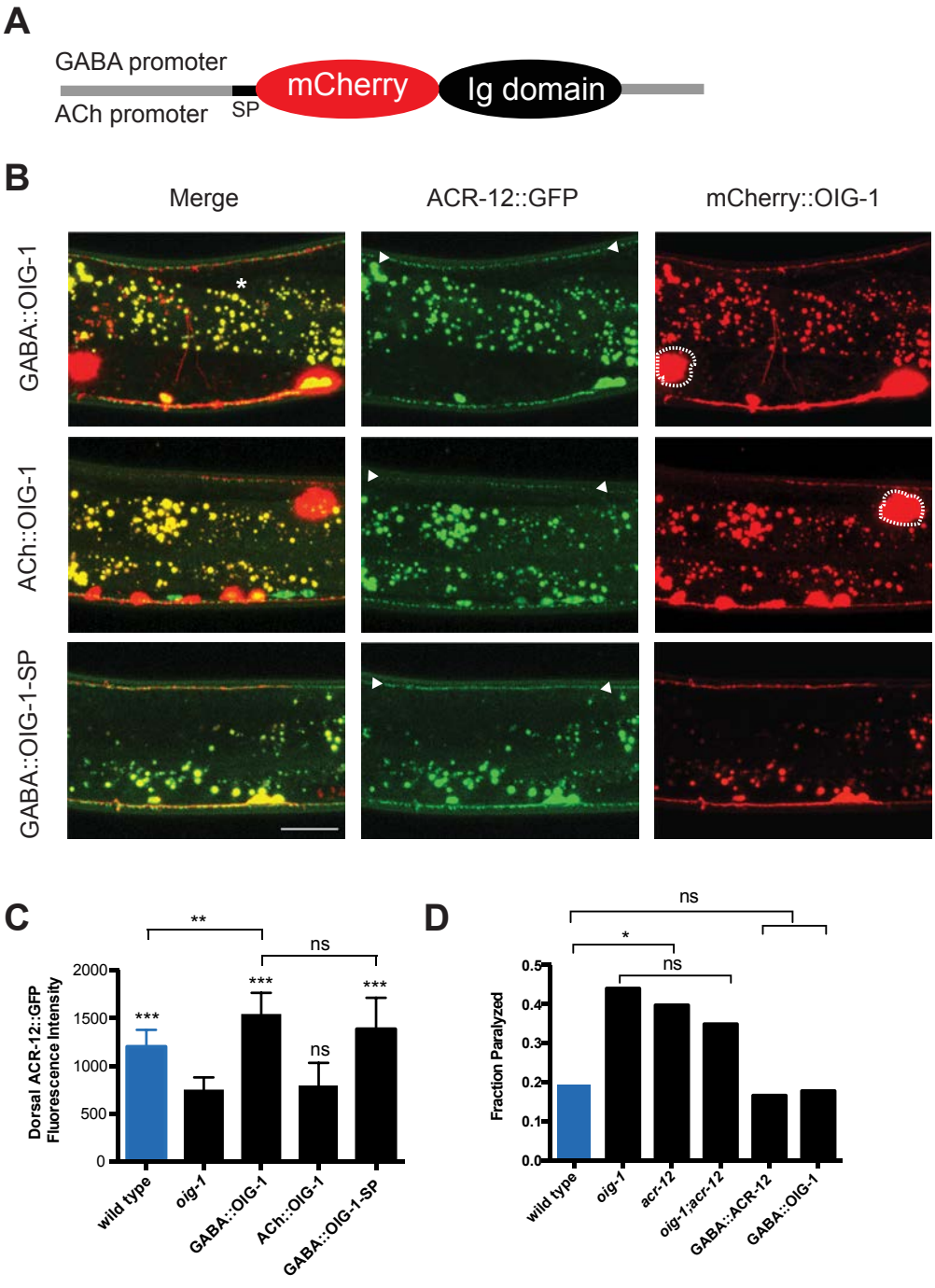
A
GABA promoter
ACh promoter
SP
mCherry
Ig domain
B
Merge
ACR-12::GFP
mCherry::OIG-1
GABA::OIG-1
ACh::OIG-1
GABA::OIG-1-SP
C
Dorsal ACR-12::GFP Fluorescence Intensity
2000
1500
1000
500
0
**
ns
***
***
***
ns
wild type
oig-1
GABA::OIG-1
ACh::OIG-1
GABA::OIG-1-SP
D
Fraction Paralyzed
0.5
0.4
0.3
0.2
0.1
0.0
ns
*
ns
wild type
oig-1
acr-12
oig-1;acr-12
GABA::ACR-12
GABA::OIG-1

Figure 2.6 Cell-autonomous expression of OIG-1 blocks postsynaptic remodeling in GABA neurons

(A) Schematic of OIG-1 fusion protein. mCherry was inserted immediately after the OIG-1 signal peptide (SP) and fused to upstream promoters for expression in either GABA or ACh (cholinergic) motor neurons in the ventral nerve cord. (B) All panels show young adults; anterior is to left, and dorsal is up. Expression of mCherry::OIG-1 in GABA neurons with the *unc-25* promoter (GABA::OIG-1) restores dorsal ACR-12::GFP puncta (arrowheads) to an *oig-1* mutant. mCherry::OIG-1 is detected in both the ventral and dorsal nerve cords and is secreted as indicated by mCherry-labeled coelomocytes (dotted outline) in the body cavity. mCherry::OIG-1 expression in cholinergic motor neurons with the *acr-2* promoter (ACh::OIG-1) does not result in significant restoration of ACR-12::GFP puncta to the dorsal nerve cord (arrowheads), although mCherry-labeled coelomocytes (dotted outline) are indicative of secretion. GABA neuron expression of a non-secreted version of mCherry::OIG-1 (GABA::OIG-1-SP) restores dorsal ACR-12::GFP (arrowheads), suggesting that secretion of the OIG-1 protein may not be required for its function in GABA neuron remodeling. Asterisk denotes gut autofluorescence. Scale bar, 20 μm. (C) Quantification of dorsal ACR-12::GFP fluorescence intensity in young adults. *oig-1* mutants (black) show reduced dorsal ACR-12::GFP signal versus wild-type (blue). Expression of mCherry::OIG-1 in GABA neurons but not in cholinergic motor neurons restores dorsal ACR-12::GFP to wild-type levels. GABA neuron expression of OIG-1-SP, the non-secreted form of mCherry::OIG-1, also rescues *oig-1*. ***$p<0.0001$ versus *oig-1*, **$p<0.001$ versus wild-type, ns ($p>0.33$), one-way ANOVA followed by Tukey multiple comparison test, n > 15 for each experimental group. Error bars, SD. (D) *acr-12(ok367)* and *oig-1(ok1687)* mutants show locomotory defects that depend on GABA motor neuron function. The number of immobilized L4 larvae at the end of a 10-min swimming assay was determined by direct observation. *oig-1(ok1687)* and *acr-12(ok367)* mutants showed a higher fraction of immobilized animals than wild-type. The swimming defect of *acr-12(ok367)* and *oig-1(ok1687)* can be rescued by expression of ACR-12 (GABA::ACR-12) and OIG-1 (GABA::OIG-1) specifically in GABA neurons, respectively. *$p<0.05$ versus wild-type. ns, $p>0.05$, n > 60 for each experimental group. All comparisons by Fisher's exact test.

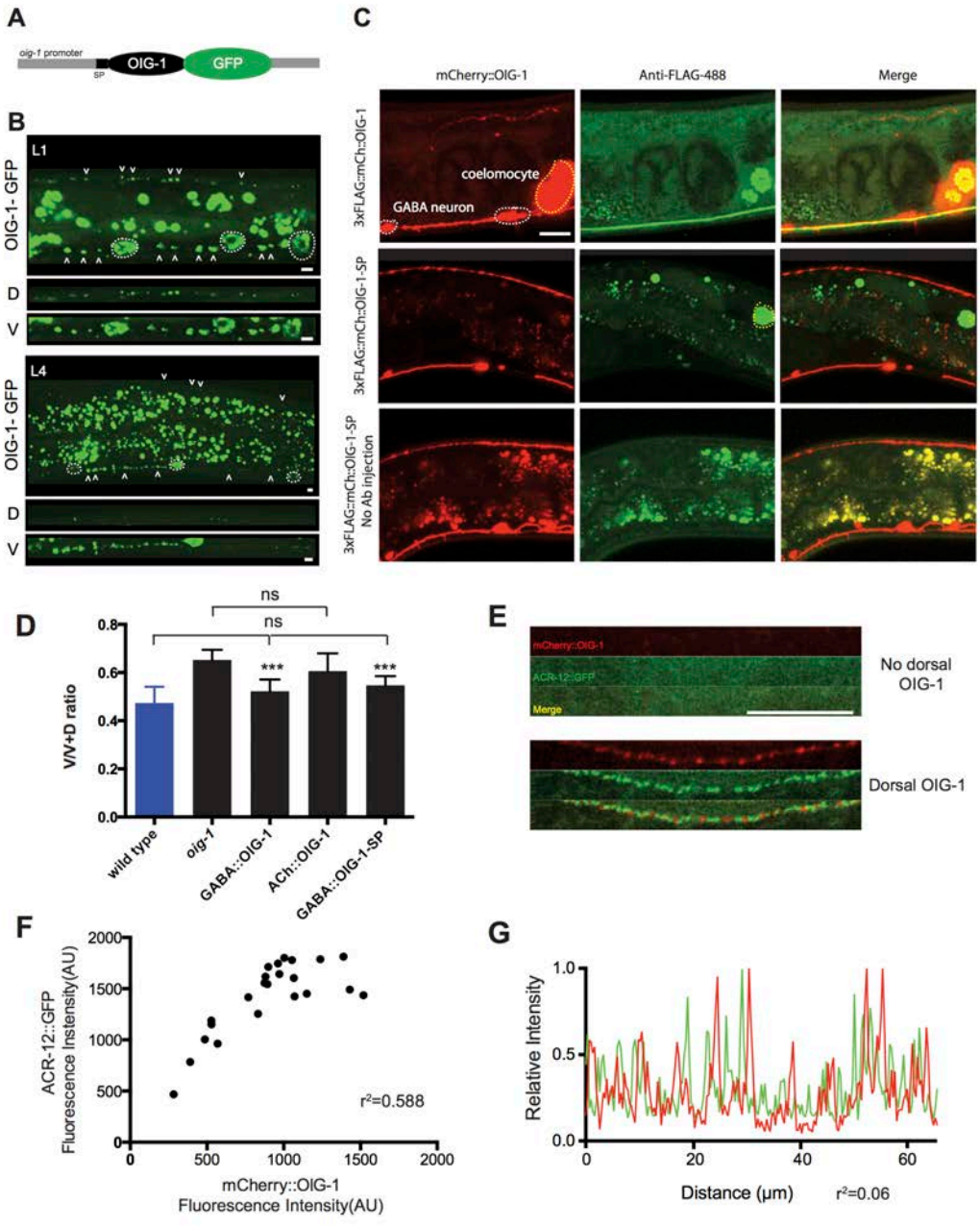
A
oig-1 promoter
SP
OIG-1
GFP
B
L1
OIG-1- GFP
D
V
L4
OIG-1- GFP
D
V
C
mCherry::OIG-1
Anti-FLAG-488
Merge
3xFLAG::mCh::OIG-1
coelomocyte
GABA neuron
3xFLAG::mCh::OIG-1-SP
3xFLAG::mCh::OIG-1-SP
No Ab injection
D
ns
ns
***
***
V/V+D ratio
0.8
0.6
0.4
0.2
0.0
wild type
oig-1
GABA::OIG-1
ACh::OIG-1
GABA::OIG-1-SP
E
mCherry::OIG-1
ACR-12::GFP
Merge
No dorsal OIG-1
Dorsal OIG-1
F
ACR-12::GFP Fluorescence Intensity(AU)
2000
1500
1000
500
0
r²=0.588
0
500
1000
1500
2000
mCherry::OIG-1 Fluorescence Intensity(AU)
G
Relative Intensity
1.0
0.5
0.0
0
20
40
60
Distance (μm)
r²=0.06

Figure 2.7 OIG-1 may stabilize AChRs through indirect interactions
(A) The *oig-1* genomic region including an upstream 2.5 kb promoter and *oig-1* coding sequence was fused to Superfolder GFP to produce C-terminal tagged OIG-1::GFP. (B) OIG-1::GFP is detected in the cell soma of GABA neurons (dotted outlines) and as discrete puncta (arrowheads) in the dorsal (D) and ventral (V) nerve cords of L1 (top) and L4 (bottom) larvae. Scale bars are 2 μm. (C) An *in vivo* immunostaining assay detects extracellular 3XFLAG::mCherry::OIG-1. All panels show adults, anterior to left, dorsal is up. The anti-FLAG-488 signal co-localizes with the signal in GABA neurons. We interpret anti-FLAG-488 staining as corresponding to 3XFLAG::mCherry::OIG-1 on the surface of secreting GABA neurons (Anti-FLAG-488 staining was also observed in the dorsal nerve cord in other injected animals, data not shown.) In contrast, removal of the OIG-1 signal peptide (SP) in the construct 3XFLAG::mCherry::OIG-1-SP does not result in detectable co-localization of anti-FLAG-488 staining with mCherry labeled GABA neurons (middle panel) but does show an anti-FLAG-488 signal in coelomocytes which is indicative of successful antibody injection into the pseudocoelom. 3XFLAG::mCherry::OIG-1-SP worms injected with buffer showed no anti-FLAG-488 signal (bottom panel). At least 20 injected animals for each group were examined. (D) Quantification of Ventral/Ventral+Dorsal ACR-12::GFP fluorescence intensity ratio (see **Figure 2.6C**). ACh and GABA rescue is in the *oig-1(ok1687)* mutant background. n>15 for each group. One way ANOVA test followed by Turkey multiple comparison. ***$p<0.001$ compared with *oig-1* mutant, ns, not significant. Error bars represent SD. (E) Dorsal localization of mCherry::OIG-1 is required for rescuing ACR-12::GFP to the dorsal nerve cord in *oig-1* mutants. Dorsal nerve cord of *oig-1* mutant strains that either lack mCherry::OIG-1 (top panels) or that show mCherry::OIG-1 (bottom panels) with the corresponding rescue of dorsal ACR-12::GFP localization. (F) Dorsal mCherry::OIG-1 fluorescence intensity is positively correlated with dorsal ACR- 12::GFP fluorescence intensity. Pearson correlation, $r^2 = 0.588$. (G) ACR-12::GFP and mCherry::OIG-1 occupy adjacent but non-overlapping domains as shown in a representative line scan of the dorsal nerve cord. (Pearson correlation, $r^2 = 0.06$).

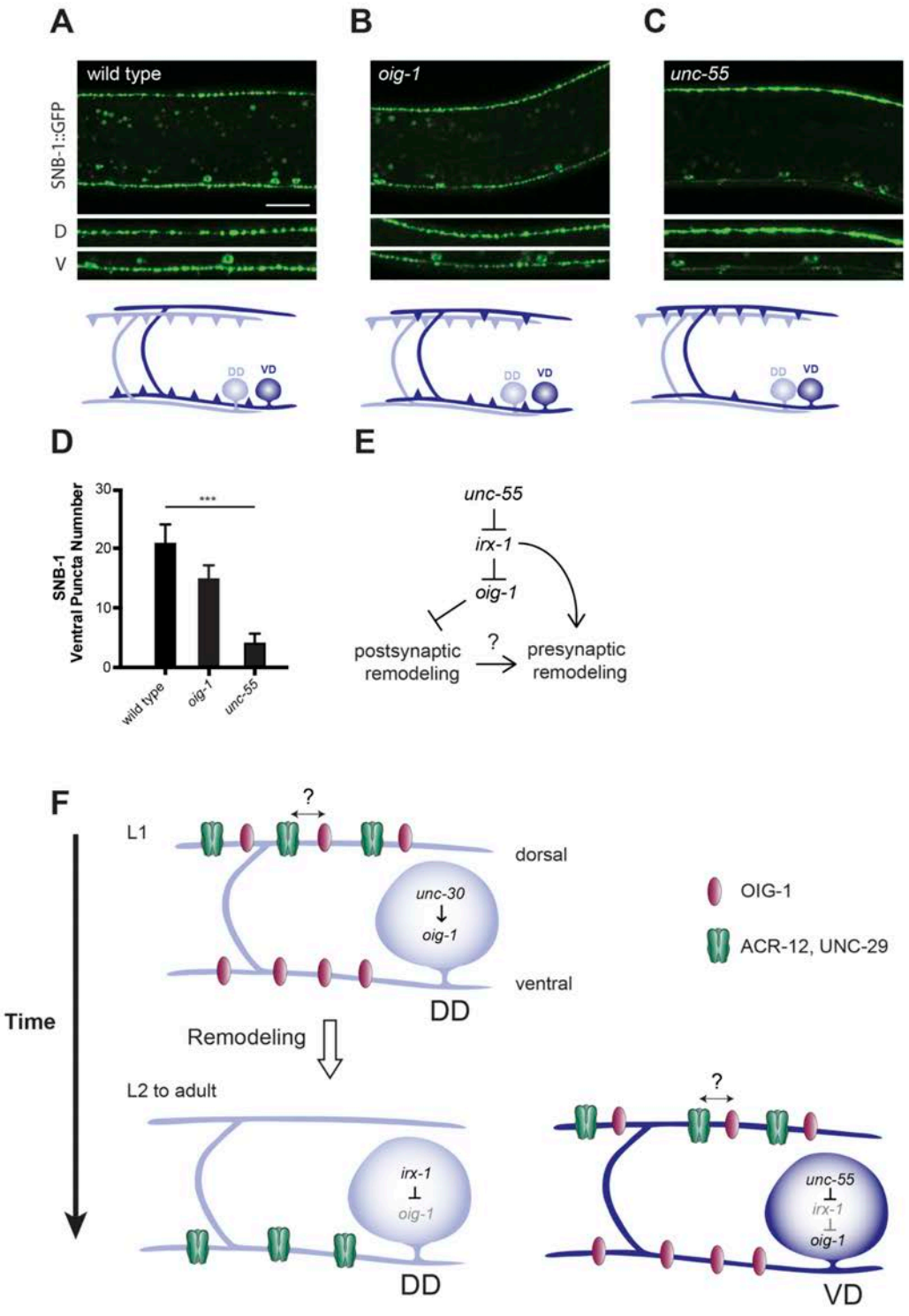
A
B
C
wild type
oig-1
unc-55
SNB-1::GFP
D
V
DD
VD
D
E
SNB-1
Ventral Puncta Numnber
30
20
10
0
***
wild type
oig-1
unc-55
unc-55
irx-1
oig-1
postsynaptic
remodeling
?
presynaptic
remodeling
F
Time
L1
?
dorsal
unc-30
oig-1
ventral
DD
Remodeling
L2 to adult
irx-1
oig-1
DD
?
unc-55
irx-1
oig-1
VD
OIG-1
ACR-12, UNC-29

Figure 2.8 OIG-1 inhibits presynaptic remodeling in GABA motor neurons
(A,B,C) Images of adults showing a presynaptic component of GABA neurons, SNB-1::GFP in wild-type (A) *oig-1* (B) and *unc-55* (C) mutants. SNB-1::GFP is evenly distributed to both dorsal and ventral nerve cords in the wild type but is relatively depleted from the ventral side in *oig-1* and *unc-55* mutants due to ectopic remodeling of VD motor neurons (bottom panels). Scale bars are 20 μm. (D) Quantification of ventral SNB-1::GFP puncta in wild-type and in *oig-1* and *unc-55* mutants. ***$p<0.001$, $n > 30$ for each group. One-way ANOVA followed by Tukey multiple comparison test. Error bars represent SD. (E) Model: *unc-55* controls a negative regulatory pathway to block synaptic remodeling in GABAergic motor neurons. *unc-55* represses *irx-1* to relieve inhibition of *oig-1*. *oig-1* antagonizes post synaptic remodeling and may indirectly inhibit presynaptic remodeling. (F) A model summarizing transcriptional regulation of OIG-1 and its role in postsynaptic remodeling. The single Ig domain protein OIG-1 is highly expressed in embryonic and L1 larval DD neurons, possibly activated by the transcription factor *unc-30* (Howell et al., 2015). During the L1 to L2 transition, *irx-1* blocks OIG-1 expression to relieve the inhibition of postsynaptic remodeling in DD neurons. OIG-1 and postsynaptic iACh receptor components (ACR-12 and UNC-29) occupy discrete subcellular domains but interact through a pathway (double-headed arrow) that antagonizes remodeling. *unc-55* blocks expression of *irx-1* to maintain high levels of OIG-1 in VD motor neurons to prevent ectopic postsynaptic remodeling.

OIG-1 inhibits presynaptic remodeling in GABAergic motor neurons

Having shown that OIG-1 antagonizes postsynaptic remodeling, we next asked whether OIG-1 also regulates the location of presynaptic proteins in the remodeling program. In the wild-type, the presynaptic marker SNB-1::GFP switches from the ventral to the dorsal side in remodeling DD motor neurons, while VD motor neurons synapse with ventral muscles throughout life. These patterns of expression produce a mature GABAergic motor circuit with SNB-1::GFP puncta in both the dorsal (DD) and ventral (VD) nerve cords (**Figure 2.8A**). In *unc-55* mutants, however, VD motor neurons undergo ectopic remodeling resulting in the net depletion of ventral SNB-1::GFP puncta (**Figure 2.8C and D**) (Hallam and Jin, 1998; Petersen et al., 2011; Walthall and Plunkett, 1995). Ventral SNB-1::GFP puncta in the GABAergic circuit are also reduced in *oig-1(ok1687)* versus the wild-type (**Figure 2.8B**), suggesting that presynaptic components are ectopically remodeled in *oig-1* mutant VD motor neurons. Our data are consistent with the observation that DD motor neurons show precocious presynaptic remodeling in *oig-1* mutant L1 larvae and that this effect is rescued by cell autonomous OIG-1 function (Howell et al., 2015). It is notable, however, that *oig-1* mutants retain a greater number of ventral SNB-1::GFP puncta than observed in *unc-55*, which suggests that ectopic presynaptic remodeling in *oig-1* mutants is incomplete and substantially less severe (**Figure 2.8D**). This difference indicates that UNC-55 likely controls an additional parallel-acting pathway involving *irx-1* that regulates presynaptic remodeling (**Figure 2.8E**) (Petersen et al., 2011).

Although synaptic refinement is crucial to the creation of a mature nervous

system, it may be equally important to maintain the architecture of established circuits by tightly controlling the activation of remodeling pathways. Our results show that the opposing roles of the conserved transcription factors IRX-1/Iroquois and UNC-55/COUP-TF orchestrate both the timing and location of synaptic remodeling in the *C. elegans* GABA motor neuron circuit (**Figure 2.4H**). *irx-1* antagonizes *oig-1* expression in late L1 stage DD neurons to permit the disassembly of the postsynaptic apparatus by the remodeling program. This inhibition of *oig-1* is blocked in the VDs by *unc-55*, which turns off *irx-1* and thus maintains high levels of OIG-1 to preserve dorsal clusters of iAChRs (**Figure 2.4H**). This negative regulatory pathway appears to function in concert with the PITX homeodomain transcription factor UNC-30, which promotes *oig-1* expression (Howell et al., 2015) (**Figure 2.8F**). However, the role of *unc-30* is likely complex because it is also required for DD expression of *irx-1* (Petersen et al., 2011).

Immunoglobulin superfamily (IgSF) proteins perform central roles in fundamental aspects of neuronal development, including cell migration, growth cone guidance, and synapse formation and function. IgSF proteins may act as cell adhesion molecules (CAMs), secreted ligands or auxiliary subunits that facilitate the function of specific receptors (Aurelio et al., 2002; Ding et al., 2007; Kolodkin and Tessier-Lavigne, 2011; Rougon and Hobert, 2003; Woo et al., 2013). In the case of OIG-1, our work suggests that OIG-1 protein inhibits the disassembly of the ACR-12 receptor complex in a mechanism that opposes remodeling of the postsynaptic region. Given our finding that a non-secreted form of OIG-1 (OIG-1-SP) is functional (**Figure 2.6B and C**), we suggest that OIG-1 might exert this effect before entering the secretory pathway (Ast et al., 2013)

such that OIG-1-SP could potentially interact with its normal physiological targets. Our results have established a key role for OIG-1 in a mechanism that regulates the relocation of a postsynaptic iAChR from the dorsal to ventral arms of remodeling GABAergic neurons. We also detected a relatively minor function for OIG-1 in the redistribution of a presynaptic component in the opposite direction (**Figure 2.8A–D**). The origin of this effect is unclear but could indicate that the removal of the postsynaptic apparatus facilitates assembly of presynaptic components in the same location. By comparison, *unc-55* exerts a strong negative effect on the ectopic relocation of SNB-1 in VD neurons (Petersen et al., 2011), perhaps indicating that other effectors regulated by *unc-55* serve parallel roles in presynaptic remodeling (**Figure 2.8E**). We have shown that the IgSF protein OIG-1 antagonizes developmental remodeling of postsynaptic iAChRs in the processes of GABAergic neurons. The molecular mechanism underlying this effect and the components of the remodeling program that OIG-1 opposes are important subjects for future studies.

Materials and Methods

Strains and Genetics

C. elegans strains were maintained under standard conditions at 15°C - 25°C. Some strains were obtained from the *Caenorhabditis* Genetics Center (CGC). Transgenic lines were generated by microinjection of plasmids or PCR products into the gonad of young hermaphrodites. Integrated lines were produced by X-ray irradiation as previously described (Schneider et al., 2012) and outcrossed to wild type. All strains are derivatives of the N2 Bristol strain (wild type). The following strains were used in this work:

Mutants

unc-55(e1170)

oig-1(ok1687)

acr-12(ok367)

Postsynaptic remodeling strains

IZ1458 *ufIs126[Pflp-13::ACR-12::GFP]*

IZ1557 *ufIs126; acr-12(ok367)*

IZ1638 *ufIs126; ufIs136[Pflp-13::mCherry::Rab3]*

IZ1410 *ufIs126; acr-12(ok367); oig-1(ok1687)*

IZ1539 *ufIs126; ufIs63[Pacr-2::mCherry::Rab3]; acr-12(ok367)*

IZ1645 *ufEx527[Pflp-13::UNC-29::GFP]*

IZ1490 *ufIs126; ufIs34[Punc-47::mCherry]; acr-12(ok367)*

IZ1750 *ufEx564[Poig-1::OIG-1-superfolderGFP]*

IZ1556 *ufIs92[Punc-47::ACR-12::GFP]; acr-12(ok367)*

NC2814 *ufIs92; unc-55(e1170); acr-12(ok367)*

NC2975 *ufIs92; unc-55(e1170)*; *acr-12(ok367); wdEx959[Pttr-39::irx-1* cDNA*; Pttr-39::irx-1* reverse*; Pttr-39::mCherry]*

NC2923 *ufIs92; oig-1(ok1687); acr-12(ok367)*

NC3025 *ufIs92; unc-55(e1170); oig-1(ok1687)*

CZ8332 *juIs223[Pttr-39::mcherry; Pttx-3::GFP]*

IZ1885 *ufIs7[Punc-29::UNC-29::GFP]; ufIs34[Punc-47::mCherry]*

OIG-1 reporter strains

OH3955 *pha-1(e2123); otEx193[C09E7.3(oig-1)::GFP; pha-1+]*

NC2941 *pha-1(e2123); otEx193[C09E7.3(oig-1)::GFP; pha-1+]; wpIs36[Punc-47::mCherry]*

NC2976 *unc-55(e1170); pha-1(e2123); otEx193[C09E7.3(oig-1)::GFP+pha-1+]*

oig-1 rescue strains

NC2951 *ufIs92; oig-1(ok1687); acr-12(ok367); wdEx954[Punc-25::3XFLAG::mCherry::OIG-1; Pstr-1::gfp]*

NC2954 *ufIs92; oig-1(ok1687); acr-12(ok367); wdEx955[Pacr-*

2::3XFLAG::mCherry::OIG-1; Pstr-1::gfp]

NC2956 *ufIs92; oig-1(ok1687); acr-12(ok367); wdEx956[Punc-25::3XFLAG::mCherry::OIG-1-SP; Pstr-1::gfp]*

NC3014 *ufIs126; oig-1(ok1687); acr-12(ok367); wdEx956[Punc-25::3XFLAG::mCherry::OIG-1-SP; str-1::gfp]*

NC3012 *ufIs126; oig-1(ok1687); acr-12(ok367); wdIs91[Punc-25::3XFLAG::mCherry::oig-1; str-1::gfp]*

In-vivo immunostaining strains

NC3026 *oig-1(ok1687); wdEx954[Punc-25::3XFLAG::mCherry::OIG-1; Pstr-1::gfp]*

NC3027 *oig-1(ok1687); wdEx956[Punc-25::3XFLAG::mCherry::OIG-1-SP; Pstr-1::gfp]*

Presynaptic remodeling strains

CZ333 *juIs1[Punc-25::SNB-1::GFP]*

NC2981 *juIs1; oig-1(ok1687)*

NC1851 *juIs1; unc-55(e1170)*

Molecular Biology and Transgenics

To build DD-specific presynaptic and postsynaptic reporter plasmids, a *flp-13* promoter fragment (-2296 bp relative to start) was cloned into pENTR-D-TOPO to generate a

Gateway entry vector as described previously (Bhattacharya et al., 2014). This entry vector was recombined with the Gateway destination vectors pDEST-38 (ACR-12::GFP), pDEST-15 (mCherry::Rab3), and pDEST-67 (UNC-29::GFP) to generate the expression plasmids pCL32 *[Pflp-13::ACR-12::GFP],* pAP43 *[Pflp-13::mCherry::Rab3],* and pAP65 *[Pflp-13::UNC-29::GFP],* respectively. pAP65 was injected into N2 to yield *ufEx527*. pCL32 and pAP43 were injected into N2 and stably integrated to produce the strains *ufIs126* and *ufIs136,* respectively.

OIG-1 expression plasmids were constructed using a combination of conventional cloning with restriction enzymes and In-fusion cloning. Briefly, *oig-1* genomic DNA was amplified by PCR and inserted into a TA cloning vector. The *oig-1* signal sequence was predicted using an online tool (http://www.cbs.dtu.dk/services/SignalP/). A 3XFLAG::mCherry fragment was inserted immediately after the *oig-1* signal sequence. The 3XFLAG::mCherry::OIG-1 fragment was then fused with either *unc-25* or *acr-2* promoter regions to create pSH24[*Punc-25*::3XFLAG::mCherry::OIG-1] and pSH25[*Pacr-2*:: 3XFLAG::mCherry::OIG-1], respectively. To create a non-secreted version of OIG-1, the start codon of pSH24 was mutated from ATG to CTG(L) with the Q5 site-directed mutagenesis kit to generate pSH26[*Punc-25*::3XFLAG::mCherry::OIG-1 no SP] such that translation is initiated from the ATG start codon of the 3XFLAG::mCherry insert. All plasmids sequences were confirmed by sequencing. All OIG-1 expression constructs were injected into an NC2923 background with a *Pstr-1::*GFP co-selectable marker.

To examine native expression of OIG-1, the *oig-1* promoter and gene (-3136bp relative to start) were PCR amplified and cloned into pENTR-D-TOPO to generate a Gateway entry vector. The entry vector was recombined with the Gateway destination vector pDest-72 (superfolder GFP) to generate the expression plasmid pAP75 *[Poig-1::oig-1-superfolder GFP]*.

The UNC-29 expression construct (pDM970) was generated by amplification of the *unc-29* promoter region (-1484 bp relative to start) and subcloning into a plasmid containing full length *unc-29*cDNA fused to GFP in the intracellular loop between transmembrane domains 3 and 4 (pDM956) (Francis et al., 2005).

Microarray Profile of DD Neurons

DD neurons, labeled with *Pttr-39*::mCherry marker, *juIs223* (Jospin et al., 2009) were isolated by FACS from a synchronized population of L1 larvae as described (Spencer et al., 2014). Total RNA was extracted from FACS-isolated DD neurons and from a reference population of synchronized L1 larvae. 5 - 10 ng of RNA for each sample was amplified with WT-Ovation Pico RNA Amplification System (NuGEN Technologies) and 5 μg of labeled target cDNA was hybridized to Affymetrix *C. elegans* GeneChip arrays. Independent data sets were collected from four DD and three L1 reference samples. Probe intensities were normalized by Robust Multiarray Analysis (RMA). Transcripts showing ≥ 2-fold difference at < 5% false discovery rate (FDR) between DD

versus L1 reference data sets were identified with two-class unpaired analysis in significance analysis of microarray (SAM) (Irizarry et al., 2003).

RNAi feeding

irx-1 RNAi knockdown by feeding used bacterial clones from the *C. elegans* RNAi library (Kamath et al., 2001) with plates created as previously described (Earls et al., 2010). For each experimental test, five L4 hermaphrodites were grown on RNAi plates overnight. Adults were removed on the second day and progeny was scored either during larval development or as young adult. For *irx-1* RNAi treatment of NC2814 [*ufIs92; unc-55(e1170); acr-12(ok367)],* adult progeny showing improved backward locomotion was selected for scoring because efficient *irx-1* RNAi knockdown suppresses the Unc-55 backward movement defect (Petersen et al., 2011). For each set of RNAi plates, *unc-55; juIs1* animals were grown as positive controls since effective *irx-1* RNAi knockdown restores ventral SNB-1::GFP puncta in this strain (Petersen et al., 2011). Hermaphrodites were also grown on the RNAi bacterial feeding strain with an empty vector (*i.e.*, L4440 containing RNAi vector with no genomic insert) as negative controls. For *irx-1* RNAi feeding experiments to assay the role of *irx-1* in DD remodeling (**Figure 2.5N**), gravid IZ1557 adults were transferred to a fresh *irx-1* RNAi plate and allowed to lay eggs for 1 hour. The mid-point of that hour was considered time = 0. The fraction of L1 larvae that had completed remodeling (ventral ACR-12::GFP puncta only) were scored after 27 hr at 25°C.

irx-1 cell-specific RNAi

To generate GABA neuron-specific *irx-1* RNAi or *irx-1(csRNAi),* we used PCR to amplify *irx-1 cDNA* (1131bp) for TOPO TA cloning to produce pSA17. The *irx-1* cDNA insert was subcloned into a *Pttr-39* promoter backbone to generate expression vectors pSA26 and pSA46 with *irx-1* inserts oriented in opposite directions. pSA26, pSA46, pMLH103 (*Pttr-39*::mCherry) and *Pstr-1::GFP* (Petersen et al., 2011) were injected into NC2814 at 25ng/µl each. The expression of *irx-1* sense and antisense RNA was confirmed by improved backward movement and the expression of *Pttr-39*::mCherry in GABA neurons.

Staging and time course of DD remodeling

The timing of DD remodeling was analyzed in synchronized animals using IZ1557 as the wild-type reference strain. Briefly, embryos for each strain were picked to separate 60mm unseeded plates and allowed to hatch for 40 minutes. Newly hatched L1 larvae were then moved to freshly seeded plates, and the midpoint of the 40 minutes in which the embryos hatched was considered time = 0. Plates were incubated at 25°C. Animals were mounted on 2% agarose pads, anesthetized with 0.3M sodium azide, and imaged with a confocal microscope at the indicated time points after hatch. The extent of remodeling was assessed by examining the fluorescence signal (ACR-12::GFP) in the ventral and dorsal nerve cords. Images were categorized based on numbers of dorsal and ventral fluorescent puncta on a scale from 1 (solely dorsal) to 5 (solely ventral), with a score of 3 representing comparable levels of dorsal and ventral expression. These scores were then

binned (1,2 dorsal; 3 dorsal=ventral; 4,5 ventral) to depict the remodeling time course. At each time point post hatch, 20 images were analyzed (n=140 per genotype throughout the time course). Results were obtained from two independent experiments for each genotype.

Laser surgery and DD remodeling experiments

The mechanism of DD remodeling was analyzed in synchronized animals using IZ1490 *[Pflp-13::ACR-12-GFP; Punc-47::mCherry; acr-12(ok367)]*. Newly hatched L1 larvae were staged as described above.

Laser surgery was performed at 5-7 hours after hatch as previously described (Gabel et al., 2008). In brief, a Ti:sapphire laser system, Mantis PulseSwitch Laser (Coherent, Inc), generated a 10 kHz train of ~100 fs pulses in the near infrared (~800 nm). The beam, focused to a diffraction limited spot (using a Nikon 40X, 1.3 NA microscope objective) resulted in vaporization and tissue disruption with pulse energies ranging from 5 to 15 nJ. Visual inspection of the targeted DD1 commissure immediately following brief laser exposure (~100–500 ms) confirmed successful axotomy. In some cases, multiple laser exposures were necessary to generate a visual break in the nerve fiber. Animals were then rescued to seeded plates, allowed to recover, and then imaged at 48-50 hours after hatch using a 3i Everest spinning-disk confocal microscope. For quantification of DD1 ventral ACR-12::GFP fluorescence following laser surgery (**Figure 2.1G**), the anterior DD1 dendrite (anterior region to the soma) was analyzed in mock *vs* experimental animals. DD1 axons showing detectable regeneration (~20%) were excluded from analysis.

in vivo antibody-binding assay

The *in vivo* antibody-binding assay was performed as described (Gottschalk and Schafer, 2006). Briefly, animals expressing 3XFLAG::mCherry::OIG-1 or 3XFLAG::mCherry::OIG-1-SP were mounted on dry agarose pads under halocarbon oil. Antibody (anti-FLAG, coupled to Alexa488, Cell Signaling) was diluted 1:200 in injection buffer (20mM K_3PO_4, 3mM K citrate, 2% PEG 6000, pH 7.5) and injected into the pseudocoelom of each adult animal with enough volume to extrude a few embryos. Animals were then transferred to NGM plates seeded with OP50 for recovery for 8 hours. Animals that moved normally, fed and laid eggs were imaged for analysis ($n > 20$ for each group). Approximately half of the injected GABA::OIG-1 animals showed *in vivo* antibody staining but none of the 20 injected GABA::OIG-1-SP transgenics were immunopositive.

Swimming assay

5-10 well-fed L4 larvae were picked onto unseeded NGM plates to allow foraging for 10 minutes and then transferred to a single well, concave glass slide with 10µL of water. The number of paralyzed L4 larvae at the end of a 10-minute swimming assay was determined by direct observation ($n > 60$ for each group). Strains used for rescue experiments are NC3026 and IZ1556.

Confocal microscopy

Nematodes were immobilized with 15mM levamisole on a 2% agarose pad in M9 buffer.

Confocal images were acquired with a Nikon A1R+ confocal microscope using either 40X or 63X objectives. All images for ACR-12::GFP fluorescence intensity quantitation were taken with the same settings. For DD remodeling experiments, images were recorded with a 3i (Intelligent Imaging Innovations) Everest spinning-disk confocal microscope collected at 0.27μm/step with a 63x objective. Nematodes were immobilized with sodium azide (0.3M) on a 2% agarose pad.

Image analysis and quantification

Intensity analysis

ND2 files generated from Nikon software were imported into ImageJ for analysis. Maximum intensity projections were generated with ImageJ. For ACR-12::GFP intensity quantification, the ventral and dorsal nerve cords between VD8 and VD9 neurons of each individual animal were traced and intensity was measured using the analyze tool. The mean fluorescence intensity of each animal was used for statistical analysis. For the quantification of *irx-1* csRNAi effect, a region on the anterior side of VD neurons was selected. Expression of *irx-1* dsRNA in VD neurons was inferred from co-expression of *Pttr-39::*mCherry (Petersen et al., 2011). A region of the anterior dorsal nerve cord was selected for the quantification of ACR-12::GFP expression in 4-hour post hatch animals.

Co-localization analysis of GFP and mCherry labeled synaptic markers

The line-tracing tool was used to mark a region of interest in either ventral or dorsal nerve cords. The fluorescence intensities of both GFP and mCherry signals were analyzed with the ImageJ plugin. Intensity data were exported to Microsoft Excel and

normalized to the corresponding highest value. Pearson's correlation efficiency was calculated for each set of images.

Scoring GABA neuron synapses

SNB-1::GFP puncta number was quantified as previously described (Petersen et al., 2011). Briefly, animals were mounted on 2% agarose pads and imaged with a Zeiss Axiovert microscope, using the micromanager software. Puncta in the ventral nerve cord between VD8 to VD9 were counted for each animal (**Figure 2.8A-D**).

Statistics

Student's t test was used to compare between two groups. A one-way ANOVA test was used for comparisons among three or more groups followed by a Tukey multiple comparison test. Fisher's Exact test was used in **Figures 2.2F, 2.4E, and 2.5N**.

Acknowledgements

We thank members of D.M.M.'s lab and V. Budnik for critical reading of the manuscript and helpful discussions, K. Howell, J. White, and O. Hobert for sharing information before publication, C. Lambert for technical assistance, Y. Jin for strain *juIs223*, and E. Lundquist for *Pstr-1::*GFP. Some nematode strains used in this work were provided by the *Caenorhabditis* Genetics Center, which is funded by the NIH National Center for Research Resources (NCRR). This work was supported by NIH grants to D.M.M. (R01NS081259), C.V.G. (R01NS077929), and M.M.F. (R01NS064263). S.H. is partially supported by the Vanderbilt International Scholar Program. A.P. is supported by an NIH predoctoral NRSA (F31DA038399). Experiments were performed in the VMC Flow Cytometry Shared Resource and by VANTAGE (supported by NIH grants, P30 CA68485, DK058404, P30 EY08126, and G20 RR030956).

CHAPTER III

Excitatory neurons sculpt GABAergic neuronal connectivity in the *C. elegans* motor circuit

Belinda Barbagallo[*], Alison Philbrook[*], Denis Touroutine, Navonil Banerjee, Devyn Oliver, Christopher M. Lambert and Michael M. Francis

Department of Neurobiology, University of Massachusetts Medical School, 364 Plantation Street, Worcester MA 01605

[*]Co-first authors

Contribution Summary

B.B. generated transgenic lines, collected confocal images, and quantified results for inhibitory synapses at the NMJ and evaluation of the tetanus toxin constructs. A.P. generated transgenic lines, collected confocal images, and quantified results for ACR-16::GFP, UNC-29::GFP, ACR-12::GFP, muscle and GABA neuron morphologies, *unc-3*::GFP, and *unc-3* rescue experiments and controls. D.T. conducted electrophysiology experiments, N.B. performed locomotory behavior assays, D.O. generated transgenic lines, and C.M.L. provided *unc-3* rescue constructs. M.M.F. and B.B. wrote the original draft, and M.M.F. and A.P. reviewed and edited the final version.

Abstract

Establishing and maintaining the appropriate number of GABA synapses is key for balancing excitation and inhibition in the nervous system, though we have only a limited understanding of the mechanisms controlling GABA circuit connectivity. Here, we show that disrupting cholinergic innervation of GABAergic neurons in the *C. elegans* motor circuit alters GABAergic neuron synaptic connectivity. These changes are accompanied by reduced frequency and increased amplitude of GABAergic synaptic events. Acute genetic disruption in early development, during the integration of post- embryonic-born GABAergic neurons into the circuit, produces irreversible effects on GABAergic synaptic connectivity that mimic those produced by chronic manipulations. In contrast, acute genetic disruption of cholinergic signaling in the adult circuit does not reproduce these effects. Our findings reveal that GABAergic signaling is regulated by cholinergic neuronal activity, probably through distinct mechanisms in the developing and mature nervous system.

Introduction

Neurons in the brain are organized into circuits, and the activity of these circuits is regulated by the integration of excitatory and inhibitory synaptic inputs. Thus, appropriate numbers and proper positioning of excitatory and inhibitory synaptic connections are key factors governing circuit performance. Indeed, disruptions in the balance of excitatory and inhibitory synaptic activity are associated with debilitating brain diseases. For instance, impaired maturation of inhibitory signaling can produce circuit hyperexcitability and a predisposition to seizure activity that is thought to be important in epilepsy (Briggs and Galanopoulou, 2011; Cossart et al., 2001; Powell et al., 2003).

Though extensive studies of excitatory synapses have produced advances in our understanding of their development and regulation, far less is known about the processes that govern inhibitory synaptogenesis and patterning. Gamma-aminobutyric acid (GABA) is the principal inhibitory neurotransmitter in the mature mammalian brain. GABAergic inhibition controls spatiotemporal patterns of activity throughout many brain areas, and robust local GABAergic innervation of excitatory neurons is central for this role. Recent work in mammals has suggested that inhibitory connectivity is shaped by sensory experience, and identified activity-dependent transcriptional pathways important for this process (Bloodgood et al., 2013; Chattopadhyaya et al., 2004; Jiao et al., 2006; Morales et al., 2002; Pieraut et al., 2014). Despite these important advances, many aspects of inhibitory network development remain inadequately understood.

Caenorhabditis elegans provides a useful model in which to study neural circuit

development and GABAergic function *in vivo*. As in mammals, inhibitory GABAergic signaling shapes *C. elegans* neural circuit activity and behavior. The identity, location and connectivity of all GABAergic neurons have been defined experimentally, and a wealth of genetic tools is available for manipulating GABAergic activity (Schuske et al., 2004). Informative genetic studies have previously identified genes involved in GABAergic synapse formation in *C. elegans*; however, the extent to which these genes identify mechanisms specific to GABAergic synapses versus more generalized roles remains unclear (Ackley et al., 2005; Dai et al., 2006; Grill et al., 2007; Hallam et al., 2002; Liao et al., 2004; Najarro et al., 2012; Schaefer et al., 2000; Zhen et al., 2000; Zhen and Jin, 1999). Here, we investigate the role of neuronal activity in the establishment and maintenance of inhibitory synaptic connections using the *C. elegans* motor circuit as a model. Prior work has provided evidence that activity-dependent processes regulate the timing of GABAergic developmental remodeling in *C. elegans* (Han et al., 2015; Thompson-Peer et al., 2012). Our studies here provide some of the first evidence that activity-dependent processes help to shape the mature pattern of synaptic connectivity in post-embryonic-born GABAergic neurons.

Results

UNC-3 transcriptional regulation coordinates cholinergic synaptic connectivity with body wall muscles

The adult pattern of synaptic connectivity in the motor circuit has been well defined (White et al., 1976). Body wall muscles receive synaptic inputs from both excitatory (acetylcholine, ACh) and inhibitory (GABA) motor neurons and these inputs shape muscle activity and sinusoidal movement (**Figure 3.1A**). Cholinergic motor neurons also provide excitatory synaptic drive onto inhibitory GABA motor neurons. GABA motor neurons then make inhibitory synaptic connections onto opposing musculature. The ventral D (VD) class GABAergic motor neurons that are the focus of our studies are integrated into the motor circuit post-embryonically following the first larval stage, and mediate inhibitory transmission onto ventral muscles in adults (Han et al., 2015; Sulston, 1976).

To address whether excitatory motor neurons are important for shaping functional connectivity in this circuit, we first examined *unc-3* mutants. *unc-3* encodes the sole *C. elegans* homolog of the COE family of transcription factors; in *unc-3* mutants, most ventral cord motor neurons completely lack expression of the genes required for cholinergic function (e.g. *cha-1* and *unc-17*) and exhibit additional defects in their organization (e.g. variable and/or disorganized process extension) (Kratsios et al., 2011; Prasad et al., 2008; Prasad et al., 1998). Thus, cholinergic transmission onto body wall muscles should be severely disrupted in these animals. To confirm this, we made whole-

cell patch clamp electrophysiology recordings of synaptic events from ventral body wall muscles of adult *unc-3* mutants (1 mM Ca^{2+}) and found significant defects in excitatory transmission (**Figure 3.1B and C**). Specifically, the frequency of endogenous excitatory postsynaptic currents (EPSCs) is significantly reduced compared with wild type (79±6% reduction, $p<0.001$). The remaining cholinergic transmission might reflect activity of cholinergic VC motor neurons, which do not require *unc-3* for expression of cholinergic markers (Kratsios et al., 2011). Prior work identified a requirement for *unc-3* in the clustering of postsynaptic ionotropic (nicotinic) acetylcholine receptors (iAChRs) in muscles (Kratsios et al., 2015). Confirming these observations, we find that the distribution of muscle iAChRs (visualized with ACR-16::GFP) is disrupted by mutation of *unc-3* (**Figure 3.1D and E**). Although the total number of ACR-16::GFP clusters is only modestly reduced compared with wild type, large accumulations of receptor are often present in the shafts of muscle arms in *unc-3* mutants, suggesting a re-distribution to non-synaptic locations. Thus, impaired terminal differentiation of cholinergic motor neurons leads to predicted defects in iAChR clustering and excitatory transmission at the cholinergic neuromuscular junction (NMJ).

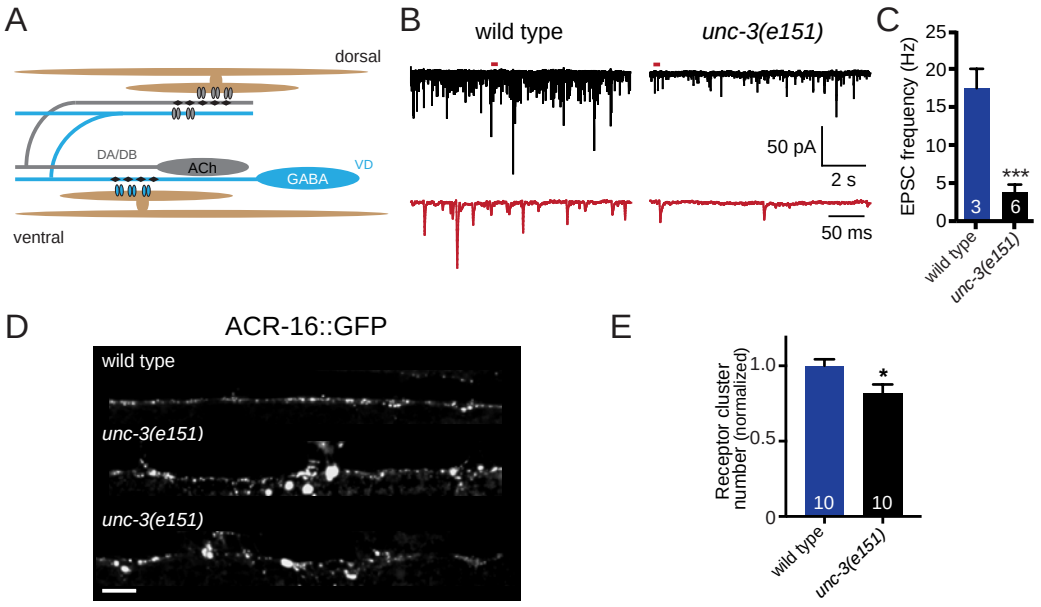

Figure 3.1 Cholinergic neuromuscular transmission is impaired in *unc-3(e151)* mutants

(A) The *C. elegans* motor circuit. Excitatory cholinergic motor neurons (gray) synapse onto inhibitory GABAergic motor neurons (blue) and onto body wall muscles (brown). (B) Representative recordings of endogenous EPSCs from body wall muscles of wild-type and *unc-3(e151)* mutant animals. Red traces are expanded views of time segments under the red bars in the upper traces. (C) The average frequency of endogenous EPSCs recorded from wild type and *unc-3(e151)* mutants. Each bar represents the mean±s.e.m., and numbers in bars indicate the n for each genotype in this figure and for all subsequent figures. ***p<0.0001; Student's t-test. (D) Confocal images of one wild-type (top) and two *unc-3(e151)* (middle and bottom) animals expressing GFP-tagged AChRs in body wall muscles (*myo3p*::ACR-16::GFP). Scale bar: 5 µm. (E) Normalized receptor cluster number per 75 µm of ventral nerve cord. *p<0.05; Student's *t*-test.

Mutation of unc-3 impairs postsynaptic iAChR clustering in GABA neurons and reduces inhibitory transmission

Given that cholinergic motor neurons also make extensive synaptic contacts with inhibitory motor neurons, we next sought to determine whether the disruption of cholinergic innervation associated with mutation of *unc-3* affected inhibitory activity. Using conditions that isolated inhibitory transmission, we measured endogenous inhibitory postsynaptic currents (IPSCs) from *unc-3* mutants. The rate of endogenous IPSCs (5 mM Ca^{2+}) is significantly lower in *unc-3* mutants compared with wild type (63% reduction, $p<0.0001$) (**Figure 3.2A and B**). Interestingly, mutation of *unc-3* also produces a shift towards larger amplitude endogenous IPSCs (**Figure 3.2C**), suggesting either altered muscle responsiveness to GABA release or increased GABA content in synaptic vesicles. Our analysis supports the notion that cholinergic neurons provide direct excitatory drive onto GABAergic motor neurons and perhaps also regulate functional attributes of GABA synaptic outputs onto muscles.

Given these findings, we next investigated whether *unc-3* is required for establishing proper synaptic connectivity between cholinergic and GABAergic motor neurons. The nicotinic AChR subunit ACR-12 is a constituent of GABA neuron iAChRs. ACR-12::GFP clusters localize opposite ACh release sites and relocate appropriately during developmental remodeling, suggesting that these clusters report mature postsynaptic structures (He et al., 2015; Petrash et al., 2013). We examined the distribution of ACR-12::GFP in the dorsal nerve cord where the majority of chemical synaptic inputs to VD neurons occur (VD synaptic contacts with muscles are exclusively

ventral) (White et al., 1986). We found that receptor clustering is severely disrupted in two independent *unc-3* mutant strains (*n3435* and *e151*) (**Figure 3.2D and E**). ACR-12 clusters are unevenly distributed and significantly reduced in number compared with wild type [e.g. 51% decrease in *unc-3(e151)*, $p<0.001$]. These effects are rescued with expression of the wild-type *unc-3* cDNA under control of a 1 kb *unc-3* promoter, but not by either GABA or muscle-specific expression (**Figure 3.2D and E**). This *unc-3* promoter region drives expression in cholinergic, but not GABAergic, motor neurons (**Figure 3.3A**). Together, these observations suggest that *unc-3* expression in cholinergic neurons is required for proper ACR-12 clustering in postsynaptic GABAergic neurons.

madd-4, the *C. elegans* homolog of mammalian punctin-1 and punctin-2 (also known as Adamtsl1 and Adamtsl3, respectively), encodes a synapse-associated extracellular scaffolding protein (Pinan-Lucarre et al., 2014). Secretion of MADD-4 from cholinergic motor neurons is required for proper iAChR localization at neuromuscular synapses (Pinan-Lucarre et al., 2014). Prior work showed that UNC-3 transcriptional regulation of *madd-4* is essential for this process (Kratsios et al., 2015). To test whether MADD-4 is similarly required at synaptic connections between cholinergic and GABAergic motor neurons, we examined ACR-12 clustering in GABAergic neurons of *madd-4* mutants. The *madd-4(ok2854)* allele is a 962 bp deletion that eliminates the two largest *madd-4* exons common to all *madd-4* isoforms, has been previously reported to be a null allele (Maro et al., 2015; Seetharaman et al., 2011), and produces significant defects in muscle AChR clustering similar to those previously observed after deletion of the entire *madd-4* locus (Pinan-Lucarre et al., 2014) (**Figure 3.3B and C**). Mutation of

madd-4 produces a slight decrease in the number of ACR-12 clusters in the dorsal nerve cord compared with wild type (18% decrease, $p<0.05$) (**Figure 3.2D and E**). Notably, this effect is much less severe than that observed for mutation of *unc-3*, indicating that the postsynaptic defects in GABAergic neurons of *unc-3* mutants cannot be accounted for by decreased *madd-4* expression. Taken together, our results indicate that UNC-3 transcriptional control of cholinergic neuron development is essential for proper iAChR clustering in GABAergic motor neurons, but MADD-4 has a comparatively minor role.

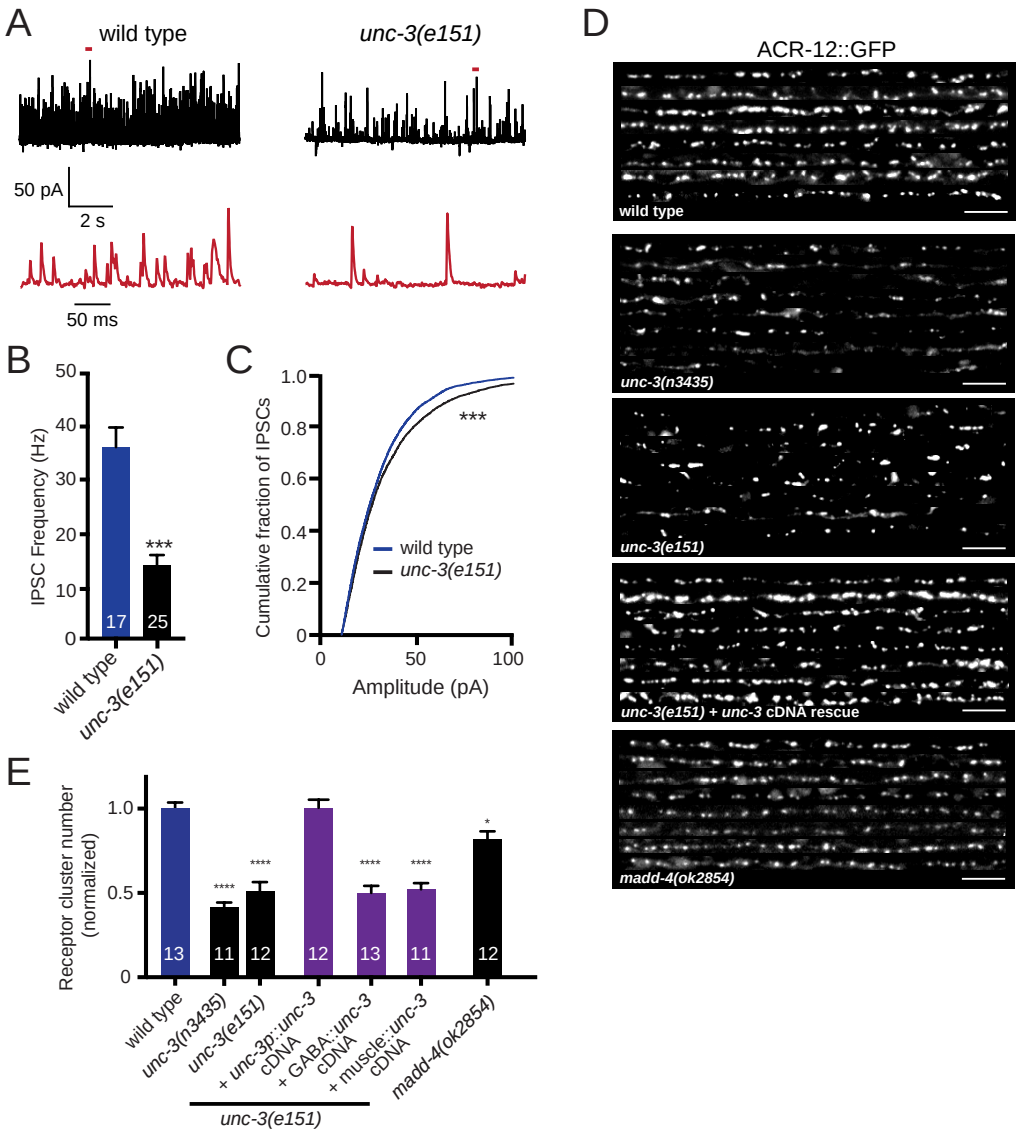

Figure 3.2 *unc-3* mutation causes defects in GABAergic transmission and iAChR clustering in GABAergic neurons

(A) Representative recordings of endogenous IPSCs from body wall muscles of wild-type animals and *unc-3(e151)* mutants. Red traces are expanded views of time segments under the red bars in the upper traces. (B) The average frequency of endogenous IPSCs recorded from wild type and *unc-3(e151)* mutants. ***p<0.0001, Student's t-test. (C) Cumulative distribution of amplitudes of endogenous IPSCs recorded from wild type and *unc-3(e151)* mutants. ***p<0.001; Kolmogorov–Smirnov test. (D) Confocal images showing the dorsal nerve cord of eight animals expressing ACR-12::GFP in GABA neurons for the genotypes indicated. Scale bars: 5 µm. (E) Quantification of the average number of receptor clusters per 85 µm of dorsal nerve cord for the genotypes indicated, normalized to wild type. *p<0.05, ****p<0.0001; ANOVA with Dunnett's multiple comparisons test.

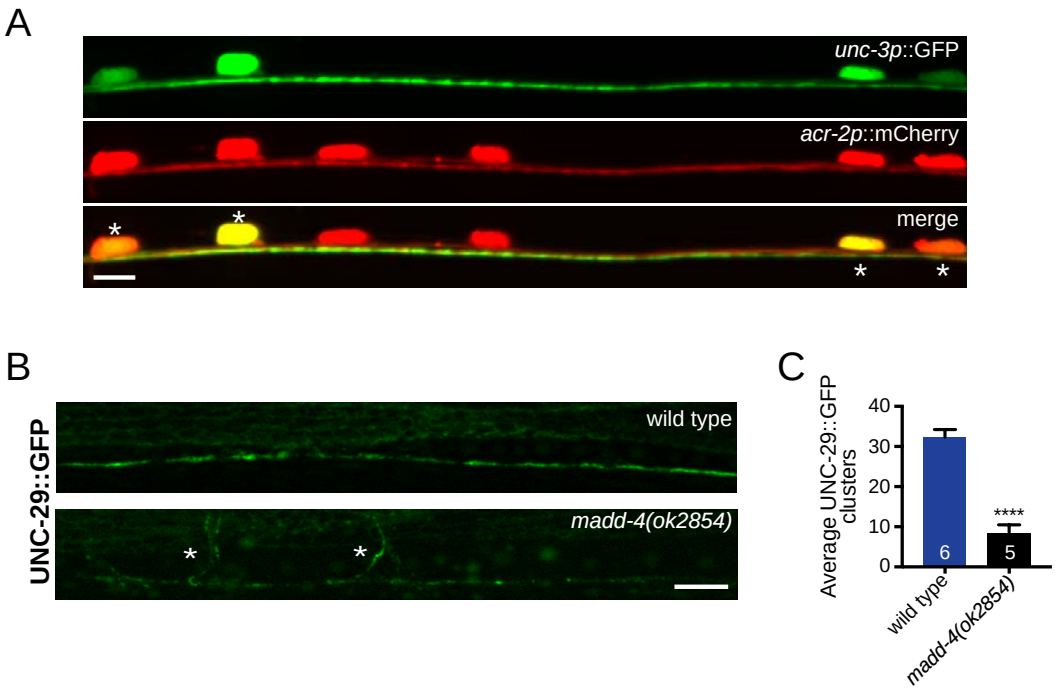

Figure 3.3 Analysis of *unc-3* expression and *madd-4(ok2854)*
(A) Confocal images of the posterior ventral nerve cord in adult animals expressing a transcriptional reporter labeling cholinergic neurons (*acr-2p*::mCherry) and an *unc-3* promoter construct fused with GFP (*unc-3p*::GFP). Asterisks indicate colocalization in cholinergic cell bodies. Scale bar, 5 μm. (B) Confocal images of UNC-29::GFP expressed specifically in body wall muscle (*myo-3p*::UNC-29::GFP) in wild type and *madd-4(ok2854)* mutant animals. Asterisks indicate UNC-29::GFP fluorescence in muscle arms. Scale bar, 5 μm. (C) Quantification of the average number of receptor clusters/80 μm of the ventral nerve cord for the genotypes indicated. Each bar represents the mean ± SEM. Numbers in bars indicate the n for each genotype. ****$p<0.0001$, student's t test.

Morphological development of body wall muscles and GABA motor neurons is not dramatically affected in unc-3 mutants

To address whether the connectivity changes we observed might reflect alterations in the gross development or assembly of the motor circuit, we examined the cellular morphology of body wall muscles and GABA motor neurons. In wild-type animals, body wall muscles project membrane extensions, called muscle arms, to the nerve cords where muscle arm termini bifurcate and project lengthwise along the nerve cord, forming *en passant* synapses with motor neurons (Dixon and Roy, 2005). We visualized muscles by specific expression of membrane-bound mCD8::GFP (*him-4p*::mCD8::GFP) (Collins and Koelle, 2013; Dixon and Roy, 2005) (**Figure 3.4A**). Variable minor morphological defects (e.g. overgrowth, membrane blebbing) are apparent in the body wall muscles of *unc-3* mutants (**Figure 3.4B**). However, consistent with a prior study (Kratsios et al., 2015), we found that overall muscle morphology is preserved – muscle arms extend normally to the nerve cord and the extent of muscle membrane contact with the nerve cord region is not appreciably altered (**Figure 3.4D**).

We visualized the morphology of GABA motor neurons using cell-specific expression of mCherry (*unc-47p*::mCherry) (**Figure 3.4A′**). Similar to the case for muscle cells, disruption of cholinergic innervation does not produce significant defects in GABA motor neuron number, positioning or gross morphology (**Figure 3.4B′; Figure 3.5A-C**). Although in some cases we noted regions of nerve cord defasciculation in *unc-3* mutants (and sometimes one fewer commissure was visible), we did not observe disruptions in the continuity of the dorsal nerve cord processes. Thus, our findings

provide evidence that gross morphological development of body wall muscles and GABA motor neurons proceeds to completion when cholinergic development is disrupted, arguing that the iAChR clustering and GABA transmission defects we observed in *unc-3* mutants are unlikely to arise secondary to impaired morphological development of these cell types.

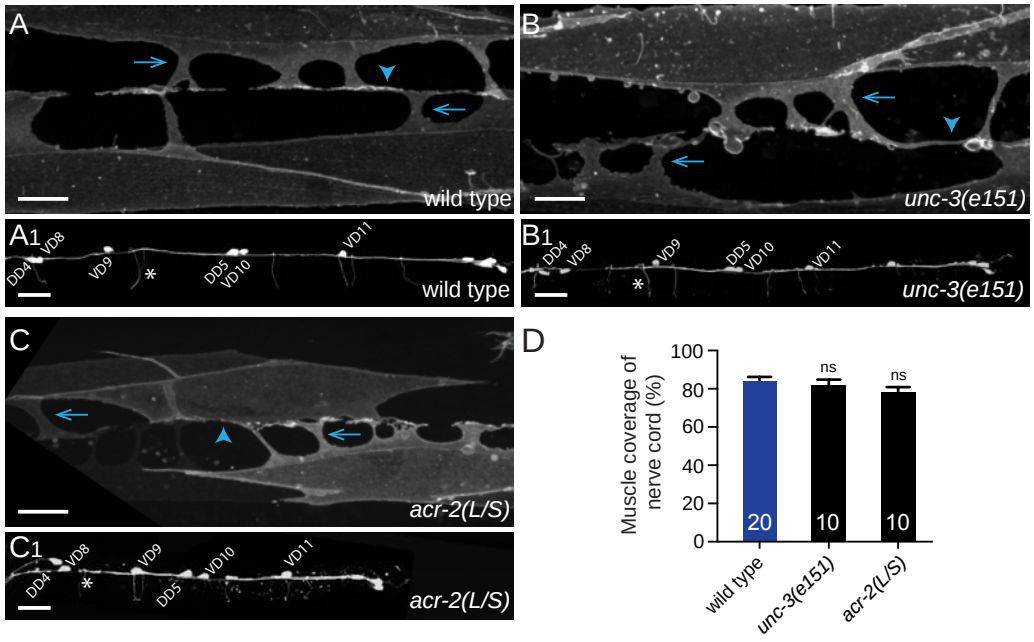

Figure 3.4 Gross morphological development of GABA motor neurons and muscles does not require cholinergic innervation

(A-C′) Confocal images of the ventral nerve cord and body wall muscles posterior to the vulva of an adult wild-type (A,A′), *unc-3(e151)* mutant (B,B′) and *acr-2(L/S)* transgenic (C,C′) animals expressing a membrane-bound GFP in the distal row of body wall muscles (*him4p*::mCD8::GFP) (A-C) or mCherry in the GABA nervous system (*unc-47p*::mCherry) (A′-C′). Arrows indicate muscle arm shafts and arrowheads indicate muscle arm termini. Asterisks indicate GABA neuron commissures. Scale bars: 10 µm (A-C); 20 µm (A′-C′). (D) Quantification of the percentage of the ventral nerve cord region covered by muscle membrane. ns, not significant; ANOVA with Dunnett's multiple comparisons test.

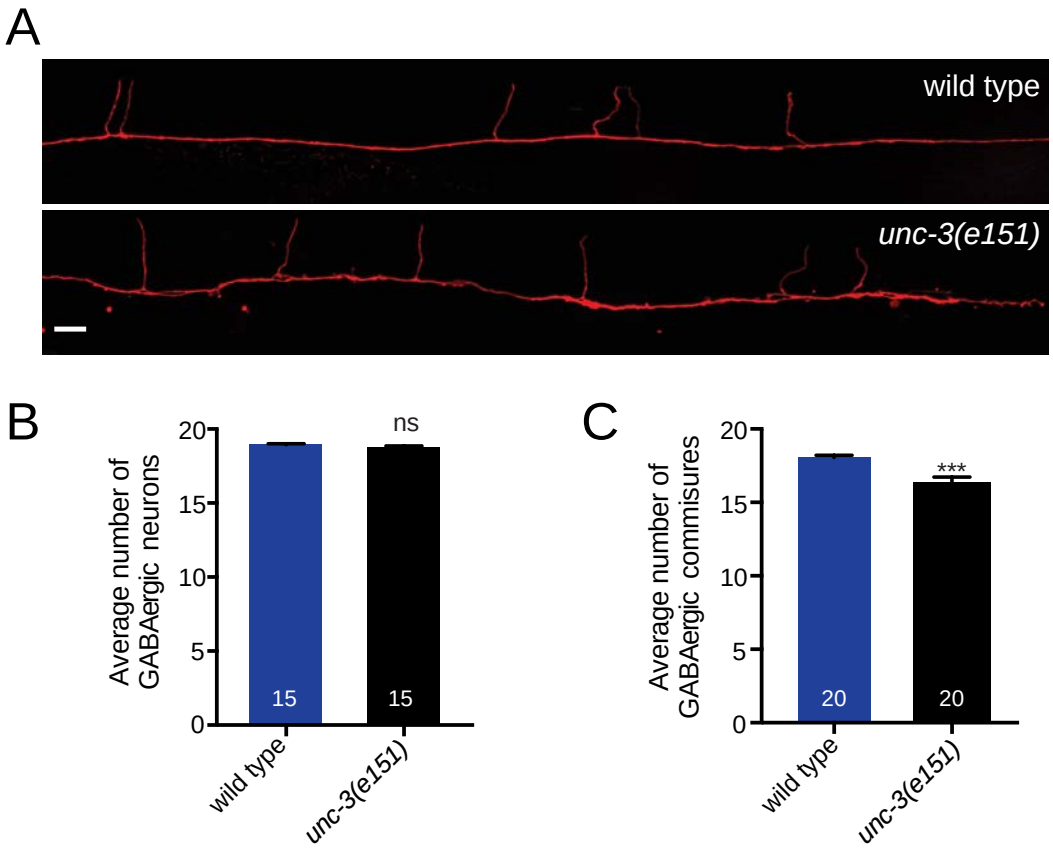

Figure 3.5 GABA neuron morphology is grossly normal in *unc-3* mutants
(A) Confocal images of the posterior dorsal nerve cord in adult animals expressing a transcriptional reporter labeling GABAergic (*unc-47p*::mCherry) neurons in wild type and *unc-3(e151)* mutant animals. Scale bar, 10 μm. (B, C) Quantification of the average number of GABAergic cell bodies (B) and commissures (C) for the genotypes indicated. Each bar represents the mean ± SEM. Numbers in bars indicate the n for each genotype. ***p<0.001, student's t test.

Cholinergic innervation refines GABA synaptic outputs

Our results described above support the idea that UNC-3 regulation of cholinergic neuron differentiation is important for the establishment of synaptic connectivity with GABAergic neurons. We next investigated whether cholinergic neurons might similarly contribute to the development of GABA synaptic outputs onto muscles. We examined GABA synapses in a transgenic strain expressing the synaptic vesicle marker mCherry::RAB-3 in GABA motor neurons together with the GFP-tagged $GABA_A$-like receptor UNC-49 in muscles (Bamber et al., 1999; Klassen and Shen, 2007) (**Figure 3.6A**). In wild-type animals, GABA synapses are evenly spaced along the ventral nerve cord, with presynaptic vesicles and postsynaptic GABA receptor clusters in close apposition (**Figure 3.6B; Figure 3.7A and D**). Mutation of *unc-3* produces striking changes in GABA synapses (**Figure 3.6C, D, G, and H**), a phenotype consistent across independent *unc-3* mutant strains (*n3435* and *e151*). Specifically, the number of pre- and post-synaptic clusters is significantly decreased, and the average size of postsynaptic UNC-49::GFP puncta is increased [e.g. by 95% in *unc-3(e151)*]. Furthermore, we noted significant regions of the ventral nerve cord lacking GABA synaptic vesicle clusters in *unc-3* mutants [e.g. 56±4% in *unc-3 (e151)*, compared with 20±2% in the wild type, $p<0.01$]. A prior study reported diffusely distributed and enlarged clusters of the active zone marker SYD-2/α-liprin in GABA neurons of *unc-3* mutants (Yeh et al., 2005), consistent with our findings.

The localization of other synaptic markers, including the synaptic vesicle marker SNB-1/synaptobrevin (Nonet, 1999) and the active zone marker UNC-10/RIM, are

similarly altered by mutation of *unc-3* (**Figure 3.6I-L**). The size and distribution of SNB-1 clusters are both affected similarly to RAB-3. The number of UNC-10 clusters is decreased significantly but we do not observe a change in their average area, suggesting that synaptic vesicle clustering is more dramatically affected than the size of the active zone itself. Despite the altered distribution of synaptic markers, we did not observe obvious changes in the apposition of presynaptic mCherry::RAB-3 and postsynaptic UNC-49::GFP fluorescent signals (**Figure 3.7D**) [wild type: 88±3%; *unc-3(e151)*: 82±4% in apposition], suggesting that trans-synaptic signaling important for establishing proper registration between pre- and post-synaptic specializations is maintained.

Most aspects of these GABA synapse defects are reversed with expression of the wild-type *unc-3* cDNA in cholinergic neurons (**Figure 3.6E, G, H**). In particular, the decreased number of GABAergic presynaptic RAB-3 clusters and the increases in synapse size are each rescued with *unc-3p*::*unc-3* expression, but not by GABA- specific expression. Although decreases in the number of GABA receptor clusters are not significantly rescued by *unc-3p*::*unc-3* expression, GABA- or muscle-specific expression enhances the severity of this phenotype, arguing against a requirement for *unc-3* expression in these cells. Finally, we noted that muscle-specific expression of *unc-3* appears to partially reverse the increases in synapse size; however, decreases in synapse number are not rescued. Together, our transgenic rescue experiments provide additional support for the idea that *unc-3* expression in cholinergic neurons is required for establishing proper GABAergic connectivity.

Surprisingly, *unc-3p*::*unc-3* cDNA expression is not sufficient to restore

movement to *unc-3* mutants. In contrast, expression of an *unc-3* minigene containing the first three *unc-3* introns under control of the same promoter improves movement and restores synaptic connectivity (**Figure 3.8**), suggesting that additional aspects of *unc-3* regulation are important for motor function and that *unc-3* intronic regions are crucial in this process.

To further test the idea that cholinergic innervation influences the number and positioning of GABAergic synapses, we ablated ACh motor neurons by expressing a putative gain-of-function variant of the ACh receptor subunit *acr-2*, *acr-2(L/S)*, that produces cell- autonomous death of cholinergic motor neurons during late embryogenesis (Barbagallo et al., 2010). Similar to *unc-3*, we did not observe gross morphological changes in GABA neurons or reduced muscle membrane contact with the nerve cord (Barbagallo et al., 2010) (**Figure 3.4C, C′, D**). Nonetheless, genetic ablation of ACh motor neurons produces striking defects in inhibitory synapses, similar to those observed for *unc-3* mutants, including a significant decrease in the number of both presynaptic mCherry::RAB-3 and postsynaptic UNC-49::GFP clusters, as well as significant increases in their size (**Figure 3.6F-H; Figure 3.7C**). Thus, impaired differentiation or genetic ablation of ACh motor neurons does not affect the gross morphology of GABA neurons but instead alters the density and size of GABA synaptic outputs. Our analysis of inhibitory synapses in *unc-3* mutants and *acr-2(L/S)* transgenic animals supports the hypothesis that presynaptic cholinergic neurons play important roles in both clustering iAChRs in GABA neurons and in shaping GABA synaptic outputs.

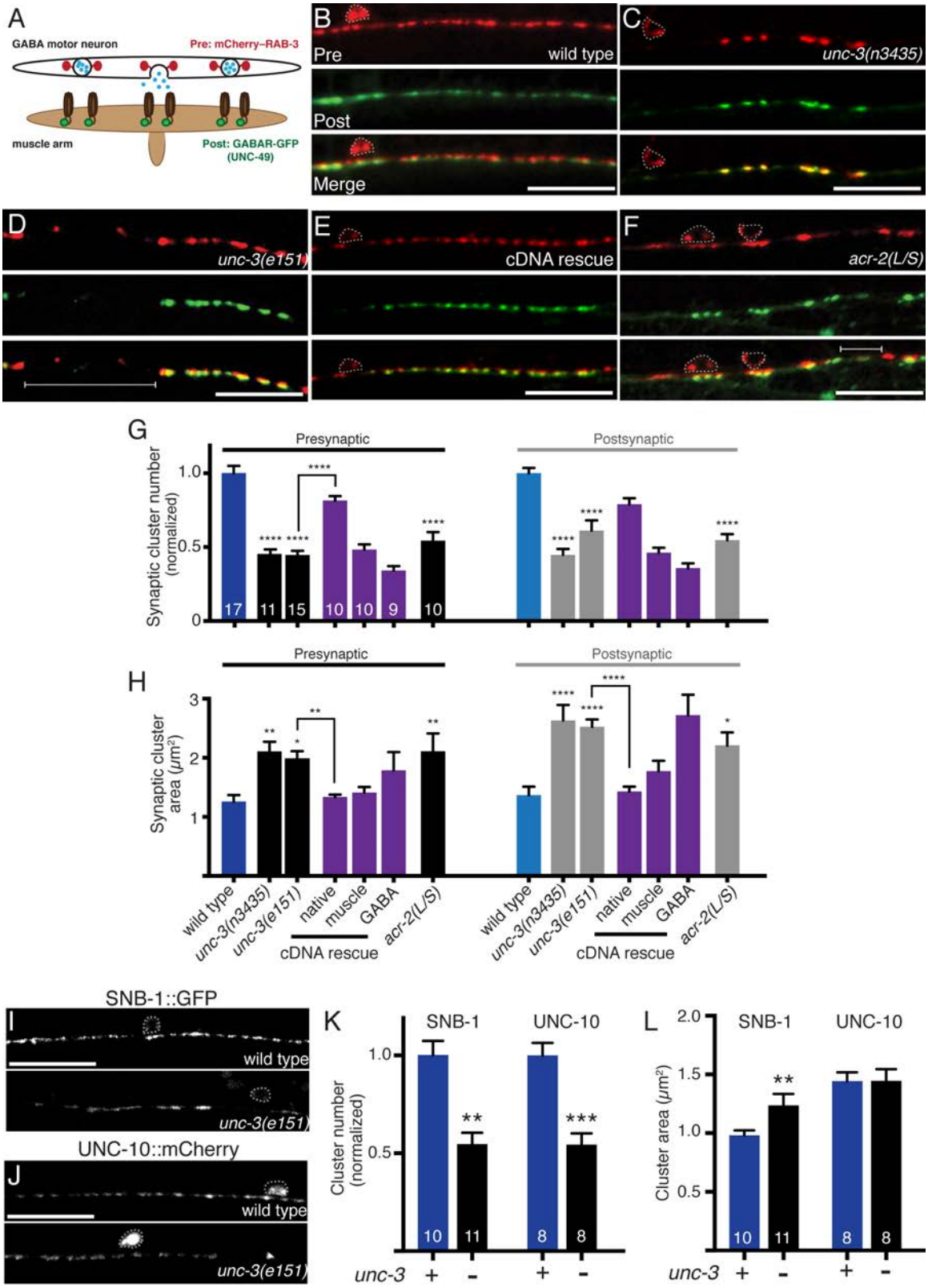
A
GABA motor neuron
Pre: mCherry–RAB-3
muscle arm
Post: GABAR-GFP (UNC-49)
B
Pre
wild type
Post
Merge
C
unc-3(n3435)
D
unc-3(e151)
E
cDNA rescue
F
acr-2(L/S)
G
Presynaptic
Postsynaptic
Synaptic cluster number (normalized)
17 11 15 10 10 9 10
H
Synaptic cluster area (μm²)
wild type
unc-3(n3435)
unc-3(e151)
native
muscle
GABA
acr-2(L/S)
cDNA rescue
SNB-1::GFP
I
wild type
unc-3(e151)
UNC-10::mCherry
J
K
SNB-1
UNC-10
Cluster number (normalized)
10 11 8 8
unc-3 + - + -
L
Cluster area (μm²)

Figure 3.6 Impaired cholinergic innervation alters the distribution and size of GABA synapses

(A) Diagram depicting the location of fluorescent reporters used to label GABA pre- (*unc-47p*::mCherry::RAB-3) and post-synaptic (UNC-49::GFP) structures. (B-F) Confocal images of the ventral nerve cord in adult wild type (B), *unc-3(n3435)* mutants (C), *unc-3(e151)* mutants (D), *unc-3(e151)* mutants expressing an *unc-3* cDNA rescuing array (*unc-3p*::*unc-3* cDNA) (E), and transgenic *acr-2(L/S)* animals (F) co-expressing *unc-47p*::mCherry::RAB-3 in GABA motor neurons with UNC-49::GFP in body wall muscles. Note areas devoid of synaptic clusters (brackets) and enlarged clusters in *unc-3* mutants and *acr-2(L/S)* transgenic animals. Motor neuron cell bodies are outlined in this figure and all subsequent figures. Scale bars: 20 µm. (G) Average number of pre- and post-synaptic clusters per 50 µm, normalized to wild type. (H) Average size of pre- and post-synaptic clusters at GABA synapses. *p<0.05, **p<0.01, ****p<0.0001 compared with either control or *unc-3* mutant as indicated; ANOVA with Dunnett's multiple comparisons test. (I,J) Confocal images of the ventral cord in wild type or *unc-3(e151)* mutants expressing the GFP-tagged synaptic vesicle marker synaptobrevin (SNB-1::GFP) (I), or the Rim1 homolog (UNC-10::mCherry) (J). Scale bars: 20 µm. (K) Quantification of synaptic cluster number per 50 µm for each marker, normalized to wild type. (L) Quantification of presynaptic cluster area for genotypes indicated. **p<0.01, ***p<0.0001; Student's *t*-test.

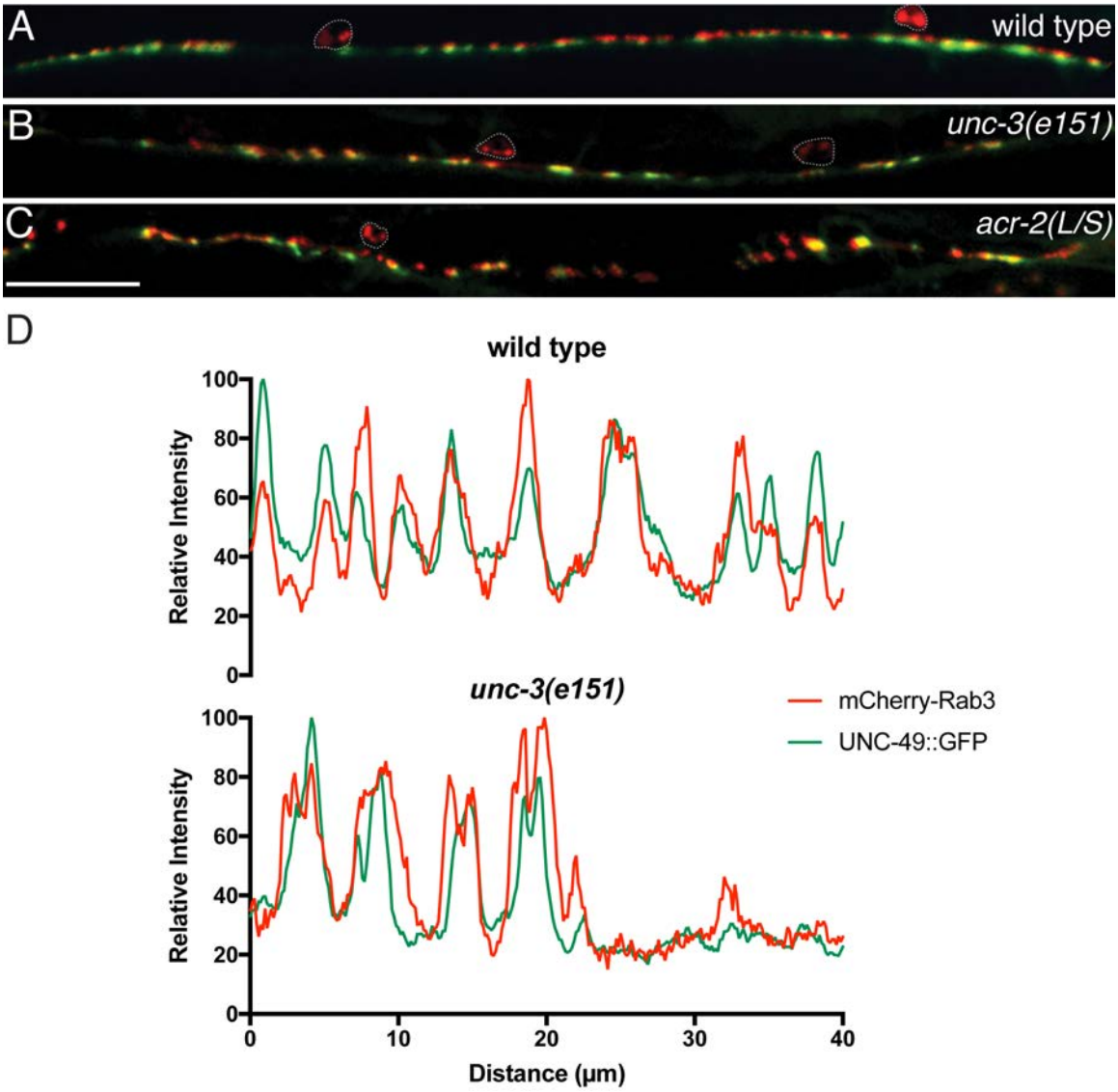

Figure 3.7 GABA synaptic distribution is altered with disruption of cholinergic neurons

(A-C) Confocal images showing the distribution of GABA synaptic markers (mCherry::RAB-3 and UNC-49::GFP) in extended regions of the ventral nerve cord of adult wild type, *unc-3(e151)*, and transgenic *acr-2(L/S)* animals. Scale bar, 20 µm. (D) Representative line scans depicting colocalization of UNC-49::GFP and mCherry::Rab3 in a 40 µm region of the ventral nerve cord in wild type and *unc-3(e151)* mutant animals. Note larger puncta and gaps in fluorescence in *unc-3* mutants.

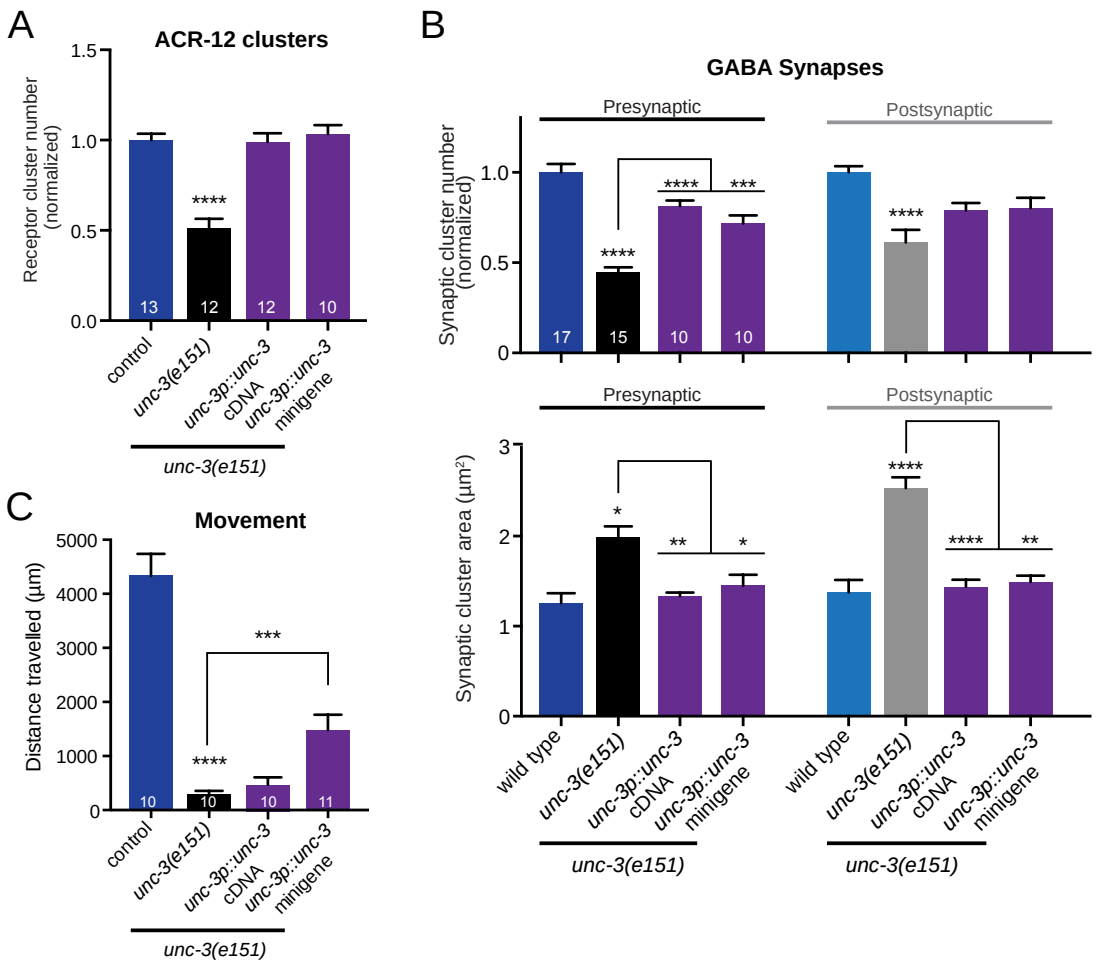

Figure 3.8 Expression of an *unc-3* minigene construct rescues synapse and movement defects in *unc-3(e151)* mutants

(A) Quantification of the average number of receptors clusters/85 µm of dorsal nerve cord for the genotypes indicated, normalized to wild type. Each bar represents the mean ± SEM. Numbers in bars indicate the n for each genotype. ****p<0.0001, ANOVA with Dunnett's multiple comparisons test. (B) Top: Average number of pre- and post-synaptic clusters/50 µm, normalized to wild type. Bottom: Average size of pre- and post-synaptic clusters at GABA synapses/50 µm. Each bar represents the mean ± SEM. Numbers in bars indicate the n for each genotype. *p<0.05, **p<0.01, ***p<0.001, ****p<0.0001 for comparisons with either wild type or *unc-3* mutant values as indicated, ANOVA with Dunnett's multiple comparisons test. For A and B, values for wild type, *unc-3* mutant and cDNA rescue were reproduced from **Figures 3.2 and 3.6** respectively. (C) Average distance travelled in 30 s for the genotypes indicated. Each bar represents the mean ± SEM. Numbers in bars indicate the n for each genotype. ****p<0.0001, ***p<0.001, ANOVA with Dunnett's multiple comparisons test.

Vesicular release from cholinergic neurons shapes GABA synapses

We next investigated whether vesicular release from cholinergic neurons is required to properly establish GABA neuron connectivity. We disrupted vesicular release by specific expression of tetanus toxin light chain (TetTx) (**Figure 3.9; Figure 3.10**). TetTx expression in cholinergic motor neurons does not affect morphology or outgrowth, but produces changes in sensitivity to the cholinesterase inhibitor aldicarb consistent with decreased transmission (**Figure 3.10**). Cholinergic expression of TetTx does not alter ACR-12 clustering in GABA neurons (**Figure 3.9A, B**). We did, however, observe significant abnormalities in GABA synaptic outputs (**Figure 3.9C-F**). These include enlargement of both presynaptic mCherry::RAB-3 and postsynaptic receptor clusters, as well as gaps in fluorescence that are similar to those observed for *unc-3* mutants and *acr-2(L/S)* transgenic animals. Thus, synaptic structures between cholinergic and GABAergic neurons appear to be properly established when vesicular release from cholinergic motor neurons is impaired. Despite this, the distribution of GABAergic synaptic outputs is disrupted, implicating vesicular signals from ACh motor neurons in contributing to this process.

To investigate the possibility that ACh itself is an important signal, we examined GABA synapses in mutant strains with specific defects in cholinergic transmission. *unc-17* mutants are defective in a vesicular transporter (vAChT) that loads ACh into synaptic vesicles (Brenner, 1974; Rand, 1989; Rand and Russell, 1984). The *unc-17(e113)* mutation disrupts the UNC-3 binding site in the *unc-17* promoter, disrupting UNC-17 and CHA-1 expression in cholinergic motor neurons (J. Rand, personal communication), and

these mutants are presumably null for ACh release from cholinergic motor neurons.

ACR-12::GFP clustering in the dorsal nerve cord is not significantly altered in *unc-17(e113)* mutants or in *madd-4;unc-17* double mutants (**Figure 3.11A, B**), consistent with the results described above for TetTx expression. In contrast, GABAergic pre- and post-synaptic clusters are significantly decreased in number in *unc-17(e113)* mutants (by 65% and 64% respectively, $p<0.001$) (**Figure 3.11D, G**). A second strongly hypomorphic *unc-17* allele *(e245)* produced similar effects. The *e245* mutation replaces a glycine with an arginine (G347R) in the ninth transmembrane domain of the vAChT protein (Alfonso et al., 1993) and decreases UNC-17 protein levels (Sandoval et al., 2006). ACR-12::GFP clustering is unchanged in *unc-17(e245)* compared with wild type (**Figure 3.11B**), but significant defects in GABA synaptic outputs are apparent. These include gaps in the distribution of synapses as well as enlarged pre- and post-synaptic clusters (**Figure 3.11E, G, H**). The increased size of GABAergic synapses in *unc-17(e245)* mutants, but not *unc-17(e113)* mutants, might indicate that partial loss of ACh release triggers changes in GABA synapse size. Alternatively, ACh release from cholinergic neurons in which *unc-17* transcriptional regulation occurs independently of *unc-3* (e.g. VC neurons) might influence GABA synapse size. Together, our analysis of *unc-17* mutants provides evidence for the involvement of cholinergic transmission in directing the development of GABA synaptic outputs. Nonetheless, these effects are less pronounced than those observed after either TetTx expression or mutation of *unc-3*, suggesting participation of additional ACh-independent signals.

To address whether the effects of decreased ACh release reflect a requirement for

ACh signaling onto muscles, we examined GABA synapses in animals lacking functional iAChRs at the NMJ (*unc-29; acr-16* double mutants) (Francis et al., 2005). Eliminating synaptic activation of muscles causes a slight reduction in the number of postsynaptic GABA receptor clusters (**Figure 3.11F-H**) but does not alter the density or positioning of presynaptic structures, suggesting that cholinergic activation of muscles is not essential for shaping GABAergic neuromuscular connectivity.

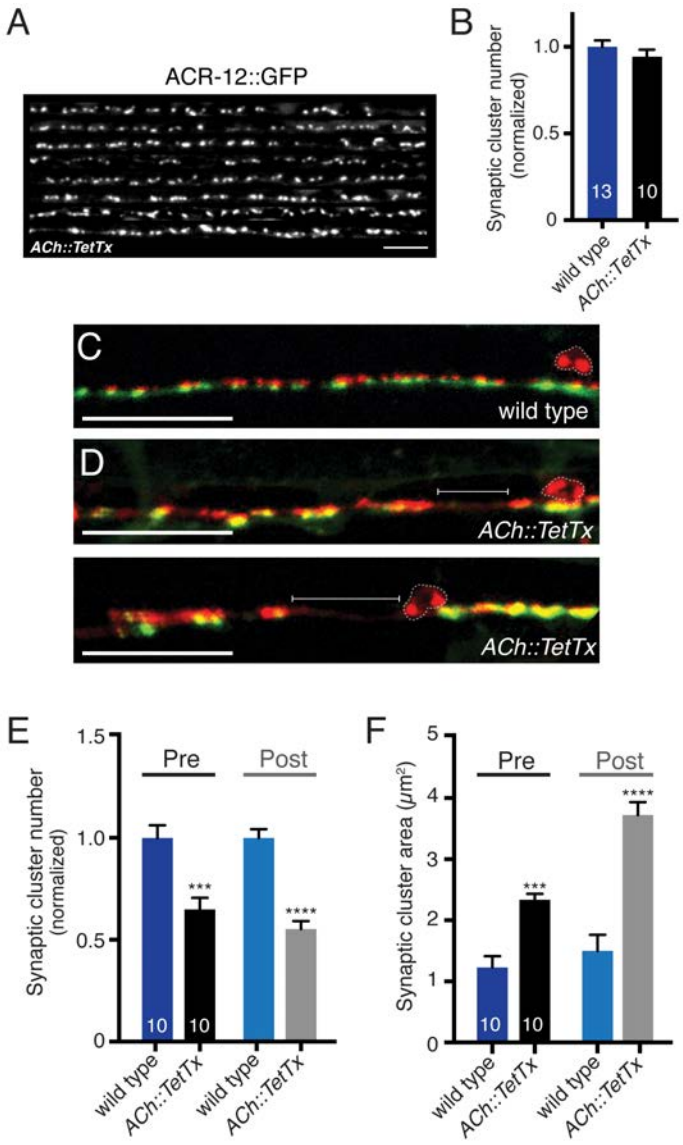

Figure 3.9 Vesicular release from cholinergic motor neurons shapes GABA synaptic outputs

(A) Confocal images showing the dorsal nerve cord of eight animals co-expressing ACR-12::GFP in GABA neurons and tetanus toxin in cholinergic neurons. Scale bar: 5 μm. (B) Quantification of the average number of receptor clusters per 85 μm of dorsal nerve cord for the genotypes indicated, normalized to wild type. (C,D) Merged confocal images of *unc-47p*::mCherry:: RAB-3 and UNC-49::GFP labeling in the ventral nerve cord of adult wild-type (C) and transgenic animals with specific TetTx expression in cholinergic neurons (D). Brackets indicate areas devoid of synaptic clusters. Scale bars: 20 μm. (E) Average number of pre- and post-synaptic clusters per 50 μm for each genotype, normalized to wild type. (F) Average area of pre- and post-synaptic clusters at GABA synapses for each genotype as indicated. ***p<0.001, ****p<0.0001; Student's t-test.

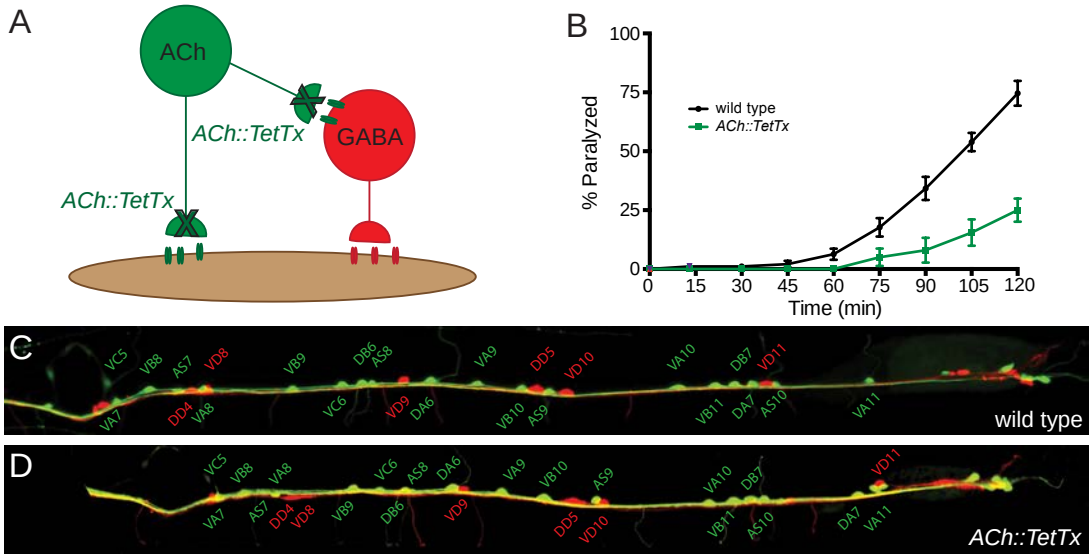

Figure 3.10 Cell specific expression of tetanus toxin in cholinergic neurons alters neuronal activity but not neuronal organization
(A) Schematic representation of the motor circuit showing connectivity of cholinergic (green) and GABAergic neurons (red). Sites of tetanus toxin action are denoted by X. (B) Time course of paralysis of adult animals on 1 mM aldicarb, an inhibitor of cholinesterase. The percentage of animals paralyzed was calculated every 15 minutes for two hours. Each data point represents the mean ± SEM of n=10 or n=8 assays for wild type or *ACh::TetTx* respectively. (C, D) Confocal images of the posterior ventral nerve cord in adult animals co-expressing transcriptional reporters labeling cholinergic (*unc-17p*::GFP) and GABAergic (*unc-47p*::mCherry) neurons in wild type or with cell-specific expression of TetTx as indicated. The identities of motor neurons based on cell body position are indicated (green, cholinergic neurons) (red, GABAergic neurons).

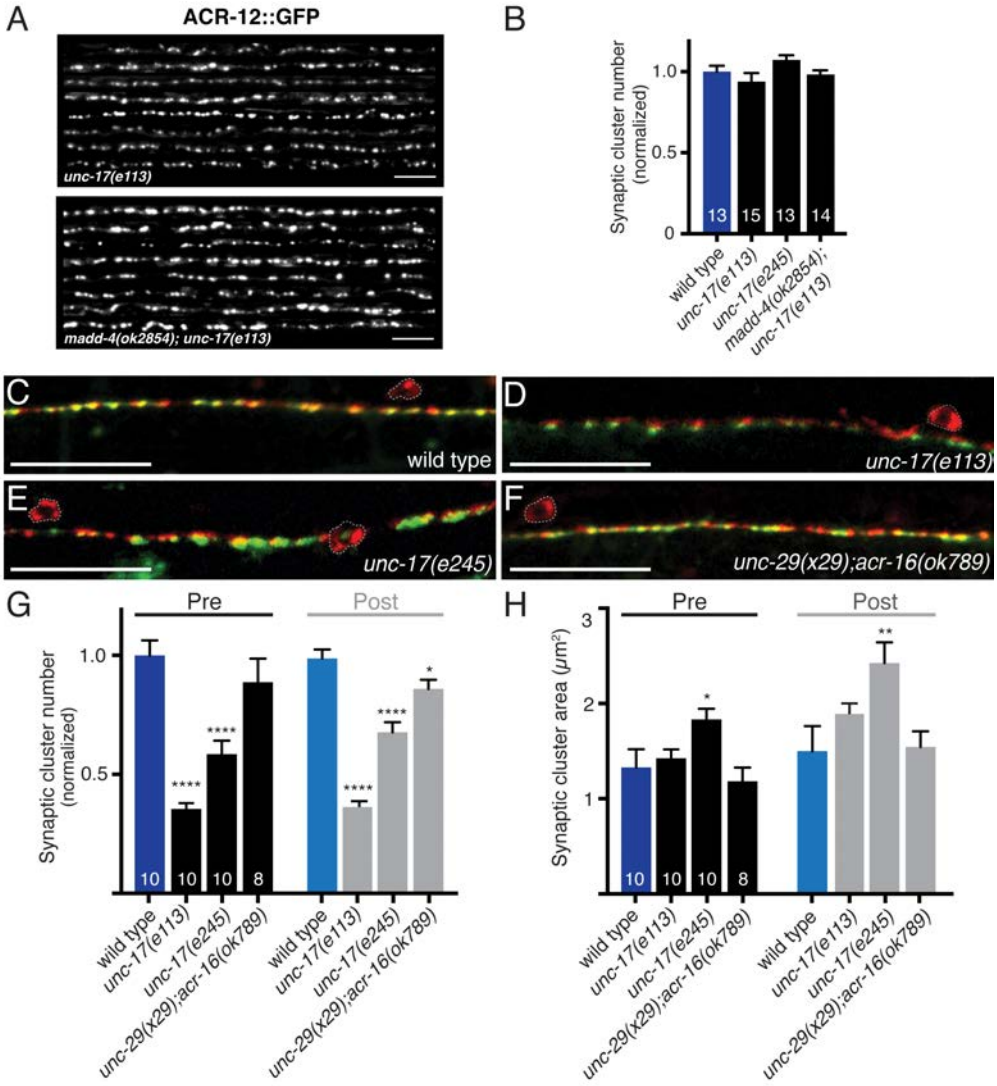

Figure 3.11 Reduced cholinergic transmission alters GABA synapse density and localization

(A) Confocal images showing the dorsal nerve cord of eight *unc-17(e113)* and *madd-4(ok2854);unc-17(e113)* animals expressing ACR-12::GFP in GABA neurons. Scale bars: 5 µm. (B) Quantification of the average number of receptor clusters per 85 µm of dorsal nerve cord for the genotypes indicated, normalized to wild type. (C-F) Merged confocal images of *unc-47p*::mCherry::RAB-3 and UNC-49::GFP labeling in the ventral nerve cord region of adult wild-type animals (C), *unc-17(e113)*/vAChT mutants (D), *unc-17(e245)*/vAChT mutants (E) or *unc-29(x29);acr-16(ok789)* double mutants, which lack functional muscle iAChRs (F). Scale bars: 20 µm. (G) Average number of GABA pre- and post-synaptic clusters per 50 µm for each genotype, normalized to wild type. (H) Average size of GABA pre- and post-synaptic clusters. *p<0.05, **p<0.01, ****p<0.0001; ANOVA with Dunnett's multiple comparisons test.

Acute reductions in cholinergic activity in adults lead to decreased GABA synapse size

Our previous genetic analysis indicated that cholinergic transmission helps to shape the distribution of GABA synaptic outputs, but did not distinguish whether these effects occur in the mature or developing nervous system. To address this question, we used a temperature- sensitive allele (*y226*) of *cha-1*/choline acetyltransferase (ChAT) (Rand and Russell, 1984). When maintained at a permissive temperature (15°C), *cha-1(y226)* mutants develop similarly to wild type, generating the full complement of cholinergic motor neurons (**Figure 3.12A**). When switched to a restrictive temperature (25°C), *cha-1 (y226)* mutants become uncoordinated within minutes, consistent with rapid impairment of cholinergic transmission, and these behavioral effects are reversible upon shifting back to the permissive temperature (Zhang et al., 2008) (**Figure 3.12B**).

We first investigated the effects of reduced cholinergic transmission in adult animals. We shifted *cha-1(y226)* mutants to 25°C for a 4 h period in early adulthood, and visualized GABA synapses immediately following this shift (**Figure 3.13A**). Interestingly, this transient reduction in cholinergic transmission does not produce appreciable changes in the distribution or number of GABA synapses. Instead, we noted a significant decrease in the size of both pre- and post-synaptic clusters (**Figure 3.13B-G**), whereas GABA synapses in wild-type animals remain unaffected. This temperature-shift paradigm also produces a significant decrease in movement velocity in *cha-1(y226)* mutants, and these effects are reversible within a 4 h recovery period at 15°C (**Figure 3.12B**). GABA synaptic clusters in *cha-1* mutants are also restored to their normal size following a 4 h recovery period (**Figure 3.13D-G**). Increasing the duration of shifts to the

restrictive temperature (8h) produces further decreases in the size of GABA pre- and post-synaptic clusters. Our findings indicate that acute changes in cholinergic activity during adulthood are sufficient to alter the size of GABA synapses, without producing obvious effects on GABA synapse positioning or density. The reversible nature of the synaptic alterations in adults provides evidence for active mechanisms that regulate the size of GABA synapses in response to changing levels of cholinergic transmission.

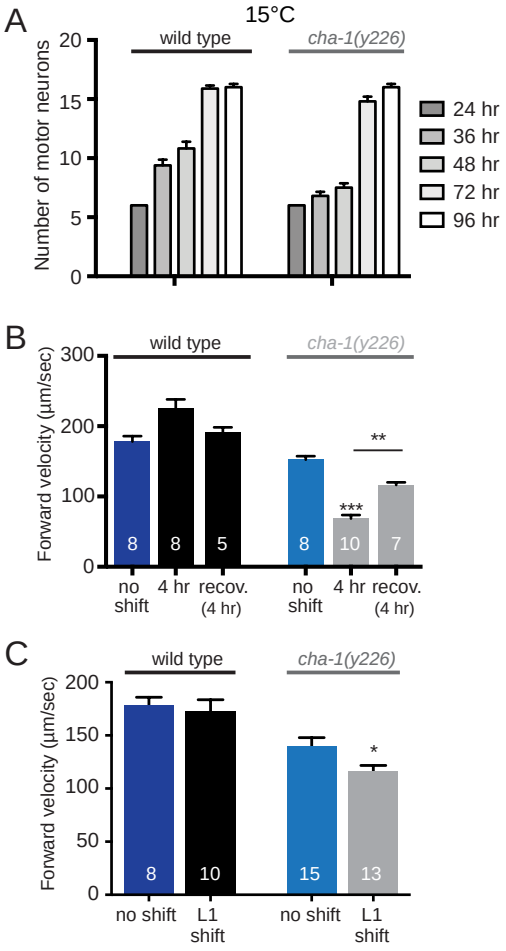

Figure 3.12 Neuronal development and locomotory behavior in *cha-1(y226)* mutant animals

(A) The number of GABA motor neuron cell bodies (visualized by *unc-47p*::mCherry expression) present in wild type or *cha-1(y226)* animals grown at 15°C at the time points indicated. All time points are taken from the 21+ cell stage. Graph represents the average number of cell bodies for 10-15 animals per time point for each genotype. (B) Forward velocity of adult wild type and *cha-1(y226)* animals following the shifts indicated. See **Figure 3.13A** for details of time shift. ***p*<0.001, ****p*<0.0001, ANOVA with Tukey's multiple comparisons test. (C) Forward velocity of young adult wild type and *cha-1(y226)* animals after being shifted to a non-permissive temperature for eight hours spanning the L1/L2 transition. See **Figure 3.14A** for details of temperature shift. **p*<0.05, student's t-test.

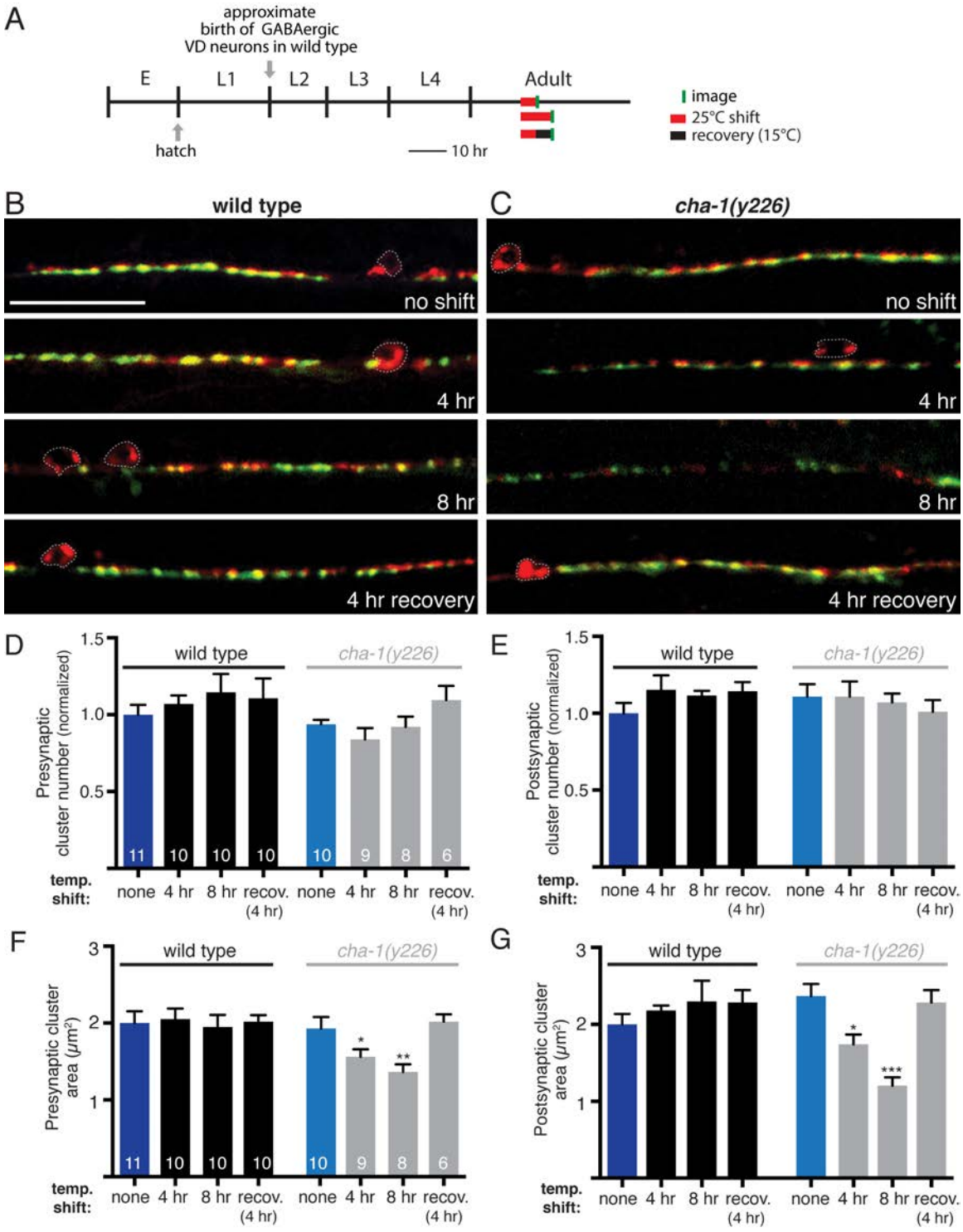
A
approximate
birth of GABAergic
VD neurons in wild type
E
L1
L2
L3
L4
Adult
hatch
10 hr
image
25°C shift
recovery (15°C)
B
wild type
C
cha-1(y226)
no shift
4 hr
8 hr
4 hr recovery
D
Presynaptic cluster number (normalized)
E
Postsynaptic cluster number (normalized)
F
Presynaptic cluster area (μm²)
G
Postsynaptic cluster area (μm²)
temp. shift:
none
4 hr
8 hr
recov. (4 hr)

Figure 3.13 Acute reduction of cholinergic transmission during adulthood produces reversible decreases in GABA synapse size
(A) Diagram indicating predicted timeline of wild-type *C. elegans* development at 15°C and temperature shifts employed. Approximate time of hatch is indicated. Temperature shifts to 25°C (red) and time of imaging (green) are indicated. E, embryo. (B,C) Merged confocal images of *unc-47p*::mCherry::RAB-3 and UNC-49::GFP labeling in the ventral nerve cord region of adult wild-type animals (B) or *cha-1(y226)* mutants (C) following a shift to 25°C for the durations indicated. Scale bar: 20 μm. (D,E) Average number of GABA presynaptic (D) and postsynaptic (E) clusters per 50 μm for wild type (black) and *cha-1(y226)* mutants (gray). (F,G) Average size of GABA presynaptic (F) and postsynaptic (G) clusters for wild type (black) and *cha-1(y226)* mutants (gray). *p<0.05, **p<0.01, ***p<0.0001; ANOVA with Dunnett's multiple comparisons test.

Acetylcholine release is required during a highly synaptogenic period for proper GABA synapse localization

We next investigated whether cholinergic activity during development might help to shape the density or distribution of GABA synapses. To address this question, we again used *cha-1(y226)* mutants, shifting animals to 25°C for 8 h periods during the first larval (L1) stage, then imaging GABA synapses later in adulthood (**Figure 3.14A**). We noted a time window beginning approximately 20 h after hatch (late L1 stage in wild type at 15°C) during which an 8 h shift to the restrictive temperature produces significant defects by adulthood. Specifically, we found the number of pre- and post-synaptic clusters is decreased by 40% and 27%, respectively, in *cha-1* mutants subjected to temperature shift (**Figure 3.14B-D**). We also noted a significant increase in the size of presynaptic clusters (**Figure 3.14E**), although the size of postsynaptic clusters does not appear to be altered (**Figure 3.14F**). These effects do not occur in control animals exposed to the same shift in temperature, or in *cha-1* mutants grown continuously at 15°C. This temperature shift paradigm also produces a modest decrease in movement velocity in *cha-1(y226)* adult animals, suggesting that transient reduction of cholinergic transmission during development might be sufficient to produce behavioral defects that extend into adulthood (**Figure 3.12C**). The timing of the 8 h temperature shift is predicted to overlap the L1/L2 transition for wild-type animals during which GABAergic VD neurons are initially integrated into the motor circuit, although the precise timing of these events can vary in mutant and transgenic strains. Thus, reduced cholinergic activity early in the development of GABAergic VD neurons affects their synaptic distribution, implicating

cholinergic signaling in defining the mature pattern of inhibitory connectivity.

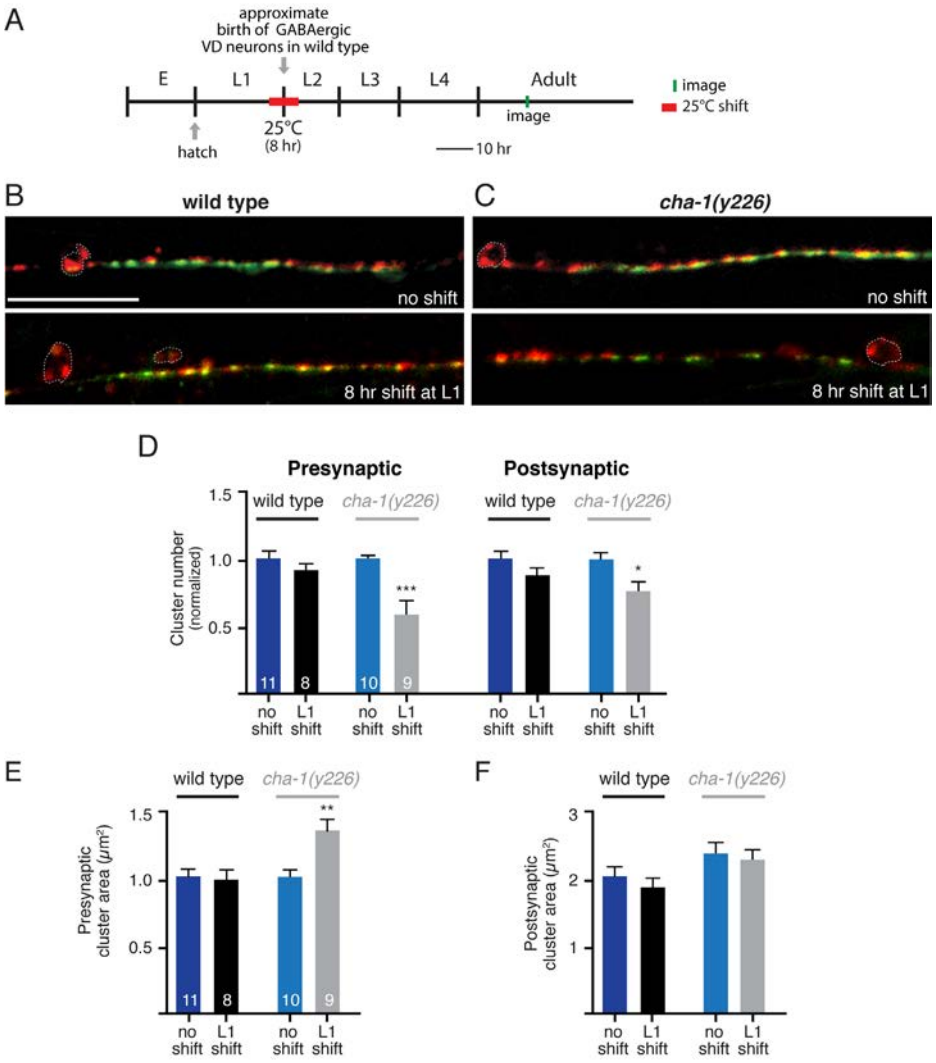

Figure 3.14 Reduced cholinergic neurotransmission during a period of GABAergic synaptogenesis alters GABAergic synaptic connectivity

(A) Diagram indicating predicted timeline of wild-type *C. elegans* development at 15°C and temperature shifts employed. Approximate time of hatch is indicated. (B,C) Confocal images of the ventral nerve cord in adult wild-type (B) and *cha-1(y226)* (C) temperature-sensitive mutant animals co-expressing GABA pre- and post-synaptic markers (*unc-47p*::mCherry::RAB-3 and UNC-49::GFP) grown at the permissive temperature and after an 8 h shift to the non-permissive temperature during the first larval stage. Note that the representative image for the *cha-1* no shift control group shown in C is the same as that displayed in Fig. 7C. Scale bar: 20 μm. (D) Average number of GABA presynaptic and postsynaptic clusters per 50 μm for wild type (black) and *cha-1(y226)* mutants (gray). (E,F) Average size of GABA presynaptic (E) and postsynaptic (F) clusters for wild type (black) and *cha-1(y226)* mutants (gray). **p*<0.05, ***p*<0.01, ****p*<0.0001; Student's *t*-test.

Discussion

Establishing the appropriate pattern of GABAergic innervation is crucial for proper inhibitory regulation of mature neural circuits. In this study, we explored the role of cholinergic motor neurons in sculpting the synaptic connectivity of GABAergic neurons in the *C. elegans* motor circuit. Our results show that integration of post-embryonic-born GABAergic VD neurons into the motor circuit is extensively regulated by cholinergic motor neurons, complementing prior studies that provided evidence for activity- dependent synaptic remodeling of embryonic-born GABAergic DD neurons (Han et al., 2015; Thompson-Peer et al., 2012). First, mutation of the COE transcription factor *unc-3,* which is required for terminal differentiation of cholinergic motor neurons, disrupts postsynaptic development (iAChR clustering) in GABAergic neurons. These effects are not strongly dependent on either cholinergic vesicular release or expression of the synaptic organizer *madd-4*, suggesting involvement of a novel molecular pathway. Second, mutation of *unc-3* produces defects in GABAergic VD neuron synaptic connectivity with muscles. Third, genetic ablation of cholinergic motor neurons or specific TetTx expression in cholinergic neurons similarly alters the size and distribution of GABA synaptic outputs to muscles. Mutation of the cholinergic vesicular transporter *unc-17* produces similar effects on GABAergic connectivity with muscles. Finally, the density of GABAergic synaptic outputs is decreased by acute reduction of cholinergic transmission during a developmental period that corresponds with the time of initial integration of GABAergic VD neurons into the circuit in wild type. Our findings suggest a model in which vesicle-borne signals from cholinergic motor neurons, both ACh and

additional signals, are important for shaping GABAergic connectivity.

Cholinergic motor neurons innervate both GABAergic motor neurons and body wall muscles. Disruption of cholinergic innervation did not impair gross morphological development or outgrowth in either of these cell types, indicating that cell-intrinsic genetic programs are sufficient to guide normal morphological development. In contrast, additional activity-dependent processes appear to be required for establishing the mature pattern of GABAergic synaptic connectivity. These results could be indicative of a functional segregation between processes underlying activity-dependent regulation of synaptic connectivity and intrinsic genetic regulation of gross morphological features. Prior work showed that elimination of glutamatergic synaptic inputs has little effect on the morphological development of mouse hippocampal neurons (Lu et al., 2013), providing support for a similar segregation between these processes in mammals.

Mutation of *unc-3* produced the most striking effects on synaptic connectivity in our experiments, both impairing postsynaptic ACR-12 iAChR clustering in VD neurons and decreasing their synaptic outputs. The requirement for UNC-3 in ACR-12 iAChR clustering is unlikely to indicate involvement of cholinergic activity-dependent regulation because neither TetTx expression nor mutation of *unc-17* altered ACR-12 clustering. Similarly, mutation of the synaptic organizer *madd-4* did not strongly affect ACR-12 iAChR clustering in VD neurons, either alone or in combination with mutation of *unc-17*, suggesting that a novel, as yet unidentified, transcriptional target of UNC-3 might be important for this process.

Our studies suggest that cholinergic activity might have a more prominent role in

directing the distribution of GABAergic synaptic outputs. Our electrophysiological analysis of *unc-3* mutants showed that GABAergic VD motor neurons are capable of sustaining inhibitory transmission. Notably, however, the frequency of GABAergic synaptic events is dramatically reduced compared with wild type, and their average amplitude increased significantly, mirroring the changes we observed in GABAergic outputs using our synaptic markers. We noted similar structural changes in GABAergic synaptic outputs when cholinergic neurons were genetically ablated [*acr-2(L/S)*], and when cholinergic vesicular release was disrupted (*ACh::TetTx*). For all of these, presynaptic alterations were paralleled by similar effects on the clustering of postsynaptic GABA receptors, suggesting that these effects reflect a change in synapse patterning/maturation rather than direct impairment of synapse formation per se.

Although synapse dynamics continue throughout the life of an animal, there is often increased plasticity earlier in development (Hensch and Fagiolini, 2005). The effects of cholinergic activity we observed might reflect an ongoing requirement for cholinergic transmission or a more specific requirement during a developmental period of increased plasticity. Our analysis of temperature-sensitive *cha-1* mutants provides support for the latter possibility. A temporally defined reduction in cholinergic transmission that overlaps with the predicted timing of the highly synaptogenic L1/L2 transition in wild type produced irreversible defects in the patterning and size of GABAergic synaptic outputs. At the L1/L2 transition, 13 GABAergic VD neurons are added to the motor circuit, forming synapses onto ventral muscles. Our findings suggest that cholinergic activity during this developmental period influences the patterning of

GABA synapses, and that deficits in transmission during this time period cannot be compensated for in later developmental stages. How might reduced cholinergic activity in early development alter GABAergic synaptic outputs in the adult? Synaptic inputs to the VDs primarily come from the dorsal A and B (DA/DB) classes of cholinergic motor neurons, which are present from hatch and are re-wired to innervate VD neurons after the L1 stage. One interesting possibility is that a reduction in cholinergic activity impairs re-wiring and DA/DB innervation of VD GABAergic neurons. According to this model, defects in GABA synapse patterning would then arise due to impaired DA/DB activation of GABAergic neurons. In contrast, acute reduction of cholinergic activity in the adult produces effects that are distinct from those during development, including changes in synapse size without decreases in synapse number, raising the possibility that homeostatic mechanisms are established after synapse patterning is completed. Similar scaling mechanisms have been reported at excitatory glutamatergic synapses in worms, flies and mammals (Davis, 2013; Grunwald et al., 2004; Turrigiano, 2008).

GABA release itself has been suggested to be key for proper inhibitory synapse maturation in mammals (Chattopadhyaya, 2011). Notably, disruption of GABA biosynthesis (*unc-25*/GAD mutants) does not impair GABA synapse formation in worms (Gally and Bessereau, 2003; Jin et al., 1999). Likewise, mutations that produce global reductions in neurotransmission (e.g. mutations in *unc-13*/Munc13 or *unc-64*/syntaxin) do not dramatically alter inhibitory synaptogenesis (Richmond et al., 1999; Saifee et al., 1998). For our studies, we used genetic tools that specifically affect cholinergic neurons. Under these conditions, inhibitory synapse formation appears to be properly initiated.

Presynaptic specializations and postsynaptic receptor clusters are in close apposition; however, the size and density of these synapses are altered, implicating vesicular signals from cholinergic neurons in the refinement or patterning of GABAergic synaptic outputs. Although the mechanism underlying this process remains to be determined, one possibility is that vesicular signals from cholinergic neurons may regulate expression of synapse-organizing molecules in GABA neurons. Several recent studies have identified genetic pathways important for GABA synapse development and regulation in worms (Maro et al., 2015; Tong et al., 2015; Tu et al., 2015). It will be interesting to investigate whether cholinergic neurons influence expression levels of these and other potential synaptic organizers. Notably, activity- dependent transcriptional cascades shape the development and placement of GABA synapses in mammals (Bloodgood et al., 2013; Lin et al., 2008). Our findings lead us to propose that similar processes might be important for integrating post- embryonic-born GABAergic VD neurons into the motor circuit and patterning their synaptic outputs.

Materials and Methods

Strains

C. elegans strains were grown at room temperature (22-24°C) on nematode growth media (NGM) plates seeded with the *Escherichia coli* strain OP50 unless otherwise noted. Wild type represents the N2 Bristol strain. Transgenic strains were obtained by microinjection to achieve germline transformation (Mello et al., 1991). Multiple independent lines were obtained for each transgenic strain, and data presented are from a single representative transgenic line. Transgenic strains were identified either by co-injection of *lin-15*(+) (pL15Ek) into *lin-15(n765ts)* mutants or by co-injection of either *lgc-11p::GFP* or *lgc-11p::mCherry* (restricted expression to the pharynx). As required, transgenes were integrated using x-ray bombardment and outcrossed to wild type. A complete list of strains is available in the **Table 3.1**.

Molecular biology

Plasmids were constructed using the two-slot Gateway Cloning system (Invitrogen) as described previously (Bhattacharya et al., 2014).

him-4p::mCD8::GFP

Entry vector: A *him-4p* promoter fragment (2156 bp) was amplified from pPRZ138.2 (a gift from Peter Roy, University of Toronto, ON, Canada) and cloned into pENTR-D-TOPO to create pENTR-3′-him4. Destination vector: mCD8::GFP (1566 bp) was

amplified from pKMC72 and ligated into pDEST-16 to create pDEST-20. pENTR-3′-him4 and pDEST-16 were recombined to generate pBB102 (*him-4p*::mCD8::GFP).

Tetanus toxin construct

Entry Vector: An *acr-2* promoter fragment (3386 bp) was amplified from pBB67 and subcloned into pENTR-D-TOPO to create pENTR-5′-acr2. Destination Vector: Tetanus toxin light chain (1374 bp) was amplified from TetTx-pWD157 to create pDEST-34. pENTR-5′-acr2 and pDEST-34 were recombined to generate pBB112 (*acr-2p*::TetTx).

unc-3 reporter and rescue constructs

Transcriptional reporter: An *unc-3* promoter fragment (−1068 bp relative to start) was amplified from genomic DNA and cloned into pENTR-D-TOPO to generate pENTR-17. pENTR-17 was recombined with pDEST-94 to generate *unc-3p*::GFP (pAP192). cDNA rescue: Wild-type *unc-3* cDNA was RT-PCR amplified from total N2 RNA and inserted into a destination vector to create pDEST-140. pDEST-140 was recombined with pENTR-17 (*unc-3* promoter), pENTR-3′-myo3 (muscle-specific promoter) and pENTR-3′-unc47 (GABA-specific promoter) to generate pAP194 (*unc-3p*::*unc-3* cDNA), pAP172 (*myo-3p*::*unc-3* cDNA) and pAP176 (*unc-47p*::*unc-3* cDNA), respectively. Minigene rescue: A 3154bp fragment extending from the *unc-3* start to exon 4 of the *unc-3* genomic locus was amplified from N2 genomic DNA and ligated into pDEST-140 to create pDEST-142. pDEST-142 was recombined with pENTR-17 to create pAP196 (*unc-3p*::*unc-3* minigene) containing the first three unc-3 introns [a 463 bp repetitive fragment

within intron 1 (+2181 relative to start) was not included] and all of the *unc-3* coding sequence.

Electrophysiology

Endogenous postsynaptic currents (PSCs) were recorded from body wall muscles as described previously (Petrash et al., 2013). The extracellular solution consisted of the following (in mM): 150 NaCl, 5 KCl, 4 $MgCl_2$, 1 or 5 $CaCl_2$ (as indicated), 15 HEPES and 10 glucose, pH 7.4, osmolarity adjusted with 20 sucrose. To facilitate analysis of *unc-3* mutants that display very low rates of GABAergic activity, recordings of GABAergic currents were performed in 5 mM $CaCl_2$. The intracellular fluid consisted of the following (in mM): 115 potassium gluconate, 25 KCl, 0.1 $CaCl_2$, 50 HEPES, 5 Mg-ATP, 0.5 Na-GTP, 0.5 cGMP, 0.5 cAMP and 1 BAPTA, pH 7.4, osmolarity adjusted with 10 sucrose. At least 60-90 s of continuous data were used in the analysis. Data analysis was performed using Igor Pro (Wavemetrics) and Mini Analysis (Synaptosoft) software.

Aldicarb assay

Aldicarb assays were performed on adult animals (24 h post L4) at room temperature (22-24°C) with the researcher blind to genotype. Staged animals (ten per plate) were transferred to NGM plates containing 1 mM Aldicarb (ChemService) and assessed for movement every 15 min for 2 h.

Microscopy and image analysis

For all imaging, nematodes were immobilized with sodium azide (0.3 M) on a 5% agarose pad. Each *n* represents analysis of the nerve cord from an independent animal. Confocal microscopy of GABA NMJ synapses was performed using an LSM Pascal 5 confocal microscope (Zeiss). Images were analyzed using ImageJ software (open source). Images were obtained using a 63× oil lens and aligned using Photoshop (Adobe) or ImageJ.

Synapse density was calculated in a 50 μm section of the ventral nerve cord directly posterior to the vulva. A minimum fluorescence threshold was set to identify synaptic peaks (1500 a.u. for cholinergic synapses and 500 a.u. for GABAergic synapses). Peaks were identified as two or more consecutive data points above threshold and spaces were defined as two or more data points below threshold. Synapse area was calculated by separating particles using the ImageJ analyze particles function. Particles $\leq 0.2\ \mu m^2$ were excluded as background.

To quantify orphan puncta at the GABAergic NMJ, the fluorescence intensities of both GFP and mCherry signals in an 85 μm region of the ventral nerve cord were analyzed. Intensity data were exported to Microsoft Excel and normalized to the corresponding highest value. Each peak of fluorescence was categorized as a colocalized puncta, presynaptic orphan puncta (mCherry signal without overlapping GFP signal) or postsynaptic orphan puncta (GFP signal without overlapping mCherry signal).
The extent of muscle membrane coverage of the ventral nerve cord region was calculated by measuring the length of the ventral midline of the posterior body wall muscles. The

length of muscle membrane along the ventral midline (visualized by *him-4p*::mCD8::GFP) was quantified and used to calculate a percentage of total nerve cord length.

ACR-12::GFP (*ufIs92*), ACR-16::GFP (*ufIs8*) and UNC-29::GFP (*ufIs2*) images were acquired using a 3i (Intelligent Imaging Innovations) Everest spinning-disk confocal microscope and collected at 0.27 μm/steps using a 63× objective.

Confocal montages of ACR-12::GFP were assembled by imaging the dorsal nerve cord posterior to the vulva in adult hermaphrodites. Identical image and laser settings were used for each genotype. Straightened dorsal cords were extracted from these images using the 'straighten to line' function.

For quantifying ACR-12::GFP, ACR-16::GFP and UNC-29::GFP puncta along the nerve cord, background fluorescence was first subtracted by calculating the average intensity of each image in a region devoid of puncta. Puncta were quantified across 80 μm of the nerve cord region with ImageJ 'analyze particles', using an intensity threshold specific for each marker. Particles ≤ 0.04 μm^2 were excluded as background.

unc-3 movement analysis

For locomotion assays, 1-day-old adults were allowed to acclimate for 1 min on NGM plates thinly seeded with a bacterial lawn. WormLab software (MBF Bioscience) was used to capture and analyze 30 s digital videos of individual worms.

cha-1 time course

Adult shifts and recovery

Wild-type and *cha-1* animals were cultured at 15°C. Animals were synchronized at the L4 stage, and then placed at 15°C for an additional 24 h. Young adult animals were then shifted to 25°C for either 4 or 8 h and imaged immediately. A third group of animals were shifted to 25°C for 4 hours, then placed back at 15°C for 4 h (recovery) before imaging.

Developmental shift

Embryos were staged at the 21+ cell stage and allowed to develop at 15°C for 20 h. Animals were then shifted to 25°C for 8 h and returned to 15°C. Animals were synchronized at the L4 stage and allowed to grow for an additional 24 h at 15°C prior to imaging.

Behavior

Temperature shifts were performed as described above. For behavioral analysis, animals were transferred individually to plates without food for a period of 5 min. Movement was quantified using Wormlab software to track animals and measure their average forward velocity over a period of 5 min.

Table 3.1 *C. elegans* strains used in this work

Genotype	Strain Name	Transgene
ufIs34	IZ829	*unc-47p*::mCherry (pPRB5)
unc-3(e151);ufIs34	IZ1265	*unc-47p*::mCherry (pPRB5)
ufIs25;ufIs34	IZ733	*acr-2(L/S)* (pBB9), *unc-47p*::mCherry (pPRB5)
acr-16(ok789);ufIs8	IZ9	*myo-3p*::ACR-16::GFP (pDM906)
unc-3(e151);acr-16(ok789); ufIs8	IZ1219	*myo-3p*::ACR-16::GFP (pDM906)
ufIs58;oxIs19	IZ930	*unc-47p*::mCherry::RAB-3 (pJRC1), UNC-49::GFP
unc-3(e151);ufIs58;oxIs19; ufEx1056	IZ2774	*unc-47p*::mCherry::RAB-3 (pJRC1), UNC-49::GFP, *unc-47p*::*unc-3* cDNA (pAP176)
unc-3(e151);ufIs58;oxIs19; ufEx1052	IZ2768	*unc-47p*::mCherry::RAB-3 (pJRC1), UNC-49::GFP, *myo-3p*::*unc-3* cDNA (pAP172)
unc-3(e151);ufIs58;oxIs19; ufEx1074	IZ2795	*unc-47p*::mCherry::RAB-3 (pJRC1), UNC-49::GFP, *unc-3p*::*unc-3* cDNA (pAP194)
unc-3(e151);ufIs58;oxIs19; ufEx1065	IZ2786	*unc-47p*::mCherry::RAB-3 (pJRC1), UNC-49::GFP, *unc-3p*::*unc-3* minigene (pAP196)
unc-3(n3435);ufIs58;oxIs19	IZ2752	*unc-47p*::mCherry::RAB-3 (pJRC1), UNC-49::GFP
unc-3(e151);ufIs58;oxIs19	IZ1256	*unc-47p*::mCherry::RAB-3 (pJRC1), UNC-49::GFP
ufIs25;ufIs58;oxIs19	IZ596	*acr-2(L/S)* (pBB9), *unc-47p*::mCherry::RAB-3 (pJRC1), UNC-49::GFP
vsIs48;ufIs34	IZ759	*unc-17p*::GFP, *unc-47p*::mCherry (pPRB5)
vsIs48;ufIs34;ufEx404	IZ1320	*unc-17p*::GFP, *unc-47p*::mCherry (pPRB5), *acr-2p*::TetTx (pBB112)
ufIs58;oxIs19;ufEx404	IZ1243	*unc-47p*::mCherry::RAB-3 (pJRC1), UNC-49::GFP, *acr-2p*::TetTx (pBB112)
unc-29(x29);acr-16(ok789); ufIs58;oxIs19	IZ1286	*unc-47p*::mCherry::RAB-3 (pJRC1), UNC-49::GFP
unc-17(e245);ufIs58;oxIs19	IZ1839	*unc-47p*::mCherry::RAB-3 (pJRC1), UNC-49::GFP

unc-17(e113);ufIs58;oxIs19	IZ1748	*unc-47p*::mCherry::RAB-3 (pJRC1), UNC-49::GFP
ufIs113	IZ1115	*him-4p*::mCD8::GFP (pBB102)
ufIs25;ufEx322	IZ1113	*him-4p*::mCD8::GFP (pBB102)
unc-3(e151);ufIs113	IZ1208	*him-4p*::mCD8::GFP (pBB102)
cha-1(y226);ufIs58;oxIs19	IZ1916	*unc-47p*::mCherry::RAB-3 (pJRC1), UNC-49::GFP
juIs1	CZ333	*unc-25p*::SNB-1::GFP
unc-3(e151);juIs1	IZ1575	*unc-25p*::SNB-1::GFP
hpIs88	ZM2246	*unc-25p*::UNC-10::mCherry
unc-3(e151);hpIs88	IZ2822	*unc-25p*::UNC-10::mCherry
acr-12(ok367);ufIs92	IZ1225	*unc-47p*::ACR-12::GFP (pHP7)
acr-12(ok367);unc-3(e151); ufIs92	IZ2128	*unc-47p*::ACR-12::GFP (pHP7)
acr-12(ok367);unc-3(e151);ufIs92;ufEx1038	IZ2726	*unc-47p*::ACR-12::GFP (pHP7), *unc-47p*::*unc-3* cDNA (pAP176)
acr-12(ok367);unc-3(e151);ufIs92;ufEx1044	IZ2744	*unc-47p*::ACR-12::GFP (pHP7), *myo-3p*::*unc-3* cDNA (pAP172)
acr-12(ok367);unc-3(e151);ufIs92;ufEx1067	IZ2788	*unc-47p*::ACR-12::GFP (pHP7), *unc-3p*::*unc-3* cDNA (pAP194)
acr-12(ok367);unc-3(e151);ufIs92;ufEx1077	IZ2798	*unc-47p*::ACR-12::GFP (pHP7), *unc-3p*::*unc-3* minigene (pAP196)
acr-12(ok367);unc-3(n3435); ufIs92	IZ2752	*unc-47p*::ACR-12::GFP (pHP7)
acr-12(ok367);unc-17(e113); ufIs92	IZ2317	*unc-47p*::ACR-12::GFP (pHP7)
acr-12(ok367);unc-17(e245); ufIs92	IZ2342	*unc-47p*::ACR-12::GFP (pHP7)
acr-12(ok367);madd-4(ok2854);ufIs92	IZ2221	*unc-47p*::ACR-12::GFP (pHP7)
acr-12(ok367);madd-4(ok2854);unc-17(e113); ufIs92	IZ2368	*unc-47p*::ACR-12::GFP (pHP7)
acr-12(ok367);ufIs92;ufEx404	IZ2345	*unc-47p*::ACR-12::GFP (pHP7); *acr-2p*::TetTx (pBB112)
ufIs43;ufEx1084	IZ2816	*acr-2p*::mCherry (pPRB6), *unc-3p*::GFP (pAP192)
ufIs2	IZ1547	*myo-3p*::UNC-29::GFP (pDM956)
ufIs2;madd-4(ok2854)	IZ2369	*myo-3p*::UNC-29::GFP (pDM956)

Acknowledgements

We would like to thank Claire Bénard and members of the Francis lab for critical reading of the manuscript, Will Joyce for technical assistance, Mei Zhen, Kevin Collins, Bruce Bamber and Peter Roy for sharing reagents. Some nematode strains used in this work were provided by the Caenorhabditis Genetics Center, which is funded by the NIH National Center for Research Resources (NCRR). This work was funded by the National Institute of Neurological Disorders and Stroke (R01NS064263 to M.M.F. and F31NS076326 to B.B.) and the National Institute on Drug Abuse (F31DA038399 to A.P.).

CHAPTER IV

Neurexin directs partner-specific synaptic connectivity in *C. elegans*

Alison Philbrook, Shankar Ramachandran, Christopher M. Lambert, Devyn Oliver, Jeremy Florman, Mark J. Alkema, Michele Lemons[1] and Michael M. Francis

Department of Neurobiology, University of Massachusetts Medical School, 364 Plantation Street, Worcester MA 01605

[1]Department of Natural Sciences, Assumption College, Worcester MA, 01609

Contribution Summary

A.P. generated transgenic lines, collected confocal images, and quantified results. S.R. performed all calcium imaging experiments, A.P and M.L. performed smFISH experiments, and J.F. collected behavioral data. A.P. and C.M.L. engineered constructs, D.O. provided several strains in the candidate genetic screen, and M.J.A. provided reagents. A.P. and M.M.F. designed and interpreted all experiments and wrote the final document.

Abstract

In neural circuits, individual neurons often make projections onto multiple postsynaptic partners. Here, we investigate molecular mechanisms by which these divergent connections are generated, using dyadic synapses in *C. elegans* as a model. We report that *C. elegans nrx-1*/neurexin directs divergent connectivity through differential actions at synapses with partnering neurons or muscles. We show that cholinergic outputs onto neurons are, unexpectedly, located at previously undefined spine-like protrusions from GABAergic dendrites. Both these spine-like features and cholinergic receptor clustering are strikingly disrupted in the absence of *nrx-1*. Excitatory transmission onto GABAergic neurons, but not neuromuscular transmission, is also disrupted. Our data indicate that NRX-1 located at presynaptic sites specifically directs postsynaptic maturation in GABAergic neurons. Our findings provide evidence that individual neurons can direct differential patterns of connectivity with their post-synaptic partners through partner-specific utilization of synaptic organizers, offering a novel view into molecular control of divergent connectivity.

Introduction

Neurons are typically wired into discrete circuits through stereotyped patterns of synaptic connections geared to perform specific functions. Individual neurons within circuits may receive convergent synaptic inputs from multiple classes of presynaptic partnering neurons, and likewise, make divergent synaptic outputs onto distinct postsynaptic targets. We have gained an understanding of some of the core mechanisms that sculpt convergent connectivity through studies of developmental processes such as activity-dependent synapse elimination (Brown et al., 1976; Campbell and Shatz, 1992; Okawa et al., 2014a; Sanes and Lichtman, 1999; Shatz and Kirkwood, 1984; Walsh and Lichtman, 2003). In contrast, the molecular processes controlling the establishment of divergent synaptic connections are not clearly defined (Okawa et al., 2014b). Neural circuit models often represent divergent connections as a means for enabling the same signal from an individual presynaptic neuron to reach many different postsynaptic target cells. However, the strength of connections with postsynaptic partners can vary widely, strongly suggesting that presynaptic neurons have the capacity to establish and regulate connections with each postsynaptic target independently. While molecular guidance cues directing axon outgrowth have been well-studied, an understanding of the molecular mechanisms responsible for directing target-specific connectivity has remained elusive.

A primary mechanism for establishing nascent synapses is through the actions of synaptic adhesion molecules, also known as synaptic organizers (de Wit and Ghosh, 2016; Missler et al., 2012). These organizers are often anchored to the pre- and post-synaptic membranes (e.g. neurexins, neuroligins, leucine-rich repeat transmembrane

proteins/LRRTMs) and promote synapse formation through trans-synaptic adhesion and signaling. The importance of these processes in establishing proper neural circuit connectivity is highlighted by the links between mutations in genes encoding these synaptic adhesion/organizing molecules and neuropsychiatric and neurodevelopmental disorders, such as autism spectrum disorder and schizophrenia (Kim et al., 2008a; Reichelt et al., 2012; Rujescu et al., 2009). Intriguingly, synaptic organizers are capable of acting in a cell-specific manner to promote synapse formation (Chen et al., 2017; Siddiqui et al., 2013; Zhang et al., 2015). Thus, an exciting possibility is that individual neurons could encode connections with alternate synaptic partners through differential deployment of synaptic organizers.

We have investigated this possibility in the motor circuit of the nematode *Caenorhabditis elegans* where individual excitatory cholinergic motor neurons form synapses with both body wall muscles and GABAergic motor neurons. Through a screen for genes that govern the formation of these divergent synaptic connections, we demonstrate that the synaptic organizer *nrx-1*/neurexin directs the outgrowth of previously uncharacterized dendritic spine-like structures and the formation of synaptic connections with GABAergic neurons, but is not required for synaptic connectivity with muscles. Conversely, genes previously shown to be required for cholinergic connectivity with muscles (Francis et al., 2005; Gally et al., 2004; Pinan-Lucarre et al., 2014) are not required for the formation of synapses onto GABAergic neurons. Our findings demonstrate that cholinergic neurons utilize distinct molecular signals to establish synapses with GABAergic motor neurons versus body wall muscles, thus revealing that a

single presynaptic neuron establishes divergent connections by employing parallel molecular strategies for the formation of connections with each postsynaptic partner.

Results

Clusters of the GFP-tagged acetylcholine receptor subunit ACR-12 are localized to spine-like dendritic protrusions on the DD1 GABAergic neuron

To establish a system to investigate mechanisms instructing synaptic connectivity, we labeled post-synaptic specializations on dorsally directed GABAergic DD neurons using cell-specific expression (*flp-13* promoter) of the GFP-tagged acetylcholine receptor subunit ACR-12. Prior work showed that ACR-12 receptors in GABAergic motor neurons are clustered opposite cholinergic terminals and mediate excitatory input onto GABAergic motor neurons (Barbagallo et al., 2017; Petrash et al., 2013). These postsynaptic ACR-12 receptor clusters relocate appropriately during developmental synaptic remodeling of the DD neurons, suggesting these clusters faithfully report synaptic inputs (He et al., 2015; Howell et al., 2015).

The morphology of DD neurons is highly polarized, facilitating clear visualization of the axonal and dendritic neuronal compartments. In the present work, we focus much of our analysis on the spatially isolated neurites of the DD1 neuron (**Figure 4.1A-C**). In adults, the anterior DD1 process extends from the soma to enter the ventral nerve cord fascicle (the dendritic compartment), where prior EM studies show that approximately 26 synaptic inputs from cholinergic neurons are concentrated (the synaptic region, **Figure 4.1C, D**) (White et al., 1978; White et al., 1976). The process then crosses the longitudinal midline of the worm via a commissural connection and enters the dorsal nerve cord where it forms *en passant* synaptic outputs onto body wall muscles (the axonal compartment) (**Figure 4.1A, B**) (White et al., 1976). We find that ACR-12::GFP

receptor clusters in DD1 are confined to the synaptic region of the ventral dendritic process in the mature animal (**Figure 4.1C**). As *C. elegans* synapses are formed *en passant*, pre- and post-synaptic specializations typically appear, at the light level, to be localized along the main shafts of neuronal processes. Surprisingly, we noted that the majority of ACR-12::GFP clusters do not appear localized to the shaft of the primary DD1 dendritic process, instead appearing to protrude from the primary DD1 dendrite shaft (**Figure 4.1C**). To investigate this finding in more detail, we examined morphological features in the synaptic region of the DD1 dendrite (**Figure 4.1D**). Intriguingly, we noted finger-like structures (~0.3 – 1 μm in length) projecting outward from the DD1 dendrite in this region (**Figure 4.1D**, **Figure 4.2A**). In contrast, these structures are not present in the asynaptic region of the process immediately adjacent to the cell soma (**Figure 4.1D**), and similarly, are not apparent in a related class of post-embryonic born, ventrally directed GABAergic neurons (VD) (data not shown). These protrusions are obscured by the processes of other ventral cord neurons when using promoters that provide for more broad expression (i.e. *unc-47*), and are therefore most clearly identifiable with specific labeling of DD neurons (**Figure 4.2B**). The dendritic protrusions concentrate clusters of ACR-12 receptors at their tips (**Figure 4.1E**), and over 60% of ACR-12::GFP clusters appear localized to protrusions (**Figure 4.1F**). The dendritic protrusions increase in abundance through larval development, and this increase correlates well with a similar developmental increase in ACR-12::GFP receptor clusters (**Figure 4.2C**). Together, our results provide evidence that cholinergic receptors cluster at morphologically distinct finger-like structures present on the DD1 dendrite, raising the

interesting possibility that these structures serve similar roles to dendritic spines in the mammalian nervous system.

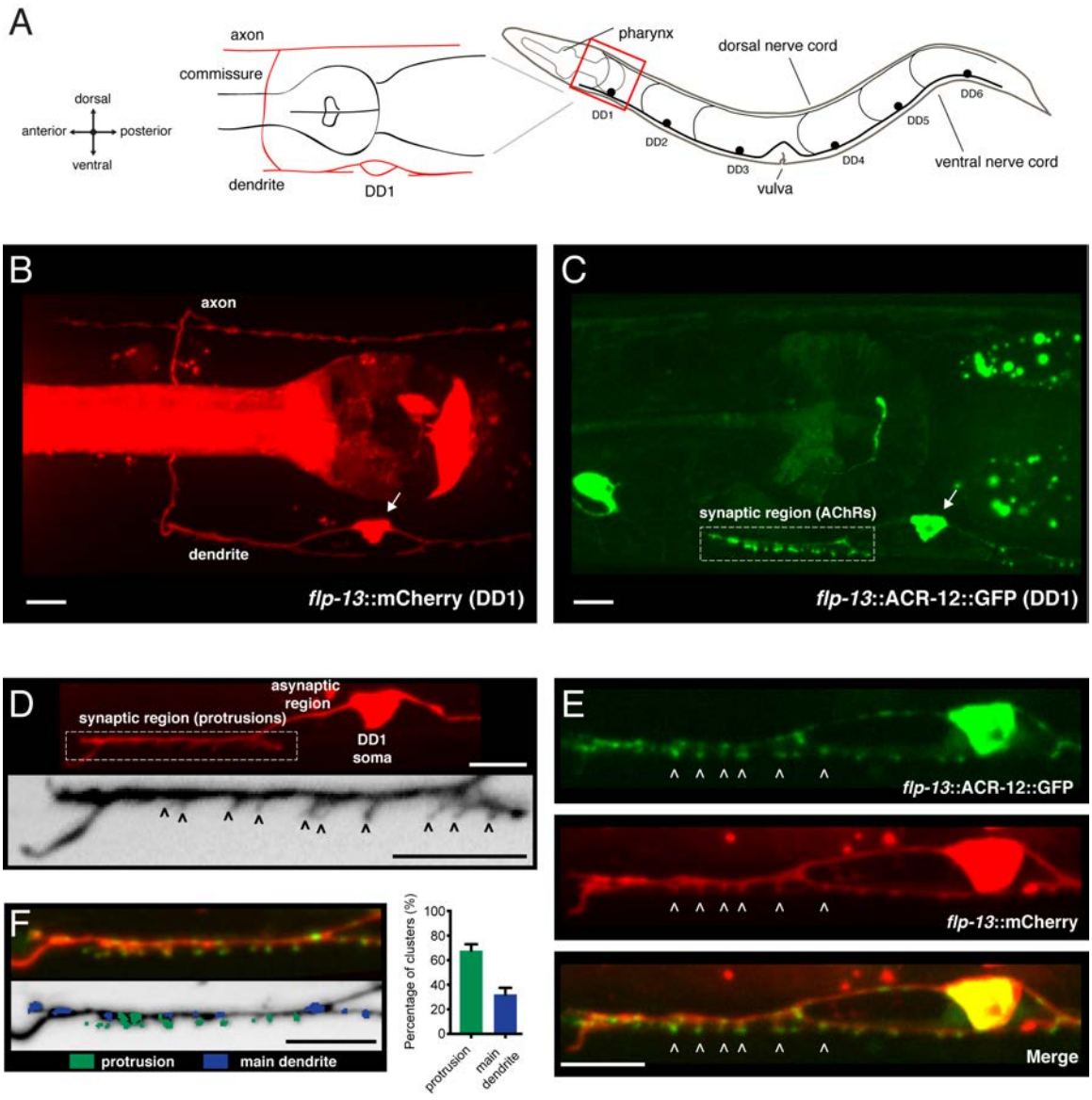
A
axon
commissure
dorsal
anterior
posterior
ventral
dendrite
DD1
pharynx
dorsal nerve cord
DD1
DD2
DD3
DD4
DD5
DD6
vulva
ventral nerve cord
B
axon
dendrite
flp-13::mCherry (DD1)
C
synaptic region (AChRs)
flp-13::ACR-12::GFP (DD1)
D
asynaptic region
synaptic region (protrusions)
DD1 soma
E
flp-13::ACR-12::GFP
flp-13::mCherry
Merge
F
protrusion
main dendrite
Percentage of clusters (%)
100
80
60
40
20
0
protrusion
main dendrite

Figure 4.1 Characterization of post-synaptic specializations in the DD1 neuron
(A) Diagrams of *C. elegans* showing the six DD GABAergic neurons in the ventral nerve cord and expanded view of DD1. After the L1/L2 transition, the DD neurons exclusively make dorsal synaptic outputs onto muscles (axon), while receiving a majority of synaptic inputs on the ventral side (dendrite). (B) Morphology of the DD1 neuron, visualized by expression of the *flp-13*::mCherry transcriptional reporter. Pharyngeal fluorescence indicates expression of the *lgc-11*::mCherry co-injection marker. Arrow indicates DD1 cell body. For this and all subsequent figures, images of L4 animals are shown unless otherwise noted. (C) Cholinergic ACR-12 receptors (*flp-13*::ACR-12::GFP) are localized to a defined region of the DD1 dendritic compartment, labeled as the synaptic region (boxed). Arrow indicates DD1 cell body. (D) Top, confocal image of the DD1 dendritic region visualized by expression of *flp-13*::mCherry. Bottom, inverted image showing expanded view of the synaptic region and dendritic protrusions (indicated by arrowheads). (E) Confocal images of DD1 soma and synaptic region with coexpression of *flp-13*::ACR-12::GFP and *flp-13*::mCherry. Arrowheads indicate ACR-12 clusters located at the tips of dendritic protrusions. (F) Left, representative confocal image showing the distribution of ACR-12::GFP clusters. ACR-12::GFP receptor clusters associated with either protrusions (green) or the main dendritic shaft (blue) are indicated. Right, the percentage of clusters classified into each category (142 receptor clusters from 11 animals were analyzed). Scale bars, 5 μm (B-F).

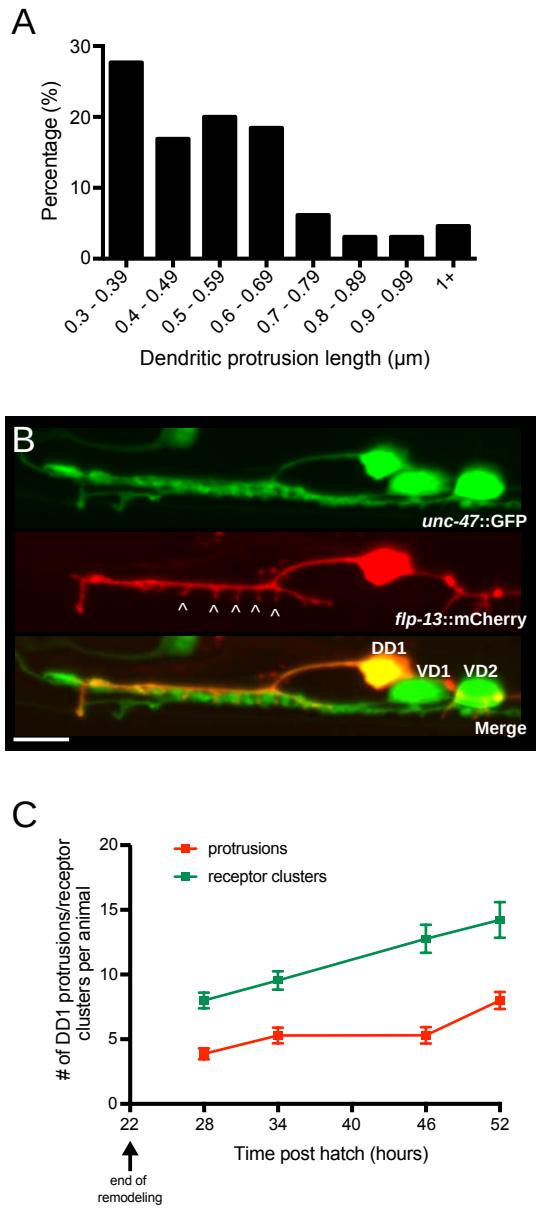

Figure 4.2 Spine-like protrusions are exclusively located on DD dendrites and increase developmentally in a correlated manner with ACR-12 receptor clusters
(A) Distribution of dendritic protrusion lengths. 65 protrusions from 11 L4 animals expressing *flp-13*::mCherry are included in the analysis. (B) DD1 and surrounding ventral cord region in an animal coexpressing *flp-13*::mCherry with *unc-47*::GFP. Spine-like protrusions are only evident with DD-specific labeling (*flp-13*). VD and DD cell bodies are indicated in the merge image. Scale bar, 5 µm. (C) Quantification of the number of DD1 spine-like protrusions (red) or receptor clusters (green) at the indicated time points after hatch. Protrusions and receptor clusters from ≥ 10 animals were analyzed for each time point.

Heteromeric ACR-12-containing AChRs are located on the cell surface opposite cholinergic release sites

To explore the above possibility further, we evaluated the spatial relationship between ACR-12 clusters located on these spine-like structures and cholinergic release sites. We found that dendritic protrusions and ACR-12 receptor clusters are both located opposite clusters of cholinergic synaptic vesicles (**Figure 4.3A, B**), indicating that these likely represent mature synapses. We therefore next investigated whether these clusters indicate post-synaptic receptors residing at the cell surface. To address this question, we inserted an HA epitope tag into the extracellular C-terminus of ACR-12::GFP (diagram in **Figure 4.3C**) (Gottschalk and Schafer, 2006). Injection of Alexa594 conjugated anti-HA antibody into live transgenic animals expressing this construct produces specific labeling in the DD1 synaptic region, and is also evident in coelomocytes (scavenger cells that take up excess antibody), confirming successful injection (**Figure 4.3C**). The anti-HA signal colocalizes with ACR-12::GFP clusters in the synaptic region of DD1, but is not evident in the cell soma. In contrast, the intracellular GFP moiety produces fluorescence that is evident in both the soma and the synaptic region of the dendrite, representing both synaptic and internal receptor pools (**Figure 4.3C**). Injection of anti-GFP antibody did not produce specific labeling, confirming that the intracellularly positioned GFP is not accessible to antibody (**Figure 4.4A**). Our analysis of ACR-12 localization in DD1 indicates that ACR-12 is incorporated into mature receptor complexes that are specifically targeted for transport to the synaptic region of the DD1 dendrite, and reside on the cell surface at post-synaptic sites in this region.

We next sought to gain an understanding of the subunit composition of ACR-12 receptors in GABAergic neurons. Most acetylcholine receptors are formed as heteromeric combinations of five subunits. Prior work has demonstrated that partially or improperly assembled acetylcholine receptor intermediates are not transported out of the ER and are instead targeted for degradation (Blount and Merlie, 1990; Merlie and Lindstrom, 1983). We therefore reasoned that genetic ablation of obligate ACR-12 partnering subunits, by interfering with assembly, transport, and synaptic targeting of ACR-12 receptor complexes, could provide an efficient strategy for identifying subunit partners. We found that single mutations in the acetylcholine receptor subunit genes *unc-38, unc-63, lev-1* or *unc-29* strongly decrease ACR-12::GFP clustering. In wild type, we observe approximately 15 receptor clusters within the DD1 synaptic region. These clusters are eliminated almost completely with mutation of these subunit genes (**Figure 4.4B, C**). In contrast, mutations in other nAChR subunit genes with previously reported neuronal expression, such as *acr-9* and *acr-14* (Cinar et al., 2005; Fox et al., 2005), do not disrupt synaptic ACR-12 clustering (**Figure 4.4B**). Mutations in genes important for AChR assembly and trafficking (*unc-50*, *unc-74,* and *ric-3*) (Boulin et al., 2008; Eimer et al., 2007; Halevi et al., 2002; Haugstetter et al., 2005) also abolish synaptic clusters of ACR-12::GFP (**Figure 4.4B, C**). GABA neuron-specific expression of wild type cDNAs encoding individual AChR subunits (UNC-63 or UNC-38) or accessory proteins in the respective mutants is sufficient to restore ACR-12 clustering to wild type levels, providing support that both gene classes act cell-autonomously in GABA neurons to promote receptor assembly, maturation and synaptic delivery (**Figure 4.4B, C**). Cell-

specific expression of either UNC-29::GFP or UNC-63::GFP in DD neurons produces punctate labeling in the DD1 synaptic region that closely resembles ACR-12::GFP clustering (**Figure 4.3D**). Mutation of *acr-12* in these transgenic animals significantly reduces UNC-29::GFP or UNC-63::GFP receptor clusters and fluorescence signal in the DD1 synaptic region (**Figure 4.3D, Figure 4.4D-E**), providing further evidence that they coassemble with ACR-12. Together, our results indicate UNC-38, UNC-63, LEV-1, UNC-29 and ACR-12 subunits coassemble into a pentameric acetylcholine receptor in GABAergic neurons.

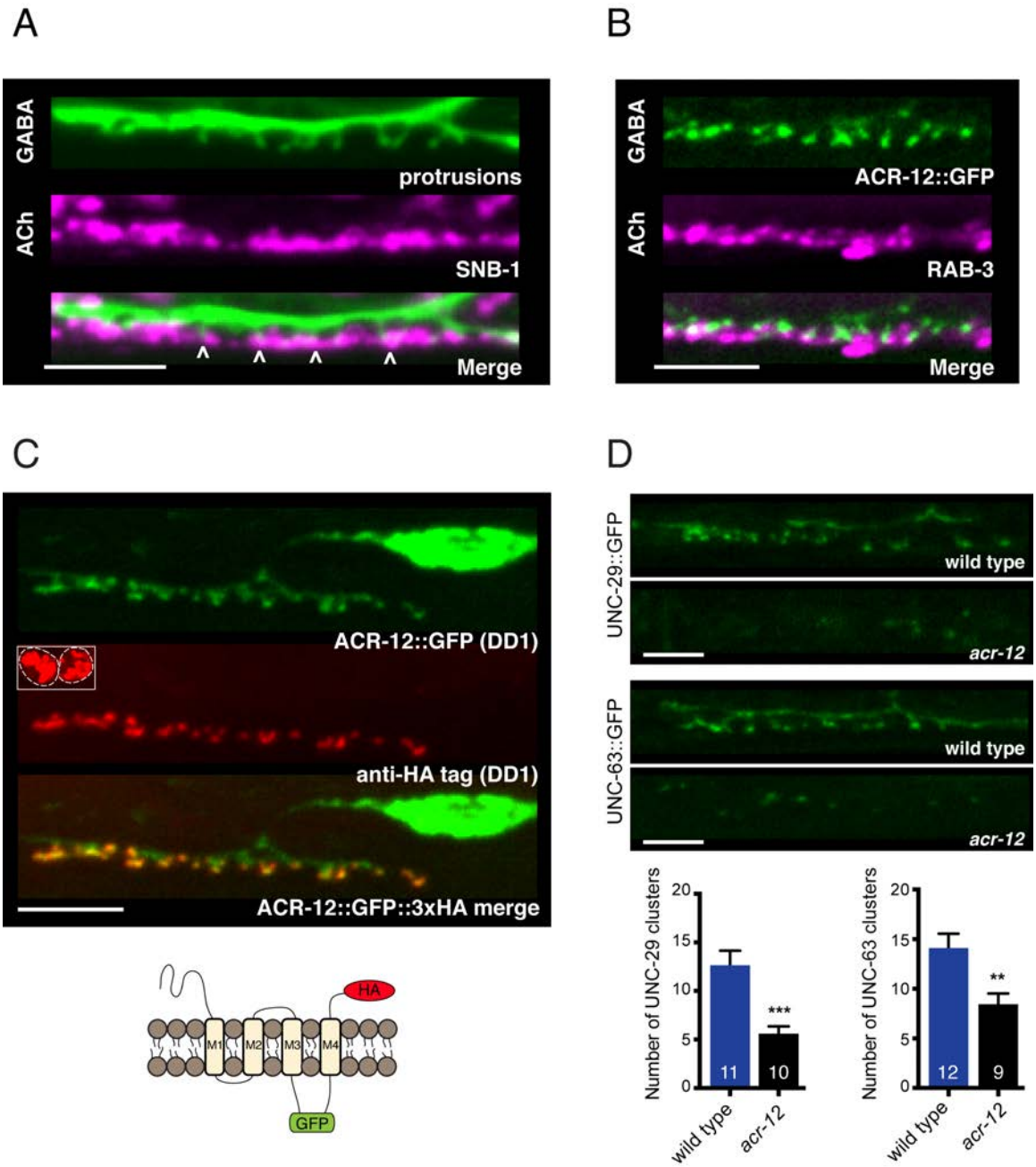
A
GABA
protrusions
ACh
SNB-1
Merge
B
GABA
ACR-12::GFP
ACh
RAB-3
Merge
C
ACR-12::GFP (DD1)
anti-HA tag (DD1)
ACR-12::GFP::3xHA merge
HA
M1
M2
M3
M4
GFP
D
UNC-29::GFP
wild type
acr-12
UNC-63::GFP
wild type
acr-12
Number of UNC-29 clusters
20
15
10
5
0
***
11
10
wild type
acr-12
Number of UNC-63 clusters
20
15
10
5
0
**
12
9
wild type
acr-12

Figure 4.3 Heteromeric ACR-12 receptors are localized at the cell surface opposite sites of release

(A) Confocal images of presynaptic (*acr-2*::SNB-1::GFP) and postsynaptic (*flp-13*::mCherry) domains in the DD1 synaptic region. Note violet/green coloring to more clearly depict presynaptic structures and protrusions (arrowheads). (B) Confocal images showing apposition of pre- and post-synaptic components with coexpression of the cholinergic synaptic vesicle marker *acr-2*::mCherry::RAB-3 (violet) and the AChR reporter ACR-12::GFP (green) in the DD1 synaptic region. (C) Top, confocal images showing ACR-12 receptor clusters as visualized by GFP fluorescence (green) or anti-HA antibody fluorescence (red) 6 hours following antibody injection. Note the extracellular location of the HA epitope tag (schematic below), enabling selective visualization of synaptic receptor clusters at the cell surface. Inset, anti-HA uptake by coelomocytes indicating successful injection. (D) Top, confocal images of UNC-29::GFP and UNC-63::GFP clusters in the DD1 dendrite (*flp-13* promoter) in wild type or *acr-12(ok367)* mutants. Bottom, quantification of the average number of UNC-29::GFP and UNC-63::GFP clusters in the DD1 dendrite for wild type and *acr-12(ok367)* mutants. Each bar represents the mean ± SEM. For this and all subsequent figures, numbers in bars indicate the n for each genotype. $^{**}p<0.01$, $^{***}p<0.001$, student's t-test. Scale bars, 5 μm (A-D).

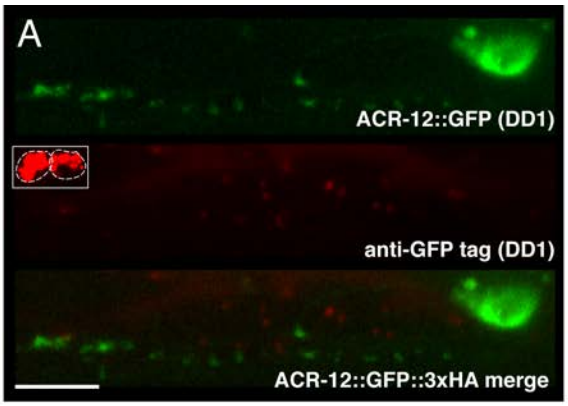
A
ACR-12::GFP (DD1)
anti-GFP tag (DD1)
ACR-12::GFP::3xHA merge

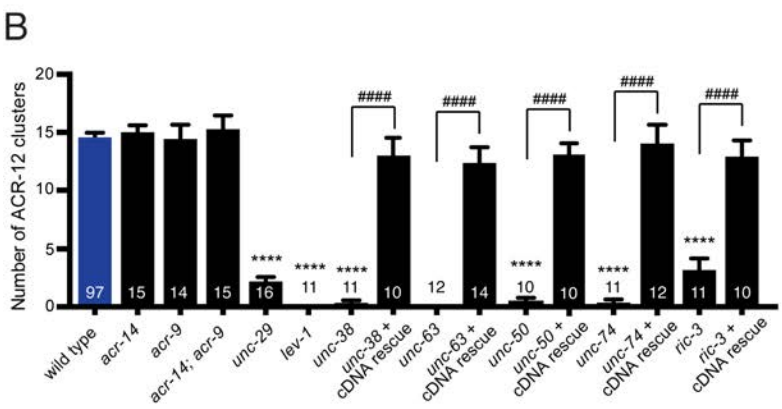
B
Number of ACR-12 clusters
20
15
10
5
0
97
15
14
15
16
11
11
10
12
14
10
10
11
12
11
10
****
####
wild type
acr-14
acr-9
acr-14; acr-9
unc-29
lev-1
unc-38
unc-38 + cDNA rescue
unc-63
unc-63 + cDNA rescue
unc-50
unc-50 + cDNA rescue
unc-74
unc-74 + cDNA rescue
ric-3
ric-3 + cDNA rescue

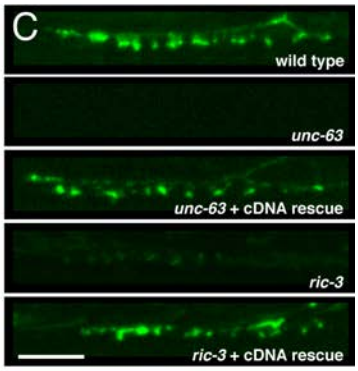
C
wild type
unc-63
unc-63 + cDNA rescue
ric-3
ric-3 + cDNA rescue

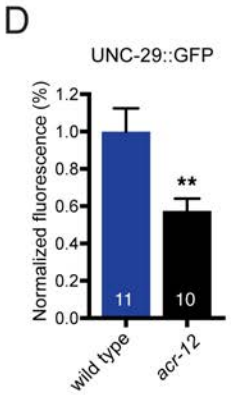
D
UNC-29::GFP
Normalized fluorescence (%)
1.2
1.0
0.8
0.6
0.4
0.2
0.0
11
10
**
wild type
acr-12

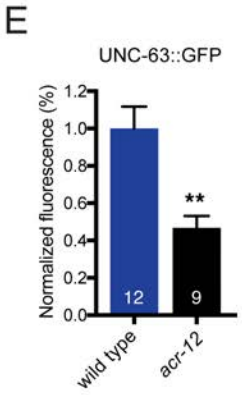
E
UNC-63::GFP
Normalized fluorescence (%)
1.2
1.0
0.8
0.6
0.4
0.2
0.0
12
9
**
wild type
acr-12

Figure 4.4 Mutations in specific AChR subunits and accessory proteins disrupt ACR-12 synaptic delivery and clustering

(A) Confocal images of the DD1 cell body and synaptic region for a wild type animal expressing *flp-13*::ACR-12::GFP::3xHA. Animals were injected with anti-GFP antibodies conjugated to Alexa594 fluorophore and imaged six hours later. Inset, anti-GFP uptake by coelomocytes indicating successful injection, but lack of synaptic ACR-12 labeling due to intracellular location of GFP moiety. Scale bar, 5 μm. (B) Quantification of the average number of ACR-12::GFP clusters in the DD1 synaptic region for the genotypes indicated. For B and C, rescue refers to specific expression of the wild type cDNAs indicated in GABAergic neurons (*unc-47* promoter). Each bar represents the mean ± SEM. ****$p<0.0001$ compared to wild type, ####$p<0.0001$ compared to the indicated mutant genotype, ANOVA with Tukey's multiple comparisons test. (C) Confocal images of ACR-12::GFP in the DD1 synaptic region for the genotypes indicated. Scale bar, 5 μm. (D-E) Quantification of the total UNC-29::GFP (D) or UNC-63::GFP (E) fluorescence in the DD1 synaptic region (*flp-13* promoter) normalized to wild type control for the genotypes indicated. **$p<0.01$, student's t-test.

Neurexin directs cholinergic connectivity with GABAergic neurons

To decipher molecular mechanisms by which these newly defined post-synaptic structures develop, we examined ACR-12::GFP labeling in DD neurons of 27 strains carrying mutations in 35 candidate genes. These candidates predominantly encode scaffold and cell-cell interaction proteins previously implicated in synapse formation, many of which have previously demonstrated expression in GABAergic neurons (Cinar et al., 2005) (**Table 4.1**). Mutations in most genes tested (77%) produce no significant disruption in ACR-12 receptor clustering (**Figure 4.5A**, light blue). A second group, comprising 7 of the 35 genes analyzed (**Figure 4.5A**, green), produces mild to moderate (28-39%) decreases in ACR-12 clustering. Many of the mutants in this second group identify genes that perform previously characterized functions in neuromuscular synapse development (e.g. *lev-10*, *madd-4*) (Gally et al., 2004; Pinan-Lucarre et al., 2014), but appear to play comparatively minor roles in establishing synaptic connectivity with GABAergic neurons.

One of the 35 mutations tested is clearly distinguishable by a striking decrease in ACR-12 clustering. Mutation of the *nrx-1* gene (orange) produces a ~70% reduction in ACR-12 receptor clustering in GABAergic neurons (*nrx-1(ok1649)*, $p<0.0001$) (**Figure 4.5A, B**). *nrx-1* encodes the sole *C. elegans* ortholog of the synaptic organizer neurexin. Neurexin has been well documented to play roles in mammalian synapse formation and function (Chen et al., 2017; Dean et al., 2003; Graf et al., 2004; Missler et al., 2003). Roles for NRX-1 in *C. elegans* synapse formation remain, by comparison, less well defined. Moreover, roles for neurexin in establishing divergent connectivity have not

been previously addressed in any system. Importantly, we do not observe appreciable alterations in the clustering of muscle AChRs in *nrx-1* mutants (**Figure 4.5C**), similar to previously reported findings (Hu et al., 2012). The profound alterations in ACR-12 localization described above, coupled with the lack of effect on muscle AChRs, therefore warranted an in-depth analysis of cholinergic synapses with GABAergic neurons in *nrx-1* mutants.

We first sought to distinguish whether *nrx-1* performs a specific role in synapse formation or serves more generalized functions in the developmental maturation of DD neurons. We studied the developmental remodeling of DD neurons, characterized by the dorsoventral repositioning of synaptic markers, which occurs at the L1/L2 transition in wild type animals (Jin and Qi, 2017; White et al., 1978). In particular, we examined the repositioning of pre- and post-synaptic markers expressed specifically in DD motor neurons (**Figure 4.6A**). Presynaptic remodeling, as measured using the synaptic vesicle marker mCherry::RAB-3, proceeds normally in *nrx-1* mutants, indicating that this process does not require neurexin expression. The clustering of ACR-12 receptors, however, is impaired both prior to and following remodeling in *nrx-1* mutants, suggesting that NRX-1 is required for receptor clustering in each of these developmental stages.

As is the case for mammals, the *C. elegans nrx-1* locus encodes both long (*nrx-1*$_L$) and short (*nrx-1*$_S$) neurexin isoforms (**Figure 4.6B**). The long isoform encodes a single pass transmembrane protein harboring intracellular PDZ binding and interleaved extracellular LNS (laminin-neurexin-sex hormone-binding globulin) and EGF-like domains (**Figure 4.5D**). The *ok1649* allele generates an in-frame deletion, eliminating

861 bp predicted to encode an extracellular LNS domain, raising the possibility that partial NRX-1 function may still be present in this strain. We therefore expanded our analysis to include larger *nrx-1* deletions, three of which (*ds1*, *tm1961*, and *nu485*) are predicted to primarily impact the long isoform, while another (*wy778*) removes the transmembrane and cytoplasmic domains shared by all NRX-1 isoforms (Calahorro and Ruiz-Rubio, 2013; Maro et al., 2015; Tong et al., 2015). All of the deletions tested disrupt ACR-12 receptor clustering in DD GABAergic neurons, with the most severe disruptions occurring in *nrx-1(wy778)* and *nrx-1(nu485)* mutants (**Figure 4.5E**). We also observe a disruption of ACR-12 receptor clustering in VD GABAergic neurons (**Figure 4.5F, G**), indicating a similar requirement for *nrx-1* at synapses with both neuron classes.

In some instances (14 of 34 animals for *nrx-1(wy778)*), we noted that a few ACR-12 receptor clusters remain detectable. We investigated whether these residual ACR-12 receptors are localized to the cell surface by injecting Alexa594 conjugated anti-HA antibody into *nrx-1* mutants expressing ACR-12::GFP::3xHA. Antibody fluorescent signal clearly colocalizes with ACR-12::GFP fluorescence, providing evidence that the few remaining receptor clusters in *nrx-1* mutants are present at the cell surface (**Figure 4.6C**). We interpret this result to indicate that neurexin is not essential for membrane insertion, but rather plays a primary role in localizing or stabilizing receptor clusters at post-synaptic sites.

We next examined whether the localization of putative ACR-12 partnering subunits is also disrupted by mutation of *nrx-1*. As noted above, ACR-12 receptors are formed as heteromeric complexes in GABAergic neurons that likely incorporate the

UNC-29 and UNC-63 AChR subunits. Neurexin deletion (*wy778*) reduces UNC-29::GFP and UNC-63::GFP clusters in DD1 by 60%, consistent with a requirement for neurexin in the proper localization of mature, heteromeric receptor complexes (**Figure 4.6D, E**). In contrast to our findings for GABAergic neurons, *nrx-1* deletion does not appreciably disrupt the clustering of AMPA-type glutamate receptors (**Figure 4.7A**), consistent with the idea that neurexin is not globally required for the establishment of synaptic connectivity in worms. Additionally, we do not observe an appreciable decrease in cholinergic synaptic vesicle clusters, although the reporter used for this analysis (*acr-2*::SNB-1::GFP) does not offer single neuron resolution (**Figure 4.7B**).

To elucidate potential mechanisms by which *nrx-1* may instruct the formation of synapses between cholinergic and GABAergic motor neurons, we evaluated mutations in the *nlg-1* gene. *nlg-1* encodes the sole *C. elegans* ortholog of neuroligin, a well characterized binding partner of neurexin (Banerjee et al., 2017; Boucard et al., 2005; Hu et al., 2012; Ichtchenko et al., 1995; Ichtchenko et al., 1996). We find that mutation of *nlg-1* produces no appreciable defects in ACR-12 receptor clustering (**Figure 4.5A, B**), indicating, surprisingly, that NRX-1 operates independently of NLG-1 to direct post-synaptic development in GABAergic neurons.

Table 4.1 Candidate-based genetic screen
Description of genes surveyed in **Figure 4.5A** and their relation to mammalian genes. Candidates predominantly encode scaffold and cell-cell interaction proteins previously implicated in synapse formation.

***C. elegans* gene**	**Description**	**References**
unc-36	α2δ calcium channel auxiliary subunit	(Saheki and Bargmann, 2009; Tong et al., 2017)
lin-7	homologous to Velis, PDZ domain containing	(Butz et al., 1998; Simske et al., 1996)
lat-2	latrophilin-like	(Willson et al., 2004)
sax-7	L1CAM	(Chen et al., 2001)
agr-1	agrin related	(Hrus et al., 2007)
dgn-2; dgn-3	dystroglycan related	(Johnson et al., 2006)
nab-1	neurabin/spinophilin related	(Hung et al., 2007)
stn-1, stn-2	syntrophins	(Grisoni et al., 2003; Zhou et al., 2008)
zig1-10	two Ig domain family	(Aurelio et al., 2002; Howell and Hobert, 2016)
lon-2	member of glypican family of heparan sulfate proteoglycans	(Gumienny et al., 2007)
casy-1	calsyntenin related	(Ikeda et al., 2008)
nlg-1	neuroligin	(Hunter et al., 2010)
oig-1	single Ig domain family	(He et al., 2015; Howell et al., 2015)
F38B6.6	transmembrane and TPR repeat containing	(Zhou et al., 2016)
unc-52	perlecan related	(Rogalski et al., 2001)
lin-2	membrane associated guanylate kinase (MAGUK) family, highly similar to CASK	(Cohen et al., 1998; Hoskins et al., 1996)
unc-40	DCC/netrin receptor	(Chan et al., 1996)
rig-3	two Ig domain family	(Schwarz et al., 2009)
cam-1	Ror receptor tyrosine kinase	(Forrester et al., 1999; Francis et al., 2005; Kim and Forrester, 2003)
madd-4	Punctin-like, ADAMTS-like family	(Pinan-Lucarre et al., 2014; Seetharaman et al., 2011)
syd-1	contains PDZ, C2, and rhoGAP-like domains	(Hallam et al., 2002)
rpy-1	rapsyn related	(Nam et al., 2009)
lev-10	CUB/LDL transmembrane containing	(Gally et al., 2004)
nrx-1	neurexin	(Haklai-Topper et al., 2011)

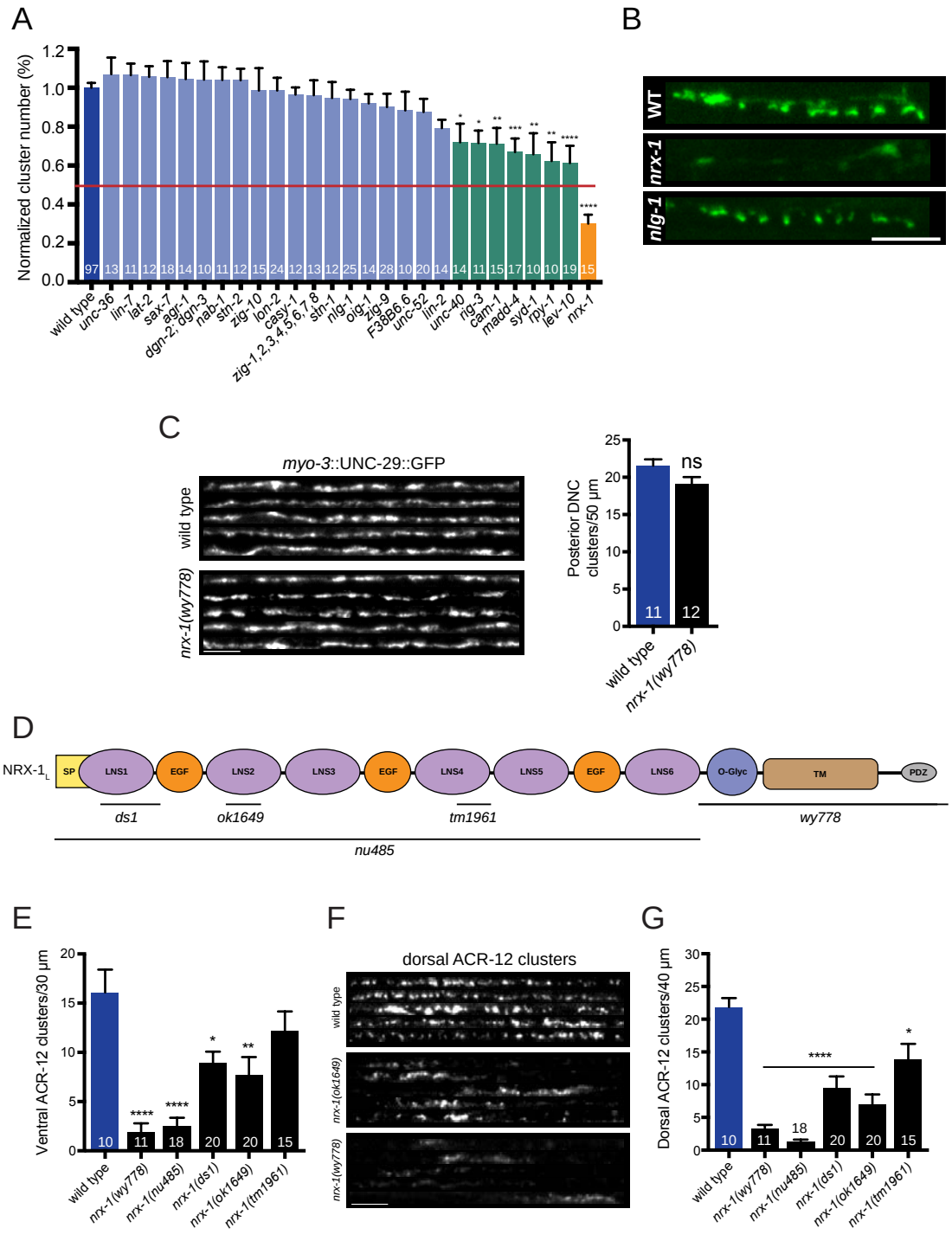
A
Normalized cluster number (%)
wild type
unc-36
lin-7
lat-2
sax-7
agr-1
dgn-2; dgn-3
nab-1
stn-2
zig-10
lon-2
casy-1
zig-1,2,3,4,5,6,7,8
stn-1
nlg-1
oig-1
zig-9
F38B6.6
unc-52
lin-2
unc-40
rig-3
cam-1
madd-4
syd-1
rpy-1
lev-10
nrx-1
B
WT
nrx-1
nlg-1
C
myo-3::UNC-29::GFP
wild type
nrx-1(wy778)
Posterior DNC clusters/50 µm
ns
D
NRX-1L
SP
LNS1
EGF
LNS2
LNS3
EGF
LNS4
LNS5
EGF
LNS6
O-Glyc
TM
PDZ
ds1
ok1649
tm1961
wy778
nu485
E
Ventral ACR-12 clusters/30 µm
F
dorsal ACR-12 clusters
G
Dorsal ACR-12 clusters/40 µm

Figure 4.5 *nrx-1/n*eurexin is required for AChR localization in GABAergic motor neurons, but not muscles

(A) Quantification of ACR-12::GFP clusters in the synaptic region of the DD1 dendrite for the genotypes indicated, normalized to wild type. Red line indicates 50% reduction in puncta number. Colored bars indicate wild type (blue), no effect (light blue), modest effect (green), and severe clustering defects (orange). **p*<0.05, ***p*<0.01, ****p*<0.001, *****p*<0.0001, ANOVA with Dunnett's multiple comparisons test. (B) Representative confocal images showing ACR-12::GFP clusters in the synaptic region of the DD1 dendrite for wild type (WT), *nrx-1(ok1649),* and *nlg-1(ok259*) mutants. Scale bar, 5 µm. (C) Left, representative confocal images of the dorsal nerve cord from five wild type and *nrx-1(wy778)* adult animals expressing *myo-3*::UNC-29::GFP. Scale bar, 5 µm. Right, quantification of UNC-29::GFP clusters in a 50 µm region of the posterior dorsal nerve cord. (D) Domain structure of the NRX-1 long isoform ($NRX\text{-}1_L$). Deletion regions are indicated (black line). N-terminal signal peptide (SP), extracellular LNS, EGF, transmembrane (TM), PDZ binding (PDZ) domains, and O-linked glycosylation site are shown. (E) Quantification of ACR-12 receptor clusters *(unc-47*::ACR-12::GFP) in the ventral nerve cord for the genotypes indicated. **p*<0.05, ***p*<0.01, *****p*<0.0001, ANOVA with Dunnett's multiple comparisons test. (F) Representative confocal images showing dorsal nerve cord ACR-12 receptor clusters for five wild type, *nrx-1(ok1649),* and *nrx-1(wy778)* animals expressing *unc-47*::ACR-12::GFP. Scale bar, 5 µm. (G) Quantification of ACR-12 receptor clusters (*unc-47*::ACR-12::GFP) in the dorsal nerve cord for the genotypes indicated. **p*<0.05, *****p*<0.0001, ANOVA with Dunnett's multiple comparisons test.

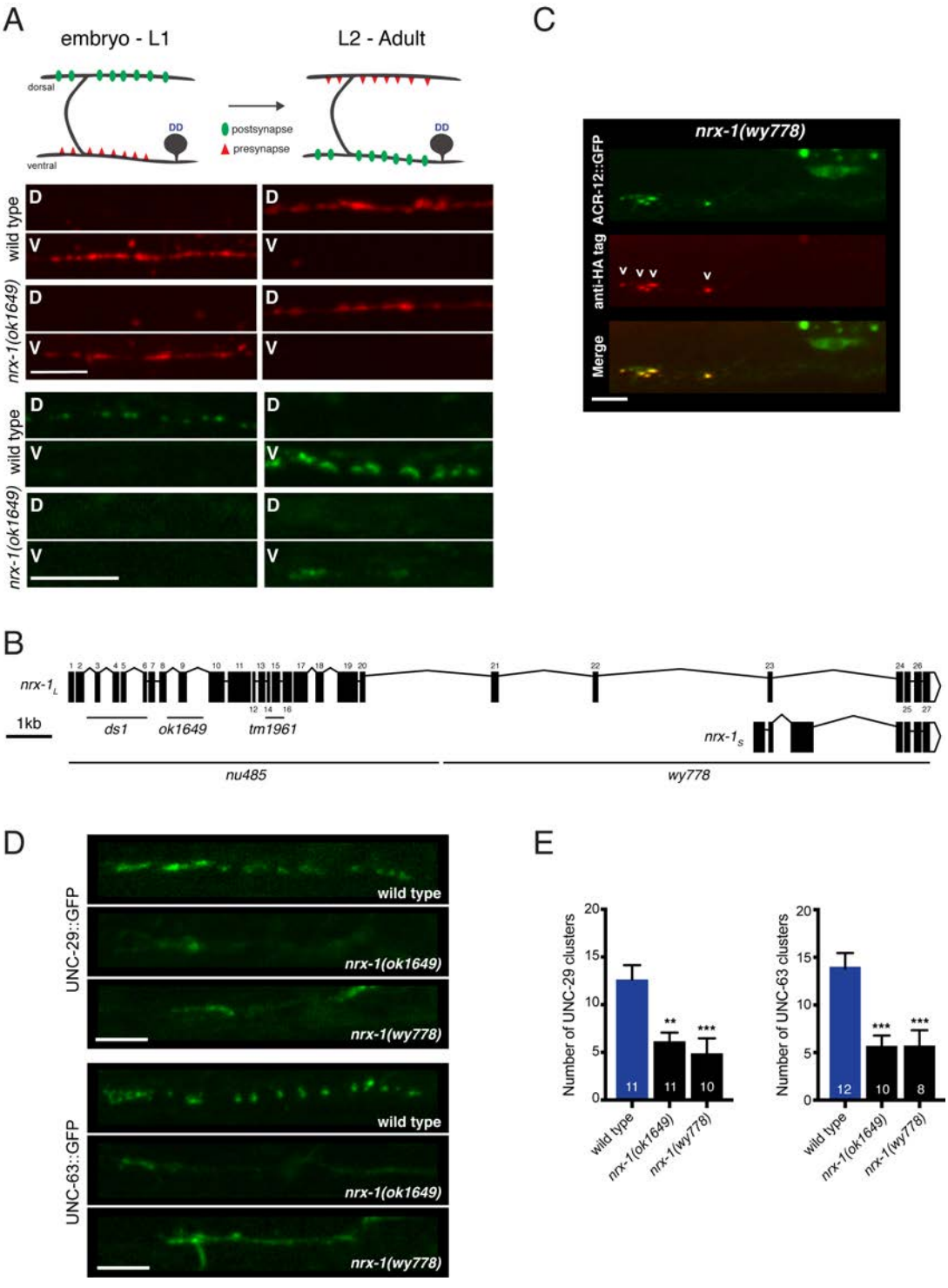
A
embryo - L1
L2 - Adult
dorsal
ventral
DD
postsynapse
presynapse
wild type
nrx-1(ok1649)
D
V
C
nrx-1(wy778)
ACR-12::GFP
anti-HA tag
Merge
B
nrx-1L
nrx-1S
1kb
ds1
ok1649
tm1961
nu485
wy778
D
UNC-29::GFP
UNC-63::GFP
wild type
nrx-1(ok1649)
nrx-1(wy778)
E
Number of UNC-29 clusters
Number of UNC-63 clusters
11
11
10
12
10
8
**
***

Figure 4.6 Loss of functional *nrx-1* disrupts ACR-12 AChR localization, but *nrx-1* is not required for AChR membrane insertion or synaptic remodeling
(A) Top, schematic depicting pre-synaptic (red) and post-synaptic (green) remodeling of DD motor neurons during development. Bottom, confocal images of wildtype and *nrx-1(ok1649)* mutants imaged before (<14 hr after hatch) and after (approximately 20 hr after hatch) the remodeling process. The presynapse is labeled with *flp-13*::mCherry::RAB-3 (red), while the postsynapse is labeled with *flp-13*::ACR-12::GFP (green). D indicates dorsal, V indicates ventral. Scale bars, 5 μm. (B) Schematic representation of the *nrx-1* locus, including long (*nrx-1*$_L$) and short (*nrx-1*$_S$) isoforms. Regions affected by available deletions are indicated (black lines). Exons (shaded boxes) are numbered and connected by lines representing introns. (C) Confocal images of the DD1 cell body and synaptic region for *nrx-1(wy778)* mutants expressing *flp-13*::ACR-12::GFP::3xHA. Animals were injected with anti-HA AlexaFluor594 antibodies (red) to label surface receptors and imaged six hours later. Scale bar, 5 μm. (D) Confocal images of UNC-29::GFP (top) and UNC-63::GFP (bottom) in the DD1 synaptic region (*flp-13* promoter) for the genotypes indicated. Scale bars, 5 μm. (E) Quantification of UNC-29::GFP (left) and UNC-63::GFP (right) clusters in the synaptic region of the DD1 dendrite in wild type and *nrx-1* mutants. ***p*<0.01, ****p*<0.001, ANOVA with Dunnett's multiple comparisons test.

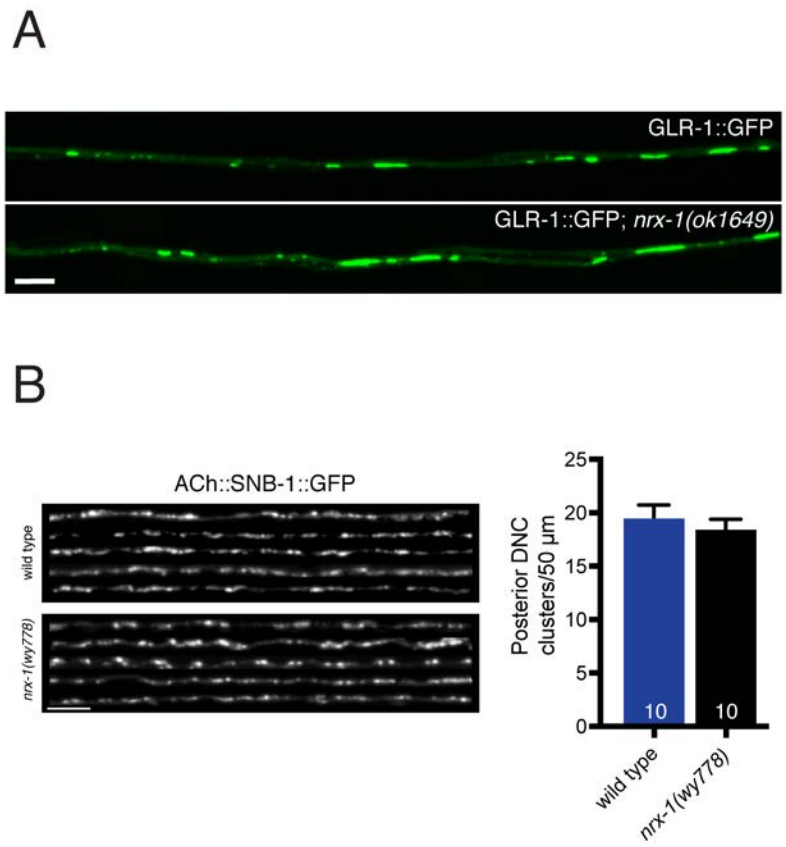

Figure 4.7 Neurexin is not essential for AMPAR localization or synaptic vesicle clusters in cholinergic motor neurons
(A) Representative confocal images of GLR-1::GFP in the anterior ventral nerve cord of adult animals. Scale bar, 5 µm. (B) Left, representative confocal images of the dorsal nerve cord from five wild type and *nrx-1(wy778)* adult animals expressing *acr-2*::SNB-1::GFP. Scale bar, 5 µm. Right, quantification of SNB-1::GFP clusters in a 50 µm region of the posterior dorsal nerve cord.

Post-synaptic morphological development requires NRX-1

We next investigated whether neurexin is required for development or maintenance of the spine-like processes we observe in the DD1 dendrite. Wild type animals (at the L4 stage) have an average of 7-8 of these spiny protrusions within the synaptic region of the anterior DD1 dendrite (**Figure 4.8A, B**). All of the *nrx-1* mutants tested have strikingly reduced numbers of spiny protrusions. For example, only two spiny protrusions are visible on average in *nrx-1(ok1649),* and *nrx-1(wy778)* mutants show a near complete absence of spines (**Figure 4.8A, B**). *nrx-1* deletion also significantly reduces spiny protrusions in L2 animals (the earliest stage at which they are visible) (**Figure 4.9A**), suggesting that neurexin is required for spine outgrowth rather than maintenance. To elucidate structural components of NRX-1 required for spine outgrowth and receptor localization, we used CRISPR to engineer specific mutations that disrupt the PDZ binding motif located at the intracellular NRX-1 C-terminus. Mutation of the NRX-1 PDZ binding domain produces a strong reduction in both receptor (**Figure 4.9B**) and spine number (**Figure 4.8A, B**), consistent with prior studies indicating the importance of this domain for interactions with intracellular partners, such as CASKs, VELIs, and Mints (Biederer and Sudhof, 2000; Butz et al., 1998; Hata et al., 1996). In accordance with our finding that *nlg-1* is not required for ACR-12::GFP localization, mutation of *nlg-1* does not alter spine number (**Figure 4.8A, B**), arguing against an essential role for neuroligin in the formation of cholinergic synapses with GABAergic neurons. Likewise, spine number is not appreciably altered in either *acr-12* or *unc-63* mutants (**Figure 4.8A,**

B), indicating that spine outgrowth proceeds normally in the absence of functional ACR-12 receptors.

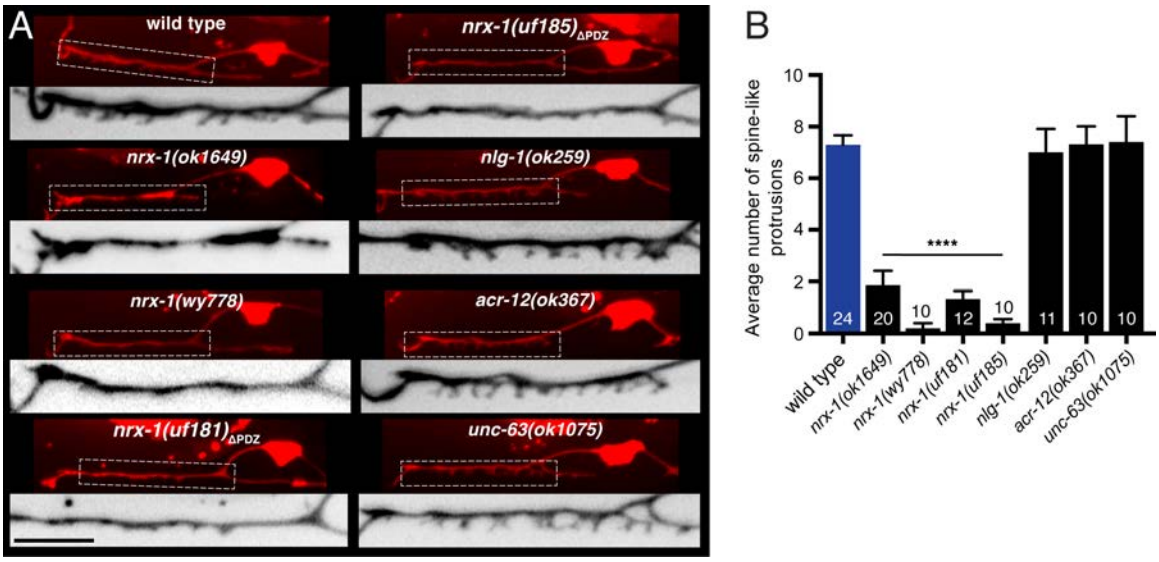

Figure 4.8 Synaptic architecture is dependent on *nrx-1*/neurexin
(A) Fluorescent confocal images of spine-like protrusions in the synaptic region of the DD1 dendrite (*flp-13*::mCherry) for the genotypes indicated. Inverted images show expanded views of the synaptic regions (indicated by dashed boxes in fluorescent images). Scale bar, 5 µm. (B) Quantification of spine-like protrusions in the DD1 dendrite for the genotypes indicated. ****p<0.0001 compared to wild type control, ANOVA with Dunnett's multiple comparisons test.

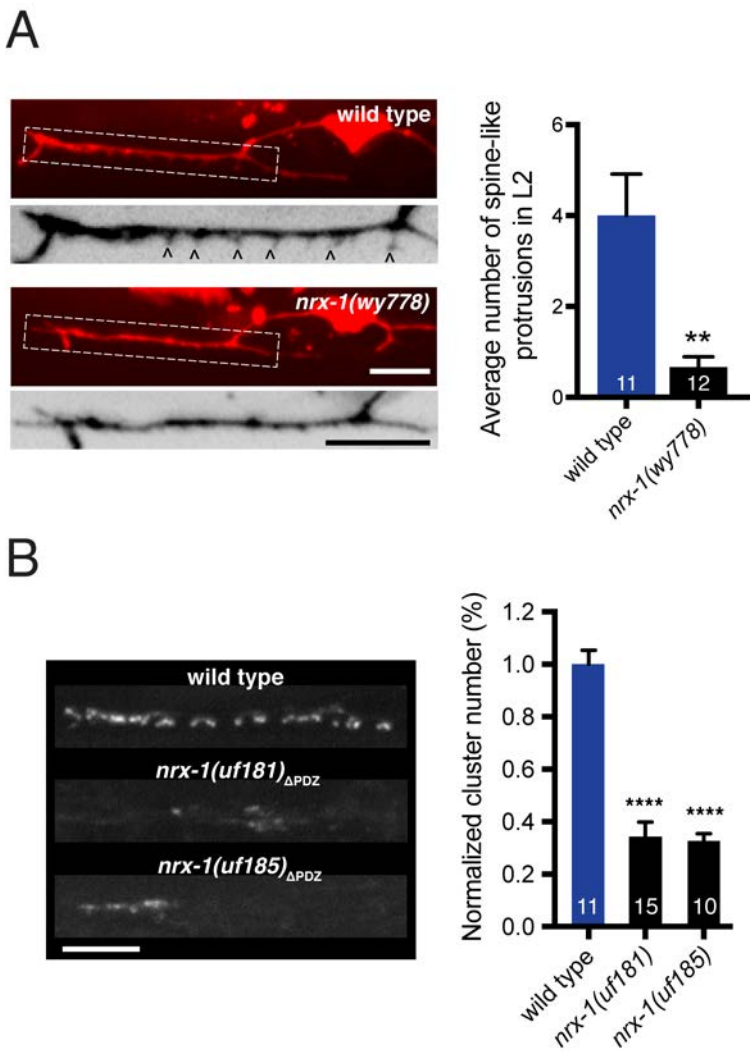

Figure 4.9 NRX-1 is required for spine outgrowth, and NRX-1 function at synapses is dependent on its intracellular PDZ binding domain

(A) Left, representative confocal images of the DD1 synaptic region in second larval stage wild type and *nrx-1(wy778)* mutants expressing *flp-13*::mCherry. Arrowheads indicate spine-like protrusions. Inverted images show expanded views of the synaptic regions (indicated by dashed boxes in fluorescent images). Scale bars, 5 µm. Right, quantification of DD1 spine-like protrusions in second larval stage animals for wild type and *nrx-1(wy778)* mutants. ***p*<0.01, student's t test. (B) Left, representative confocal images of ACR-12::GFP clusters in the DD1 synaptic region for the genotypes indicated. Scale bar, 5 µm. Right, quantification of ACR-12::GFP clusters in the synaptic region of the DD1 dendrite for the genotypes indicated, normalized to control (*ufEx441*). *****p*<0.0001, ANOVA with Dunnett's multiple comparisons test.

nrx-1 is expressed and functionally required in cholinergic motor neurons

To understand how NRX-1 regulates the formation of cholinergic synapses with GABAergic neurons, we sought to define the requirements for *nrx-1* expression. We first examined expression of a *nrx-1*$_L$::GFP transcriptional reporter incorporating ~4.8 kb of sequence upstream of the *nrx-1*$_L$ start site, and found that this reporter is strongly expressed in cholinergic motor neurons (**Figure 4.10A**). We next asked whether specific *nrx-1* expression in cholinergic neurons is sufficient to rescue the post-synaptic maturation defects of *nrx-1* mutants. We found that expression of a *nrx-1*$_L$ rescuing construct in cholinergic neurons is sufficient to reverse the ACR-12 clustering defects of *nrx-1(wy778)* mutants, while expression in either GABAergic neurons or muscles fails to rescue (**Figure 4.10B-D**). Notably, cholinergic-specific expression of *nrx-1*$_L$ also restores spine-like protrusions in *nrx-1* mutants (**Figure 4.11A**). Thus, our results suggest that presynaptic NRX-1 acts non-autonomously to direct post-synaptic assembly in GABAergic neurons. To investigate this possibility in more detail, we examined the subcellular localization of NRX-1 by expressing GFP-tagged NRX-1$_L$ (NRX-1$_L$::GFP) (Maro et al., 2015) in a subset of cholinergic neurons (DA/DB). Expression of *unc-129*::NRX-1$_L$::GFP produces discrete puncta along the dorsal nerve cord where the synaptic outputs of DA/DB neurons are exclusively located (**Figure 4.11B**, left). NRX-1$_L$::GFP clusters colocalize with clusters of mCherry::RAB-3 fluorescence, providing evidence that NRX-1$_L$ is preferentially localized to cholinergic presynaptic sites (**Figure 4.10E, F**). Loss of *nlg-1* function does not affect NRX-1$_L$::GFP (**Figure 4.11B**), arguing against a requirement for NLG-1 in NRX-1 localization to presynaptic sites. NRX-

1_L::GFP localization is not appreciably altered by *acr-12* deletion, suggesting that the positioning of NRX-1 at presynaptic terminals occurs independently of post-synaptic receptor clustering (**Figure 4.11C**). Our results indicate NRX-1 positioning at presynaptic sites occurs independently of post-synaptic receptor localization, and raise the intriguing possibility that NRX-1 localization to the presynaptic domain may serve as an initiation signal for developmental maturation of post-synaptic specializations in GABAergic neurons.

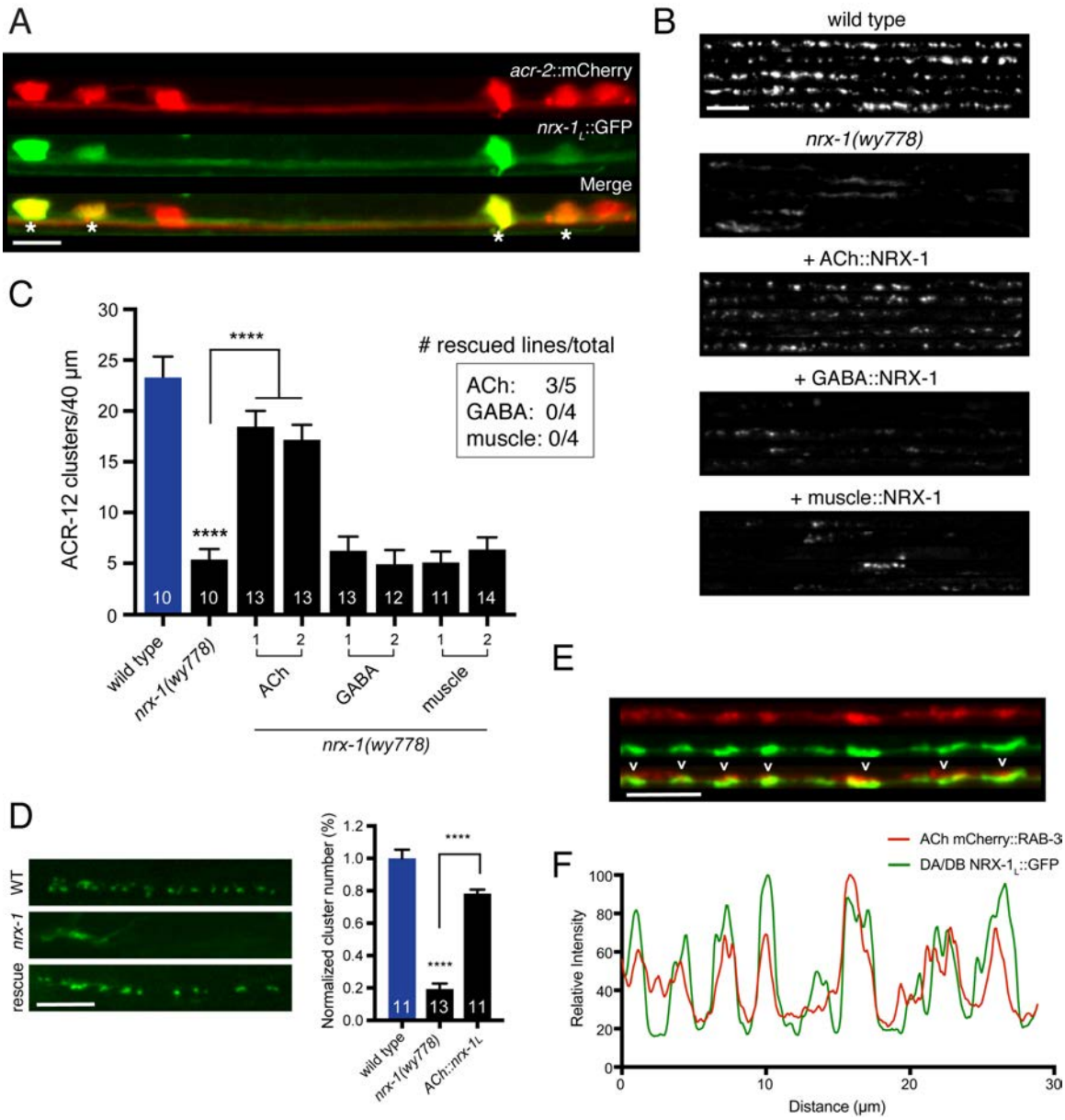
A
acr-2::mCherry
nrx-1L::GFP
Merge
B
wild type
nrx-1(wy778)
+ ACh::NRX-1
+ GABA::NRX-1
+ muscle::NRX-1
C
ACR-12 clusters/40 µm
rescued lines/total
ACh: 3/5
GABA: 0/4
muscle: 0/4
wild type
nrx-1(wy778)
ACh
GABA
muscle
nrx-1(wy778)
D
WT
nrx-1
rescue
Normalized cluster number (%)
wild type
nrx-1(wy778)
ACh::nrx-1L
E
F
ACh mCherry::RAB-3
DA/DB NRX-1L::GFP
Relative Intensity
Distance (µm)

Figure 4.10 Cell-specific expression of neurexin in cholinergic motor neurons restores ACR-12 localization to synapses

(A) Confocal images of the ventral nerve cord in a transgenic strain expressing *nrx-1*$_L$::GFP together with the cholinergic motor neuron marker *acr-2*::mCherry. Asterisks indicate coexpression. Scale bar, 5 µm. (B) Confocal images of the dorsal nerve cord (*unc-47*::ACR-12::GFP) for the genotypes indicated. For each, five representative images are shown. In B and C, rescue was evaluated by cholinergic (*unc-17β* promoter), GABAergic (*unc-47* promoter), or muscle-specific (*myo-3* promoter) expression of a NRX-1$_L$ minigene in *nrx-1(wy778)* mutants. Scale bar, 5 µm. (C) Quantification of ACR-12::GFP receptor clusters in the dorsal nerve cord for the genotypes indicated. ****p<0.0001, ANOVA with Tukey's multiple comparisons test. Two transgenic lines are shown for each rescue construct. Inset, number of rescuing lines/total transgenic lines tested for each construct. (D) Left, confocal images of ACR-12::GFP clusters in the DD1 synaptic region for the genotypes indicated. Rescue refers to cholinergic-specific expression (*ufEx1114*, line #1 in **Figure 4.10C**) of NRX-1$_L$ in *nrx-1(wy778)* mutants. Scale bar, 5 µm. Right, quantification of ACR-12::GFP clusters in the DD1 synaptic region for the genotypes indicated, normalized to control (*ufEx441*). ****p<0.0001, ANOVA with Tukey's multiple comparisons test. (E) Confocal images of the dorsal nerve cord in an adult animal expressing NRX-1$_L$::GFP (*unc-129* promoter) with mCherry::RAB-3 (*acr-2* promoter). Colocalization is indicated by arrowheads. Scale bar, 5 µm. (F) Line scans showing relative fluorescent intensity of NRX-1$_L$::GFP (green) and mCherry::RAB-3 (red) for a 30 µm region of the dorsal nerve cord.

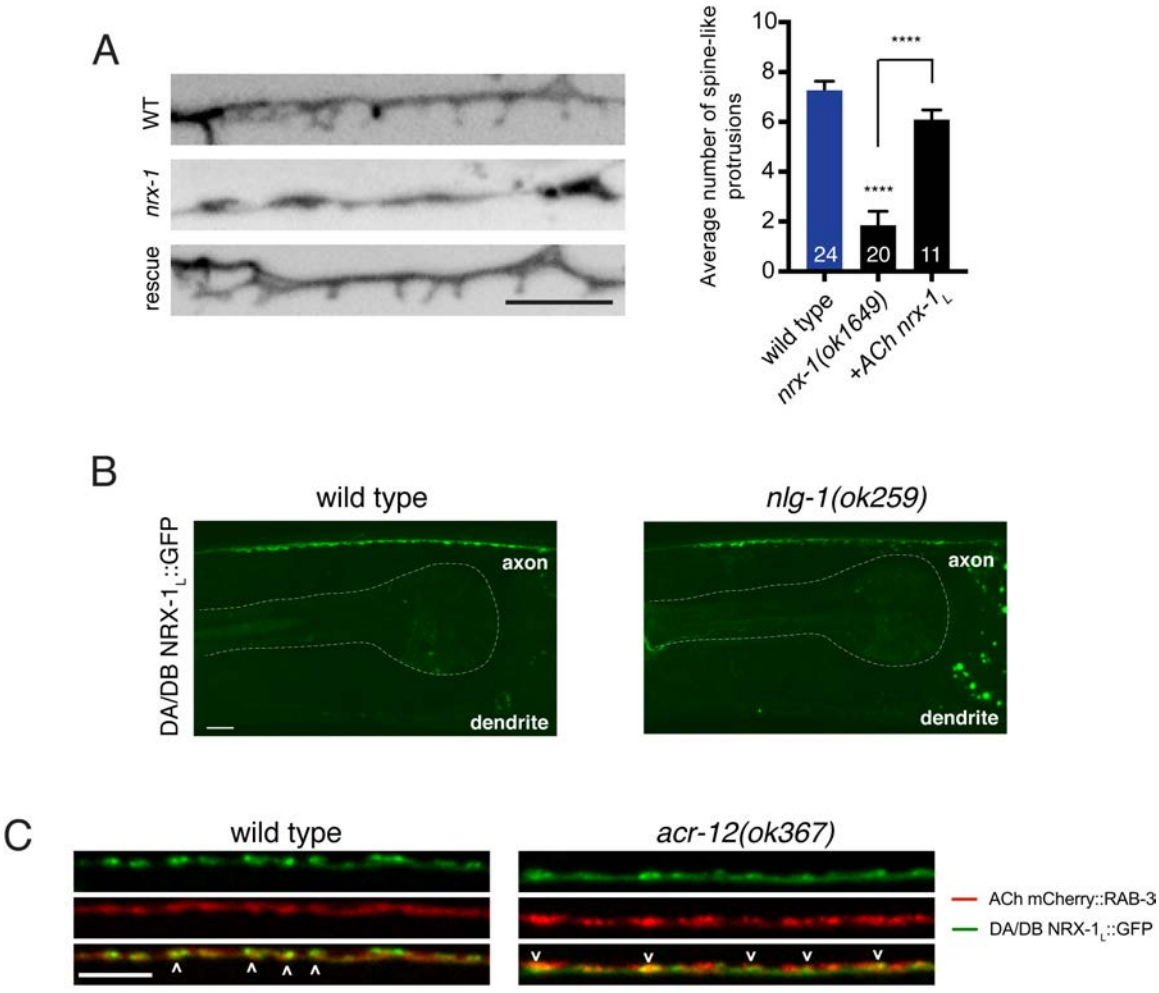

Figure 4.11 NRX-1 acts presynaptically to regulate spine outgrowth, and loss of *nlg-1* or *acr-12* does not affect NRX-1 localization to synapses
(A) Left, inverted images of spine-like protrusions in the synaptic region of the DD1 dendrite (*flp-13*::mCherry) for the genotypes indicated. Rescue refers to cholinergic expression (*ufEx1114*) of NRX-1_L in *nrx-1(ok1649)* mutants. Scale bar, 5 µm. Right, quantification of spine-like protrusions in the DD1 dendrite for the genotypes indicated. ****p<0.0001, ANOVA with Tukey's multiple comparisons test. (B) Confocal images of NRX-1_L::GFP in the dorsal nerve cord of wild type or *nlg-1(ok259)* mutant. Pharynx is outlined by white dashed line. Scale bar, 5 µm. (C) Confocal images of the dorsal nerve cord in adult animals expressing NRX-1_L::GFP (*unc-129*::NRX-1_L::GFP) with mCherry::RAB-3 (*acr-2*::mCherry::RAB-3) in wild type and *acr-12(ok367)* mutant. Colocalization is indicated by arrowheads. Scale bar, 5 µm.

The COE-type transcription factor unc-3 directly controls neurexin expression

We have previously demonstrated that mutation of the COE-type (Collier/Olf/Ebf) transcription factor *unc-3* disrupts ACR-12 clustering in VD GABAergic neurons (Barbagallo et al., 2017). In light of our findings here that *nrx-1* deletion similarly disrupts ACR-12 clustering and spine-like protrusion outgrowth in DD neurons (**Figure 4.12A, B),** we next investigated the role of UNC-3 transcriptional regulation in the development of cholinergic connectivity with GABAergic DD neurons. Prior work has shown that activity of UNC-3 is essential for the specification of cholinergic neurotransmitter identity (Kratsios et al., 2015; Kratsios et al., 2011). To investigate the requirement for *unc-3* in ACR-12 clustering, we first evaluated whether cholinergic transmission itself is critical for the development of post-synaptic specializations on DD neurons. We found that mutations in the *unc-17* cholinergic vesicular ACh transporter produced no appreciable changes in spine-like protrusion number or ACR-12 clusters (**Figure 4.12B**), arguing against a strong requirement for cholinergic transmission in the formation of these structures.

We next asked whether UNC-3 transcriptional regulation of *nrx-1* expression is critical for the development of cholinergic connectivity with GABAergic neurons. To address this question, we tested whether *unc-3* is required for expression of the *nrx-1*$_L$::GFP transcriptional reporter described above. We found that mutation of *unc-3* significantly reduces *nrx-1*$_L$::GFP fluorescence in motor neuron cell bodies of the ventral nerve cord, as well as the majority of fluorescence in ventral cord processes (**Figure 4.12C, D).** The remaining ventral cord GFP fluorescence is associated with the processes

of head neurons that project into the nerve cord, which are presumably not subject to *unc-3* regulation. We next used fluorescent *in situ* hybridization (FISH) to determine the effects of *unc-3* mutation on *nrx-1* mRNA abundance. Fluorescent signals indicating *nrx-1* mRNA (primarily targeting the *nrx-1*$_L$ isoforms) are clearly associated with cholinergic motor neuron cell bodies (co-labeled with *unc-17*::GFP) in wild type animals (**Figure 4.12E**), consistent with our prior analysis using the *nrx-1*$_L$::GFP transcriptional reporter. The smFISH signals are strongly diminished in *nrx-1(nu485)* deletion mutants (**Figure 4.12E, F**), confirming they accurately report *nrx-1* mRNA abundance. The number of labeled *nrx-1* mRNA signals in cholinergic motor neurons is strikingly reduced by mutation of *unc-3*, consistent with the possibility that *nrx-1* is a transcriptional target of *unc-3* (**Figure 4.12E, F**).

We noted that a second *nrx-1*$_L$ transcriptional reporter incorporating only ~2 kb of *nrx-1* regulatory sequence did not produce strong fluorescence in ventral cord motor neurons (**Figure 4.12C, D**). We reasoned that regulatory elements required for *nrx-1* expression in these neurons may be present in the sequence that differs across these two transcriptional reporters (2 kb versus 4.8 kb) (**Figure 4.12C, D**). As both mammalian COE transcription factors and UNC-3 bind a conserved COE binding motif (TCCCNN$^{G}/_{A}{}^{G}/_{A}{}^{G}/_{A}{}^{G}/_{A}$) to regulate transcription of target genes (Kim et al., 2005; Kratsios et al., 2011; Wang et al., 2015; Wang et al., 1993), we searched for COE binding motifs within this region. We identified a potential COE motif (TCCCAAAGGG) located approximately 20 bp downstream from the 5' end of the 4.8 kb *nrx-1*$_L$::GFP transcriptional reporter. Mutation of this site (T<u>CCC</u>AAAGGG >> T<u>AAA</u>AAAGGG)

within the 4.8 kb *nrx-1*$_L$::GFP transcriptional reporter eliminates all fluorescence from ventral cord motor neurons, while fluorescence in the processes extending from head neurons remains visible (**Figure 4.12C, D**), offering evidence that UNC-3 directly regulates *nrx-1* transcription in ventral cord neurons.

We reasoned that forced expression of *nrx-1*$_L$ in cholinergic neurons using a promoter not subject to *unc-3* regulation may allow NRX-1 to coordinate synapse development independently of UNC-3 transcriptional regulation. We expressed the *nrx-1*$_L$ isoform using a regulatory region of the *unc-3* gene that drives expression in ventral cord cholinergic neurons (Barbagallo et al., 2017). We found that cholinergic-specific expression of the *nrx-1*$_L$ isoform significantly restored receptor clusters in the dendritic region of *unc-3* animals (**Figure 4.12G**), indicating that the lack of ACR-12 receptor clusters in *unc-3* mutants is due to the absence of *nrx-1* expression. Our findings define the gene regulatory mechanisms controlling neurexin expression in presynaptic neurons and illustrate their involvement in the establishment of synaptic connectivity.

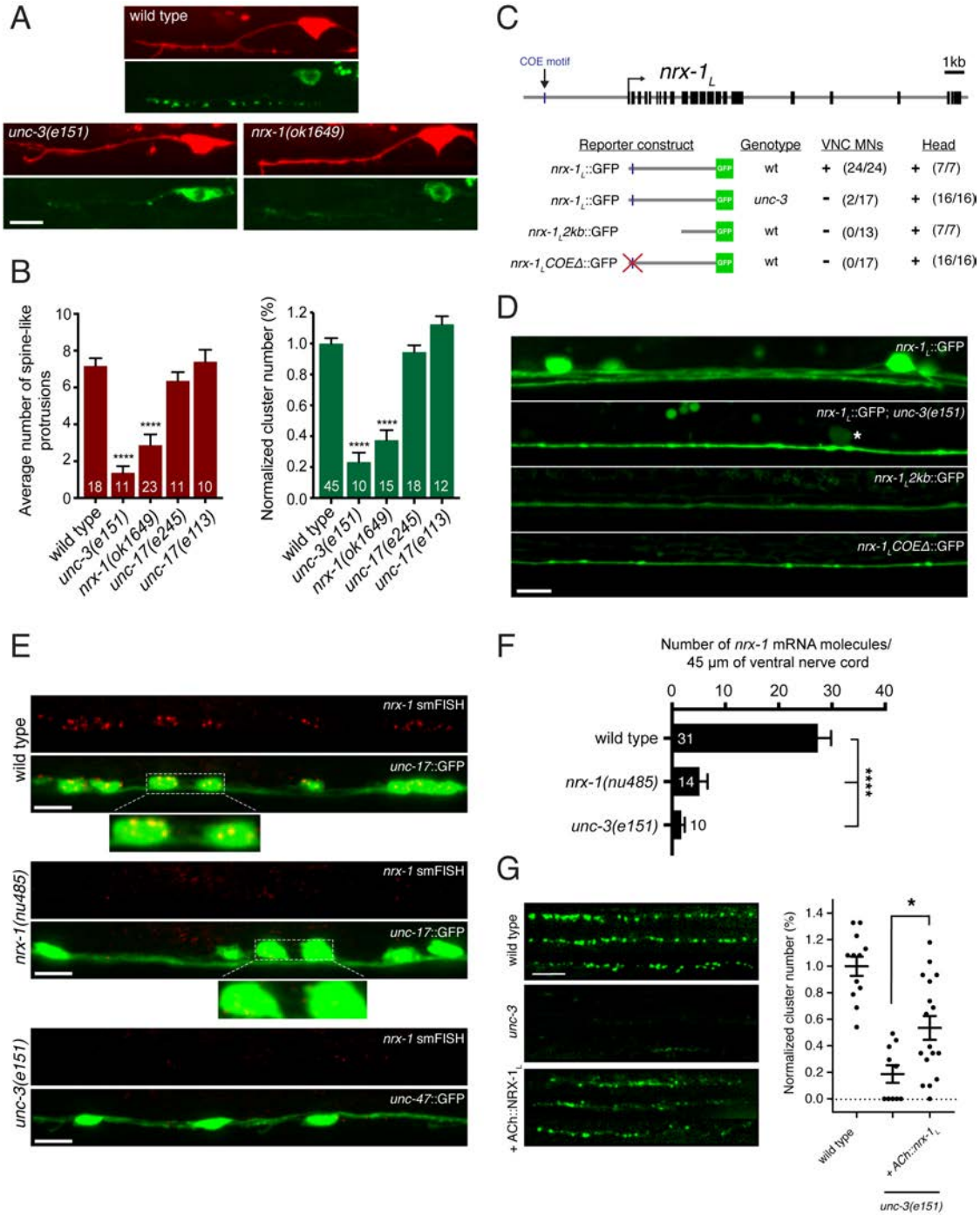
A
wild type
unc-3(e151)
nrx-1(ok1649)
B
Average number of spine-like protrusions
wild type
unc-3(e151)
nrx-1(ok1649)
unc-17(e245)
unc-17(e113)
Normalized cluster number (%)
C
COE motif
nrx-1L
1kb
Reporter construct
Genotype
VNC MNs
Head
nrx-1L::GFP
wt
+ (24/24)
+ (7/7)
unc-3
- (2/17)
+ (16/16)
nrx-1L2kb::GFP
- (0/13)
nrx-1LCOEΔ::GFP
- (0/17)
D
nrx-1L::GFP
nrx-1L::GFP; unc-3(e151)
nrx-1L2kb::GFP
nrx-1LCOEΔ::GFP
E
nrx-1 smFISH
unc-17::GFP
nrx-1(nu485)
unc-3(e151)
unc-47::GFP
F
Number of nrx-1 mRNA molecules/ 45 µm of ventral nerve cord
wild type
nrx-1(nu485)
unc-3(e151)
G
+ ACh::NRX-1L
Normalized cluster number (%)
+ ACh::nrx-1L
unc-3(e151)

Figure 4.12 Transcriptional control of neurexin expression in ACh motor neurons by UNC-3

(A) Confocal images of the DD1 synaptic region and cell soma in wild type and *nrx-1(ok1649)* and *unc-3(e151)* mutants expressing *flp-13*::mCherry (upper) or *flp-13*::ACR-12::GFP (lower). Note the absence of spine-like protrusions and ACR-12 receptor clusters in *unc-3* and *nrx-1* mutants. Although we also note variable defects in neurite extension in *unc-3* mutants, reductions in spine-like protrusions and ACR-12 clusters are clearly evident when neurite extension appears unaffected. Notably, *flp-13*::mCherry fluorescence is not altered by mutation of *unc-3*, arguing against *unc-3* regulation of the *flp-13* promoter. (B) Left, quantification of spine-like protrusions in the DD1 dendrite for the genotypes indicated. ****p<0.0001, ANOVA with Dunnett's multiple comparisons test. Right, quantification of ACR-12::GFP clusters in the DD1 synaptic region for the genotypes indicated, normalized to control (*ufIs126)*. ****p<0.0001, ANOVA with Dunnett's multiple comparisons test. (C) Mutational analysis of the regulatory region of the *nrx-1*$_L$ promoter. Upper, genomic organization of the *nrx-1* locus. Black boxes, exons. Blue line, COE motif upstream of the *nrx-1* start site. Lower, schematics of promoter regions fused with GFP (green) corresponding to the images in D. (+) indicates strong expression in ventral nerve cord or head neurons of fourth larval stage animals, (-) indicates lack of expression. Number of animals with GFP expression in either ventral nerve cord or head neurons is indicated in parentheses. (D) Confocal images of *nrx-1*$_L$::GFP expression in the ventral nerve cord for the genotypes indicated. Note the decreased *nrx-1*$_L$::GFP fluorescence in *unc-3(e151)* mutants, with expression from a truncated (2 kb) promoter (*nrx-1*$_L$*2kb*), or with disruption of the COE motif (*nrx-1*$_L$*COE∆*). The remaining fluorescent signal is associated with processes originating from head neurons. (E) Fluorescent *in situ* hybridization (FISH) signals indicating *nrx-1* mRNA abundance in wild type, *nrx-1(nu485),* and *unc-3(e151)* mutant animals expressing *unc-17*::GFP or *unc-47*::GFP to visualize the ventral nerve cord. mRNA molecules are labeled by CAL Fluor® Red 590 Dye conjugated probes and appear as red dots. Insets, expanded views of mRNA labeling associated with cholinergic motor neuron cell bodies. (F) Quantification of *nrx-1* mRNA molecules per 45 µm segment of the ventral nerve cord for the genotypes indicated. ****p<0.0001, ANOVA with Dunnett's multiple comparisons test. (G) Left, representative confocal images showing ACR-12::GFP clusters in the dorsal nerve cord for three wild type, *unc-3(e151)* or *unc-3* rescue animals expressing *unc-47*::ACR-12::GFP. Rescue refers to cholinergic-specific (*unc-3* promoter) expression of NRX-1$_L$ in *unc-3(e151)* mutants (*ACh::nrx-1*$_L$*)*. Right, scatterplot of ACR-12::GFP clusters in a 40 µm region of the dorsal nerve cord for the genotypes indicated, normalized to control. *p<0.05, ANOVA with Tukey's multiple comparisons test. Scale bars, 5 µm (A, D-E, G).

nrx-1 deletion impairs cholinergic neurotransmission onto GABAergic neurons

To investigate how *nrx-1* deletion impacts the spatial arrangement of pre- and post-synaptic specializations, we examined strains coexpressing ACR-12::GFP in GABAergic neurons with the synaptic vesicle marker mCherry::RAB-3 in cholinergic neurons. In the wild type, ACR-12 receptor clusters at the tips of spiny protrusions are submerged within the presynaptic domains of cholinergic axons, where synaptic contacts are presumably located (**Figure 4.13A**, left). In *nrx-1* mutants, however, we noted a prominent gap between the neurites of the pre- and post-synaptic neurons (**Figure 4.13A**, right), suggesting that *nrx-1* coordinates the extension of receptor-bearing spiny protrusions to presynaptic domains of cholinergic axons. These results, in combination with the lack of an appreciable effect on muscle synapses described above, predict that *nrx-1* deletion would impair cholinergic synaptic activation of GABAergic neurons, while cholinergic transmission onto muscles would remain unaffected.

We recorded Ca^{2+} transients from either GABAergic motor neurons or muscles immediately following presynaptic cholinergic depolarization in order to address this question (**Figure 4.14A**). We used combined cell-specific expression of Chrimson for cholinergic depolarization (Klapoetke et al., 2014; Larsch et al., 2015), and GCaMP6s for monitoring [Ca^{2+}] changes (Chen et al., 2013) in either post-synaptic GABAergic motor neurons or body wall muscles (**Figure 4.13B, E**). Strikingly, we found that *nrx-1* deletion disrupts GABA neuron Ca^{2+} transients in response to cholinergic stimulation, but produces no appreciable effect on muscle Ca^{2+} transients, consistent with a specific

requirement for *nrx-1* in the development of functional connectivity between cholinergic and GABAergic neuron, but not muscle, synaptic partners (**Figure 4.13B-G**).

Cholinergic depolarization (5 s) evokes robust stimulus-coupled Ca^{2+} transients in both GABAergic neurons (67% responding during 5 second stimulation) and muscles (88% responding during 5 second stimulation) that occur within 250 ms of stimulus onset (average response latency: 0.22±0.06 s in motor neurons and 0.25±0.02 s in muscles). These transients are not observed in the absence of cholinergic Chrimson expression or in the absence of retinal (**Figure 4.14B, C**), consistent with a requirement for presynaptic Chrimson-mediated depolarization. In both cell types, evoked Ca^{2+} transients rise rapidly following stimulation (τ_{rise}: 0.48±0.08 s in GABA neurons; 0.74±0.06 s in muscles), and persist throughout the duration of stimuli before decaying to baseline. Motor neuron transients are typically shorter in duration (mean duration: 7.7±1 s in GABA neurons; 10.8±0.5 s in muscles) and decay more rapidly (τ_{decay}: 1.1±0.4 s in GABA neurons; 4.6±0.6 s in muscles) compared with muscle transients, likely reflecting differences in both synaptic connectivity and physiology across the two cell types.

For both GABA neurons and muscles, evoked Ca^{2+} responses are eliminated almost completely by mutations that impair post-synaptic AChR function in the respective cell types (*acr-12* or *unc-29;acr-16*, respectively). Specifically, *acr-12* deletion reduces the mean peak amplitude of GABA neuron calcium responses to cholinergic stimulation by 60% (**Figure 4.13C-D**, **Figure 4.14D**) and increases the failure rate (no response to stimulation) by 53% compared to wild type, consistent with prior electrophysiology studies (Petrash et al., 2013). Similarly, for muscles, the mean

peak amplitude of calcium responses to cholinergic stimulation is reduced by 95% in *unc-29;acr-16* double mutants (**Figure 4.13F-G**, **Figure 4.14E**), and the failure rate is increased roughly 15-fold to 77%, consistent with prior electrophysiology studies of evoked synaptic responses in these double mutants (Francis et al., 2005).

nrx-1 deletion reduces the mean peak amplitude of GABA neuron calcium responses to cholinergic stimulation by roughly 71% (**Figure 4.13C-D**, **Figure 4.14D**), and increases the failure rate for GABA neuron recordings by 47%. By comparison, *nrx-1* deletion does not produce a significant decrease in either mean peak fluorescence (**Figure 4.13F-G**, **Figure 4.14E**) or the failure rate in recordings of evoked muscle activity. Together, these findings support a specific requirement for *nrx-1* in cholinergic transmission onto GABA neurons, while *nrx-1* appears dispensable for transmission onto muscles under our recording conditions. Notably, both the failure rate and mean peak amplitude of evoked GABA neuron Ca^{2+} responses are restored to wild type levels with expression of a rescuing *nrx-1*$_L$ transgene in *nrx-1* mutants using a cholinergic neuron-specific promoter (**Figure 4.13C-D**, **Figure 4.14D**).

Consistent with a requirement for NRX-1 in cholinergic synaptic connectivity with GABAergic motor neurons, automated worm track analysis showed that *nrx-1* mutants display defects in the amplitude of dorsoventral bending, a feature of worm movement previously associated with GABAergic function (McIntire et al., 1993; Petrash et al., 2013). These effects are rescued with cell-specific expression of *nrx-1*$_L$ in cholinergic neurons (**Figure 4.14F**). Thus, presynaptic *nrx-1* expression in cholinergic neurons is required for synaptic connectivity between cholinergic and GABAergic motor

neurons, and deficits in these connections alter motor performance. Together, our data indicate that NRX-1 located in presynaptic cholinergic neurons is required for establishing synaptic connectivity with partnering GABAergic neurons, but not muscle cells. NRX-1 signaling promotes both receptor clustering and the outgrowth of post-synaptic spine-like morphological features in GABAergic dendrites. Our findings support a model where distinct synaptic organizers, acting on specific post-synaptic targets, are coordinately regulated with neuronal identity, perhaps offering a mechanism for independent developmental regulation of synaptic outputs across alternate partners (**Figure 4.15**).

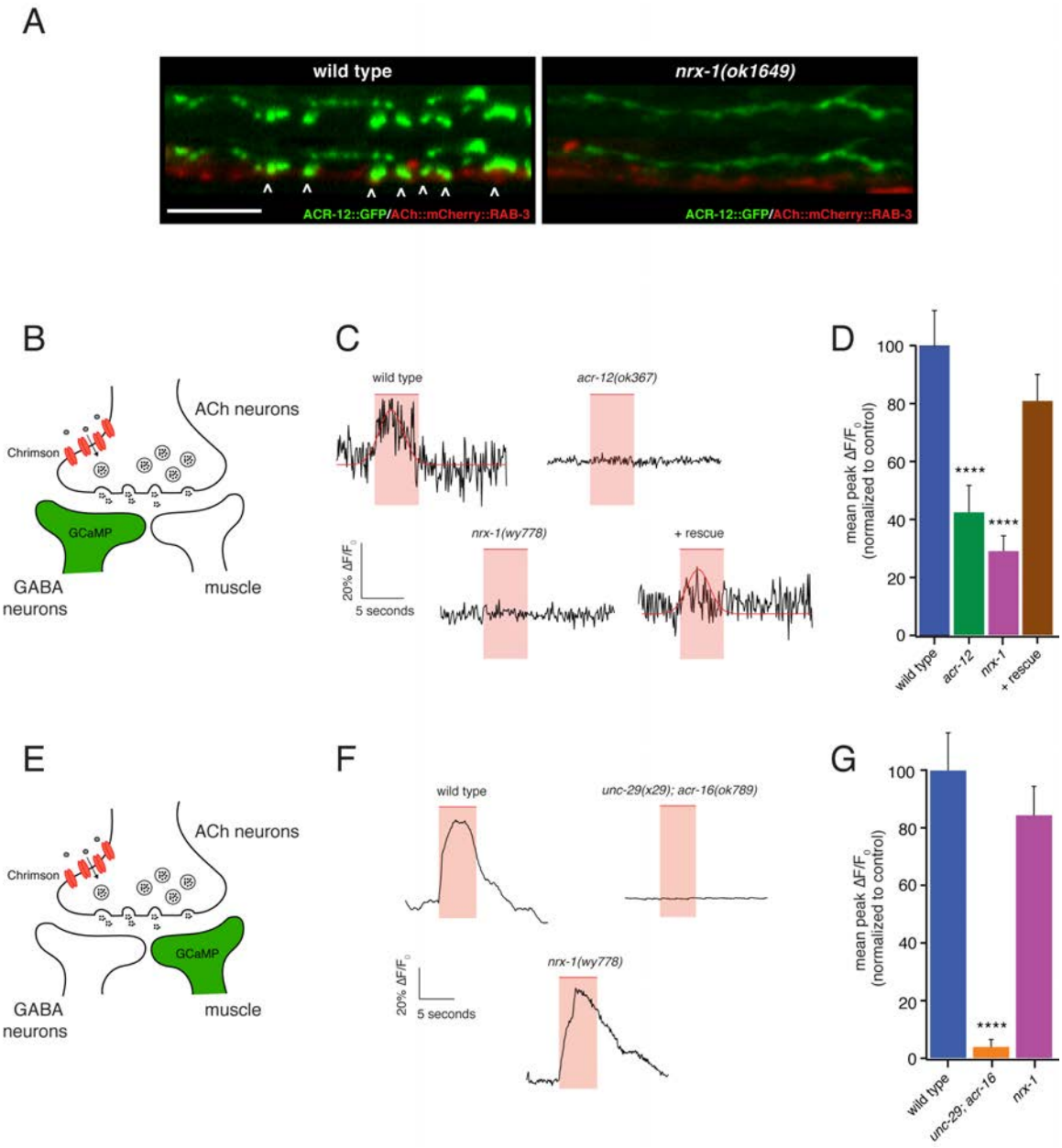
A
wild type
nrx-1(ok1649)
ACR-12::GFP/ACh::mCherry::RAB-3
ACR-12::GFP/ACh::mCherry::RAB-3
B
ACh neurons
Chrimson
GCaMP
GABA neurons
muscle
C
wild type
acr-12(ok367)
nrx-1(wy778)
+ rescue
20% ΔF/F0
5 seconds
D
mean peak ΔF/F0 (normalized to control)
100
80
60
40
20
0
****
****
wild type
acr-12
nrx-1
+ rescue
E
ACh neurons
Chrimson
GCaMP
GABA neurons
muscle
F
wild type
unc-29(x29); acr-16(ok789)
nrx-1(wy778)
20% ΔF/F0
5 seconds
G
mean peak ΔF/F0 (normalized to control)
100
80
60
40
20
0
****
wild type
unc-29; acr-16
nrx-1

Figure 4.13 *nrx-1* mutants show functional defects in synaptic connectivity
(A) Confocal images of pre-synaptic (*acr-2*::mCherry::RAB-3) and post-synaptic (*flp-13*::ACR-12::GFP) specializations in the DD1 synaptic region for the genotypes indicated. Arrowheads indicate receptor-bearing spiny protrusions extending into the presynaptic region of cholinergic axons in wild type. Note gap between the pre- and post-synaptic regions in *nrx-1(ok1649)* mutants. Scale bar, 5 μm. (B) Cartoon depicting specific expression of Chrimson (*acr-2*::Chrimson) in cholinergic neurons together with GCaMP (*ttr-39*::GCaMP6s::SL2::mCherry, green) in GABAergic neurons, applies to C-D. (C) Representative calcium transients in GABAergic motor neurons evoked by light stimulation (red shaded region) of cholinergic neurons for the genotypes indicated. Rescue refers to cholinergic-specific expression of NRX-1_L in *nrx-1(wy778)* mutants (C-D). Red line indicates Gaussian fit to the wild type and rescue traces. (D) Quantification of the mean peak $\Delta F/F_0$ upon Chrimson stimulation for the genotypes indicated, normalized to control (*ufIs155; ufIs157)*. ****p<0.0001, ANOVA with Dunnett's multiple comparisons test. (E) Cartoon depicting specific expression of Chrimson (*acr-2*::Chrimson) in cholinergic neurons together with GCaMP (*myo-3*::NLSwCherry::SL2::GCaMP6s, green) in muscles, applies to F-G. (F) Representative calcium transients in muscle cells evoked by light stimulation (red shaded region) of cholinergic motor neurons for the genotypes indicated. (G) Quantification of the mean peak $\Delta F/F_0$ upon Chrimson stimulation for the genotypes indicated, normalized to control (*zfEx813; ufIs157)*. ****p<0.0001, ANOVA with Dunnett's multiple comparisons test.

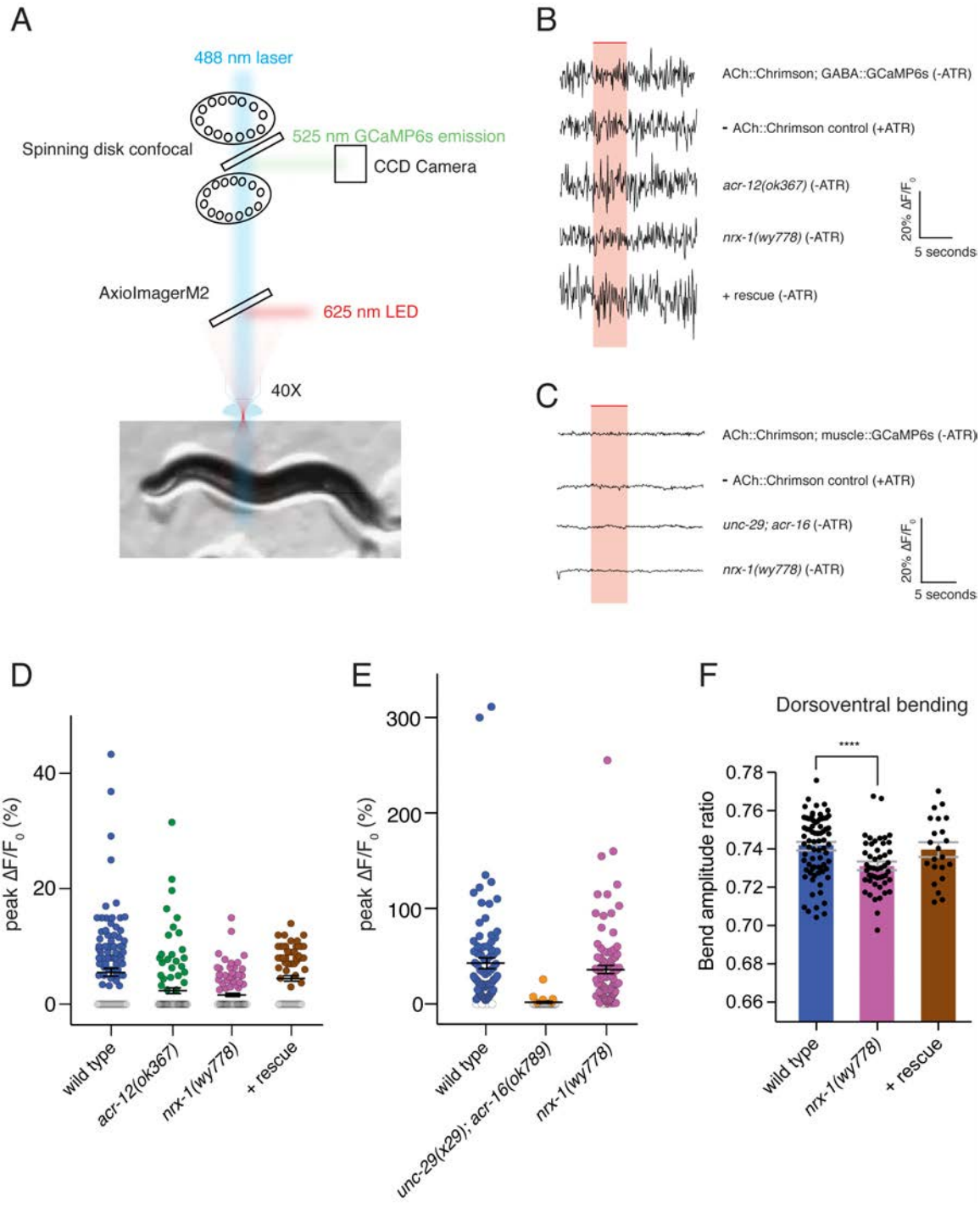
A
488 nm laser
Spinning disk confocal
525 nm GCaMP6s emission
CCD Camera
AxioImagerM2
625 nm LED
40X
B
ACh::Chrimson; GABA::GCaMP6s (-ATR)
- ACh::Chrimson control (+ATR)
acr-12(ok367) (-ATR)
nrx-1(wy778) (-ATR)
+ rescue (-ATR)
20% ΔF/F0
5 seconds
C
ACh::Chrimson; muscle::GCaMP6s (-ATR)
- ACh::Chrimson control (+ATR)
unc-29; acr-16 (-ATR)
nrx-1(wy778) (-ATR)
20% ΔF/F0
5 seconds
D
peak ΔF/F0 (%)
wild type
acr-12(ok367)
nrx-1(wy778)
+ rescue
E
peak ΔF/F0 (%)
wild type
unc-29(x29); acr-16(ok789)
nrx-1(wy778)
F
Dorsoventral bending
Bend amplitude ratio
****
wild type
nrx-1(wy778)
+ rescue

Figure 4.14 *nrx-1* mutants have defects in transmission onto GABAergic neurons and abnormalities in dorsoventral bending

(A) Simplified schematic of experimental setup for calcium imaging studies. GCaMP6s fluorescence was recorded in GABAergic neurons or body wall muscle cells in a single focal plane over a 20 second recording (**Figure 4.13**). Chrimson stimulation was elicited using a 625 nm LED. GCaMP excitation (488 nm) and emission (525 nm) acquisition and Chrimson activation were achieved using a 556 nm short-pass dichroic beam splitter inserted into the light path. (B-C) Representative calcium transients in GABAergic neurons (B) or muscle cells (C) evoked by light stimulation (red shaded region) of cholinergic motor neurons (*acr-2*::Chrimson) for the genotypes indicated. ATR, all-trans retinal. Rescue refers to cholinergic expression of NRX-1_L in *nrx-1(wy778)* mutants. (D-E) Scatterplots of peak evoked calcium responses ($\Delta F/F_0$, closed circles) in GABAergic neurons (D) or muscle cells (E) for the genotypes indicated. $\Delta F/F_0$ of 0 indicates a failure and is represented by open circles. Black bars indicate mean ± SEM. (F) Ratio of maximum dorsoventral bending amplitude measured using automated worm track analysis (see Materials and Methods) (Yemini et al., 2013). Rescue refers to cholinergic expression of NRX-1_L in *nrx-1(wy778)* mutants. Each data point indicates an individual worm analyzed, and gray bars indicate mean ± SEM. n > 20 for each genotype. ****p<0.0001 compared to wild type control, ANOVA with Dunnett's multiple comparisons test.

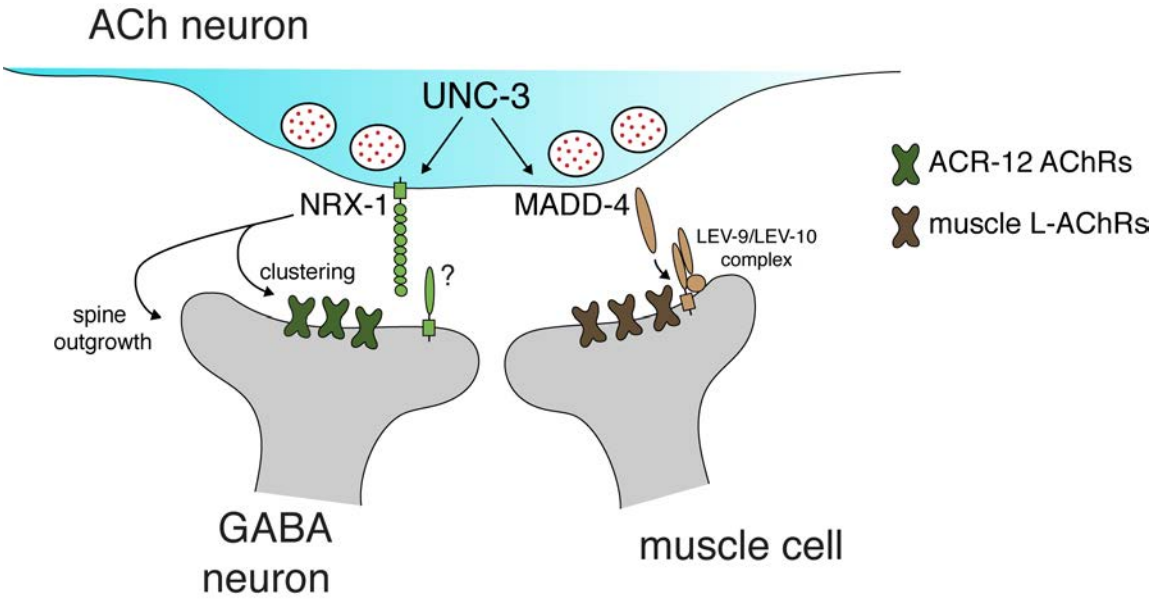

Figure 4.15 Distinct molecular scaffolds direct partner-specific connectivity
Distinct molecular scaffolds coordinate post-synaptic development in GABAergic neurons vs muscle. NRX-1/neurexin located at sites of presynaptic cholinergic release acts to coordinate ACR-12 receptor localization (green) and spine outgrowth in GABA neurons. A complex of proteins, including MADD-4, LEV-9, and LEV-10, direct receptor clustering (brown) at the neuromuscular junction (Gally et al., 2004; Gendrel et al., 2009; Pinan-Lucarre et al., 2014; Rapti et al., 2011). NRX-1 and MADD-4 (Kratsios et al., 2015) expression in cholinergic neurons is transcriptionally co-regulated with neurotransmitter identity by the COE transcription factor UNC-3.

Discussion

Neurons often make divergent synaptic connections onto multiple postsynaptic partners, and these connections are critical for proper neural circuit performance in the brain. In this study, we use dyadic *C. elegans* synapses between cholinergic motor neurons and their muscle and GABAergic motor neuron postsynaptic partners as a model to define novel molecular mechanisms controlling divergent connectivity. First, we identify spine-like dendritic specializations on GABAergic DD neurons. We find that heteromeric post-synaptic AChR complexes composed of the ACR-12, UNC-63, UNC-38, UNC-29 and LEV-1 subunits are localized to these structures. Second, we identify a novel neurexin signaling pathway required both for the formation of post-synaptic specializations and for AChR clustering. In contrast, *nrx-1*/neurexin is not required for the development of cholinergic synapses onto muscles, which instead require molecularly distinct pathways that have been described previously (Francis et al., 2005; Gally et al., 2004; Gendrel et al., 2009; Jensen et al., 2012; Pinan-Lucarre et al., 2014; Rapti et al., 2011). Third, we find that presynaptic *nrx-1* expression in cholinergic neurons is required for the establishment of synapses with GABAergic neurons, and transcriptional regulation of *nrx-1* is achieved through actions of the COE transcription factor *unc-3*. These findings suggest a model where cholinergic expression of *nrx-1* initiates synapse formation with GABAergic neurons via NRX-1 mediated trans-synaptic signaling. Finally, the ACh-GABA connectivity defects that we observe in *nrx-1* mutants are paralleled by significant impairment of evoked cholinergic transmission onto GABAergic neurons, and altered sinusoidal movement. In contrast, functional connectivity with

muscles is unaffected. Together, our findings provide evidence that distinct molecular signaling pathways act in parallel to establish divergent connections at dyadic synapses in the motor circuit, raising the interesting possibility that differential use of synaptic organizers may be similarly utilized in the brain to provide a molecular code directing divergent connectivity (**Figure 4.15**).

Heteromeric ACR-12 receptor complexes cluster in specialized post-synaptic domains of GABAergic DD dendrites

Using candidate deletion analysis and cell-specific rescue, we identified AChR subunits and accessory proteins required for the assembly and localization of ACR-12 receptors in GABAergic neurons, defining the subunit composition of this neuronal receptor. Our findings implicate four additional receptor subunits (UNC-38, UNC-63, UNC-29, LEV-1) that co-assemble with ACR-12 to form pentameric receptor complexes in GABAergic neurons, and demonstrate that three accessory proteins (UNC-74, UNC-50, RIC-3) with more generalized roles in AChR assembly and maturation are also required (Boulin et al., 2008; Halevi et al., 2002; Jospin et al., 2009). These findings provide evidence that ACR-12 receptors in GABA neurons are similar in subunit composition to muscle L-AChRs, differing only in the inclusion of the ACR-12 subunit in GABA neurons, whereas muscle L-AChRs incorporate the LEV-8 subunit (Boulin et al., 2008; Towers et al., 2005). Consistent with our analysis, a prior study showed that ACR-12 can be co-purified with the UNC-29 or LEV-1 subunits (Gottschalk et al., 2005). We have previously shown that *unc-29* is expressed in GABAergic motor neurons, and UNC-29::GFP localizes similarly

to ACR-12::GFP in DD neurons, both in the mature animal and during developmental remodeling of these neurons (He et al., 2015).

We show that ACR-12 receptor complexes are concentrated at the tips of spine-like dendritic protrusions in GABAergic DD neurons. Spiny processes associated with D-type GABAergic neurons had been noted in prior electron microscopy studies (White et al., 1976), but to our knowledge, were not characterized further. We find that these AChR-containing dendritic protrusions are apposed by presynaptic clusters of cholinergic vesicles and increase in number during the course of larval development, perhaps representing new synaptic connections formed with post-embryonic born cholinergic neurons that are integrated into the circuit following the L1/L2 transition (White et al., 1978). While further investigation of these structures will undoubtedly reveal additional insights, the characteristics we define here raise the interesting possibility that these dendritic protrusions are structural specializations for housing neurotransmitter receptors and other proteins required for post-synaptic signaling, perhaps representing an evolutionary precursor to mammalian dendritic spines.

The synaptic organizer neurexin directs post-synaptic development in a partner-specific manner

nrx-1 deletion impairs both AChR localization and spiny outgrowths in DD neurons, creating a gap between the pre- and post-synaptic neurons. Similarly, in *Drosophila,* mutation of the single neurexin gene *dnrx* causes disorganization of synaptic structure at the neuromuscular junction (Li et al., 2007). Knockout of two out of the three mouse

alpha neurexins reduces dendrite length and total spine number in the cortex (Dudanova et al., 2007), though significant numbers of dendritic spines remain detectable. In our studies, we find that *nrx-1* is required for ACR-12 receptor localization in GABAergic DD and VD neurons, although we observe spine-like protrusions only in DD neurons. These findings argue that NRX-1 is not solely involved in directing spine development, but serves an additional role in receptor clustering. Further, we show that dendritic protrusions form independently of a requirement for AChRs containing either ACR-12 or UNC-63, offering additional support that spine outgrowth and receptor clustering are independently regulated by NRX-1. Similarly, dendritic spines on mouse CA1 pyramidal neurons form normally in the absence of functional glutamate receptors (Lu et al., 2013).

Although GABA neuron ACR-12 AChRs and muscle L-AChRs share very similar subunit composition (Boulin et al., 2008; Lewis et al., 1980), we find that genes required for proper localization of muscle L-AChRs (e.g. *madd-4, lev-10*) play comparatively minor roles at synapses onto GABA neurons. Conversely, loss of *nrx-1* function specifically affects GABAergic, but not muscle, AChR clustering and cholinergic transmission onto muscles appears largely unaffected. Our cell-specific rescue experiments indicate *nrx-1* acts in cholinergic neurons to coordinate post-synaptic development in GABAergic neurons via trans-synaptic signaling.

Numerous studies support neuroligin as a primary trans-synaptic binding partner with neurexin (Boucard et al., 2005; Comoletti et al., 2006; Ichtchenko et al., 1995; Ichtchenko et al., 1996; Nguyen and Sudhof, 1997). Indeed, *C. elegans* NRX-1/neurexin function has been characterized almost exclusively in the context of its partnership with

NLG-1/neuroligin. A retrograde neurexin-neuroligin signaling pathway that regulates neurotransmitter release has been described, involving signaling through the Ca^{2+} channel auxiliary subunit UNC-36/α2δ (Hu et al., 2012; Tong et al., 2017). Consistent with this representing a distinct mechanism from that described in our work, mutation of *unc-36* has no appreciable effect on synapse development in our experiments. Postsynaptic expression of NLG-1/neuroligin is required at GABAergic synapses. However, MADD-4/Punctin likely acts as a major presynaptic partner for NLG-1 in this case, with NRX-1 playing a comparatively minor role (Maro et al., 2015; Tong et al., 2015; Tu et al., 2015). Finally, recent work also implicates neurexin-neuroligin signaling in sexually dimorphic neurite plasticity (Hart and Hobert, 2018). In contrast to these studies, we find that NRX-1 operates independently of NLG-1 to direct the formation of cholinergic synapses with GABAergic neurons. How therefore might presynaptic neurexin direct postsynaptic maturation? Our analysis shows that presynaptic NRX-1 localizes properly in the absence of *acr-12,* arguing against a requirement for direct binding of neurexin to the postsynaptic receptor. Prior studies offer strong evidence for alternate neurexin binding partners that support trans-synaptic signaling (Boucard et al., 2012; de Wit et al., 2009; Ko et al., 2009; Missler et al., 1998; Petrenko et al., 1996; Pettem et al., 2013; Sugita et al., 2001; Uemura et al., 2010). For several of these gene families (e.g. neurexophilins, cerebellins), clear *C. elegans* orthologs are not present. Others are included in our candidate analysis (e.g. *casy-1*/calsyntenin, *lat-2*/latrophilin), but single gene mutations do not produce post-synaptic defects comparable to mutation of *nrx-1*, suggesting either the possibility of a novel post-synaptic *nrx-1* binding partner or redundant post-synaptic mechanisms.

Additional genetic or proteomic studies will be required to distinguish between these possibilities and address this important question.

Transcriptional control of partner-specific synaptic connectivity

Transcriptional regulators of neurexin expression are only beginning to be elucidated (Runkel et al., 2013). Previously, we found that mutation of the COE-type transcription factor *unc-3* disrupts AChR clustering in GABAergic dendrites (Barbagallo et al., 2017). These disrupted clusters are unlikely to reflect a requirement for acetylcholine release in AChR clustering, as neither tetanus toxin expression nor mutation of *unc-17*/vAChT produces appreciable defects in ACR-12 clustering (Barbagallo et al., 2017) (this study). Here, we find that neurexin is a transcriptional target of UNC-3, and we propose that UNC-3 regulation of *nrx-1* expression directs development of postsynaptic specializations in GABAergic neurons. Prior work indicates that UNC-3 transcriptional regulation of MADD-4/Punctin is essential for proper development of cholinergic synapses with muscles (Kratsios et al., 2015). However, *madd-4* is dispensable for cholinergic synapse formation with neighboring GABAergic neurons (Barbagallo et al., 2017) (this study). Thus, cholinergic connectivity with distinct synaptic targets–muscles and GABAergic neurons–is coordinately regulated with cholinergic neuronal identity by *unc-3* transcriptional control of alternate synaptic organizers.

Our work here defines a novel yet essential role for NRX-1 during synapse formation. Neurexin acts in a target-specific manner to coordinate postsynaptic development/maturation. Presynaptic neurexin instructs receptor localization and the

development of spine-like processes in postsynaptic GABAergic neurons, and *nrx-1* expression is critical for cholinergic transmission onto GABAergic neurons, while not required for signaling onto neighboring muscle. Our work suggests synaptic target-specific utilization of organizers such as neurexin may specify divergent connectivity, and provide a molecular mechanism for target-specific regulation of synapse development.

Materials and Methods

Strains

C. elegans strains were maintained at room temperature (22-24°C) on nematode growth media plates (NGM) seeded with the *Escherichia coli* strain OP50. All strains are derivatives of the N2 Bristol strain (wild type). Transgenic strains were obtained by microinjection to achieve germline transformation (Mello et al., 1991) and identified with co-injection markers as previously (Barbagallo et al., 2017). Integrated lines were produced by X-ray irradiation and outcrossed to wild type. A complete list of all strains used in this work is included in **Table 4.2**.

Molecular Biology

Plasmids were constructed using the two-slot Gateway Cloning system (Invitrogen) as described previously (Bhattacharya et al., 2014) and confirmed by restriction digest and/or sequencing as appropriate.

Tagged receptor constructs: To generate *flp-13*::ACR-12::GFP::3xHA, ACR-12::GFP was amplified from pDEST-38, removing the original stop codon and adding a 3X HA tag. The product (3195 bp) was ligated into a destination vector to generate pDEST-113. pDEST-113 was recombined with pENTR-3'-*flp-13* to create pAP138 (*flp-13*::ACR-12::GFP::3xHA). To generate *flp-13::*UNC-63::GFP, 5' and 3' fragments of *unc-63* cDNA were PCR amplified from pDEST-57, ligated into pPD117.01 (*mec-7*::GFP), converted into the destination vector pDEST-79, and recombined with pENTR-5'-*flp-13*

to create pAP84 (*flp-13*::UNC-63::GFP), where GFP is inserted into the intracellular loop of UNC-63.

AChR subunit and accessory rescue constructs: Wild type *unc-38* (1536 bp), *unc-63* (1509 bp), *unc-74* (1344 bp), *unc-50* (906 bp), and *ric-3* (1137 bp) rescue constructs were PCR amplified and ligated into destination vectors to generate pDEST-51, pDEST-57, pDEST-58, pDEST-56, and pDEST-59, respectively. Each of these was recombined with pENTR-*unc-47* to create pAP45 (*unc-47*::*unc-38 cDNA*), pAP59 (*unc-47*::*unc-63 cDNA*), pAP53 (*unc-47*::*unc-74 cDNA*), pAP57 (*unc-47*::*unc-50 cDNA*), and pAP55 (*unc-47*::*ric-3 cDNA*).

nrx-1 reporter and rescue constructs: To generate the 5 kb *nrx-1*$_L$::GFP transcriptional reporter, the *nrx-1*$_L$ promoter was amplified from wild type genomic DNA (-4786 bp relative to start) and cloned into pENTR-D-TOPO to generate pENTR-5'-*nrx-1*$_L$. pENTR-5'-*nrx-1*$_L$ was then recombined with pDEST-93 (GFP) to generate pAP156 (*nrx-1*$_L$::GFP). The 2 kb *nrx-1*$_L$ promoter::GFP fusion construct (-2033 bp relative to start) was created using the same strategy, recombining pENTR-5'-*nrx1*$_L$*2kb* with pDEST-93 to create pAP118 (*nrx-1*$_L$*2kb*::GFP). *nrx-1*$_L$*COEΔ*::GFP (pAP178) was generated by PCR amplification using mutant primers that disrupt the COE motif (T<u>CCC</u>AAAGGG > T<u>AAA</u>AAAGGG).

Rescuing NRX-1$_L$ minigene constructs were generated by ligation of a 10,598 bp NheI fragment of the *nrx-1* genomic locus extending from the *nrx-1*$_L$ start to exon 21 (amplified from cosmid C29A12) with a 715 bp fragment of the *nrx-1* cDNA (isoform A) amplified from a plasmid containing the *nrx-1* coding sequence (GM470, provided by

Kang Shen (Maro et al., 2015)), and converted into the destination vector pDEST-143. For cell-specific rescue, pDEST-143 was recombined with pENTR-3'-*unc17β*, pENTR-3'-*unc47*, pENTR-3'-*myo3*, and pENTR-3'-*unc3* to create minigene plasmids pAP204 (*unc-17β*::*nrx-1*$_L$), pAP206 (*unc-47*::*nrx-1*$_L$), pAP208 *(myo-3*::*nrx-1*$_L$), and pAP202 *(unc-3*::*nrx-1*$_L$), respectively.

unc-129::NRX-1$_L$::GFP was generated by conversion of the NRX-1$_L$::GFP plasmid GM477 (provided by Kang Shen (Maro et al., 2015)) into the destination vector pDEST-99 and recombination with pENTR-3'-*unc129* to create pAP120 (*unc-129*::NRX-1$_L$::GFP).

Chrimson and GCaMP constructs: To generate *acr-2*::Chrimson, Chrimson coding sequence was amplified from *odr-7*::Chrimson (construct provided by Dirk Albrecht (Larsch et al., 2015)) and ligated into a destination vector to create pDEST-104. pDEST-104 was recombined with pENTR-5'-*acr2* to create pRB2 (*acr-2*::Chrimson). To generate *ttr-39*::GCaMP6s::SL2::mCherry, GCaMP6s was amplified from pGP-CMV-GCaMP6s (Addgene) and ligated into a destination vector to create pDEST-95. pDEST-95 was recombined with pENTR-5'-*ttr39* (promoter provided by David Miller (Petersen et al., 2011)) to create pAP130 (*ttr-39*::GCaMP6s::SL2::mCherry).

CRISPR/Cas9-mediated gene disruption of *nrx-1* PDZ binding domain

gRNA plasmids were made as previously described (Arribere et al., 2014). Target sequences were selected on exons 26 and 27 of *nrx-1*$_L$ (or exons 6 and 7 of *nrx-1*$_S$) for the PDZ binding domain mutants (*uf181* and *uf185)*. Cas9 plasmid (pDD162 (Dickinson et

al., 2013)) (50 ng/μL), gRNA plasmids (25 ng/μL each), gRNA plasmid pJA58 (*dpy-10* target) (50 ng/μL), and ssODN repair template for *dpy-10* (*dpy-10(cn64)*) (20 ng/μL) were injected into N2 (wild type) worms. Mutant lines were identified based on Rol and/or Dpy phenotypes, F2 progeny were screened by PCR for indels disrupting the PDZ binding domain, and mutations were confirmed by sequencing. *nrx-1(uf181)* contains an 80 bp insertion (within exon 26) 258 bp upstream of the PDZ binding domain, resulting in a frameshift and early stop prior to this domain. *nrx-1(uf185)* contains a 67 bp deletion 51 bp upstream of the PDZ binding domain (within exon 27), deleting this domain, removing the stop codon, and creating a new stop within the 3'UTR.

Confocal microscopy

For all imaging, nematodes were immobilized with sodium azide (0.3 M) on a 2% or 5% agarose pad. Each n represents analysis of the nerve cord from an independent animal. Images were obtained using either a 3i (Intelligent Imaging Innovations) Everest spinning-disk confocal microscope or Olympus BX51WI spinning disk confocal equipped with a 63x objective. All DD1 confocal images were obtained by imaging L4 hermaphrodites of similar size in the region near the pharynx using identical image and laser settings for each marker, and receptor clusters were quantified in a region from the DD1 cell body to connecting commissure (i.e. the synaptic region).

Analysis of synapse number/fluorescence intensity was conducted using either Volocity 6.3 or ImageJ software (open source) using defined intensity threshold values acquired from control experiments for each fluorescent marker. Specifically, the "find objects" function in Volocity was used, excluding objects >10 μm^2 and <0.2 μm^2.

Alternatively, the “analyze particles” function of ImageJ was used. For ImageJ analyses, background fluorescence was first subtracted by calculating the average intensity of each image in a region devoid of puncta. In some cases, fluorescence intensity within a region of interest was also measured and normalized to wild type control as indicated. Confocal montages of the nerve cord were assembled by using the “straighten to line” function in ImageJ. Only images where the DD1 neuron was clearly distinguishable from neighboring cells were included in analyses.

For measurements of dendritic morphology, post-synaptic protrusions in the ventral dendritic region anterior to the DD1 soma (i.e. the synaptic region) were quantified in L4 hermaphrodites. All protrusions ≥ 0.3 μm were analyzed, measuring from the base of the main dendritic process to the tip of the protrusion.

For imaging and quantification of *flp-13*::ACR-12::GFP in **Figures 4.5A** and **Figure 4.4B**, strains IZ1458 (*ufIs126*) and IZ1557 (*ufIs126; acr-12(ok367))* were included in the analysis as wild type control. There was no appreciable difference in the number of receptor clusters between the two strains (*ufIs126; acr-12(ok367)* 14.4 ± 0.6, n = 49; *ufIs126* 14.8 ± 0.6, n = 48).

Staging and timecourse of receptors/protrusion growth during development

Spine and receptor cluster number in the DD1 synaptic region were analyzed in synchronized animals using strains IZ1458 and IZ1464 as described previously (He et al., 2015). Briefly, embryos for each strain were picked to separate 60 mm unseeded plates and allowed to hatch for 40 minutes. Newly hatched L1 larvae were moved to freshly

seeded plates, and the midpoint of the 40 minutes in which the embryos hatched was considered t=0. Plates were incubated at 25°C for 28, 34, 46, and 52 hours. Developing protrusions ≥ 0.2 μm in the synaptic region were analyzed, and ACR-12 receptor clusters were quantified as above.

Single molecule RNA fluorescent *in situ* hybridization (FISH) and imaging

Custom Stellaris FISH probes against *nrx-1* mRNA were obtained from Biosearch Technologies as a mix of 48 probes conjugated to CAL Fluor® Red 590 Dye. Experiments were performed using wild type, *unc-3(e151)* mutants, and *nrx-1(nu485)* mutants expressing either *unc-47*::GFP (*oxIs12*), *unc-4*::GFP (*wdIs5*), or *unc-17::GFP* (*vsIs48*) markers to label populations of GABA and ACh motor neurons. Synchronized populations of L3-L4 larval animals were fixed and hybridized as described previously (Ji and van Oudenaarden, 2012; Raj et al., 2008). Images were obtained using spinning disk microscopy as above. Z-projections were analyzed in ImageJ using the "analyze particles" function. Following background subtraction, the total number of *nrx-1* mRNA molecules was calculated for a 45 μm x 5.5 μm straightened region of the anterior ventral nerve cord using a defined intensity threshold across all images.

Injection of fluorescent antibodies for *in vivo* labeling of nAChRs

For staining of ACR-12 receptors at the cell surface, mouse monoclonal α-HA antibodies (16B12) coupled to Alexa594 were diluted in injection buffer (20 mM K_3PO_4, 3 mM K citrate, 2% PEG 6000, pH 7.5). Antibody was injected into the pseudocoelom of

early L4 stage wild type or *nrx-1(wy778)* animals as described previously (Gottschalk and Schafer, 2006). Animals were allowed to recover for six hours on seeded NGM plates. Only animals in which fluorescence was observed in coelomocytes (indicating uptake of excess antibody and successful injection) were included in the analysis. Injections of anti-GFP Alexa594 antibody followed the same protocol.

nrx-1 behavioral assays

One-day old adults were placed on thinly seeded NGM plates and tracked for a period of 5 minutes using Single Worm Tracker 2.0 (WT2) (Yemini et al., 2011). Worm tracker software version 2.0.3.1, created by Eviatar Yemini and Tadas Jucikas (Schafer lab, MRC, Cambridge, UK), was used to analyze movement.

Calcium imaging

Transgenic animals expressing *ttr-39*::GCaMP6s::SL2::mCherry (GABA neurons) or *myo-3*::NLSwCherry::SL2::GCaMP6s (muscle, from M. Alkema) along with *acr-2*::Chrimson (cholinergic neurons) were placed on plates seeded with OP50 containing 2.75 mM All-Trans Retinal (ATR) for 24 hours prior to experiments. Young adults were immobilized on 5% agarose pads in 2,3-Butanedione monoxime (BDM) (30 mg/ml). For all genotypes, control animals grown in the absence of ATR were imaged.

Imaging was carried out on a Yokogawa CSU-X1-A1N spinning disk confocal system equipped with EM-CCD camera (Hammamatsu, C9100-50) and 40X C-Apochromat 1.2 NA water immersion objective. Optogenetic stimulation experiments

employed a 625 nm (40 W) LED (Mightex Systems). Optical output through the objective was 0.3 mW/mm^2 at the focal plane of the specimen. Simultaneous GCaMP excitation (488 nm) and emission (525 nm) acquisition and Chrimson activation were achieved using a 556 nm edge BrightLine® single-edge short-pass dichroic beam splitter positioned in the light path (Semrock).

Data were acquired using Volocity software. Images were binned at 4x4 during acquisition and sampled at 10 Hz. GABA motor neuron and muscle ROIs in respective experiments were identified by mCherry fluorescence. Recordings from motor neuron cell bodies were obtained systematically, beginning at the anterior end of the ventral nerve cord and moving in a posterior direction. Each field typically contained 1-5 GABA motor neurons. Only recordings of neurons located anterior to the vulva were included in the analysis. Muscle recordings were obtained either directly anterior or posterior to the vulva.

Photobleaching correction was carried out by fitting an exponential function to the data (CorrectBleach plugin, ImageJ). A linear fit (Igor Pro, Wavemetrics) of the background fluorescence was subtracted from the cell body fluorescence across all time points. Pre-stimulus baseline fluorescence (F_0) was calculated as the average of the corrected background-subtracted data points in the first 4 seconds of the recording and the corrected fluorescence data was normalized to prestimulus baseline as $\Delta F/F_0$, where $\Delta F = F - F_0$. Peak $\Delta F/F_0$ was determined by fitting a Gaussian function to the $\Delta F/F_0$ time sequence using Multi peak 2.0 (Igor Pro, WaveMetrics). All data collected were analyzed, including failures (no response to stimulation). Peak $\Delta F/F_0$ values were

calculated from recordings of >10 animals per genotype. Mean peaks ± SEM were calculated from all peak $\Delta F/F_0$ data values and normalized to the wild type mean. Latency was calculated as the time required from stimulus onset for fluorescence ($\Delta F/F_0$) to reach two times the pre-stimulus baseline standard deviation (Larsch et al., 2015). Duration was measured as the time between the onset of the transient and the completion of the decay back to the baseline. Rise and decay time constants were determined from the time constant of exponential fits between the baseline and peak fluorescence as appropriate.

Table 4.2 *C. elegans* strains used in this work

Genotype	Strain Name	Transgene
ufIs126	IZ1458	*flp-13*::ACR-12::GFP (pCL32)
ufIs126; acr-12(ok367)	IZ1557	*flp-13*::ACR-12::GFP (pCL32)
ufIs137	IZ1687	*flp-13*::mCherry::RAB-3 (pAP43)
ufIs137; nrx-1(ok1649); oxIs22	IZ2030	*flp-13*::mCherry::RAB-3 (pAP43); *unc-49*::UNC-49::GFP
ufEx527	IZ1645	*flp-13*::UNC-29::GFP (pAP65)
ufEx527; nrx-1(ok1649)	IZ1822	*flp-13*::UNC-29::GFP (pAP65)
ufEx527; nrx-1(wy778)	IZ2507	*flp-13*::UNC-29::GFP (pAP65)
ufEx527; acr-12(ok367)	IZ1799	*flp-13*::UNC-29::GFP (pAP65)
ufEx577	IZ1815	*flp-13*::UNC-63::GFP (pAP84)
ufEx577; nrx-1(ok1649)	IZ1911	*flp-13*::UNC-63::GFP (pAP84)
ufEx577; nrx-1(wy778)	IZ2503	*flp-13*::UNC-63::GFP (pAP84)
ufEx577; acr-12(ok367)	IZ2441	*flp-13*::UNC-63::GFP (pAP84)
juIs20; ufIs128	IZ1858	*acr-2*::SNB-1::GFP; *flp-13*::mCherry (pAP31)
juIs20	CZ637	*acr-2*::SNB-1::GFP
juIs20; nrx-1(wy778)	IZ2223	*acr-2*::SNB-1::GFP
nuIs25	VM4177	*glr-1*::GLR-1::GFP
nuIs25; nrx-1(ok1649)	IZ1743	*glr-1*::GLR-1::GFP
ufIs2; unc-29(x29)	IZ109	*myo-3*::UNC-29::GFP (pDM956)
ufIs2; unc-29(x29); nrx-1(wy778)	IZ2271	*myo-3*::UNC-29::GFP (pDM956)
ufIs126; ufIs63; acr-12(ok367)	IZ1539	*flp-13*::ACR-12::GFP (pCL32); *acr-2*::mCherry::RAB-3 (pPRB47)
ufIs126; ufIs63; nrx-1(ok1649)	IZ1742	*flp-13*::ACR-12::GFP (pCL32); *acr-2*::mCherry::RAB-3 (pPRB47)
wdIs950; acr-12(ok367)	NC2920	*unc-47*::ACR-12::GFP (pHP7)
wdIs950; acr-12(ok367); nrx-1(ok1649)	IZ1693	*unc-47*::ACR-12::GFP (pHP7)
wdIs950; acr-12(ok367); nrx-1(tm1961)	IZ1867	*unc-47*::ACR-12::GFP (pHP7)
wdIs950; acr-12(ok367); nrx-1(ds1)	IZ1869	*unc-47*::ACR-12::GFP (pHP7)
wdIs950; acr-12(ok367); nrx-1(wy778)	IZ2098	*unc-47*::ACR-12::GFP (pHP7)
wdIs950; acr-12(ok367); nrx-1(nu485)	IZ2676	*unc-47*::ACR-12::GFP (pHP7)
wdIs950; acr-12(ok367); unc-3(e151)	IZ3044	*unc-47*::ACR-12::GFP (pHP7)

wdIs950; acr-12(ok367); unc-3(e151); ufEx1200	IZ3008	*unc-47*::ACR-12::GFP (pHP7); *unc-3*::*nrx-1*$_L$ cDNA (pAP202) at 10ng/µL
ufIs126; ufEx523	IZ1599	*flp-13*::ACR-12::GFP (pCL32); *flp-13*::mCherry (pAP31)
ufIs128; oxIs12	IZ2288	*flp-13*::mCherry (pAP31); *unc-47*::GFP
wdIs950; acr-12(ok367); nrx-1(wy778); ufEx1114 and *wdIs950; acr-12(ok367); nrx-1(wy778); ufEx1137*	IZ2869 and IZ2903	*unc-47*::ACR-12::GFP (pHP7); *unc-17β*::*nrx-1*$_L$ minigene at 10ng/µL (pAP204)
wdIs950; acr-12(ok367); nrx-1(wy778); ufEx1128 and *wdIs950; acr-12(ok367); nrx-1(wy778); ufEx1129*	IZ2891 and IZ2892	*unc-47*::ACR-12::GFP (pHP7); *unc-47*::*nrx-1*$_L$ minigene at 10ng/µL (pAP206)
wdIs950; acr-12(ok367); nrx-1(wy778); ufEx1134 and *wdIs950; acr-12(ok367); nrx-1(wy778); ufEx1136*	IZ2900 and IZ2902	*unc-47*::ACR-12::GFP (pHP7); *myo-3*::*nrx-1*$_L$ minigene at 10ng/µL (pAP208)
ufIs128	IZ1464	*flp-13*::mCherry (pAP31)
ufIs128; acr-12(ok367)	IZ1802	*flp-13*::mCherry (pAP31)
ufIs128; unc-63(ok1075)	IZ2428	*flp-13*::mCherry (pAP31)
ufIs128; nlg-1(ok259)	IZ2078	*flp-13*::mCherry (pAP31)
ufIs128; nrx-1(ok1649)	IZ1712	*flp-13*::mCherry (pAP31)
ufIs128; nrx-1(wy778)	IZ2176	*flp-13*::mCherry (pAP31)
ufIs128; nrx-1(uf181)	IZ2755	*flp-13*::mCherry (pAP31)
ufIs128; nrx-1(uf185)	IZ2882	*flp-13*::mCherry (pAP31)
ufIs128; unc-17(e113)	IZ1717	*flp-13*::mCherry (pAP31)
ufIs128; unc-17(e245)	IZ1770	*flp-13*::mCherry (pAP31)
ufIs128; unc-3(e151)	IZ1499	*flp-13*::mCherry (pAP31)
ufIs128; nrx-1(ok1649); ufEx1114	IZ2987	*flp-13*::mCherry (pAP31); *unc-17β*::*nrx-1*$_L$ minigene at 10ng/µL (pAP204)
ufIs126; acr-14(ok1155); acr-12(ok367)	IZ1488	*flp-13*::ACR-12::GFP (pCL32)
ufIs126; acr-9(ok933)	IZ1460	*flp-13*::ACR-12::GFP (pCL32)
ufIs126; acr-9(ok933); acr-14(ok1155)	IZ1489	*flp-13*::ACR-12::GFP (pCL32)
ufIs126; unc-38(e264); acr-12(ok367)	IZ1565	*flp-13*::ACR-12::GFP (pCL32)

ufIs126; unc-38(e264); acr-12(ok367); ufEx1213	IZ3045	*flp-13*::ACR-12::GFP (pCL32); *unc-47*::*unc-38 cDNA* (pAP45)
ufIs126; unc-63(ok1075)	IZ1427	*flp-13*::ACR-12::GFP (pCL32)
ufIs126; unc-63(ok1075); ufEx514	IZ1582	*flp-13*::ACR-12::GFP (pCL32); *unc-47*::*unc-63 cDNA* (pAP59)
ufIs126; lev-1(e211)	IZ1454	*flp-13*::ACR-12::GFP (pCL32)
ufIs126; unc-29(x29)	IZ1487	*flp-13*::ACR-12::GFP (pCL32)
ufIs126; unc-74(e883)	IZ1597	*flp-13*::ACR-12::GFP (pCL32)
ufIs126; unc-74(e883); ufEx1146	IZ2918	*flp-13*::ACR-12::GFP (pCL32); *unc-47*::*unc-74 cDNA* (pAP53)
ufIs126; unc-50(e306); acr-12(ok367)	IZ1566	*flp-13*::ACR-12::GFP (pCL32)
ufIs126; unc-50(e306); acr-12(ok367); ufEx1143	IZ2933	*flp-13*::ACR-12::GFP (pCL32); *unc-47*::*unc-50 cDNA* (pAP57)
ufIs126; ric-3(hm9); acr-12(ok367)	IZ1425	*flp-13*::ACR-12::GFP (pCL32)
ufIs126; ric-3(hm9); acr-12(ok367); ufEx537	IZ1679	*flp-13*::ACR-12::GFP (pCL32); *unc-47*::*ric-3 cDNA* (pAP55)
ufIs126; unc-36(e251)	IZ3187	*flp-13*::ACR-12::GFP (pCL32)
ufIs126; lin-7(n106)	IZ2931	*flp-13*::ACR-12::GFP (pCL32)
ufIs126; lat-2(ok301)	IZ2666	*flp-13*::ACR-12::GFP (pCL32)
ufIs126; dgn-2(ok209); dgn-3(tm1092)	IZ3005	*flp-13*::ACR-12::GFP (pCL32)
ufIs126; sax-7(nj48)	IZ2047	*flp-13*::ACR-12::GFP (pCL32)
ufIs126; nab-1(ok943)	IZ2669	*flp-13*::ACR-12::GFP (pCL32)
ufIs126; stn-2(ok2417)	IZ2907	*flp-13*::ACR-12::GFP (pCL32)
ufIs126; agr-1(tm2051)	IZ2110	*flp-13*::ACR-12::GFP (pCL32)
ufIs126; zig-10(tm6327)	IZ2989	*flp-13*::ACR-12::GFP (pCL32)
ufIs126; lon-2(e678)	IZ2048	*flp-13*::ACR-12::GFP (pCL32)
ufIs126; casy-1(tm718)	IZ1790	*flp-13*::ACR-12::GFP (pCL32)
ufEx534; zig-1(ot81); zig-2(ok696); zig-3(tm924); zig-4(gk34); zig-5(ok1065); zig-6(ok273); zig-7(ok2329); zig-8(ok561)	IZ1672	*flp-13*::ACR-12::GFP (pCL32)
ufIs126; stn-1(ok292)	IZ1697	*flp-13*::ACR-12::GFP (pCL32)
ufIs126; nlg-1(ok259)	IZ1650	*flp-13*::ACR-12::GFP (pCL32)
ufIs126; oig-1(ok1687); acr-12(ok367)	IZ1410	*flp-13*::ACR-12::GFP (pCL32)
ufIs126; F38B6.6(ok3009)	IZ1706	*flp-13*::ACR-12::GFP (pCL32)
ufIs126; zig-9(tm5230)	IZ2017	*flp-13*::ACR-12::GFP (pCL32)
ufIs126; unc-52(e444)	IZ1984	*flp-13*::ACR-12::GFP (pCL32)
ufIs126; lin-2(n397)	IZ2979	*flp-13*::ACR-12::GFP (pCL32)

ufIs126; unc-40(e1430); dpy-5(e61)	IZ2898	*flp-13*::ACR-12::GFP (pCL32)
ufIs126; rig-3(ok2156)	IZ1709	*flp-13*::ACR-12::GFP (pCL32)
ufIs126; cam-1(ak37)	IZ1670	*flp-13*::ACR-12::GFP (pCL32)
ufIs126; F53B6.2(ok2854)	IZ1731	*flp-13*::ACR-12::GFP (pCL32)
ufIs126; syd-1(ju82)	IZ2004	*flp-13*::ACR-12::GFP (pCL32)
ufIs126; rpy-1(ok145); acr-12(ok367)	IZ1497	*flp-13*::ACR-12::GFP (pCL32)
ufIs126; lev-10(ok2111)	IZ1604	*flp-13*::ACR-12::GFP (pCL32)
ufIs126; nrx-1(ok1649)	IZ1696	*flp-13*::ACR-12::GFP (pCL32)
ufIs126; unc-17(e113)	IZ1678	*flp-13*::ACR-12::GFP (pCL32)
ufIs126; unc-17(e245)	IZ1570	*flp-13*::ACR-12::GFP (pCL32)
ufIs126; unc-3(e151)	IZ1496	*flp-13*::ACR-12::GFP (pCL32)
ufEx441	IZ2374	*flp-13*::ACR-12::GFP (pCL32)
ufEx441; nrx-1(wy778)	IZ2312	*flp-13*::ACR-12::GFP (pCL32)
ufEx441; nrx-1(uf181)	IZ2739	*flp-13*::ACR-12::GFP (pCL32)
ufEx441; nrx-1(uf185)	IZ2873	*flp-13*::ACR-12::GFP (pCL32)
ufEx441; ufEx1114; nrx-1(wy778)	IZ2981	*flp-13*::ACR-12::GFP (pCL32); *unc-17β*::*nrx-1*$_L$ minigene at 10ng/µL (pAP204)
ufIs164	IZ2513	*flp-13*::ACR-12::GFP::3xHA (pAP138)
ufIs164; nrx-1(wy778)	IZ2628	*flp-13*::ACR-12::GFP::3xHA (pAP138)
oxIs12	EG1306	*unc-47*::GFP
oxIs12; unc-3(e151)	IZ2496	*unc-47*::GFP
oxIs12; nrx-1(nu485)	IZ2660	*unc-47*::GFP
wdIs5; dpy-20(e1282)	NC2484	*unc-4*::GFP
vsIs48; lin-15(n765ts)	LX949	*unc-17*::GFP
ufEx766; lin-15(n765ts)	IZ2173	*nrx-1*$_L$*2kb*::GFP (pAP118)
ufEx996	IZ2626	*nrx-1*$_L$::GFP (pAP156)
ufEx996; unc-3(e151)	IZ2611	*nrx-1*$_L$::GFP (pAP156)
ufEx996; ufIs43	IZ2617	*nrx-1*$_L$::GFP (pAP156); *acr-2*::mCherry (pPRB6)
ufEx1046, ufEx1042; ufEx1041; ufEx1040	IZ2746, IZ2733, IZ2732, IZ2731	*nrx-1*$_L$*COEΔ*::GFP (pAP178)
ufEx847	IZ2359	*unc-129*::NRX-1$_L$::GFP (pAP120)
ufEx847; ufIs63	IZ2769	*unc-129*::NRX-1$_L$::GFP (pAP120); *acr-2*::mCherry::RAB-3 (pPRB47)
ufEx847; nlg-1(ok259)	IZ2766	*unc-129*::NRX-1$_L$::GFP (pAP120)
ufEx847; ufIs63; acr-12(ok367)	IZ2857	*unc-129*::NRX-1$_L$::GFP (pAP120); *acr-2*::mCherry::RAB-3 (pPRB47)
ufIs155	IZ2670	*ttr-39*::GCaMP6s::SL2::mCherry

		(pAP130)
ufIs155; ufIs157	IZ2695	*ttr-39*::GCaMP6s::SL2::mCherry (pAP130); *acr-2*::Chrimson (pRB2)
ufIs155; ufIs157; nrx-1(wy778)	IZ2840	*ttr-39*::GCaMP6s::SL2::mCherry (pAP130); *acr-2*::Chrimson (pRB2)
ufIs155; ufIs157; acr-12(ok367)	IZ2865	*ttr-39*::GCaMP6s::SL2::mCherry (pAP130); *acr-2*::Chrimson (pRB2)
ufEx1114; ufIs155; ufIs157; nrx-1(wy778)	IZ2985	*unc-17β*::*nrx-1*$_L$ minigene (pAP204); *ttr-39*::GCaMP6s::SL2::mCherry (pAP130); *acr-2*::Chrimson (pRB2)
zfEx813; lin-15(n765ts)	QW1646	*myo-3*::NLSwCherry::SL2::GCaMP6s
zfEx813; ufIs157	IZ2838	*myo-3*::NLSwCherry::SL2::GCaMP6s*;* *acr-2*::Chrimson (pRB2)
zfEx813; ufIs157; nrx-1(wy778)	IZ2880	*myo-3*::NLSwCherry::SL2::GCaMP6s*;* *acr-2*::Chrimson (pRB2)
zfEx813; ufIs157; unc-29(x29); acr-16(ok789)	IZ2958	*myo-3*::NLSwCherry::SL2::GCaMP6s; *acr-2*::Chrimson (pRB2)
ufEx1114; nrx-1(wy778)	IZ2924	*unc-17β*::*nrx-1*$_L$ minigene (pAP204)

Acknowledgements

We would like to thank Dori Schafer, Vivian Budnik, Alexandra Byrne and members of the Francis lab for critical reading of the manuscript, Claire Bénard, Kang Shen, and David Miller for sharing reagents, and Michael Gorczyca, Will Joyce, and the UMMS Model Organism CRISPR Core for technical assistance. Some nematode strains used in this work were provided by the *Caenorhabditis* Genetics Center, which is funded by the NIH National Center for Research Resources (NCRR). This research was supported by NIH NINDS R01 NS064263 (MMF), NIH NIDA F31 DA038399 (AP), and NIH NIGMS R01 GM084491 (MJA).

CHAPTER V

Discussion

Nervous system function is dependent upon the construction and refinement of neural circuits. The regulation of synaptic connectivity by synaptic organizers and neuronal activity is central to this process. My thesis work takes advantage of the simple, well-characterized nervous system of *C. elegans* to address the cellular and molecular mechanisms involved in developmental synaptic remodeling, activity-dependent shaping of neural circuits, and establishing partner-specific connectivity. In Chapter II, my work identifies the single Ig domain protein OIG-1 as an important regulator of developmental remodeling. Expression of OIG-1 regulates the timing of remodeling, likely through the stabilization of postsynaptic receptors, but is less critical for mature synapse formation. Additionally, I show that postsynaptic remodeling involves de novo synthesis of receptors, in contrast to the deconstruction and trafficking of presynaptic components that has been characterized previously (Park et al., 2011). In Chapter III, I characterize cell-type specific roles for neuronal activity in the development and stabilization of synaptic connections. Disruption of cholinergic signaling early in development alters GABAergic connectivity with muscle, while synapses onto GABAergic neurons do not require neurotransmission for their formation. Lastly, my work in Chapter IV describes an instructive role for neurexin in directing partner-specific connectivity. I show that *nrx-1*/neurexin is required for the development of postsynaptic spine-like processes as well as the localization of acetylcholine receptors in GABAergic dendrites. *nrx-1* expression is required in presynaptic cholinergic neurons and this expression is subject to transcriptional regulation by the same pathway that determines cholinergic neurotransmitter identity. In contrast, cholinergic connectivity with their other

postsynaptic partners, muscle cells, is unaffected by *nrx-1* deletion. Thus, distinct molecular signals govern the establishment of synaptic connectivity with these two cell types. This work also provides the first characterization of spiny protrusions in *C. elegans* inhibitory neurons that resemble mammalian dendritic spines, providing exciting avenues for future investigation of spine outgrowth and maintenance. Altogether, my thesis explores fundamental mechanisms governing neural circuit connectivity, shedding light onto how the enormous complexity of the brain is established.

Part I. Transcriptional regulation of the single immunoglobulin domain protein OIG-1 controls synaptic remodeling

40 years ago, electron microscopy studies demonstrated the clear rewiring of synaptic connections in GABAergic DD neurons, indicated by the dorsoventral repositioning of active zones in DD neurites during the transition from the L1 to L2 stage of larval development (White et al., 1978). Numerous follow up studies have addressed genetic mechanisms controlling remodeling of presynaptic components in DD neurons using fluorescent markers to label synaptic vesicles and active zone components (Hallam and Jin, 1998; Park et al., 2011; Petersen et al., 2011; Thompson-Peer et al., 2012). Investigation of the genetic pathways driving postsynaptic remodeling had remained a challenge, however, due to the lack of suitable postsynaptic markers for *in vivo* light microscopy studies. The recent development of GFP-tagged AChR subunits in the Francis laboratory to label the postsynaptic specializations of DD neurons, in particular the ACR-12 subunit, has substantially changed this situation (Petrash et al., 2013). Using this tool, I examined postsynaptic remodeling during development and identified the single immunoglobulin domain protein OIG-1 as a critical regulator of the remodeling program. In contrast, OIG-1 plays only a minor role in the redistribution of presynaptic components. This work highlights the importance of Ig domain proteins in circuit refinement, suggesting that IgSF proteins may similarly regulate postsynaptic plasticity in the brain.

OIG-1 is required for setting the timing of postsynaptic remodeling

I investigated the role of OIG-1 in synaptic remodeling after the discovery that *oig-1* is highly expressed in early L1 DD motor neurons by cell-specific microarray analysis. In *oig-1* mutants, DD postsynaptic remodeling is initiated much earlier than wild type, with precocious removal of dorsal ACR-12 receptors coinciding with their earlier appearance on the ventral side. This result suggests that OIG-1 normally acts to inhibit the remodeling program. The temporal pattern of *oig-1* expression is consistent with this model. *oig-1* expression in DD neurons is high in the L1, then drops after the L1/L2 transition when remodeling occurs. VD neurons, which do not normally remodel, maintain high levels of *oig-1* expression throughout development, and loss of *oig-1* results in ectopic remodeling of ACR-12 receptors to the ventral side. Together, this work indicates that OIG-1 antagonizes the remodeling program in GABAergic neurons. My work and others also demonstrate that OIG-1 inhibits presynaptic remodeling (Howell et al., 2015), although these effects are less prominent (discussed further below).

Transcriptional control of OIG-1 expression

Previous work has indicated that several transcription factors act to coordinate the remodeling of presynaptic components (Hallam and Jin, 1998; Petersen et al., 2011; Thompson-Peer et al., 2012). One transcription factor that blocks presynaptic remodeling specifically in VD neurons is the COUP-TF family transcription factor UNC-55 (Petersen et al., 2011). In *unc-55* mutants, VD neurons (that do not normally undergo remodeling) remodel ectopically, and synaptic outputs relocate to the dorsal side (Petersen et al.,

2011; Shan et al., 2005). One of the transcriptional targets of *unc-55* is the Iroquois homeodomain-containing transcription factor *irx-1*. *unc-55* inhibits *irx-1* expression in VD neurons, which then inhibits remodeling. Thus, de-repression of *irx-1* promotes VD remodeling (Petersen et al., 2011). While *unc-55* is not detected in DD neurons (Shan et al., 2005), *irx-1* is also required for remodeling of presynaptic components in this cell type (Petersen et al., 2011).

In Chapter II, I further elucidate the roles of the transcription factors *unc-55* and *irx-1* in synaptic remodeling, characterizing a genetic program that orchestrates remodeling through regulation of *oig-1* expression. I find that *oig-1* is a downstream transcriptional target of *unc-55*, and that *irx-1* acts as an intermediate in this pathway. Specifically, UNC-55 blocks *irx-1* expression in VD neurons, allowing OIG-1 inhibition of the remodeling program (**Figure 5.1**). In *unc-55* mutants, the de-repression of *irx-1* inhibits *oig-1* expression, which results in VD ectopic remodeling. Further, *irx-1* RNAi results in ectopic expression of *oig-1* in DD neurons throughout development and delayed postsynaptic remodeling, indicating that *irx-1* normally functions to inhibit *oig-1* expression (**Figure 5.1**). In wild type DD neurons, IRX-1 levels rise during the L1/L2 transition to block OIG-1 expression, allowing DD postsynaptic remodeling to occur. UNC-55 expression in VD neurons inhibits expression of IRX-1 to maintain high levels of OIG-1 throughout development, which antagonizes remodeling.

Further work has revealed additional transcriptional regulators of *oig-1* expression. The PITX homeodomain transcription factor *unc-30* acts to promote *oig-1*

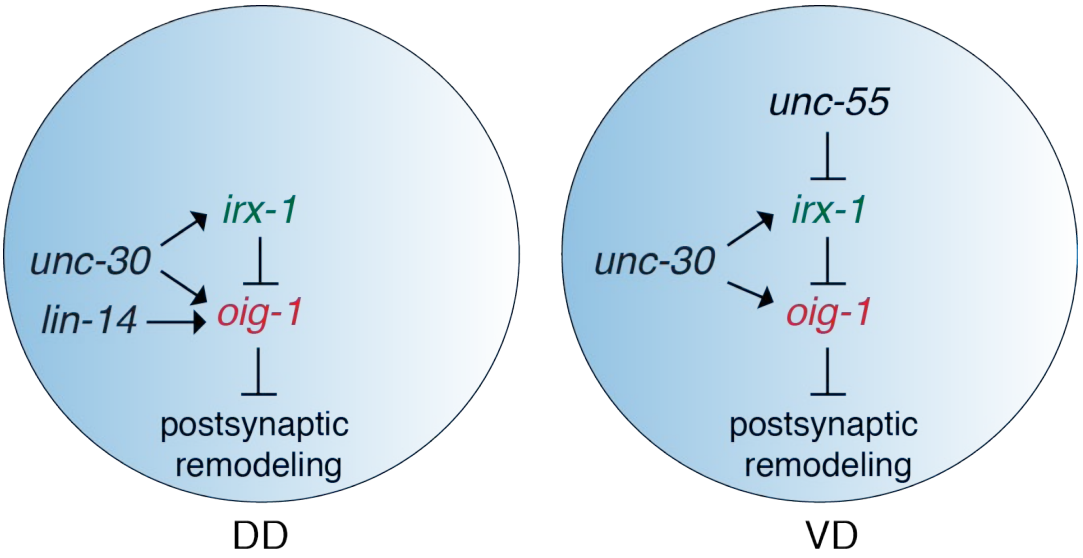

Figure 5.1 Factors that regulate the timing of postsynaptic remodeling
A transcriptional program modulates GABAergic DD and VD remodeling to regulate expression of factors that promote (green) and inhibit (red) remodeling (He et al., 2015; Howell et al., 2015; Kurup and Jin, 2016; Petersen et al., 2011).

expression (Cinar et al., 2005; Howell et al., 2015), however its role in synaptic remodeling is complex as it also regulates the expression of *irx-1* (Petersen et al., 2011). In VD neurons, *unc-30* acts together with *unc-55* to prevent aberrant wiring by controlling the expression levels of *oig-1*. Alternatively, *unc-30* acts with the transcription factor *lin-14* in DD neurons to regulate *oig-1* expression. Thus, intersectional transcriptional strategies control synapse rewiring (**Figure 5.1**) (Howell et al., 2015).

Proposed mechanism of OIG-1 action

The localization of mCherry::OIG-1 in coelomocytes clearly indicates that OIG-1 is secreted. Surprisingly, however, this secretion is not required for its function in controlling synaptic remodeling, and OIG-1 acts cell-autonomously in GABAergic neurons. Expression of secreted OIG-1 in neighboring cholinergic neurons, for example, did not rescue remodeling defects of *oig-1* mutants, while GABAergic expression of mutated OIG-1 that is not predicted to be secreted is sufficient to restore ACR-12::GFP levels. Another *C. elegans* IgSF protein RIG-3 similarly does not require secretion for its function at synapses. At the NMJ, presynaptic RIG-3 regulates the clustering of ACR-16 receptors in muscle. Although RIG-3 can be secreted, membrane-associated RIG-3 primarily mediates its anti-plasticity function at synapses (Babu et al., 2011). One intriguing possibility is that the secreted version of OIG-1 may play additional roles in the nervous system. Loss of the two Ig domain protein ZIG-3, for example, results in the mispositioning of axonal tracts in the nerve cord, and rescue of these defects requires

secretion (Benard et al., 2009). Further characterization of nervous system function in *oig-1* mutants could lend insight into this question, utilizing rescue approaches with secreted or non-secreted OIG-1 protein.

Early in development in young L1 animals, *oig-1* mutants display dorsal ACR-12::GFP expression in DD neurons, but the intensity of fluorescence is significantly decreased compared to wild type. Could OIG-1 help stabilize nascent ACR-12 clusters? In support of this, overexpression of OIG-1 increases ACR-12::GFP fluorescence intensity. While OIG-1 expression in GABAergic neurons restores ACR-12 receptor clustering, ACR-12::GFP and mCherry::OIG-1 occupy non-overlapping domains. One possibility is that OIG-1 interacts with other unidentified scaffolding proteins to help stabilize ACR-12 receptors. Immunoprecipitation to pull down interacting proteins with OIG-1 or ACR-12 may help elucidate this complex.

At the *C. elegans* neuromuscular junction, the single Ig domain protein OIG-4 physically interacts with a postsynaptic scaffold that anchors L-AChRs in muscle (Rapti et al., 2011). A similar mechanism may act to stabilize ACR-12 AChRs in GABA neurons. This model would predict that ACR-12 receptors in the L1 animal may be more mobile in the absence of OIG-1. Fluorescence recovery after photobleaching (FRAP) in the L1 could help address this question. If OIG-1 acts to stabilize ACR-12 receptors in L1 animals, ACR-12::GFP fluorescence should recover more quickly in *oig-1* mutants after photobleaching. However, while both OIG-1 and OIG-4 are secreted, OIG-1 acts cell-autonomously in GABAergic neurons to regulate ACR-12 receptor clusters, while OIG-4 is thought to interact with LEV-10/LEV-9/L-AChR complexes extracellularly (Rapti et

al., 2011). To further test this model described by the Bessereau lab (Rapti et al., 2011), it would be interesting to determine if a non-secreted version of OIG-4 expressed in muscle could potentially rescue the synaptic defects of *oig-4* mutants. Additionally, can OIG-1 and OIG-4 act interchangeably? These questions warrant further study into the distinction between OIG-1 and OIG-4's functions at synapses.

OIG-1 also plays a minor role in the redistribution of presynaptic components. Specific mechanisms that coordinate pre- and post-synaptic remodeling, and the role of OIG-1 in this process, remain unclear. One possibility is that the removal of the postsynaptic apparatus may facilitate presynaptic remodeling, where presynaptic components occupy the same sites that were previously designated as postsynaptic. Further work utilizing a transgenic strain that labels both pre- and post-synaptic components (i.e. *flp-13*::mCherry::RAB-3 and *flp-13*::ACR-12::GFP for pre- and post-synaptic labeling, respectively) could aid in addressing this question. Specifically, time-lapse imaging during the remodeling process (approximately 14-18 hours after hatch) would show the simultaneous repositioning of pre- and post-synaptic structures, although currently the immobilization of young animals for long periods remains a technical limitation. New techniques for the immobilization and high-resolution imaging of *C. elegans*, such as microfluidic devices (Keil et al., 2017) or the use of nanoparticles (Kim et al., 2013) will help overcome this obstacle.

Mechanism of postsynaptic DD remodeling

Ablation of the DD1 commissure prior to rewiring uncouples the axonal and dendritic compartments, but does not disrupt adult expression of ACR-12 receptors later in development, suggesting de novo ventral synthesis of receptors. In contrast, remodeling of presynaptic components requires ventral disassembly and trafficking to the dorsal nerve cord (Park et al., 2011). My results suggest that pre- and post-synaptic remodeling occur via distinct mechanisms, but do not eliminate the possibility that the relocation of postsynaptic components along the DD commissure also contributes to postsynaptic remodeling. Tagging of the ACR-12 receptor with photoactivatable or photoconvertible fluorescent proteins will help evaluate this possibility. Additionally, it will be interesting to evaluate whether genes that coordinate the disassembly and trafficking of presynaptic components, including *cyy-1* and *cdk-5* (Park et al., 2011), also act to regulate remodeling of the postsynapse.

Alternatively, trafficking of ACR-12 receptors from the dorsal to the ventral side may not contribute to adult synapses. This could suggest that remodeling of postsynaptic components involves the concurrent degradation/removal of synapses dorsally with the new synthesis of receptors ventrally. Ongoing genetic experiments in the Francis lab provide additional support for this model. Several mutants with sustained ACR-12::GFP expression in the dorsal nerve cord in the adult have recently been retrieved from a forward genetic screen. These mutants may define genes required for the removal of dorsal ACR-12::GFP clusters. Importantly, the distribution of ventral ACR-12 receptors is unaffected in these mutants, suggesting that ventral expression of ACR-12 receptors

occurs independently of the dorsal removal of synapses. It will be interesting to determine if the timing of ventral ACR-12::GFP expression is affected in these conditions: i.e. does the removal of dorsal ACR-12::GFP receptor clusters trigger the synthesis of cholinergic receptors ventrally? Identification of genes from the forward genetic screen may help answer this question.

Notably, loss of *oig-1* does not disrupt DD ACR-12 receptor clustering in the adult. Thus, distinct machinery may be required for the stabilization of cholinergic receptors in the developing vs mature animal. In Chapter IV, I identify *nrx-1*/neurexin as a critical regulator of mature synapse formation, and I further discuss its mechanism of action in Part III of the Discussion.

Additional questions to address

My work here offers insight into the mechanisms driving postsynaptic DD remodeling and describes transcriptional regulation of a key molecule that shapes the timing of this process. An important question that remains unaddressed, however, is what role synaptic activity plays in postsynaptic remodeling. Prior work has shown that the transcription factor *hbl-1* acts to promote DD remodeling of presynaptic structures, and expression of this gene is activity-dependent (Thompson-Peer et al., 2012). Mutations that decrease circuit activity (i.e. *unc-13* or *unc-18*) decrease *hbl-1* expression, resulting in delayed DD presynaptic remodeling (Thompson-Peer et al., 2012). While transcriptional programs specify the timecourse of DD remodeling, this work demonstrates that this process is not solely the result of genetically hard-wired

programming (Thompson-Peer et al., 2012). Rather, GABAergic DD remodeling is also subject to activity-dependent regulation. In preliminary work, I have found that disruption of *unc-13* does not disrupt the localization of ACR-12::GFP receptor clusters before or after the remodeling process. To address whether the timing of postsynaptic remodeling is activity-dependent, a more detailed analysis of the remodeling timecourse in *unc-13* and *unc-18* mutants is required. Further, do specific alterations in cholinergic signaling (i.e. *unc-17* or *cha-1* mutants) also disrupt the timing of DD remodeling, or does this plasticity require global changes in activity? This work has the potential to elucidate key mechanisms that drive the activity-dependent refinement of neural circuits.

DD remodeling in *C. elegans* enables the correct wiring with newly born cholinergic VA/VB motor neurons. In *oig-1* mutants, remodeling is initiated approximately six hours earlier than wild type, presumably before the birth of these neurons. A closer examination of these synapses in the adult is required to determine if they represent functional connections. Are pre- and post-synaptic structures closely apposed? Is cholinergic neurotransmission onto GABAergic DD neurons disrupted? Locomotory defects in *oig-1* mutants in the adult are consistent with GABA neuron dysfunction, however, it is unclear whether this is the result of disrupted cholinergic receptor localization in VD and/or DD GABAergic neurons. It remains possible that the timing of DD remodeling is critical for establishing the correct synaptic contacts in the mature animal. Further investigation of these adult synapses in *oig-1* mutants will help us better understand how the timing of nervous system refinement shapes mature connectivity.

The involvement of transcription factors in synaptic remodeling has been well documented (Boulanger et al., 2011; West and Greenberg, 2011). My work in combination with others (**Figure 5.1**) has shown that transcriptional programs act in GABAergic neurons in *C. elegans* by ultimately controlling the expression of the single immunoglobulin domain protein OIG-1. IgSF proteins have been implicated in several aspects of neuronal development, including cell migration and synapse formation (Aurelio et al., 2002; Ding et al., 2007; Rougon and Hobert, 2003). While there are many uncharacterized IgSF proteins expressed in the nervous system, work in both vertebrates and *C. elegans* indicates that IgSF members serve important and specific roles in nervous system function (Cherra and Jin, 2016; Howell and Hobert, 2016; Rapti et al., 2011; Usardi et al., 2017). My work here suggests that the single Ig domain protein OIG-1 antagonizes synaptic remodeling by potentially stabilizing AChRs. Many questions remain to be addressed about the mechanism of OIG-1 function at synapses, and these studies will contribute to our understanding of how IgSF proteins play such diverse roles in the brain.

Part II. Excitatory neurons shape GABAergic connectivity

Following the end of the first larval stage, a second population of ventrally directed VD GABAergic neurons are born. To integrate these neurons into the motor circuit, the DD neurons remodel as described above, where postsynaptic components are removed dorsally and new inputs are established onto the ventral dendrites. The newly born VD inhibitory neurons also contain spatially separated dendritic and axonal compartments, with dendrites located dorsally and axons ventrally. In the dorsal dendrite, VD neurons express iAChRs containing the AChR subunit ACR-12. The ventral axon sends projections onto ventral body wall muscle, acting via postsynaptic GABAergic UNC-49 receptors. Fluorescently tagged synaptic components (e.g. ACR-12::GFP, UNC-49::GFP) allow for clear visualization of GABA inputs and outputs in the nerve cord (**Figure 5.2**).

Chapter III focuses on how excitatory neurons shape GABAergic connectivity by examining the processes underlying the integration of these VD GABAergic neurons into the motor circuit. This study aims to address a fundamental question in neurobiology: what role does neuronal activity play in the development of neural circuits? While studies have demonstrated that neurotransmitter secretion may not be absolutely essential for initial synapse formation (Varoqueaux et al., 2002; Verhage et al., 2000), activity-dependent regulation of neural connectivity is well-established and understanding the mechanisms underlying this process is an area of intense interest. The wealth of tools available in *C. elegans* provides us with a useful model in which to study neural circuit

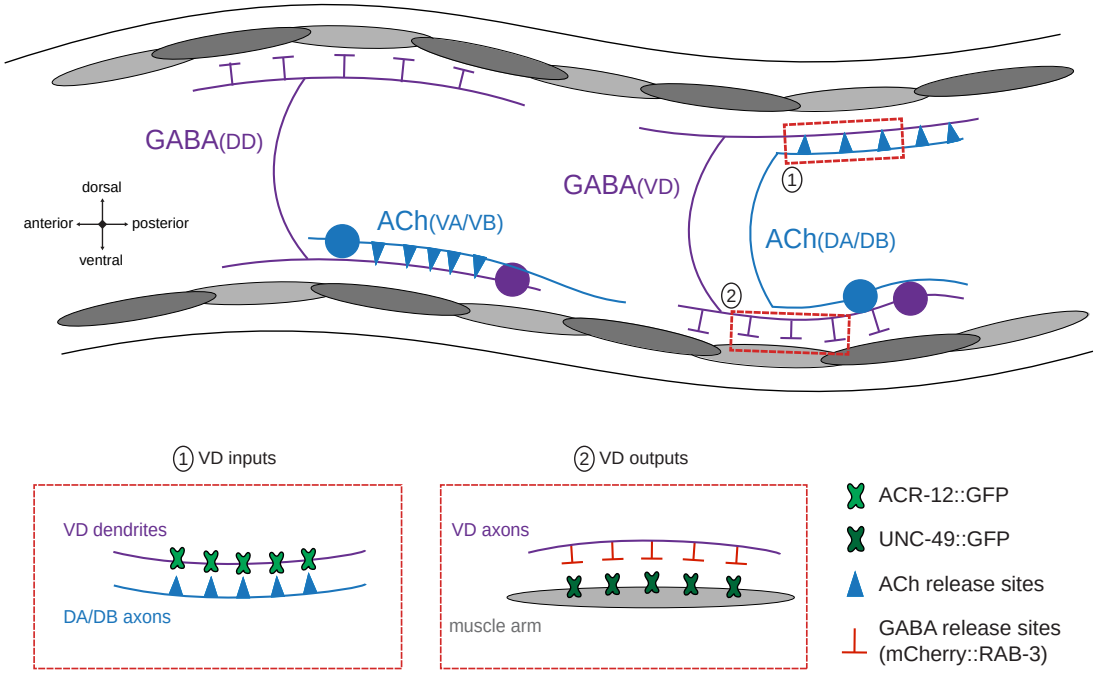

Figure 5.2 Toolkit to study the incorporation of VD GABAergic neurons into the motor circuit

Top: Schematic of *C. elegans* motor circuit. Blue coloring indicates GABAergic motor neurons (DD/VD), purple coloring indicates cholinergic motor neurons (VA/VB and DA/DB). Gray shading represents body wall muscles. Regions of excitatory inputs onto VD neurons (1) and VD inhibitory outputs onto muscle (2) are indicated in red dashed boxes.

Bottom: Expanded views of regions indicated by red boxes above. (1) GABAergic VD inputs are labeled by the tagged AChR ACR-12::GFP, localized opposite sites of ACh release. (2) GABAergic VD outputs are labeled by the fluorescent reporter mCherry::RAB-3. Inhibitory receptors in muscle are labeled by reporter UNC-49::GFP.

development *in vivo* (**Figure 5.2**).

Cholinergic neurons play important roles in both clustering iAChRs in GABA neurons and in shaping GABA synaptic outputs

To investigate how activity regulates GABAergic circuitry, I first examined a requirement for the COE-type transcription factor *unc-3* in inhibitory signaling. *unc-3* mutants lack expression of genes required for cholinergic neuron identity, including *cha-1* and *unc-17* (Prasad et al., 2008), and these mutants show expected disruptions in excitatory neurotransmission and postsynaptic excitatory receptor clustering, consistent with a prior report (Kratsios et al., 2015). Surprisingly, loss of *unc-3* disrupts inhibitory neurotransmission, with reduced frequency and increased amplitude of GABAergic synaptic events. I hypothesized that this defect may be the result of altered synapses onto GABAergic neurons or onto muscle, so I therefore examined VD GABAergic inputs and outputs (**Figure 5.2**). My results demonstrate that mutation of *unc-3* disrupts synapse development at both of these locations, although the mechanisms involved appear specific to each cell type. ACR-12 receptor clusters located in VD dendrites are severely disrupted in *unc-3* mutants, showing abnormal distribution and fewer receptor number in the dorsal nerve cord. GABA synapses at the NMJ in *unc-3* mutants are similarly disrupted, with gaps in synaptic vesicle clusters and fewer postsynaptic GABAergic receptor clusters. Ablation of cholinergic motor neurons using an *acr-2(gf)* transgene results in comparable alterations in synapse number at the NMJ. The changes observed both pre- and post-synaptically are not caused by alterations in the gross morphology of

GABAergic neurons or body wall muscles, as only minor morphological defects are observed in *unc-3* or *acr-2(gf)* mutants (e.g. overgrowth in muscle and some ventral nerve cord defasciculation). I therefore dissected roles for *unc-3* in the establishment of synapses onto both of these cell types.

Excitatory neurotransmission is not required for ACh – GABA connectivity

My work demonstrates that excitatory neurotransmission is severely disrupted in *unc-3* mutants, and these animals show abnormal ACR-12 receptor clustering. However, the disruptions in ACR-12 receptors observed in *unc-3* mutants does not appear to result from a loss of cholinergic transmission. I analyzed *unc-17*/vAChT mutants, which are null for ACh release from cholinergic motor neurons, and transgenic animals expressing tetanus toxin light chain specifically in cholinergic motor neurons. Using both of these approaches, I found that ACR-12 receptor clustering is unaltered. Thus, cholinergic neurotransmission is not required for the formation of cholinergic synapses onto GABAergic neurons.

These results do not eliminate the possibility, however, that neuronal activity can shape synaptic connections onto GABAergic neurons. The effects of activity on circuit refinement and maintenance have been well documented, particularly in the visual system and at the vertebrate neuromuscular junction (Katz and Shatz, 1996; Sanes and Lichtman, 1999). It would be interesting to test if synapses onto GABAergic neurons demonstrate plasticity in response to acute manipulations in activity. Optogenetic and chemical tools developed in *C. elegans* provide spatial and temporal precision in order to approach this

question. For example, cholinergic-specific expression of channelrhodopsin or histamine-gated chloride channels would aid in exciting or inhibiting this cell type, respectively. While synapses onto GABAergic neurons may not require cholinergic neurotransmission for their initial formation, alterations in activity may shape the strengthening or weakening of existing synaptic connections.

An unidentified transcriptional target of unc-3 shapes synapses onto GABA neurons

How does loss of *unc-3* result in the altered distribution of cholinergic receptors in GABAergic neurons? *unc-3* establishes a "cholinergic gene battery" in *C. elegans*, regulating the expression of cholinergic receptors (e.g. *acr-5, acr-2*) and cholinergic pathway genes (e.g. *unc-17, cho-1*) through the binding to COE motifs (Kratsios et al., 2011). Additionally, many other genes such as secreted signaling molecules, axon guidance genes, and other transcription factors are subject to *unc-3* regulation (Kratsios et al., 2015; Kratsios et al., 2011). *unc-3* transcriptional control of genes that control neurotransmitter identity cannot explain the disruptions in ACR-12 receptor clustering, as demonstrated by the tetanus toxin experiments and analysis of *unc-17* mutants. These results point to the exciting possibility that an unidentified transcriptional target of *unc-3* may regulate cholinergic receptor clustering in the postsynaptic cell, perhaps through trans-synaptic signaling.

The synapse-organizing molecule *madd-4/*Punctin appeared to be an excellent candidate. *madd-4* is the *C. elegans* ortholog of mammalian Punctin-1 and Punctin-2, belonging to the ADAMTS-like family (Pinan-Lucarre et al., 2014). *madd-4* is essential

for both excitatory and inhibitory synapse development at the NMJ, and both isoforms are expressed in cholinergic neurons (Pinan-Lucarre et al., 2014), which form synapses onto both GABAergic neurons and body wall muscle. Additionally, *unc-3* directly controls the expression of *madd-4* (Kratsios et al., 2015). However, *madd-4* is not essential for synapses onto GABAergic neurons. Although mutation of *madd-4* produces a slight decrease in ACR-12 receptor clusters, the effect is much less severe than the abnormal distribution of receptors seen in *unc-3* mutants. Thus, the transcriptional target of *unc-3* responsible for clustering ACR-12 receptors had yet to be identified. Through a candidate approach surveying 35 genes that predominantly encode scaffold and cell-cell interaction proteins previously implicated in synapse formation, I identified this gene to be *nrx-1*/neurexin (Chapter IV).

ACh release shapes GABA synapses at the NMJ

While ACh neurotransmitter release is dispensable for synapses onto GABAergic neurons, my work suggests that cholinergic signaling plays an important role in synapse development at the inhibitory neuromuscular junction. Expression of cholinergic-specific tetanus toxin or mutation of *unc-17* results in reduced pre- and post-synaptic clusters (as measured by GABA::mCherry::RAB-3 and muscle::UNC-49::GFP, respectively), as well as gaps in fluorescence that are similar to *unc-3* mutants and transgenic animals expressing *acr-2(gf)*. Cholinergic activation of muscle is not essential for GABA synapse development, as animals lacking functional iAChRs at the NMJ (*unc-29;acr-16* double

mutants) have only minor defects in receptor number, indicating that the disruptions in GABA synapses are not secondary to defects at the excitatory NMJ.

Notably, the defects observed in *unc-17* mutants or in transgenic animals expressing cholinergic-specific tetanus toxin are less pronounced than loss of *unc-3.* Thus, additional acetylcholine-independent signals are likely required for inhibitory synapses at the NMJ. For example, cholinergic motor neurons express a short isoform of *madd-4*/Punctin which is transcriptionally regulated by *unc-3*, and specific disruption of this isoform results in altered expression of UNC-49 receptors in muscle (Kratsios et al., 2015; Pinan-Lucarre et al., 2014). Analysis of *unc-17;madd-4* double mutants will help address this idea by examining whether defects in GABA synapses in these mutants phenocopy the disruptions seen with mutation of *unc-3.*

While loss of *unc-3* disrupts synapse number and size at the GABAergic NMJ, the apposition of pre- and post-synaptic components is preserved. Similar phenotypes are observed in *unc-17* mutants or with cholinergic-specific expression of tetanus toxin. Thus, GABA synapses still form in the absence of cholinergic activity, however, there are fewer overall connections. My work supports prior studies examining the loss of synaptic release and effects on overall synapse number (Bouwman et al., 2004; Brandon et al., 2003). Munc18 deficient mice, for example, lack synaptic release and display fewer synapses in the neocortex at multiple timepoints during development (Bouwman et al., 2004). To examine whether cholinergic signaling is specifically required for synapse formation rather than the maintenance of existing connections, it would be important to

also study GABAergic synapses of *unc-17* mutants early in development, when the VD GABAergic motor neurons are born and first form synapses with ventral muscle.

Plasticity of mature GABA synapses at the NMJ

As noted above, the analysis of *unc-17* mutants suggests that cholinergic transmission is critical for the patterning of GABA synapses, but does not distinguish whether this signal is required in the mature or developing animal. Disrupting cholinergic signaling in the adult animal (either for 4 or 8 hours using a temperature-sensitive *cha-1* allele) reduces the size of pre- and post-synaptic clusters, without effecting synapse number, and these effects are reversible. These effects are distinct from chronic manipulation of cholinergic transmission; in *unc-17* mutants, by comparison, the size of pre- and post-synaptic clusters increases, and there are fewer synapses in the nerve cord.

The reduction in synapse size following acute reduction of cholinergic transmission in adults may suggest that homeostatic mechanisms act to stabilize *E/I* signaling in the adult nervous system, and that cholinergic neuronal activity shapes GABAergic signaling through distinct mechanisms in the developing and mature animal. The balance of excitatory and inhibitory signaling onto *C. elegans* muscle is essential for proper sinusoidal movement: excess excitatory signaling, for example, can lead to convulsive behavior (Jospin et al., 2009), while the addition of the GABA agonist muscimol causes the worm to elongate (Han et al., 2015; Schaeffer and Bergstrom, 1988). The transient loss of excitatory signaling in the adult animal may result in compensatory decreases in GABA synapse size in an attempt to maintain this *E/I* balance.

How this effect is mediated is unclear, but this process could involve the internalization of surface GABA receptors. The majority of UNC-49::GFP fluorescence appears to represent cell surface receptors (Tong et al., 2015), and increased receptor internalization may represent a means to scale inhibitory signaling. Depolarization of cultured hippocampal neurons, for example, results in an increase in GABA receptor number and size through decreases in the internalization rate (Rannals and Kapur, 2011). Specific examination of cell surface UNC-49 receptors, potentially using a pH-sensitive GFP (pHluorin) tag, will help address this question. Additionally, improved imaging techniques may reveal an increase in the lateral diffusion of GABA receptors, which could also explain the observed decreases in synapse size.

As the homeostatic mechanisms driving receptor turnover at inhibitory synapses are not well defined, further work examining genes required for these activity-induced changes in synapse size will advance our understanding of this process. One gene that has been previously linked to the homeostatic regulation of inhibitory synapses in the hippocampus is the cell adhesion molecule dystroglycan (Pribiag et al., 2014). Prolonged neuronal activity upregulates dystroglycan expression, increasing dystroglycan localization to synapses and GABA receptor abundance (Pribiag et al., 2014). Although dystroglycan homologs are not thought to be expressed in *C. elegans* muscle (Johnson et al., 2006), it is possible that other genes may play similar roles in the scaling of GABAergic receptors at the neuromuscular junction.

A possible critical period for GABA synapse development at the NMJ

While acute loss of cholinergic activity in the mature animal decreases synapse size, disruptions of excitatory neurotransmission early in development, when the VD motor neurons are born and first integrated into the motor circuit, mimic the effects seen in *unc-17* mutants. An eight-hour block in ACh neurotransmission at the end of the L1 stage results in fewer synapses and larger presynaptic clusters later in adulthood. Thus, loss of activity during this time period produces irreversible defects in synapse patterning. These results suggest that the wiring of VD neurons may be shaped by a critical or sensitive period, a concept first described in the visual system (Hubel and Wiesel, 1970), where neuronal circuits are more susceptible to enhanced plasticity in development.

GABA synapses are sensitive to loss of neuronal activity at the end of the L1 stage. One possibility is that reductions in ACh activity during this time period, when the DA/DB motor neurons are first forming synaptic connections with the newly born VD GABAergic neurons, impairs synapse rewiring. The defects in VD GABA synapses at the NMJ are likely not due to impaired release of inhibitory neurotransmitter, as disruption of GABA biosynthesis does not alter GABA synapses in worms (Gally and Bessereau, 2003; Jin et al., 1999). Vesicular signals from cholinergic neurons may control the expression of synaptogenic molecules, acting in GABAergic neurons to regulate their outputs onto muscle. For example, the transcription factor Npas4 is activated by excitatory activity, and in turn triggers the formation of inhibitory synapses in mouse hippocampal neurons (Bloodgood et al., 2013; Lin et al., 2008). Genes induced by

changes in neuronal activity help mediate plastic changes in synapse structure and function (Hayashi et al., 2012; West and Greenberg, 2011). Using microarray analysis to look for genes whose expression levels are altered in *cha-1* temperature-shifted animals vs wild type controls, future work could identify genes involved in activity-dependent changes at the *C. elegans* inhibitory NMJ.

The role of activity in the development of neural circuits

My results here suggest that synaptic connections are differentially sensitive to alterations in activity, supporting recent work highlighting cell-type specific effects (Andreae and Burrone, 2014; Bleckert and Wong, 2011; Dunn et al., 2013; Morgan et al., 2011; Soto et al., 2012). For example, in the retina, neurotransmission differentially regulates glutamatergic synapses onto a single postsynaptic retinal ganglion cell (Morgan et al., 2011). The motor circuit in *C. elegans* provides an excellent model to address this idea due to its relative wiring simplicity and the availability of cell type-specific synaptic markers. In Chapter III, I find that cholinergic synapses onto GABAergic neurons develop normally in the absence of presynaptic activity, while ACh drive is critical for the distribution and density of inhibitory synapses at the NMJ. Based on this work in combination with others (Dunn et al., 2013; Morgan et al., 2011; Soto et al., 2012), it is unlikely that one mechanism (or mechanisms) drives activity-dependent changes in connectivity. Rather, different cell types may employ different strategies to regulate their circuitry in response to activity.

Future studies identifying genes responsible for activity-dependent changes at the inhibitory NMJ in *C. elegans* will help address this question. Based on my work examining the requirements of cholinergic signaling during different time periods in development, I expect that distinct processes may be involved in the developing vs mature animal. The regulation of inhibitory synapses is critical for establishing *E/I* balance in the brain, as deficits are associated with disorders such as epilepsy (Cossart et al., 2001; Powell et al., 2003). Studies aimed at identifying the processes underlying activity-dependent changes at synapses will shed light onto how *E/I* balance is established and maintained in the brain.

Part III. The synaptic organizer neurexin coordinates cholinergic synaptic connectivity with GABAergic motor neurons

The analysis of GABAergic connectivity in Chapter III suggested that a transcriptional target of *unc-3* may be required for the development of cholinergic synapses onto GABAergic neurons. Cholinergic motor neurons in the *C. elegans* motor circuit form dyadic synapses onto both body wall muscle and inhibitory GABAergic neurons. Interestingly, *unc-3* regulation of the synaptogenic molecule *madd-4/*Punctin is required for cholinergic synapses onto body wall muscle (Pinan-Lucarre et al., 2014), but is not essential for connectivity onto GABAergic neurons (Chapter III). What are the molecular mechanisms underlying these synapse-type specific differences?

To address this question, I searched for genes that specifically disrupt ACh – GABA connectivity. Through this work, I identified the cell adhesion molecule *nrx-1*/neurexin. My results characterize a novel role for neurexin in establishing divergent connectivity, advancing our understanding of how synaptic organizers may direct neuronal circuitry in the brain.

Heteromeric AChRs are localized to spiny processes on the DD1 GABAergic neuron

First, I established a model to examine cholinergic synapses with single neuron resolution *in vivo.* There are six DD GABAergic motor neurons along the length of the worm, and DD1 is spatially separated from the remaining DD neurons, offering clear visualization of neuronal processes. By examining the anterior DD1 dendritic process, I

was able to study cholinergic synapses onto a single dendrite, an approach that is unattainable in other systems.

Using this model, I found that the DD1 dendrite contains finger-like protrusions that contact presynaptic cholinergic motor neuron axons. Similar to mammalian dendritic spines, these structures harbor excitatory neurotransmitter receptors at their tips, increase in number during development, and display variation in their size and shape. Prior work using electron microscopy also noted the presence of spiny processes in D-type neurons (White et al., 1976, 1986), but these structures have not been characterized further. Thus, my finding introduces the exciting possibility that some synapses in *C. elegans* may occur on the surface of dendritic spines, similar to the majority of excitatory synapses in the mammalian brain. Additional ultrastructural studies will help categorize these processes by their morphology, as examination of spine shape in worms is difficult to determine at the light microscopy level.

Excitatory iAChRs containing the ACR-12 subunit concentrate at the tips of these protrusions, extending into the presynaptic domain. Using candidate deletion analysis and cell-specific rescue, I defined the subunit composition of this neuronal receptor. My studies indicate that four acetylcholine receptor subunits (LEV-1, UNC-29, UNC-63, and UNC-38) likely coassemble with ACR-12 to form a pentameric receptor. Genetic ablation of this receptor (i.e. mutation of *acr-12* or *unc-63*) does not disrupt spine number or morphology, suggesting that spines can still form in the absence of iAChRs. However, mutation of *acr-12* does not completely eliminate inhibitory signaling (Petrash et al., 2013) or GABA neuron calcium responses to cholinergic stimulation (Chapter IV), which

may indicate that unidentified iAChRs also help mediate excitatory signaling onto GABAergic neurons. Genetic ablation of *acr-12* in combination with iAChR subunit genes known to be expressed in GABAergic neurons (such as *acr-9* or *acr-14*) may help to address this question. How AChR subtypes expressed within the same cell are localized to specific synapses is another potential area for further study.

Through a candidate-based genetic screen, I found that *nrx-1*/neurexin is required for the localization of ACR-12 containing receptors to spiny processes. The 35 genes surveyed predominantly encode scaffold and cell-cell interaction proteins previously implicated in synapse formation. Future work employing an unbiased forward genetic screen may reveal novel regulators of synapse development. Additionally, GABA-specific RNAi approaches may help target genes that are linked to lethality, such as *pan-1*, which encodes a predicted transmembrane protein with leucine-rich repeat domains (Gissendanner and Kelley, 2013) that may be important for protein-protein interactions at synapses.

Within the candidates surveyed, several genes that are required for muscle AChR clustering produce mild to moderate decreases (28-39%) in ACR-12 receptor clustering. L-AChRs are similar in subunit composition to ACR-12 receptors, differing by only one α subunit (ACR-12 in GABAergic neurons, LEV-8 in muscle) (Boulin et al., 2008; Towers et al., 2005). It would be interesting to test if genes essential for L-AChR clustering also act cell-autonomously in GABAergic neurons, playing a minor role in ACR-12 receptor clustering. Alternatively, disruption of L-AChRs at the NMJ may affect

ACR-12 clustering in neighboring GABAergic neurons. Examination of *lev-8* mutants, to specifically disrupt L-AChRs, will help address this question.

A trans-synaptic role for neurexin in the development of the postsynapse

In mammals, neurexin plays important roles in both excitatory and inhibitory synapse development, acting via trans-synaptic partners to connect pre- and post-synaptic neurons at synapses. Neurexin's most well-characterized extracellular binding partner is neuroligin (Boucard et al., 2005; Comoletti et al., 2006; Ichtchenko et al., 1995; Ichtchenko et al., 1996; Nguyen and Sudhof, 1997). While loss of *nlg-1*/neuroligin in *C. elegans* has been associated with the disruption of GABAergic synapses at the neuromuscular junction (Maro et al., 2015; Tu et al., 2015), single gene mutations in *nrx-1*/neurexin have not been previously demonstrated to alter synapse formation. In Chapter IV, I provide the first evidence for neurexin regulation of synapse development in worms. Specifically, I find that loss of *nrx-1*/neurexin disrupts the clustering of ACR-12 receptors in both DD and VD GABAergic neurons, with fewer receptor number and increased diffuse fluorescence in the dendritic processes. *nrx-1* is also required for spine outgrowth, while the gross morphology of GABAergic neurons is unaffected. In contrast, mutation of *nlg-1*/neuroligin produces no appreciable defects in ACR-12 receptor clustering or spine outgrowth. My work demonstrates that *nrx-1* acts independently of *nlg-1* to regulate cholinergic synapses onto GABAergic neurons, suggesting the involvement of an alternative binding partner for neurexin.

Previous studies in vertebrates have shown that neurexins are highly concentrated

at presynaptic nerve terminals (Hata et al., 1993; Ushkaryov et al., 1992) and act to regulate synaptic release, primarily through coupling Ca^{+2} channels to the presynaptic machinery (Dean et al., 2003; Missler et al., 2003). Additionally, there is little evidence to suggest that neurexin is required for spine formation; while knockout of two out of the three mouse alpha neurexins reduces dendrite length and total spine number in the cortex, this is only a mild effect and synaptic ultrastructure remains unaffected (Dudanova et al., 2007). In my work, I find that neurexin is similarly expressed in presynaptic cholinergic motor neurons and localizes to axon terminals. However, loss of *nrx-1*/neurexin does not appear to affect presynaptic development or ACh signaling onto body wall muscle. Instead, I demonstrate a specific requirement for neurexin presynaptically to regulate the postsynaptic domain. My work reflects an emerging view for neurexins in the brain, where neurexins serve as context-dependent synaptic organizers (Chen et al., 2017). At the neuromuscular junction in *C. elegans*, for example, neurexins play a minor role in GABAergic synapse formation, acting in a complex with MADD-4/Punctin and NLG-1/neuroligin (Maro et al., 2015; Tu et al., 2015), while also mediating a retrograde signaling pathway to regulate the strength of cholinergic neurotransmitter release (Hu et al., 2012; Tong et al., 2017). Understanding neurexin's role in the brain requires the dissection of neurexin function at each synapse type. This question is difficult to address in mammals, which express three neurexin genes and thousands of different isoforms, and triple knockout of all alpha neurexins results in lethality (Missler et al., 2003). In *C. elegans* there is just one neurexin homolog, and the simplicity of neural circuits has enabled the investigation of neurexin function. As mutations in neurexin have been

associated with neuropsychiatric and neurodevelopmental disorders, such as autism spectrum disorder and schizophrenia (Kim et al., 2008a; Reichelt et al., 2012; Rujescu et al., 2009), there is a critical need to examine the molecular mechanisms underlying neurexin's differential roles at synapses.

Proposed mechanism of NRX-1 signaling

As is the case for mammals, the *C. elegans nrx-1* locus encodes both long and short isoforms (*nrx-1*$_L$ and *nrx-1*$_S$). Specific re-expression of *nrx-1*$_L$ in mutants that contain disruptions in both isoforms rescues receptor clustering and spine outgrowth, indicating that *nrx-1*$_L$ is required for postsynaptic development. To date, work investigating *C. elegans nrx-1*/neurexin has only implicated the long isoform (Hart and Hobert, 2018; Hu et al., 2012; Maro et al., 2015), and roles for *nrx-1*$_S$ are unknown. In the brain, both isoforms are capable of binding trans-synaptic partners, such as neuroligin (Boucard et al., 2005). Future work examining mutants with specific disruptions in *nrx-1*$_S$ may help unravel functions for this isoform in *C. elegans* nervous system development.

The long isoform of *C. elegans* neurexin encodes a single pass transmembrane protein containing intracellular PDZ binding and extracellular LNS and EGF-like domains, similar to mammalian neurexins. My work suggests that intracellular interactions are critical for neurexin's function at synapses. Disruption of the PDZ binding domain reduces ACR-12 receptor clustering and spine outgrowth, and these effects are equally as severe as *nrx-1* null mutants (*wy778*). Prior work has shown that neurexins can interact with a complex of PDZ domain containing proteins such as

CASKs, Velis, and Mints (Biederer and Sudhof, 2000; Butz et al., 1998; Hata et al., 1996). Interestingly, mutation of *lin-2* or *lin-7, C. elegans* homologs of CASK and Veli, respectively, does not disrupt receptor clustering. However, binding of mammalian neurexins to these proteins is thought to be critical for the recruitment of Munc18 to the plasma membrane and subsequent neurotransmitter release (Biederer and Sudhof, 2000), and loss of *C. elegans nrx-1* does not disrupt ACh release or synaptic vesicle clustering. One possibility is that NRX-1's PDZ binding domain is important for its recruitment to axon terminals, and the mislocalization of NRX-1 disrupts its trans-synaptic function as a synaptic organizer. For example, in *Drosophila*, the presynaptic active zone protein *Syd-1* recruits neurexin to active zones at the neuromuscular junction, and loss of either *Syd-1* or *dnrx-1* disrupts synapse formation (Owald et al., 2012). In the candidate-based genetic screen, I found that loss of *C. elegans syd-1* significantly reduces cholinergic receptor clustering in GABAergic dendrites. Future work investigating the role of SYD-1 and additional PDZ domain containing proteins will help reveal intracellular NRX-1 binding partners and their functions at synapses.

My analysis of multiple *nrx-1* deletion strains demonstrates that extracellular interactions are also critical for neurexin's function as a synaptic organizer. The *ok1649* allele, for example, generates an in-frame deletion, eliminating a region predicted to encode an extracellular LNS domain (LNS2), and these mutants demonstrate severe disruptions in both ACR-12 receptor localization and spine outgrowth. Multiple extracellular binding partners are capable of interacting with mammalian neurexins via this domain (Missler et al., 1998; Sugita et al., 2001), suggesting that its removal could

disrupt binding of *C. elegans nrx-1* partners. Notably, NRX-1/neurexin acts trans-synaptically to regulate the postsynapse independently of its typical postsynaptic binding partner NLG-1/neuroligin. Although mammalian neurexins are capable of binding to several extracellular partners besides neuroligin, less is known about their roles in synapse formation and function. Additionally, work to date examining *C. elegans* nervous system development has described roles for neurexin solely in the context of its partnership with neuroligin (Hart and Hobert, 2018; Hu et al., 2012; Maro et al., 2015; Tong et al., 2015). Thus, my investigation of neurexin signaling at *C. elegans* neuronal synapses provides an opportunity to dissect novel roles for neurexins.

How does presynaptic NRX-1 coordinate postsynaptic development in GABAergic neurons? Mammalian neurexins are capable of directly binding to postsynaptic GABAergic receptors (Zhang et al., 2010), suggesting that *C. elegans* NRX-1 may bind directly to ACR-12 iAChRs. Mutation of *acr-12* does not disrupt NRX-1 localization to synapses, arguing against this idea. Many of the described binding partners for mammalian neurexins, including neurexophilins (Beglopoulos et al., 2005; Missler et al., 1998; Missler and Sudhof, 1998; Petrenko et al., 1996), LRRTMs (de Wit et al., 2009; Ko et al., 2009; Siddiqui et al., 2010; Um et al., 2016), and cerebellins (Joo et al., 2011; Matsuda and Yuzaki, 2011; Uemura et al., 2010) have no clear *C. elegans* orthologs. I tested several other known neurexin binding partners in the candidate gene approach, such as *casy-1*/calsyntenin (Lu et al., 2014; Pettem et al., 2013; Um et al., 2014), *dgn-2;dgn-3*/dystroglycan (Reissner et al., 2014; Sugita et al., 2001), *lat-2*/latrophilin (Boucard et al., 2012), and *madd-4*/Punctin (Maro et al., 2015), but these

mutants did not produce the severe defects seen with mutation of *nrx-1*. These results could implicate a novel postsynaptic binding partner for neurexin or possible redundancy between neurexin binding partners. An unbiased forward genetic screen may help address the first possibility, combined with surveying *C. elegans* genes encoding protein-protein interaction domains. While there are no obvious orthologs for LRRTMs, for example, there are *C. elegans* proteins with similar domain architectures (Dolan et al., 2007; Hobert, 2013), and many of these are expressed in neurons (Liu and Shen, 2011). Alternatively, there may be redundancy between multiple postsynaptic binding partners. Multiple cell adhesion interactions, for example, specify the wiring of mating circuits in the *C. elegans* adult male (Kim and Emmons, 2017). This possibility may reflect how complex circuitry is established, and would require the analysis of double or triple mutants to decipher neurexin partners.

Known extracellular neurexin binding partner	***C. elegans* ortholog(s)**	**Effect on ACR-12 iAChRs**
neuroligins	*nlg-1*	no effect
dystroglycans	*dgn-1, dgn-2, dgn-3*	*dgn-1* sterile no effect in *dgn-2; dgn-3*
calsyntenins	*casy-1*	no effect
latrophilins	*lat-1, lat-2*	*lat-1* L1 arrest no effect in *lat-2*
neurexophilins	no clear ortholog (Hobert, 2013; Missler and Sudhof, 1998)	N/A
cerebellins	no clear ortholog (Hobert, 2013)	N/A
LRRTMs	no clear ortholog (Hobert, 2013)	N/A

Table 5.1 Extracellular binding partners for neurexins

In combination with these genetic approaches to identify trans-synaptic binding partners, biochemical analysis may provide additional insight. Immunoprecipitation to pull down interacting proteins with neurexin or postsynaptic AChRs could help elucidate this signaling pathway. It would also be interesting to test whether NRX-1 and OIG-1, which are both required for AChR localization in first larval stage animals, physically interact. However, Ig domain containing proteins most frequently bind to other Ig domains (Missler et al., 2012), and the defects in AChR clustering are distinct in *nrx-1* and *oig-1* mutants, perhaps suggesting separate pathways.

Future work characterizing postsynaptic binding partners will advance our understanding of how neurexins coordinate iAChR clustering and spine outgrowth. Studies investigating the role of cell surface molecules and spine development in vertebrates, for example, have suggested that trans-synaptic signaling may be linked to the organization of the actin cytoskeleton (Liu et al., 2016; Penzes et al., 2003). Further examination of F-actin organization in the spine-like processes of GABAergic dendrites will help test this idea, in both *nrx-1* mutants and with mutation of their downstream partners.

Transcriptional control of nrx-1 expression

My analysis of ACR-12 clustering in Chapter III suggested that a transcriptional target of *unc-3* controls receptor localization in GABAergic dendrites. In Chapter IV, I identify this target to be *nrx-1*/neurexin. My results suggest that *unc-3* directly regulates *nrx-1* expression through a COE binding motif located upstream of the *nrx-1*$_L$ start site.

Forced expression of *nrx-1*/neurexin in *unc-3* mutants restores ACR-12 receptor clusters, indicating that the lack of receptors in *unc-3* mutants is due to the absence of *nrx-1*. In mammals, neurexin isoforms demonstrate cell-type specific expression patterns, indicating that neurexin mRNA expression is tightly regulated (Fuccillo et al., 2015). In Chapter IV, I find that *unc-3* controls the expression of *nrx-1*/neurexin in *C. elegans* motor neurons, while mRNA signal in head neurons is unaffected in *unc-3* mutants. Thus, *unc-3* regulates the cell-type specific expression pattern of neurexin in the nervous system. It will be interesting to determine if expression of *nrx-1*$_S$, which utilizes an independent promoter, is also subject to *unc-3* transcriptional regulation.

My findings support growing evidence that genetic programs can specify both synaptic connectivity and neurotransmitter identity. While *unc-3* expression is required for ACh neurotransmitter release, it also directly controls the expression of two synaptogenic molecules, *madd-4*/Punctin (Kratsios et al., 2015) and *nrx-1*/neurexin. These features suggest that synapse formation can be genetically hardwired. In support of this, loss of ACh neurotransmission does not affect cholinergic receptor localization or spine outgrowth in the DD1 dendrite. In mouse hippocampal neurons, complete loss of glutamate release similarly does not disrupt dendritic morphology, highlighting the importance of neuron-intrinsic programs in synapse formation (Sando et al., 2017; Sigler et al., 2017). However, my work from Chapter III in combination with previous studies (Dunn et al., 2013; Morgan et al., 2011; Soto et al., 2012) reflect a model where synapses are differentially sensitive to alterations in activity. Further characterization of

cholinergic synapses in *C. elegans* in response to acute manipulations in activity may help address the potential plasticity of these connections.

COE (Collifer/Olf1/EBF)-type transcription factors play a variety of roles, including axonal pathfinding and neuronal specification, and they are expressed in the developing nervous system (Garel et al., 1997; Wang et al., 1997). Given the strong conservation of these genes across systems (Dubois and Vincent, 2001), my results suggest that COE-type transcription factors may similarly promote synapse formation in the brain. In support of this idea, the *Drosophila* COE-type transcriptional regulator Knot controls the formation of class IV dendritic arbors (Hattori et al., 2007) through the regulation of downstream target genes (Hattori et al., 2013). Further investigation of mammalian COE/EBF proteins and their regulation of target genes (Green and Vetter, 2011) in the developing nervous system may reveal conserved roles for these transcription factors in synapse establishment.

Partner-specific synaptic connectivity

unc-3 directly controls the expression of two synaptogenic molecules, MADD-4 and NRX-1. While loss of *nrx-1* disrupts ACR-12 receptor clustering and spine outgrowth in GABAergic dendrites, *nrx-1* is not required for AChR clustering in muscle, consistent with a previous report (Hu et al., 2012). Conversely, *madd-4* is required for the development of the excitatory neuromuscular junction (Pinan-Lucarre et al., 2014), but is not essential for the formation of synapses onto GABAergic neurons. This work suggests that transcriptional control of distinct synaptic organizers may specify divergent

connectivity. In support of this, loss of *nrx-1* specifically impairs evoked ACh transmission onto inhibitory neurons, but not muscles. Thus, a single presynaptic neuron coordinates synapse formation with its postsynaptic partners through the differential deployment of synaptic organizers. This work provides evidence for neurexin regulation of divergent connectivity, and suggests the exciting possibility that neurexins may play similar roles in the brain.

BIBLIOGRAPHY

Ackley, B.D., Harrington, R.J., Hudson, M.L., Williams, L., Kenyon, C.J., Chisholm, A.D., and Jin, Y. (2005). The two isoforms of the *Caenorhabditis elegans* leukocyte-common antigen related receptor tyrosine phosphatase PTP-3 function independently in axon guidance and synapse formation. J Neurosci 25, 7517-7528.

Alfonso, A., Grundahl, K., Duerr, J.S., Han, H.P., and Rand, J.B. (1993). The *Caenorhabditis elegans unc-17* gene: a putative vesicular acetylcholine transporter. Science 261, 617-619.

Andreae, L.C., and Burrone, J. (2014). The role of neuronal activity and transmitter release on synapse formation. Curr Opin Neurobiol 27, 47-52.

Aoki, C., Venkatesan, C., Go, C.G., Mong, J.A., and Dawson, T.M. (1994). Cellular and subcellular localization of NMDA-R1 subunit immunoreactivity in the visual cortex of adult and neonatal rats. J Neurosci 14, 5202-5222.

Apel, E.D., Glass, D.J., Moscoso, L.M., Yancopoulos, G.D., and Sanes, J.R. (1997). Rapsyn is required for MuSK signaling and recruits synaptic components to a MuSK-containing scaffold. Neuron 18, 623-635.

Arribere, J.A., Bell, R.T., Fu, B.X., Artiles, K.L., Hartman, P.S., and Fire, A.Z. (2014). Efficient marker-free recovery of custom genetic modifications with CRISPR/Cas9 in *Caenorhabditis elegans*. Genetics 198, 837-846.

Ast, T., Cohen, G., and Schuldiner, M. (2013). A network of cytosolic factors targets SRP-independent proteins to the endoplasmic reticulum. Cell 152, 1134-1145.

Aurelio, O., Hall, D.H., and Hobert, O. (2002). Immunoglobulin-domain proteins required for maintenance of ventral nerve cord organization. Science 295, 686-690.

Babu, K., Hu, Z., Chien, S.C., Garriga, G., and Kaplan, J.M. (2011). The immunoglobulin super family protein RIG-3 prevents synaptic potentiation and regulates Wnt signaling. Neuron 71, 103-116.

Baer, K., Burli, T., Huh, K.H., Wiesner, A., Erb-Vogtli, S., Gockeritz-Dujmovic, D., Moransard, M., Nishimune, A., Rees, M.I., Henley, J.M., et al. (2007). PICK1 interacts with alpha7 neuronal nicotinic acetylcholine receptors and controls their clustering. Mol Cell Neurosci 35, 339-355.

Bamber, B.A., Beg, A.A., Twyman, R.E., and Jorgensen, E.M. (1999). The *Caenorhabditis elegans unc-49* locus encodes multiple subunits of a heteromultimeric GABA receptor. J Neurosci 19, 5348-5359.

Banerjee, S., Venkatesan, A., and Bhat, M.A. (2017). Neurexin, Neuroligin and Wishful Thinking coordinate synaptic cytoarchitecture and growth at neuromuscular junctions. Mol Cell Neurosci 78, 9-24.

Barbagallo, B., Philbrook, A., Touroutine, D., Banerjee, N., Oliver, D., Lambert, C.M., and Francis, M.M. (2017). Excitatory neurons sculpt GABAergic neuronal connectivity in the *C. elegans* motor circuit. Development 144, 1807-1819.

Barbagallo, B., Prescott, H.A., Boyle, P., Climer, J., and Francis, M.M. (2010). A dominant mutation in a neuronal acetylcholine receptor subunit leads to motor neuron degeneration in *Caenorhabditis elegans*. J Neurosci 30, 13932-13942.

Beglopoulos, V., Montag-Sallaz, M., Rohlmann, A., Piechotta, K., Ahmad, M., Montag, D., and Missler, M. (2005). Neurexophilin 3 is highly localized in cortical and cerebellar regions and is functionally important for sensorimotor gating and motor coordination. Mol Cell Biol 25, 7278-7288.

Benard, C., Tjoe, N., Boulin, T., Recio, J., and Hobert, O. (2009). The small, secreted immunoglobulin protein ZIG-3 maintains axon position in *Caenorhabditis elegans*. Genetics 183, 917-927.

Bhattacharya, R., Touroutine, D., Barbagallo, B., Climer, J., Lambert, C.M., Clark, C.M., Alkema, M.J., and Francis, M.M. (2014). A conserved dopamine-cholecystokinin signaling pathway shapes context-dependent *Caenorhabditis elegans* behavior. PLoS Genet 10, e1004584.

Biederer, T., and Sudhof, T.C. (2000). Mints as adaptors. Direct binding to neurexins and recruitment of munc18. J Biol Chem 275, 39803-39806.

Bleckert, A., and Wong, R.O. (2011). Identifying roles for neurotransmission in circuit assembly: insights gained from multiple model systems and experimental approaches. Bioessays 33, 61-72.

Bloodgood, B.L., Sharma, N., Browne, H.A., Trepman, A.Z., and Greenberg, M.E. (2013). The activity-dependent transcription factor NPAS4 regulates domain-specific inhibition. Nature 503, 121-125.

Blount, P., and Merlie, J.P. (1990). Mutational analysis of muscle nicotinic acetylcholine receptor subunit assembly. J Cell Biol 111, 2613-2622.

Boucard, A.A., Chubykin, A.A., Comoletti, D., Taylor, P., and Sudhof, T.C. (2005). A splice code for trans-synaptic cell adhesion mediated by binding of neuroligin 1 to alpha- and beta-neurexins. Neuron 48, 229-236.

Boucard, A.A., Ko, J., and Sudhof, T.C. (2012). High affinity neurexin binding to cell adhesion G-protein-coupled receptor CIRL1/latrophilin-1 produces an intercellular adhesion complex. J Biol Chem 287, 9399-9413.

Boulanger, A., Clouet-Redt, C., Farge, M., Flandre, A., Guignard, T., Fernando, C., Juge, F., and Dura, J.M. (2011). ftz-f1 and Hr39 opposing roles on EcR expression during *Drosophila* mushroom body neuron remodeling. Nat Neurosci 14, 37-44.

Boulin, T., Gielen, M., Richmond, J.E., Williams, D.C., Paoletti, P., and Bessereau, J.L. (2008). Eight genes are required for functional reconstitution of the *Caenorhabditis elegans* levamisole-sensitive acetylcholine receptor. Proc Natl Acad Sci U S A 105, 18590-18595.

Bouwman, J., Maia, A.S., Camoletto, P.G., Posthuma, G., Roubos, E.W., Oorschot, V.M., Klumperman, J., and Verhage, M. (2004). Quantification of synapse formation and maintenance *in vivo* in the absence of synaptic release. Neuroscience 126, 115-126.

Brandon, E.P., Lin, W., D'Amour, K.A., Pizzo, D.P., Dominguez, B., Sugiura, Y., Thode, S., Ko, C.P., Thal, L.J., Gage, F.H., et al. (2003). Aberrant patterning of neuromuscular synapses in choline acetyltransferase-deficient mice. J Neurosci 23, 539-549.

Brenner, S. (1974). The genetics of *Caenorhabditis elegans*. Genetics 77, 71-94.

Briggs, S.W., and Galanopoulou, A.S. (2011). Altered GABA signaling in early life epilepsies. Neural Plast 2011, 527605.

Brown, M.C., Jansen, J.K., and Van Essen, D. (1976). Polyneuronal innervation of skeletal muscle in new-born rats and its elimination during maturation. J Physiol 261, 387-422.

Buffelli, M., Burgess, R.W., Feng, G., Lobe, C.G., Lichtman, J.W., and Sanes, J.R. (2003). Genetic evidence that relative synaptic efficacy biases the outcome of synaptic competition. Nature 424, 430-434.

Butz, S., Okamoto, M., and Sudhof, T.C. (1998). A tripartite protein complex with the potential to couple synaptic vesicle exocytosis to cell adhesion in brain. Cell 94, 773-782.

Cajal, S.R. (1888). Estructura de los centros nerviosos de las aves.

Cajal, S.R. (1891). Sur la structure de l'écorce cérébrale de quelques mammifères (Typ. de Joseph van In & Cie.; Aug. Peeters, lib).

Calahorro, F., and Ruiz-Rubio, M. (2013). Human alpha- and beta-NRXN1 isoforms rescue behavioral impairments of *Caenorhabditis elegans* neurexin-deficient mutants. Genes Brain Behav 12, 453-464.

Campbell, G., and Shatz, C.J. (1992). Synapses formed by identified retinogeniculate axons during the segregation of eye input. J Neurosci 12, 1847-1858.

Chan, S.S., Zheng, H., Su, M.W., Wilk, R., Killeen, M.T., Hedgecock, E.M., and Culotti, J.G. (1996). UNC-40, a *C. elegans* homolog of DCC (Deleted in Colorectal Cancer), is required in motile cells responding to UNC-6 netrin cues. Cell 87, 187-195.

Chattopadhyaya, B. (2011). Molecular mechanisms underlying activity-dependent GABAergic synapse development and plasticity and its implications for neurodevelopmental disorders. Neural Plast 2011, 734231.

Chattopadhyaya, B., Di Cristo, G., Higashiyama, H., Knott, G.W., Kuhlman, S.J., Welker, E., and Huang, Z.J. (2004). Experience and activity-dependent maturation of perisomatic GABAergic innervation in primary visual cortex during a postnatal critical period. J Neurosci 24, 9598-9611.

Chen, C., and Regehr, W.G. (2000). Developmental remodeling of the retinogeniculate synapse. Neuron 28, 955-966.

Chen, L., Ong, B., and Bennett, V. (2001). LAD-1, the *Caenorhabditis elegans* L1CAM homologue, participates in embryonic and gonadal morphogenesis and is a substrate for fibroblast growth factor receptor pathway-dependent phosphotyrosine-based signaling. J Cell Biol 154, 841-855.

Chen, L.Y., Jiang, M., Zhang, B., Gokce, O., and Sudhof, T.C. (2017). Conditional Deletion of All Neurexins Defines Diversity of Essential Synaptic Organizer Functions for Neurexins. Neuron 94, 611-625 e614.

Chen, T.W., Wardill, T.J., Sun, Y., Pulver, S.R., Renninger, S.L., Baohan, A., Schreiter, E.R., Kerr, R.A., Orger, M.B., Jayaraman, V., et al. (2013). Ultrasensitive fluorescent proteins for imaging neuronal activity. Nature 499, 295-300.

Cherra, S.J., 3rd, and Jin, Y. (2016). A Two-Immunoglobulin-Domain Transmembrane Protein Mediates an Epidermal-Neuronal Interaction to Maintain Synapse Density. Neuron 89, 325-336.

Chih, B., Engelman, H., and Scheiffele, P. (2005). Control of excitatory and inhibitory synapse formation by neuroligins. Science 307, 1324-1328.

Chilton, J.K. (2006). Molecular mechanisms of axon guidance. Dev Biol 292, 13-24.

Christopherson, K.S., Ullian, E.M., Stokes, C.C., Mullowney, C.E., Hell, J.W., Agah, A., Lawler, J., Mosher, D.F., Bornstein, P., and Barres, B.A. (2005). Thrombospondins are astrocyte-secreted proteins that promote CNS synaptogenesis. Cell 120, 421-433.

Cinar, H., Keles, S., and Jin, Y. (2005). Expression profiling of GABAergic motor neurons in *Caenorhabditis elegans*. Curr Biol 15, 340-346.

Cohen, A.R., Woods, D.F., Marfatia, S.M., Walther, Z., Chishti, A.H., and Anderson, J.M. (1998). Human CASK/LIN-2 binds syndecan-2 and protein 4.1 and localizes to the basolateral membrane of epithelial cells. J Cell Biol 142, 129-138.

Collins, K.M., and Koelle, M.R. (2013). Postsynaptic ERG potassium channels limit muscle excitability to allow distinct egg-laying behavior states in *Caenorhabditis elegans*. J Neurosci 33, 761-775.

Comoletti, D., Flynn, R.E., Boucard, A.A., Demeler, B., Schirf, V., Shi, J., Jennings, L.L., Newlin, H.R., Sudhof, T.C., and Taylor, P. (2006). Gene selection, alternative splicing, and post-translational processing regulate neuroligin selectivity for beta-neurexins. Biochemistry 45, 12816-12827.

Conroy, W.G., Liu, Z., Nai, Q., Coggan, J.S., and Berg, D.K. (2003). PDZ-containing proteins provide a functional postsynaptic scaffold for nicotinic receptors in neurons. Neuron 38, 759-771.

Consortium, C.e.S. (1998). Genome sequence of the nematode *C. elegans*: a platform for investigating biology. Science 282, 2012-2018.

Cossart, R., Dinocourt, C., Hirsch, J.C., Merchan-Perez, A., De Felipe, J., Ben-Ari, Y., Esclapez, M., and Bernard, C. (2001). Dendritic but not somatic GABAergic inhibition is decreased in experimental epilepsy. Nat Neurosci 4, 52-62.

Culetto, E., Baylis, H.A., Richmond, J.E., Jones, A.K., Fleming, J.T., Squire, M.D., Lewis, J.A., and Sattelle, D.B. (2004). The *Caenorhabditis elegans unc-63* gene encodes a levamisole-sensitive nicotinic acetylcholine receptor alpha subunit. J Biol Chem 279, 42476-42483.

Dai, Y., Taru, H., Deken, S.L., Grill, B., Ackley, B., Nonet, M.L., and Jin, Y. (2006). SYD-2 Liprin-alpha organizes presynaptic active zone formation through ELKS. Nat Neurosci 9, 1479-1487.

Dani, J.A., and Bertrand, D. (2007). Nicotinic acetylcholine receptors and nicotinic cholinergic mechanisms of the central nervous system. Annu Rev Pharmacol Toxicol 47, 699-729.

Davis, E.K., Zou, Y., and Ghosh, A. (2008). Wnts acting through canonical and noncanonical signaling pathways exert opposite effects on hippocampal synapse formation. Neural Dev 3, 32.

Davis, G.W. (2013). Homeostatic signaling and the stabilization of neural function. Neuron 80, 718-728.

de Wit, J., and Ghosh, A. (2016). Specification of synaptic connectivity by cell surface interactions. Nat Rev Neurosci 17, 22-35.

de Wit, J., Sylwestrak, E., O'Sullivan, M.L., Otto, S., Tiglio, K., Savas, J.N., Yates, J.R., 3rd, Comoletti, D., Taylor, P., and Ghosh, A. (2009). LRRTM2 interacts with Neurexin1 and regulates excitatory synapse formation. Neuron 64, 799-806.

Dean, C., Scholl, F.G., Choih, J., DeMaria, S., Berger, J., Isacoff, E., and Scheiffele, P. (2003). Neurexin mediates the assembly of presynaptic terminals. Nat Neurosci 6, 708-716.

DeChiara, T.M., Bowen, D.C., Valenzuela, D.M., Simmons, M.V., Poueymirou, W.T., Thomas, S., Kinetz, E., Compton, D.L., Rojas, E., Park, J.S., et al. (1996). The receptor tyrosine kinase MuSK is required for neuromuscular junction formation *in vivo*. Cell 85, 501-512.

Deneris, E.S., Connolly, J., Rogers, S.W., and Duvoisin, R. (1991). Pharmacological and functional diversity of neuronal nicotinic acetylcholine receptors. Trends Pharmacol Sci 12, 34-40.

Dickinson, D.J., Ward, J.D., Reiner, D.J., and Goldstein, B. (2013). Engineering the *Caenorhabditis elegans* genome using Cas9-triggered homologous recombination. Nat Methods 10, 1028-1034.

Dickson, B.J. (2002). Molecular mechanisms of axon guidance. Science 298, 1959-1964.

Ding, M., Chao, D., Wang, G., and Shen, K. (2007). Spatial regulation of an E3 ubiquitin ligase directs selective synapse elimination. Science 317, 947-951.

Dixon, S.J., and Roy, P.J. (2005). Muscle arm development in *Caenorhabditis elegans*. Development 132, 3079-3092.

Dolan, J., Walshe, K., Alsbury, S., Hokamp, K., O'Keeffe, S., Okafuji, T., Miller, S.F., Tear, G., and Mitchell, K.J. (2007). The extracellular leucine-rich repeat superfamily; a comparative survey and analysis of evolutionary relationships and expression patterns. BMC Genomics 8, 320.

Dubois, L., and Vincent, A. (2001). The COE--Collier/Olf1/EBF--transcription factors: structural conservation and diversity of developmental functions. Mech Dev 108, 3-12.

Dudanova, I., Tabuchi, K., Rohlmann, A., Sudhof, T.C., and Missler, M. (2007). Deletion of alpha-neurexins does not cause a major impairment of axonal pathfinding or synapse formation. J Comp Neurol 502, 261-274.

Dunn, F.A., Della Santina, L., Parker, E.D., and Wong, R.O. (2013). Sensory experience shapes the development of the visual system's first synapse. Neuron 80, 1159-1166.

Earls, L.R., Hacker, M.L., Watson, J.D., and Miller, D.M., 3rd (2010). Coenzyme Q protects *Caenorhabditis elegans* GABA neurons from calcium-dependent degeneration. Proc Natl Acad Sci U S A 107, 14460-14465.

Eimer, S., Gottschalk, A., Hengartner, M., Horvitz, H.R., Richmond, J., Schafer, W.R., and Bessereau, J.L. (2007). Regulation of nicotinic receptor trafficking by the transmembrane Golgi protein UNC-50. EMBO J 26, 4313-4323.

Farris, S.M., Robinson, G.E., and Fahrbach, S.E. (2001). Experience- and age-related outgrowth of intrinsic neurons in the mushroom bodies of the adult worker honeybee. J Neurosci 21, 6395-6404.

Feng, G., Steinbach, J.H., and Sanes, J.R. (1998). Rapsyn clusters neuronal acetylcholine receptors but is inessential for formation of an interneuronal cholinergic synapse. J Neurosci 18, 4166-4176.

Feng, J., Yan, Z., Ferreira, A., Tomizawa, K., Liauw, J.A., Zhuo, M., Allen, P.B., Ouimet, C.C., and Greengard, P. (2000). Spinophilin regulates the formation and function of dendritic spines. Proc Natl Acad Sci U S A 97, 9287-9292.

Feng, Z., and Ko, C.P. (2008). Schwann cells promote synaptogenesis at the neuromuscular junction via transforming growth factor-beta1. J Neurosci 28, 9599-9609.

Fleming, J.T., Squire, M.D., Barnes, T.M., Tornoe, C., Matsuda, K., Ahnn, J., Fire, A., Sulston, J.E., Barnard, E.A., Sattelle, D.B., et al. (1997). *Caenorhabditis elegans* levamisole resistance genes *lev-1*, *unc-29*, and *unc-38* encode functional nicotinic acetylcholine receptor subunits. J Neurosci 17, 5843-5857.

Flores, C.E., Nikonenko, I., Mendez, P., Fritschy, J.M., Tyagarajan, S.K., and Muller, D. (2015). Activity-dependent inhibitory synapse remodeling through gephyrin phosphorylation. Proc Natl Acad Sci U S A 112, E65-72.

Forrester, W.C., Dell, M., Perens, E., and Garriga, G. (1999). A *C. elegans* Ror receptor tyrosine kinase regulates cell motility and asymmetric cell division. Nature 400, 881-885.

Fox, R.M., Von Stetina, S.E., Barlow, S.J., Shaffer, C., Olszewski, K.L., Moore, J.H., Dupuy, D., Vidal, M., and Miller, D.M., 3rd (2005). A gene expression fingerprint of *C. elegans* embryonic motor neurons. BMC Genomics 6, 42.

Frambach, I., Rossler, W., Winkler, M., and Schurmann, F.W. (2004). F-actin at identified synapses in the mushroom body neuropil of the insect brain. J Comp Neurol 475, 303-314.

Francis, M.M., Evans, S.P., Jensen, M., Madsen, D.M., Mancuso, J., Norman, K.R., and Maricq, A.V. (2005). The Ror receptor tyrosine kinase CAM-1 is required for ACR-16-mediated synaptic transmission at the *C. elegans* neuromuscular junction. Neuron 46, 581-594.

Fritschy, J.M. (2008). Epilepsy, E/I Balance and GABA(A) Receptor Plasticity. Front Mol Neurosci 1, 5.

Fuccillo, M.V., Foldy, C., Gokce, O., Rothwell, P.E., Sun, G.L., Malenka, R.C., and Sudhof, T.C. (2015). Single-Cell mRNA Profiling Reveals Cell-Type-Specific Expression of Neurexin Isoforms. Neuron 87, 326-340.

Gabel, C.V., Antoine, F., Chuang, C.F., Samuel, A.D., and Chang, C. (2008). Distinct cellular and molecular mechanisms mediate initial axon development and adult-stage axon regeneration in *C. elegans*. Development 135, 1129-1136.

Gally, C., and Bessereau, J.L. (2003). GABA is dispensable for the formation of junctional GABA receptor clusters in *Caenorhabditis elegans*. J Neurosci 23, 2591-2599.

Gally, C., Eimer, S., Richmond, J.E., and Bessereau, J.L. (2004). A transmembrane protein required for acetylcholine receptor clustering in *Caenorhabditis elegans*. Nature 431, 578-582.

Gao, S., and Zhen, M. (2011). Action potentials drive body wall muscle contractions in *Caenorhabditis elegans*. Proc Natl Acad Sci U S A 108, 2557-2562.

Garel, S., Marin, F., Mattei, M.G., Vesque, C., Vincent, A., and Charnay, P. (1997). Family of Ebf/Olf-1-related genes potentially involved in neuronal differentiation and regional specification in the central nervous system. Dev Dyn 210, 191-205.

Gautam, M., Noakes, P.G., Moscoso, L., Rupp, F., Scheller, R.H., Merlie, J.P., and Sanes, J.R. (1996). Defective neuromuscular synaptogenesis in agrin-deficient mutant mice. Cell 85, 525-535.

Gautam, M., Noakes, P.G., Mudd, J., Nichol, M., Chu, G.C., Sanes, J.R., and Merlie, J.P. (1995). Failure of postsynaptic specialization to develop at neuromuscular junctions of rapsyn-deficient mice. Nature 377, 232-236.

Gendrel, M., Rapti, G., Richmond, J.E., and Bessereau, J.L. (2009). A secreted complement-control-related protein ensures acetylcholine receptor clustering. Nature 461, 992-996.

Gillespie, S.K., Balasubramanian, S., Fung, E.T., and Huganir, R.L. (1996). Rapsyn clusters and activates the synapse-specific receptor tyrosine kinase MuSK. Neuron 16, 953-962.

Gissendanner, C.R., and Kelley, T.D. (2013). The *C. elegans* gene *pan-1* encodes novel transmembrane and cytoplasmic leucine-rich repeat proteins and promotes molting and the larva to adult transition. BMC Dev Biol 13, 21.

Glantz, L.A., and Lewis, D.A. (2000). Decreased dendritic spine density on prefrontal cortical pyramidal neurons in schizophrenia. Arch Gen Psychiatry 57, 65-73.

Goodman, M.B., Hall, D.H., Avery, L., and Lockery, S.R. (1998). Active currents regulate sensitivity and dynamic range in *C. elegans* neurons. Neuron 20, 763-772.

Gotti, C., Clementi, F., Fornari, A., Gaimarri, A., Guiducci, S., Manfredi, I., Moretti, M., Pedrazzi, P., Pucci, L., and Zoli, M. (2009). Structural and functional diversity of native brain neuronal nicotinic receptors. Biochem Pharmacol 78, 703-711.

Gottschalk, A., Almedom, R.B., Schedletzky, T., Anderson, S.D., Yates, J.R., 3rd, and Schafer, W.R. (2005). Identification and characterization of novel nicotinic receptor-associated proteins in *Caenorhabditis elegans*. EMBO J 24, 2566-2578.

Gottschalk, A., and Schafer, W.R. (2006). Visualization of integral and peripheral cell surface proteins in live *Caenorhabditis elegans*. J Neurosci Methods 154, 68-79.

Gotz, M., and Huttner, W.B. (2005). The cell biology of neurogenesis. Nat Rev Mol Cell Biol 6, 777-788.

Graf, E.R., Zhang, X., Jin, S.X., Linhoff, M.W., and Craig, A.M. (2004). Neurexins induce differentiation of GABA and glutamate postsynaptic specializations via neuroligins. Cell 119, 1013-1026.

Gray, E.G. (1959). Electron microscopy of synaptic contacts on dendrite spines of the cerebral cortex. Nature 183, 1592-1593.

Green, Y.S., and Vetter, M.L. (2011). EBF factors drive expression of multiple classes of target genes governing neuronal development. Neural Dev 6, 19.

Grill, B., Bienvenut, W.V., Brown, H.M., Ackley, B.D., Quadroni, M., and Jin, Y. (2007). *C. elegans* RPM-1 regulates axon termination and synaptogenesis through the Rab GEF GLO-4 and the Rab GTPase GLO-1. Neuron 55, 587-601.

Grisoni, K., Gieseler, K., Mariol, M.C., Martin, E., Carre-Pierrat, M., Moulder, G., Barstead, R., and Segalat, L. (2003). The *stn-1* syntrophin gene of *C.elegans* is functionally related to dystrophin and dystrobrevin. J Mol Biol 332, 1037-1046.

Grunwald, M.E., Mellem, J.E., Strutz, N., Maricq, A.V., and Kaplan, J.M. (2004). Clathrin-mediated endocytosis is required for compensatory regulation of GLR-1 glutamate receptors after activity blockade. Proc Natl Acad Sci U S A 101, 3190-3195.

Gumienny, T.L., MacNeil, L.T., Wang, H., de Bono, M., Wrana, J.L., and Padgett, R.W. (2007). Glypican LON-2 is a conserved negative regulator of BMP-like signaling in *Caenorhabditis elegans*. Curr Biol 17, 159-164.

Haklai-Topper, L., Soutschek, J., Sabanay, H., Scheel, J., Hobert, O., and Peles, E. (2011). The neurexin superfamily of *Caenorhabditis elegans*. Gene Expr Patterns 11, 144-150.

Halevi, S., McKay, J., Palfreyman, M., Yassin, L., Eshel, M., Jorgensen, E., and Treinin, M. (2002). The *C. elegans ric-3* gene is required for maturation of nicotinic acetylcholine receptors. EMBO J 21, 1012-1020.

Halevi, S., Yassin, L., Eshel, M., Sala, F., Sala, S., Criado, M., and Treinin, M. (2003). Conservation within the RIC-3 gene family. Effectors of mammalian nicotinic acetylcholine receptor expression. J Biol Chem 278, 34411-34417.

Hall, A.C., Lucas, F.R., and Salinas, P.C. (2000). Axonal remodeling and synaptic differentiation in the cerebellum is regulated by WNT-7a signaling. Cell 100, 525-535.

Hall, D.H., and Altun, Z.F. (2008). *C. elegans* atlas (Cold Spring Harbor, N.Y.: Cold Spring Harbor Laboratory Press).

Hallam, S., Singer, E., Waring, D., and Jin, Y. (2000). The *C. elegans* NeuroD homolog *cnd-1* functions in multiple aspects of motor neuron fate specification. Development 127, 4239-4252.

Hallam, S.J., Goncharov, A., McEwen, J., Baran, R., and Jin, Y. (2002). SYD-1, a presynaptic protein with PDZ, C2 and rhoGAP-like domains, specifies axon identity in *C. elegans*. Nat Neurosci 5, 1137-1146.

Hallam, S.J., and Jin, Y. (1998). *lin-14* regulates the timing of synaptic remodelling in *Caenorhabditis elegans*. Nature 395, 78-82.

Han, B., Bellemer, A., and Koelle, M.R. (2015). An evolutionarily conserved switch in response to GABA affects development and behavior of the locomotor circuit of *Caenorhabditis elegans*. Genetics 199, 1159-1172.

Harris, K.M., Jensen, F.E., and Tsao, B. (1992). Three-dimensional structure of dendritic spines and synapses in rat hippocampus (CA1) at postnatal day 15 and adult ages: implications for the maturation of synaptic physiology and long-term potentiation. J Neurosci 12, 2685-2705.

Harris, K.M., and Stevens, J.K. (1989). Dendritic spines of CA 1 pyramidal cells in the rat hippocampus: serial electron microscopy with reference to their biophysical characteristics. J Neurosci 9, 2982-2997.

Hart, M.P., and Hobert, O. (2018). Neurexin controls plasticity of a mature, sexually dimorphic neuron. Nature 553, 165.

Hata, Y., Butz, S., and Sudhof, T.C. (1996). CASK: a novel dlg/PSD95 homolog with an N-terminal calmodulin-dependent protein kinase domain identified by interaction with neurexins. J Neurosci 16, 2488-2494.

Hata, Y., Davletov, B., Petrenko, A.G., Jahn, R., and Sudhof, T.C. (1993). Interaction of synaptotagmin with the cytoplasmic domains of neurexins. Neuron 10, 307-315.

Hattori, Y., Sugimura, K., and Uemura, T. (2007). Selective expression of Knot/Collier, a transcriptional regulator of the EBF/Olf-1 family, endows the *Drosophila* sensory system with neuronal class-specific elaborated dendritic patterns. Genes Cells 12, 1011-1022.

Hattori, Y., Usui, T., Satoh, D., Moriyama, S., Shimono, K., Itoh, T., Shirahige, K., and Uemura, T. (2013). Sensory-neuron subtype-specific transcriptional programs controlling dendrite morphogenesis: genome-wide analysis of Abrupt and Knot/Collier. Dev Cell 27, 530-544.

Haugstetter, J., Blicher, T., and Ellgaard, L. (2005). Identification and characterization of a novel thioredoxin-related transmembrane protein of the endoplasmic reticulum. J Biol Chem 280, 8371-8380.

Hayashi, M.K., Tang, C., Verpelli, C., Narayanan, R., Stearns, M.H., Xu, R.M., Li, H., Sala, C., and Hayashi, Y. (2009). The postsynaptic density proteins Homer and Shank form a polymeric network structure. Cell 137, 159-171.

Hayashi, Y., Okamoto, K.-i., Bosch, M., and Futai, K. (2012). Roles of Neuronal Activity-Induced Gene Products in Hebbian and Homeostatic Synaptic Plasticity, Tagging, and Capture. In Synaptic Plasticity: Dynamics, Development and Disease, M.R. Kreutz, and C. Sala, eds. (Vienna: Springer Vienna), pp. 335-354.

Hayashi-Takagi, A., Yagishita, S., Nakamura, M., Shirai, F., Wu, Y.I., Loshbaugh, A.L., Kuhlman, B., Hahn, K.M., and Kasai, H. (2015). Labelling and optical erasure of synaptic memory traces in the motor cortex. Nature 525, 333-338.

He, S., Philbrook, A., McWhirter, R., Gabel, C.V., Taub, D.G., Carter, M.H., Hanna, I.M., Francis, M.M., and Miller, D.M., 3rd (2015). Transcriptional Control of Synaptic Remodeling through Regulated Expression of an Immunoglobulin Superfamily Protein. Curr Biol 25, 2541-2548.

Hebb, D.O. (1949). Organization of behavior. New York: Wiley, 1949, pp. 335. Journal of Clinical Psychology 6, 307-307.

Heisenberg, M., Borst, A., Wagner, S., and Byers, D. (1985). *Drosophila* mushroom body mutants are deficient in olfactory learning. J Neurogenet 2, 1-30.

Hendry, S.H., Schwark, H.D., Jones, E.G., and Yan, J. (1987). Numbers and proportions of GABA-immunoreactive neurons in different areas of monkey cerebral cortex. J Neurosci 7, 1503-1519.

Hensch, T.K., and Fagiolini, M. (2005). Excitatory-inhibitory balance and critical period plasticity in developing visual cortex. Prog Brain Res 147, 115-124.

Henson, M.A., Tucker, C.J., Zhao, M., and Dudek, S.M. (2017). Long-term depression-associated signaling is required for an *in vitro* model of NMDA receptor-dependent synapse pruning. Neurobiol Learn Mem 138, 39-53.

Hobert, O. (2013). The neuronal genome of *Caenorhabditis elegans*. WormBook, 1-106.

Hoskins, R., Hajnal, A.F., Harp, S.A., and Kim, S.K. (1996). The *C. elegans* vulval induction gene *lin-2* encodes a member of the MAGUK family of cell junction proteins. Development 122, 97-111.

Howell, K., and Hobert, O. (2016). Small Immunoglobulin Domain Proteins at Synapses and the Maintenance of Neuronal Features. Neuron 89, 239-241.

Howell, K., White, J.G., and Hobert, O. (2015). Spatiotemporal control of a novel synaptic organizer molecule. Nature 523, 83-87.

Hrus, A., Lau, G., Hutter, H., Schenk, S., Ferralli, J., Brown-Luedi, M., Chiquet-Ehrismann, R., and Canevascini, S. (2007). *C. elegans* agrin is expressed in pharynx, IL1 neurons and distal tip cells and does not genetically interact with genes involved in synaptogenesis or muscle function. PLoS One 2, e731.

Hu, Z., Hom, S., Kudze, T., Tong, X.J., Choi, S., Aramuni, G., Zhang, W., and Kaplan, J.M. (2012). Neurexin and neuroligin mediate retrograde synaptic inhibition in *C. elegans*. Science 337, 980-984.

Hubel, D.H., and Wiesel, T.N. (1970). The period of susceptibility to the physiological effects of unilateral eye closure in kittens. J Physiol 206, 419-436.

Hung, W., Hwang, C., Po, M.D., and Zhen, M. (2007). Neuronal polarity is regulated by a direct interaction between a scaffolding protein, Neurabin, and a presynaptic SAD-1 kinase in *Caenorhabditis elegans*. Development 134, 237-249.

Hunter, J.W., Mullen, G.P., McManus, J.R., Heatherly, J.M., Duke, A., and Rand, J.B. (2010). Neuroligin-deficient mutants of *C. elegans* have sensory processing deficits and are hypersensitive to oxidative stress and mercury toxicity. Dis Model Mech 3, 366-376.

Hutsler, J.J., and Zhang, H. (2010). Increased dendritic spine densities on cortical projection neurons in autism spectrum disorders. Brain Res 1309, 83-94.

Ichtchenko, K., Hata, Y., Nguyen, T., Ullrich, B., Missler, M., Moomaw, C., and Sudhof, T.C. (1995). Neuroligin 1: a splice site-specific ligand for beta-neurexins. Cell 81, 435-443.

Ichtchenko, K., Nguyen, T., and Sudhof, T.C. (1996). Structures, alternative splicing, and neurexin binding of multiple neuroligins. J Biol Chem 271, 2676-2682.

Ikeda, D.D., Duan, Y., Matsuki, M., Kunitomo, H., Hutter, H., Hedgecock, E.M., and Iino, Y. (2008). CASY-1, an ortholog of calsyntenins/alcadeins, is essential for learning in *Caenorhabditis elegans*. Proc Natl Acad Sci U S A 105, 5260-5265.

Irie, M., Hata, Y., Takeuchi, M., Ichtchenko, K., Toyoda, A., Hirao, K., Takai, Y., Rosahl, T.W., and Sudhof, T.C. (1997). Binding of neuroligins to PSD-95. Science 277, 1511-1515.

Irizarry, R.A., Bolstad, B.M., Collin, F., Cope, L.M., Hobbs, B., and Speed, T.P. (2003). Summaries of Affymetrix GeneChip probe level data. Nucleic Acids Res 31, e15.

Jensen, M., Hoerndli, F.J., Brockie, P.J., Wang, R., Johnson, E., Maxfield, D., Francis, M.M., Madsen, D.M., and Maricq, A.V. (2012). Wnt signaling regulates

acetylcholine receptor translocation and synaptic plasticity in the adult nervous system. Cell 149, 173-187.

Ji, N., and van Oudenaarden, A. (2012). Single molecule fluorescent *in situ* hybridization (smFISH) of *C. elegans* worms and embryos. WormBook, 1-16.

Jiao, Y., Zhang, C., Yanagawa, Y., and Sun, Q.Q. (2006). Major effects of sensory experiences on the neocortical inhibitory circuits. J Neurosci 26, 8691-8701.

Jin, Y., Jorgensen, E., Hartwieg, E., and Horvitz, H.R. (1999). The *Caenorhabditis elegans* gene *unc-25* encodes glutamic acid decarboxylase and is required for synaptic transmission but not synaptic development. J Neurosci 19, 539-548.

Jin, Y., and Qi, Y.B. (2017). Building stereotypic connectivity: mechanistic insights into structural plasticity from *C. elegans*. Curr Opin Neurobiol 48, 97–105.

Johnson, R.P., Kang, S.H., and Kramer, J.M. (2006). *C. elegans* dystroglycan DGN-1 functions in epithelia and neurons, but not muscle, and independently of dystrophin. Development 133, 1911-1921.

Joo, J.Y., Lee, S.J., Uemura, T., Yoshida, T., Yasumura, M., Watanabe, M., and Mishina, M. (2011). Differential interactions of cerebellin precursor protein (Cbln) subtypes and neurexin variants for synapse formation of cortical neurons. Biochem Biophys Res Commun 406, 627-632.

Jospin, M., Qi, Y.B., Stawicki, T.M., Boulin, T., Schuske, K.R., Horvitz, H.R., Bessereau, J.L., Jorgensen, E.M., and Jin, Y. (2009). A neuronal acetylcholine receptor regulates the balance of muscle excitation and inhibition in *Caenorhabditis elegans*. PLoS Biol 7, e1000265.

Kamath, R.S., Martinez-Campos, M., Zipperlen, P., Fraser, A.G., and Ahringer, J. (2001). Effectiveness of specific RNA-mediated interference through ingested double-stranded RNA in *Caenorhabditis elegans*. Genome Biol 2, RESEARCH0002.

Katz, L.C., and Shatz, C.J. (1996). Synaptic activity and the construction of cortical circuits. Science 274, 1133-1138.

Keil, W., Kutscher, L.M., Shaham, S., and Siggia, E.D. (2017). Long-Term High-Resolution Imaging of Developing *C. elegans* Larvae with Microfluidics. Dev Cell 40, 202-214.

Kilman, V., van Rossum, M.C., and Turrigiano, G.G. (2002). Activity deprivation reduces miniature IPSC amplitude by decreasing the number of postsynaptic GABA(A) receptors clustered at neocortical synapses. J Neurosci 22, 1328-1337.

Kim, B., and Emmons, S.W. (2017). Multiple conserved cell adhesion protein interactions mediate neural wiring of a sensory circuit in *C. elegans*. Elife 6.

Kim, C., and Forrester, W.C. (2003). Functional analysis of the domains of the *C elegans* Ror receptor tyrosine kinase CAM-1. Dev Biol 264, 376-390.

Kim, C.H., Xiong, W.C., and Mei, L. (2003). Regulation of MuSK expression by a novel signaling pathway. J Biol Chem 278, 38522-38527.

Kim, E., Sun, L., Gabel, C.V., and Fang-Yen, C. (2013). Long-term imaging of *Caenorhabditis elegans* using nanoparticle-mediated immobilization. PLoS One 8, e53419.

Kim, H.G., Kishikawa, S., Higgins, A.W., Seong, I.S., Donovan, D.J., Shen, Y., Lally, E., Weiss, L.A., Najm, J., Kutsche, K., et al. (2008a). Disruption of neurexin 1 associated with autism spectrum disorder. Am J Hum Genet 82, 199-207.

Kim, K., Colosimo, M.E., Yeung, H., and Sengupta, P. (2005). The UNC-3 Olf/EBF protein represses alternate neuronal programs to specify chemosensory neuron identity. Dev Biol 286, 136-148.

Kim, N., Stiegler, A.L., Cameron, T.O., Hallock, P.T., Gomez, A.M., Huang, J.H., Hubbard, S.R., Dustin, M.L., and Burden, S.J. (2008b). Lrp4 is a receptor for Agrin and forms a complex with MuSK. Cell 135, 334-342.

Klapoetke, N.C., Murata, Y., Kim, S.S., Pulver, S.R., Birdsey-Benson, A., Cho, Y.K., Morimoto, T.K., Chuong, A.S., Carpenter, E.J., Tian, Z., et al. (2014). Independent optical excitation of distinct neural populations. Nat Methods 11, 338-346.

Klassen, M.P., and Shen, K. (2007). Wnt signaling positions neuromuscular connectivity by inhibiting synapse formation in *C. elegans*. Cell 130, 704-716.

Ko, J., Fuccillo, M.V., Malenka, R.C., and Sudhof, T.C. (2009). LRRTM2 functions as a neurexin ligand in promoting excitatory synapse formation. Neuron 64, 791-798.

Kolodkin, A.L., and Tessier-Lavigne, M. (2011). Mechanisms and molecules of neuronal wiring: a primer. Cold Spring Harb Perspect Biol 3.

Kratsios, P., Pinan-Lucarre, B., Kerk, S.Y., Weinreb, A., Bessereau, J.L., and Hobert, O. (2015). Transcriptional coordination of synaptogenesis and neurotransmitter signaling. Curr Biol 25, 1282-1295.

Kratsios, P., Stolfi, A., Levine, M., and Hobert, O. (2011). Coordinated regulation of cholinergic motor neuron traits through a conserved terminal selector gene. Nat Neurosci 15, 205-214.

Kurup, N., and Jin, Y. (2016). Neural circuit rewiring: insights from DD synapse remodeling. Worm 5, e1129486.

Larsch, J., Flavell, S.W., Liu, Q., Gordus, A., Albrecht, D.R., and Bargmann, C.I. (2015). A Circuit for Gradient Climbing in *C. elegans* Chemotaxis. Cell Rep 12, 1748-1760.

Lee, T., Lee, A., and Luo, L. (1999). Development of the *Drosophila* mushroom bodies: sequential generation of three distinct types of neurons from a neuroblast. Development 126, 4065-4076.

Lee, T., Marticke, S., Sung, C., Robinow, S., and Luo, L. (2000). Cell-autonomous requirement of the USP/EcR-B ecdysone receptor for mushroom body neuronal remodeling in *Drosophila*. Neuron 28, 807-818.

Lee, V., and Maguire, J. (2013). Impact of inhibitory constraint of interneurons on neuronal excitability. J Neurophysiol 110, 2520-2535.

Lee, V., and Maguire, J. (2014). The impact of tonic GABAA receptor-mediated inhibition on neuronal excitability varies across brain region and cell type. Front Neural Circuits 8, 3.

Leiss, F., Koper, E., Hein, I., Fouquet, W., Lindner, J., Sigrist, S., and Tavosanis, G. (2009). Characterization of dendritic spines in the *Drosophila* central nervous system. Dev Neurobiol 69, 221-234.

Lewis, J.A., Wu, C.H., Berg, H., and Levine, J.H. (1980). The genetics of levamisole resistance in the nematode *Caenorhabditis elegans*. Genetics 95, 905-928.

Li, J., Ashley, J., Budnik, V., and Bhat, M.A. (2007). Crucial role of *Drosophila* neurexin in proper active zone apposition to postsynaptic densities, synaptic growth, and synaptic transmission. Neuron 55, 741-755.

Liao, E.H., Hung, W., Abrams, B., and Zhen, M. (2004). An SCF-like ubiquitin ligase complex that controls presynaptic differentiation. Nature 430, 345-350.

Lin, W., Burgess, R.W., Dominguez, B., Pfaff, S.L., Sanes, J.R., and Lee, K.F. (2001). Distinct roles of nerve and muscle in postsynaptic differentiation of the neuromuscular synapse. Nature 410, 1057-1064.

Lin, Y., Bloodgood, B.L., Hauser, J.L., Lapan, A.D., Koon, A.C., Kim, T.K., Hu, L.S., Malik, A.N., and Greenberg, M.E. (2008). Activity-dependent regulation of inhibitory synapse development by Npas4. Nature 455, 1198-1204.

Lisman, J., Yasuda, R., and Raghavachari, S. (2012). Mechanisms of CaMKII action in long-term potentiation. Nat Rev Neurosci 13, 169-182.

Liu, A., Zhou, Z., Dang, R., Zhu, Y., Qi, J., He, G., Leung, C., Pak, D., Jia, Z., and Xie, W. (2016). Neuroligin 1 regulates spines and synaptic plasticity via LIMK1/cofilin-mediated actin reorganization. J Cell Biol 212, 449-463.

Liu, O.W., and Shen, K. (2011). The transmembrane LRR protein DMA-1 promotes dendrite branching and growth in *C. elegans*. Nat Neurosci 15, 57-63.

Livet, J., Sigrist, M., Stroebel, S., De Paola, V., Price, S.R., Henderson, C.E., Jessell, T.M., and Arber, S. (2002). ETS gene Pea3 controls the central position and terminal arborization of specific motor neuron pools. Neuron 35, 877-892.

Lu, W., Bushong, E.A., Shih, T.P., Ellisman, M.H., and Nicoll, R.A. (2013). The cell-autonomous role of excitatory synaptic transmission in the regulation of neuronal structure and function. Neuron 78, 433-439.

Lu, Z., Wang, Y., Chen, F., Tong, H., Reddy, M.V., Luo, L., Seshadrinathan, S., Zhang, L., Holthauzen, L.M., Craig, A.M., et al. (2014). Calsyntenin-3 molecular architecture and interaction with neurexin 1alpha. J Biol Chem 289, 34530-34542.

Luikart, B.W., Zhang, W., Wayman, G.A., Kwon, C.H., Westbrook, G.L., and Parada, L.F. (2008). Neurotrophin-dependent dendritic filopodial motility: a convergence on PI3K signaling. J Neurosci 28, 7006-7012.

Luo, L., Hensch, T.K., Ackerman, L., Barbel, S., Jan, L.Y., and Jan, Y.N. (1996). Differential effects of the Rac GTPase on Purkinje cell axons and dendritic trunks and spines. Nature 379, 837-840.

Markus, E.J., and Petit, T.L. (1987). Neocortical synaptogenesis, aging, and behavior: lifespan development in the motor-sensory system of the rat. Exp Neurol 96, 262-278.

Maro, G.S., Gao, S., Olechwier, A.M., Hung, W.L., Liu, M., Ozkan, E., Zhen, M., and Shen, K. (2015). MADD-4/Punctin and Neurexin Organize *C. elegans* GABAergic Postsynapses through Neuroligin. Neuron 86, 1420-1432.

Martin, L.J., Blackstone, C.D., Levey, A.I., Huganir, R.L., and Price, D.L. (1993). AMPA glutamate receptor subunits are differentially distributed in rat brain. Neuroscience 53, 327-358.

Martinez-Mir, A., Gonzalez-Perez, A., Gayan, J., Antunez, C., Marin, J., Boada, M., Lopez-Arrieta, J.M., Fernandez, E., Ramirez-Lorca, R., Saez, M.E., et al. (2013). Genetic study of neurexin and neuroligin genes in Alzheimer's disease. J Alzheimers Dis 35, 403-412.

Marty, S., Wehrle, R., and Sotelo, C. (2000). Neuronal activity and brain-derived neurotrophic factor regulate the density of inhibitory synapses in organotypic slice cultures of postnatal hippocampus. J Neurosci 20, 8087-8095.

Martynoga, B., Drechsel, D., and Guillemot, F. (2012). Molecular control of neurogenesis: a view from the mammalian cerebral cortex. Cold Spring Harb Perspect Biol 4.

Mathew, D., Ataman, B., Chen, J., Zhang, Y., Cumberledge, S., and Budnik, V. (2005). Wingless signaling at synapses is through cleavage and nuclear import of receptor DFrizzled2. Science 310, 1344-1347.

Matsuda, K., and Yuzaki, M. (2011). Cbln family proteins promote synapse formation by regulating distinct neurexin signaling pathways in various brain regions. Eur J Neurosci 33, 1447-1461.

Matsuzaki, M., Honkura, N., Ellis-Davies, G.C., and Kasai, H. (2004). Structural basis of long-term potentiation in single dendritic spines. Nature 429, 761-766.

Matus, A., Ackermann, M., Pehling, G., Byers, H.R., and Fujiwara, K. (1982). High actin concentrations in brain dendritic spines and postsynaptic densities. Proc Natl Acad Sci U S A 79, 7590-7594.

McGuire, S.E., Le, P.T., and Davis, R.L. (2001). The role of *Drosophila* mushroom body signaling in olfactory memory. Science 293, 1330-1333.

McIntire, S.L., Jorgensen, E., Kaplan, J., and Horvitz, H.R. (1993). The GABAergic nervous system of *Caenorhabditis elegans*. Nature 364, 337-341.

McMahan, U.J. (1990). The agrin hypothesis. Cold Spring Harb Symp Quant Biol 55, 407-418.

Meinecke, D.L., and Peters, A. (1987). GABA immunoreactive neurons in rat visual cortex. J Comp Neurol 261, 388-404.

Mello, C.C., Kramer, J.M., Stinchcomb, D., and Ambros, V. (1991). Efficient gene transfer in *C.elegans*: extrachromosomal maintenance and integration of transforming sequences. EMBO J 10, 3959-3970.

Meng, J., Ma, X., Tao, H., Jin, X., Witvliet, D., Mitchell, J., Zhu, M., Dong, M.Q., Zhen, M., Jin, Y., et al. (2017). Myrf ER-Bound Transcription Factors Drive *C. elegans* Synaptic Plasticity via Cleavage-Dependent Nuclear Translocation. Dev Cell 41, 180-194 e187.

Merlie, J.P., and Lindstrom, J. (1983). Assembly *in vivo* of mouse muscle acetylcholine receptor: identification of an alpha subunit species that may be an assembly intermediate. Cell 34, 747-757.

Messeant, J., Ezan, J., Delers, P., Glebov, K., Marchiol, C., Lager, F., Renault, G., Tissir, F., Montcouquiol, M., Sans, N., et al. (2017). Wnt proteins contribute to neuromuscular junction formation through distinct signaling pathways. Development 144, 1712-1724.

Miller-Fleming, T.W., Petersen, S.C., Manning, L., Matthewman, C., Gornet, M., Beers, A., Hori, S., Mitani, S., Bianchi, L., Richmond, J., et al. (2016). The DEG/ENaC cation channel protein UNC-8 drives activity-dependent synapse removal in remodeling GABAergic neurons. Elife 5.

Missler, M., Hammer, R.E., and Sudhof, T.C. (1998). Neurexophilin binding to alpha-neurexins. A single LNS domain functions as an independently folding ligand-binding unit. J Biol Chem 273, 34716-34723.

Missler, M., and Sudhof, T.C. (1998). Neurexophilins form a conserved family of neuropeptide-like glycoproteins. J Neurosci 18, 3630-3638.

Missler, M., Sudhof, T.C., and Biederer, T. (2012). Synaptic cell adhesion. Cold Spring Harb Perspect Biol 4, a005694.

Missler, M., Zhang, W., Rohlmann, A., Kattenstroth, G., Hammer, R.E., Gottmann, K., and Sudhof, T.C. (2003). Alpha-neurexins couple Ca2+ channels to synaptic vesicle exocytosis. Nature 423, 939-948.

Morales, B., Choi, S.Y., and Kirkwood, A. (2002). Dark rearing alters the development of GABAergic transmission in visual cortex. J Neurosci 22, 8084-8090.

Morey, M., Yee, S.K., Herman, T., Nern, A., Blanco, E., and Zipursky, S.L. (2008). Coordinate control of synaptic-layer specificity and rhodopsins in photoreceptor neurons. Nature 456, 795-799.

Morgan, J.L., Soto, F., Wong, R.O., and Kerschensteiner, D. (2011). Development of cell type-specific connectivity patterns of converging excitatory axons in the retina. Neuron 71, 1014-1021.

Najarro, E.H., Wong, L., Zhen, M., Carpio, E.P., Goncharov, A., Garriga, G., Lundquist, E.A., Jin, Y., and Ackley, B.D. (2012). *Caenorhabditis elegans* flamingo cadherin *fmi-1* regulates GABAergic neuronal development. J Neurosci 32, 4196-4211.

Nam, S., Min, K., Hwang, H., Lee, H.O., Lee, J.H., Yoon, J., Lee, H., Park, S., and Lee, J. (2009). Control of rapsyn stability by the CUL-3-containing E3 ligase complex. J Biol Chem 284, 8195-8206.

Neff, R.A., 3rd, Gomez-Varela, D., Fernandes, C.C., and Berg, D.K. (2009). Postsynaptic scaffolds for nicotinic receptors on neurons. Acta Pharmacol Sin 30, 694-701.

Nguyen, T., and Sudhof, T.C. (1997). Binding properties of neuroligin 1 and neurexin 1beta reveal function as heterophilic cell adhesion molecules. J Biol Chem 272, 26032-26039.

Nonet, M.L. (1999). Visualization of synaptic specializations in live *C. elegans* with synaptic vesicle protein-GFP fusions. J Neurosci Methods 89, 33-40.

O'Brien, R.J., Kamboj, S., Ehlers, M.D., Rosen, K.R., Fischbach, G.D., and Huganir, R.L. (1998). Activity-dependent modulation of synaptic AMPA receptor accumulation. Neuron 21, 1067-1078.

Okawa, H., Della Santina, L., Schwartz, G.W., Rieke, F., and Wong, R.O. (2014a). Interplay of cell-autonomous and nonautonomous mechanisms tailors synaptic connectivity of converging axons *in vivo*. Neuron 82, 125-137.

Okawa, H., Hoon, M., Yoshimatsu, T., Della Santina, L., and Wong, R.O.L. (2014b). Illuminating the multifaceted roles of neurotransmission in shaping neuronal circuitry. Neuron 83, 1303-1318.

Owald, D., Khorramshahi, O., Gupta, V.K., Banovic, D., Depner, H., Fouquet, W., Wichmann, C., Mertel, S., Eimer, S., Reynolds, E., et al. (2012). Cooperation of Syd-1 with Neurexin synchronizes pre- with postsynaptic assembly. Nat Neurosci 15, 1219-1226.

Packard, M., Koo, E.S., Gorczyca, M., Sharpe, J., Cumberledge, S., and Budnik, V. (2002). The *Drosophila* Wnt, wingless, provides an essential signal for pre- and postsynaptic differentiation. Cell 111, 319-330.

Park, M., Watanabe, S., Poon, V.Y., Ou, C.Y., Jorgensen, E.M., and Shen, K. (2011). CYY-1/cyclin Y and CDK-5 differentially regulate synapse elimination and formation for rewiring neural circuits. Neuron 70, 742-757.

Penzes, P., Beeser, A., Chernoff, J., Schiller, M.R., Eipper, B.A., Mains, R.E., and Huganir, R.L. (2003). Rapid induction of dendritic spine morphogenesis by trans-synaptic ephrinB-EphB receptor activation of the Rho-GEF kalirin. Neuron 37, 263-274.

Peters, A., and Kaiserman-Abramof, I.R. (1970). The small pyramidal neuron of the rat cerebral cortex. The perikaryon, dendrites and spines. Am J Anat 127, 321-355.

Petersen, S.C., Watson, J.D., Richmond, J.E., Sarov, M., Walthall, W.W., and Miller, D.M., 3rd (2011). A transcriptional program promotes remodeling of GABAergic synapses in *Caenorhabditis elegans*. J Neurosci 31, 15362-15375.

Petrash, H.A., Philbrook, A., Haburcak, M., Barbagallo, B., and Francis, M.M. (2013). ACR-12 ionotropic acetylcholine receptor complexes regulate inhibitory motor neuron activity in *Caenorhabditis elegans*. J Neurosci 33, 5524-5532.

Petrenko, A.G., Ullrich, B., Missler, M., Krasnoperov, V., Rosahl, T.W., and Sudhof, T.C. (1996). Structure and evolution of neurexophilin. J Neurosci 16, 4360-4369.

Pettem, K.L., Yokomaku, D., Luo, L., Linhoff, M.W., Prasad, T., Connor, S.A., Siddiqui, T.J., Kawabe, H., Chen, F., Zhang, L., et al. (2013). The specific alpha-neurexin interactor calsyntenin-3 promotes excitatory and inhibitory synapse development. Neuron 80, 113-128.

Philbrook, A., and Francis, M.M. (2016). Emerging Technologies in the Analysis of *C. elegans* Nicotinic Acetylcholine Receptors. In Nicotinic Acetylcholine Receptor Technologies, M.D. Li, ed. (New York, NY: Springer New York), pp. 77-96.

Pieraut, S., Gounko, N., Sando, R., 3rd, Dang, W., Rebboah, E., Panda, S., Madisen, L., Zeng, H., and Maximov, A. (2014). Experience-dependent remodeling of basket cell networks in the dentate gyrus. Neuron 84, 107-122.

Pinan-Lucarre, B., Tu, H., Pierron, M., Cruceyra, P.I., Zhan, H., Stigloher, C., Richmond, J.E., and Bessereau, J.L. (2014). *C. elegans* Punctin specifies cholinergic versus GABAergic identity of postsynaptic domains. Nature 511, 466-470.

Powell, E.M., Campbell, D.B., Stanwood, G.D., Davis, C., Noebels, J.L., and Levitt, P. (2003). Genetic disruption of cortical interneuron development causes region- and GABA cell type-specific deficits, epilepsy, and behavioral dysfunction. J Neurosci 23, 622-631.

Prange, O., Wong, T.P., Gerrow, K., Wang, Y.T., and El-Husseini, A. (2004). A balance between excitatory and inhibitory synapses is controlled by PSD-95 and neuroligin. Proc Natl Acad Sci U S A 101, 13915-13920.

Prasad, B., Karakuzu, O., Reed, R.R., and Cameron, S. (2008). *unc-3*-dependent repression of specific motor neuron fates in *Caenorhabditis elegans*. Dev Biol 323, 207-215.

Prasad, B.C., Ye, B., Zackhary, R., Schrader, K., Seydoux, G., and Reed, R.R. (1998). *unc-3*, a gene required for axonal guidance in *Caenorhabditis elegans*, encodes a member of the O/E family of transcription factors. Development 125, 1561-1568.

Pribiag, H., Peng, H., Shah, W.A., Stellwagen, D., and Carbonetto, S. (2014). Dystroglycan mediates homeostatic synaptic plasticity at GABAergic synapses. Proc Natl Acad Sci U S A 111, 6810-6815.

Probst, A., Basler, V., Bron, B., and Ulrich, J. (1983). Neuritic plaques in senile dementia of Alzheimer type: a Golgi analysis in the hippocampal region. Brain Res 268, 249-254.

Raj, A., van den Bogaard, P., Rifkin, S.A., van Oudenaarden, A., and Tyagi, S. (2008). Imaging individual mRNA molecules using multiple singly labeled probes. Nat Methods 5, 877-879.

Rakic, P., Bourgeois, J.P., Eckenhoff, M.F., Zecevic, N., and Goldman-Rakic, P.S. (1986). Concurrent overproduction of synapses in diverse regions of the primate cerebral cortex. Science 232, 232-235.

Rand, J.B. (1989). Genetic analysis of the *cha-1-unc-17* gene complex in *Caenorhabditis*. Genetics 122, 73-80.

Rand, J.B. (2007). Acetylcholine. WormBook, 1-21.

Rand, J.B., and Russell, R.L. (1984). Choline acetyltransferase-deficient mutants of the nematode *Caenorhabditis elegans*. Genetics 106, 227-248.

Rannals, M.D., and Kapur, J. (2011). Homeostatic strengthening of inhibitory synapses is mediated by the accumulation of GABA(A) receptors. J Neurosci 31, 17701-17712.

Raper, J., and Mason, C. (2010). Cellular strategies of axonal pathfinding. Cold Spring Harb Perspect Biol 2, a001933.

Rapti, G., Richmond, J., and Bessereau, J.L. (2011). A single immunoglobulin-domain protein required for clustering acetylcholine receptors in *C. elegans*. EMBO J 30, 706-718.

Reichelt, A.C., Rodgers, R.J., and Clapcote, S.J. (2012). The role of neurexins in schizophrenia and autistic spectrum disorder. Neuropharmacology 62, 1519-1526.

Reissner, C., Stahn, J., Breuer, D., Klose, M., Pohlentz, G., Mormann, M., and Missler, M. (2014). Dystroglycan binding to alpha-neurexin competes with neurexophilin-1 and neuroligin in the brain. J Biol Chem 289, 27585-27603.

Richmond, J.E., Davis, W.S., and Jorgensen, E.M. (1999). UNC-13 is required for synaptic vesicle fusion in *C. elegans*. Nat Neurosci 2, 959-964.

Richmond, J.E., and Jorgensen, E.M. (1999). One GABA and two acetylcholine receptors function at the *C. elegans* neuromuscular junction. Nat Neurosci 2, 791-797.

Robichaux, M.A., and Cowan, C.W. (2014). Signaling mechanisms of axon guidance and early synaptogenesis. Curr Top Behav Neurosci 16, 19-48.

Rogalski, T.M., Mullen, G.P., Bush, J.A., Gilchrist, E.J., and Moerman, D.G. (2001). UNC-52/perlecan isoform diversity and function in *Caenorhabditis elegans*. Biochem Soc Trans 29, 171-176.

Rougon, G., and Hobert, O. (2003). New insights into the diversity and function of neuronal immunoglobulin superfamily molecules. Annu Rev Neurosci 26, 207-238.

Rujescu, D., Ingason, A., Cichon, S., Pietilainen, O.P., Barnes, M.R., Toulopoulou, T., Picchioni, M., Vassos, E., Ettinger, U., Bramon, E., et al. (2009). Disruption of the neurexin 1 gene is associated with schizophrenia. Hum Mol Genet 18, 988-996.

Runkel, F., Rohlmann, A., Reissner, C., Brand, S.M., and Missler, M. (2013). Promoter-like sequences regulating transcriptional activity in neurexin and neuroligin genes. J Neurochem 127, 36-47.

Saheki, Y., and Bargmann, C.I. (2009). Presynaptic CaV2 calcium channel traffic requires CALF-1 and the alpha(2)delta subunit UNC-36. Nat Neurosci 12, 1257-1265.

Sahores, M., Gibb, A., and Salinas, P.C. (2010). Frizzled-5, a receptor for the synaptic organizer Wnt7a, regulates activity-mediated synaptogenesis. Development 137, 2215-2225.

Saifee, O., Wei, L., and Nonet, M.L. (1998). The *Caenorhabditis elegans unc-64* locus encodes a syntaxin that interacts genetically with synaptobrevin. Mol Biol Cell 9, 1235-1252.

Sala, C., Piech, V., Wilson, N.R., Passafaro, M., Liu, G., and Sheng, M. (2001). Regulation of dendritic spine morphology and synaptic function by Shank and Homer. Neuron 31, 115-130.

Sando, R., Bushong, E., Zhu, Y., Huang, M., Considine, C., Phan, S., Ju, S., Uytiepo, M., Ellisman, M., and Maximov, A. (2017). Assembly of Excitatory Synapses in the Absence of Glutamatergic Neurotransmission. Neuron 94, 312-321 e313.

Sandoval, G.M., Duerr, J.S., Hodgkin, J., Rand, J.B., and Ruvkun, G. (2006). A genetic interaction between the vesicular acetylcholine transporter VAChT/UNC-17 and synaptobrevin/SNB-1 in *C. elegans*. Nat Neurosci 9, 599-601.

Sanes, J.R., and Lichtman, J.W. (1999). Development of the vertebrate neuromuscular junction. Annu Rev Neurosci 22, 389-442.

Sanes, J.R., and Lichtman, J.W. (2001). Induction, assembly, maturation and maintenance of a postsynaptic apparatus. Nat Rev Neurosci 2, 791-805.

Schaefer, A.M., Hadwiger, G.D., and Nonet, M.L. (2000). *rpm-1*, a conserved neuronal gene that regulates targeting and synaptogenesis in *C. elegans*. Neuron 26, 345-356.

Schaeffer, J.M., and Bergstrom, A.R. (1988). Identification of gamma-aminobutyric acid and its binding sites in *Caenorhabditis elegans*. Life Sci 43, 1701-1706.

Schafer, D.P., Lehrman, E.K., Kautzman, A.G., Koyama, R., Mardinly, A.R., Yamasaki, R., Ransohoff, R.M., Greenberg, M.E., Barres, B.A., and Stevens, B. (2012). Microglia sculpt postnatal neural circuits in an activity and complement-dependent manner. Neuron 74, 691-705.

Schafer, D.P., and Stevens, B. (2015). Microglia Function in Central Nervous System Development and Plasticity. Cold Spring Harb Perspect Biol 7, a020545.

Schneider, J., Skelton, R.L., Von Stetina, S.E., Middelkoop, T.C., van Oudenaarden, A., Korswagen, H.C., and Miller, D.M., 3rd (2012). UNC-4 antagonizes Wnt signaling to regulate synaptic choice in the *C. elegans* motor circuit. Development 139, 2234-2245.

Schuske, K., Beg, A.A., and Jorgensen, E.M. (2004). The GABA nervous system in *C. elegans*. Trends Neurosci 27, 407-414.

Schwarz, V., Pan, J., Voltmer-Irsch, S., and Hutter, H. (2009). IgCAMs redundantly control axon navigation in *Caenorhabditis elegans*. Neural Dev 4, 13.

Seetharaman, A., Selman, G., Puckrin, R., Barbier, L., Wong, E., D'Souza, S.A., and Roy, P.J. (2011). MADD-4 is a secreted cue required for midline-oriented guidance in *Caenorhabditis elegans*. Dev Cell 21, 669-680.

Shan, G., Kim, K., Li, C., and Walthall, W.W. (2005). Convergent genetic programs regulate similarities and differences between related motor neuron classes in *Caenorhabditis elegans*. Dev Biol 280, 494-503.

Shatz, C.J., and Kirkwood, P.A. (1984). Prenatal development of functional connections in the cat's retinogeniculate pathway. J Neurosci 4, 1378-1397.

Shi, S.H., Hayashi, Y., Petralia, R.S., Zaman, S.H., Wenthold, R.J., Svoboda, K., and Malinow, R. (1999). Rapid spine delivery and redistribution of AMPA receptors after synaptic NMDA receptor activation. Science 284, 1811-1816.

Shinza-Kameda, M., Takasu, E., Sakurai, K., Hayashi, S., and Nose, A. (2006). Regulation of layer-specific targeting by reciprocal expression of a cell adhesion molecule, capricious. Neuron 49, 205-213.

Shoop, R.D., Martone, M.E., Yamada, N., Ellisman, M.H., and Berg, D.K. (1999). Neuronal acetylcholine receptors with alpha7 subunits are concentrated on somatic spines for synaptic signaling in embryonic chick ciliary ganglia. J Neurosci 19, 692-704.

Siddiqui, T.J., Pancaroglu, R., Kang, Y., Rooyakkers, A., and Craig, A.M. (2010). LRRTMs and neuroligins bind neurexins with a differential code to cooperate in glutamate synapse development. J Neurosci 30, 7495-7506.

Siddiqui, T.J., Tari, P.K., Connor, S.A., Zhang, P., Dobie, F.A., She, K., Kawabe, H., Wang, Y.T., Brose, N., and Craig, A.M. (2013). An LRRTM4-HSPG complex mediates excitatory synapse development on dentate gyrus granule cells. Neuron 79, 680-695.

Sigler, A., Oh, W.C., Imig, C., Altas, B., Kawabe, H., Cooper, B.H., Kwon, H.B., Rhee, J.S., and Brose, N. (2017). Formation and Maintenance of Functional Spines in the Absence of Presynaptic Glutamate Release. Neuron 94, 304-311 e304.

Simske, J.S., Kaech, S.M., Harp, S.A., and Kim, S.K. (1996). LET-23 receptor localization by the cell junction protein LIN-7 during *C. elegans* vulval induction. Cell 85, 195-204.

Singh, S.K., Stogsdill, J.A., Pulimood, N.S., Dingsdale, H., Kim, Y.H., Pilaz, L.J., Kim, I.H., Manhaes, A.C., Rodrigues, W.S., Jr., Pamukcu, A., et al. (2016). Astrocytes Assemble Thalamocortical Synapses by Bridging NRX1alpha and NL1 via Hevin. Cell 164, 183-196.

Smith, A.D., and Bolam, J.P. (1990). The neural network of the basal ganglia as revealed by the study of synaptic connections of identified neurones. Trends Neurosci 13, 259-265.

Smith-Trunova, S., Prithviraj, R., Spurrier, J., Kuzina, I., Gu, Q., and Giniger, E. (2015). Cdk5 regulates developmental remodeling of mushroom body neurons in *Drosophila*. Dev Dyn 244, 1550-1563.

Song, J.Y., Ichtchenko, K., Sudhof, T.C., and Brose, N. (1999). Neuroligin 1 is a postsynaptic cell-adhesion molecule of excitatory synapses. Proc Natl Acad Sci U S A 96, 1100-1105.

Soto, F., Ma, X., Cecil, J.L., Vo, B.Q., Culican, S.M., and Kerschensteiner, D. (2012). Spontaneous activity promotes synapse formation in a cell-type-dependent manner in the developing retina. J Neurosci 32, 5426-5439.

Spencer, W.C., McWhirter, R., Miller, T., Strasbourger, P., Thompson, O., Hillier, L.W., Waterston, R.H., and Miller, D.M., 3rd (2014). Isolation of specific neurons from *C. elegans* larvae for gene expression profiling. PLoS One 9, e112102.

Spencer, W.C., Zeller, G., Watson, J.D., Henz, S.R., Watkins, K.L., McWhirter, R.D., Petersen, S., Sreedharan, V.T., Widmer, C., Jo, J., et al. (2011). A spatial and temporal map of *C. elegans* gene expression. Genome Res 21, 325-341.

Sterky, F.H., Trotter, J.H., Lee, S.J., Recktenwald, C.V., Du, X., Zhou, B., Zhou, P., Schwenk, J., Fakler, B., and Sudhof, T.C. (2017). Carbonic anhydrase-related protein CA10 is an evolutionarily conserved pan-neurexin ligand. Proc Natl Acad Sci U S A 114, E1253-E1262.

Sugita, S., Saito, F., Tang, J., Satz, J., Campbell, K., and Sudhof, T.C. (2001). A stoichiometric complex of neurexins and dystroglycan in brain. J Cell Biol 154, 435-445.

Sulston, J.E. (1976). Post-embryonic development in the ventral cord of *Caenorhabditis elegans*. Philos Trans R Soc Lond B Biol Sci 275, 287-297.

Sulston, J.E., and Horvitz, H.R. (1977). Post-embryonic cell lineages of the nematode, *Caenorhabditis elegans*. Dev Biol 56, 110-156.

Tavazoie, S.F., and Reid, R.C. (2000). Diverse receptive fields in the lateral geniculate nucleus during thalamocortical development. Nat Neurosci 3, 608-616.

Thompson-Peer, K.L., Bai, J., Hu, Z., and Kaplan, J.M. (2012). HBL-1 patterns synaptic remodeling in *C. elegans*. Neuron 73, 453-465.

Togashi, H., Abe, K., Mizoguchi, A., Takaoka, K., Chisaka, O., and Takeichi, M. (2002). Cadherin regulates dendritic spine morphogenesis. Neuron 35, 77-89.

Tong, X.J., Hu, Z., Liu, Y., Anderson, D., and Kaplan, J.M. (2015). A network of autism linked genes stabilizes two pools of synaptic GABA(A) receptors. Elife 4, e09648.

Tong, X.J., Lopez-Soto, E.J., Li, L., Liu, H., Nedelcu, D., Lipscombe, D., Hu, Z., and Kaplan, J.M. (2017). Retrograde Synaptic Inhibition Is Mediated by alpha-Neurexin Binding to the alpha2delta Subunits of N-Type Calcium Channels. Neuron 95, 326-340 e325.

Touroutine, D., Fox, R.M., Von Stetina, S.E., Burdina, A., Miller, D.M., 3rd, and Richmond, J.E. (2005). *acr-16* encodes an essential subunit of the levamisole-resistant nicotinic receptor at the *Caenorhabditis elegans* neuromuscular junction. J Biol Chem 280, 27013-27021.

Towers, P.R., Edwards, B., Richmond, J.E., and Sattelle, D.B. (2005). The *Caenorhabditis elegans lev-8* gene encodes a novel type of nicotinic acetylcholine receptor alpha subunit. J Neurochem 93, 1-9.

Tu, H., Pinan-Lucarre, B., Ji, T., Jospin, M., and Bessereau, J.L. (2015). *C. elegans* Punctin Clusters GABA(A) Receptors via Neuroligin Binding and UNC-40/DCC Recruitment. Neuron 86, 1407-1419.

Turrigiano, G.G. (2008). The self-tuning neuron: synaptic scaling of excitatory synapses. Cell 135, 422-435.

Turrigiano, G.G., Leslie, K.R., Desai, N.S., Rutherford, L.C., and Nelson, S.B. (1998). Activity-dependent scaling of quantal amplitude in neocortical neurons. Nature 391, 892-896.

Uemura, T., Lee, S.J., Yasumura, M., Takeuchi, T., Yoshida, T., Ra, M., Taguchi, R., Sakimura, K., and Mishina, M. (2010). Trans-synaptic interaction of GluRdelta2 and Neurexin through Cbln1 mediates synapse formation in the cerebellum. Cell 141, 1068-1079.

Ullrich, B., Ushkaryov, Y.A., and Sudhof, T.C. (1995). Cartography of neurexins: more than 1000 isoforms generated by alternative splicing and expressed in distinct subsets of neurons. Neuron 14, 497-507.

Um, J.W., Choi, T.Y., Kang, H., Cho, Y.S., Choii, G., Uvarov, P., Park, D., Jeong, D., Jeon, S., Lee, D., et al. (2016). LRRTM3 Regulates Excitatory Synapse Development through Alternative Splicing and Neurexin Binding. Cell Rep 14, 808-822.

Um, J.W., Pramanik, G., Ko, J.S., Song, M.Y., Lee, D., Kim, H., Park, K.S., Sudhof, T.C., Tabuchi, K., and Ko, J. (2014). Calsyntenins function as synaptogenic adhesion molecules in concert with neurexins. Cell Rep 6, 1096-1109.

Usardi, A., Iyer, K., Sigoillot, S.M., Dusonchet, A., and Selimi, F. (2017). The immunoglobulin-like superfamily member IGSF3 is a developmentally regulated protein that controls neuronal morphogenesis. Dev Neurobiol 77, 75-92.

Ushkaryov, Y.A., Petrenko, A.G., Geppert, M., and Sudhof, T.C. (1992). Neurexins: synaptic cell surface proteins related to the alpha-latrotoxin receptor and laminin. Science 257, 50-56.

Varoqueaux, F., Sigler, A., Rhee, J.S., Brose, N., Enk, C., Reim, K., and Rosenmund, C. (2002). Total arrest of spontaneous and evoked synaptic transmission but normal synaptogenesis in the absence of Munc13-mediated vesicle priming. Proc Natl Acad Sci U S A 99, 9037-9042.

Verhage, M., Maia, A.S., Plomp, J.J., Brussaard, A.B., Heeroma, J.H., Vermeer, H., Toonen, R.F., Hammer, R.E., van den Berg, T.K., Missler, M., et al. (2000). Synaptic assembly of the brain in the absence of neurotransmitter secretion. Science 287, 864-869.

Walsh, M.K., and Lichtman, J.W. (2003). *In vivo* time-lapse imaging of synaptic takeover associated with naturally occurring synapse elimination. Neuron 37, 67-73.

Walthall, W.W., and Plunkett, J.A. (1995). Genetic transformation of the synaptic pattern of a motoneuron class in *Caenorhabditis elegans*. J Neurosci 15, 1035-1043.

Wang, J., Chitturi, J., Ge, Q., Laskova, V., Wang, W., Li, X., Ding, M., Zhen, M., and Huang, X. (2015). The *C. elegans* COE transcription factor UNC-3 activates lineage-specific apoptosis and affects neurite growth in the RID lineage. Development 142, 1447-1457.

Wang, M.M., Tsai, R.Y., Schrader, K.A., and Reed, R.R. (1993). Genes encoding components of the olfactory signal transduction cascade contain a DNA binding site that may direct neuronal expression. Mol Cell Biol 13, 5805-5813.

Wang, S.S., Tsai, R.Y., and Reed, R.R. (1997). The characterization of the Olf-1/EBF-like HLH transcription factor family: implications in olfactory gene regulation and neuronal development. J Neurosci 17, 4149-4158.

Wassef, A., Baker, J., and Kochan, L.D. (2003). GABA and schizophrenia: a review of basic science and clinical studies. J Clin Psychopharmacol 23, 601-640.

West, A.E., and Greenberg, M.E. (2011). Neuronal activity-regulated gene transcription in synapse development and cognitive function. Cold Spring Harb Perspect Biol 3.

White, J.G., Albertson, D.G., and Anness, M.A. (1978). Connectivity changes in a class of motoneurone during the development of a nematode. Nature 271, 764-766.

White, J.G., Southgate, E., Thomson, J.N., and Brenner, S. (1976). The structure of the ventral nerve cord of *Caenorhabditis elegans*. Philos Trans R Soc Lond B Biol Sci 275, 327-348.

White, J.G., Southgate, E., Thomson, J.N., and Brenner, S. (1986). The structure of the nervous system of the nematode *Caenorhabditis elegans*. Philos Trans R Soc Lond B Biol Sci 314, 1-340.

Willson, J., Amliwala, K., Davis, A., Cook, A., Cuttle, M.F., Kriek, N., Hopper, N.A., O'Connor, V., Harder, A., Walker, R.J., et al. (2004). Latrotoxin receptor signaling engages the UNC-13-dependent vesicle-priming pathway in *C. elegans*. Curr Biol 14, 1374-1379.

Wilson, C.J., Groves, P.M., Kitai, S.T., and Linder, J.C. (1983). Three-dimensional structure of dendritic spines in the rat neostriatum. J Neurosci 3, 383-388.

Woo, J., Kwon, S.K., Nam, J., Choi, S., Takahashi, H., Krueger, D., Park, J., Lee, Y., Bae, J.Y., Lee, D., et al. (2013). The adhesion protein IgSF9b is coupled to neuroligin 2 via S-SCAM to promote inhibitory synapse development. J Cell Biol 201, 929-944.

Woolf, T.B., Shepherd, G.M., and Greer, C.A. (1991). Local information processing in dendritic trees: subsets of spines in granule cells of the mammalian olfactory bulb. J Neurosci 11, 1837-1854.

Yang, G., Pan, F., and Gan, W.B. (2009a). Stably maintained dendritic spines are associated with lifelong memories. Nature 462, 920-924.

Yang, K.C., Jin, G.Z., and Wu, J. (2009b). Mysterious alpha6-containing nAChRs: function, pharmacology, and pathophysiology. Acta Pharmacol Sin 30, 740-751.

Yang, X., Arber, S., William, C., Li, L., Tanabe, Y., Jessell, T.M., Birchmeier, C., and Burden, S.J. (2001). Patterning of muscle acetylcholine receptor gene expression in the absence of motor innervation. Neuron 30, 399-410.

Yang, Y., Paspalas, C.D., Jin, L.E., Picciotto, M.R., Arnsten, A.F., and Wang, M. (2013). Nicotinic alpha7 receptors enhance NMDA cognitive circuits in dorsolateral prefrontal cortex. Proc Natl Acad Sci U S A 110, 12078-12083.

Yeh, E., Kawano, T., Weimer, R.M., Bessereau, J.L., and Zhen, M. (2005). Identification of genes involved in synaptogenesis using a fluorescent active zone marker in *Caenorhabditis elegans*. J Neurosci 25, 3833-3841.

Yemini, E., Jucikas, T., Grundy, L.J., Brown, A.E., and Schafer, W.R. (2013). A database of *Caenorhabditis elegans* behavioral phenotypes. Nat Methods 10, 877-879.

Yemini, E., Kerr, R.A., and Schafer, W.R. (2011). Preparation of samples for single-worm tracking. Cold Spring Harb Protoc 2011, 1475-1479.

Zhang, B., Chen, L.Y., Liu, X., Maxeiner, S., Lee, S.J., Gokce, O., and Sudhof, T.C. (2015). Neuroligins Sculpt Cerebellar Purkinje-Cell Circuits by Differential Control of Distinct Classes of Synapses. Neuron 87, 781-796.

Zhang, C., Atasoy, D., Arac, D., Yang, X., Fucillo, M.V., Robison, A.J., Ko, J., Brunger, A.T., and Sudhof, T.C. (2010). Neurexins physically and functionally interact with GABA(A) receptors. Neuron 66, 403-416.

Zhang, M., Chung, S.H., Fang-Yen, C., Craig, C., Kerr, R.A., Suzuki, H., Samuel, A.D., Mazur, E., and Schafer, W.R. (2008). A self-regulating feed-forward circuit controlling *C. elegans* egg-laying behavior. Curr Biol 18, 1445-1455.

Zhen, M., Huang, X., Bamber, B., and Jin, Y. (2000). Regulation of presynaptic terminal organization by *C. elegans* RPM-1, a putative guanine nucleotide exchanger with a RING-H2 finger domain. Neuron 26, 331-343.

Zhen, M., and Jin, Y. (1999). The liprin protein SYD-2 regulates the differentiation of presynaptic termini in *C. elegans*. Nature 401, 371-375.

Zhen, M., and Samuel, A.D. (2015). *C. elegans* locomotion: small circuits, complex functions. Curr Opin Neurobiol 33, 117-126.

Zhou, H.M., and Walthall, W.W. (1998). UNC-55, an orphan nuclear hormone receptor, orchestrates synaptic specificity among two classes of motor neurons in *Caenorhabditis elegans*. J Neurosci 18, 10438-10444.

Zhou, Q., Homma, K.J., and Poo, M.M. (2004). Shrinkage of dendritic spines associated with long-term depression of hippocampal synapses. Neuron 44, 749-757.

Zhou, Q., Li, H., Li, H., Nakagawa, A., Lin, J.L., Lee, E.S., Harry, B.L., Skeen-Gaar, R.R., Suehiro, Y., William, D., et al. (2016). Mitochondrial endonuclease G mediates breakdown of paternal mitochondria upon fertilization. Science 353, 394-399.

Zhou, S., Opperman, K., Wang, X., and Chen, L. (2008). *unc-44* Ankyrin and *stn-2* gamma-syntrophin regulate *sax-7* L1CAM function in maintaining neuronal positioning in *Caenorhabditis elegans*. Genetics 180, 1429-1443.

Ziv, N.E., and Smith, S.J. (1996). Evidence for a role of dendritic filopodia in synaptogenesis and spine formation. Neuron 17, 91-102.

Zong, Y., Zhang, B., Gu, S., Lee, K., Zhou, J., Yao, G., Figueiredo, D., Perry, K., Mei, L., and Jin, R. (2012). Structural basis of agrin-LRP4-MuSK signaling. Genes Dev 26, 247-258.

Zuo, Y., Lin, A., Chang, P., and Gan, W.B. (2005). Development of long-term dendritic spine stability in diverse regions of cerebral cortex. Neuron 46, 181-189.